AWARD NUMBER: W81XWH-19-1-0167 / CA181344

TITLE: Therapeutic Targeting of Immune Dysfunction in Langerhans Cell Histiocytosis

PRINCIPAL INVESTIGATOR: Rikhia Chaudhury Chakraborty

CONTRACTING ORGANIZATION: Baylor College of Medicine, One Baylor Plaza, Houston, TX 77030

REPORT DATE: December 2021

TYPE OF REPORT: Final Report

PREPARED FOR: U.S. Army Medical Research and Development Command
Fort Detrick, Maryland 21702-5012

DISTRIBUTION STATEMENT: Approved for Public Release;
Distribution Unlimited

The views, opinions and/or findings contained in this report are those of the author(s) and should not be construed as an official Department of the Army position, policy or decision unless so designated by other documentation.

# REPORT DOCUMENTATION PAGE

*Form Approved*
*OMB No. 0704-0188*

Public reporting burden for this collection of information is estimated to average 1 hour per response, including the time for reviewing instructions, searching existing data sources, gathering and maintaining the data needed, and completing and reviewing this collection of information. Send comments regarding this burden estimate or any other aspect of this collection of information, including suggestions for reducing this burden to Department of Defense, Washington Headquarters Services, Directorate for Information Operations and Reports (0704-0188), 1215 Jefferson Davis Highway, Suite 1204, Arlington, VA 22202-4302. Respondents should be aware that notwithstanding any other provision of law, no person shall be subject to any penalty for failing to comply with a collection of information if it does not display a currently valid OMB control number. **PLEASE DO NOT RETURN YOUR FORM TO THE ABOVE ADDRESS.**

| 1. REPORT DATE | 2. REPORT TYPE | 3. DATES COVERED |
|---|---|---|
| December 2021 | Final Report | 10/01/2019 – 08/16/2021 |

**4. TITLE AND SUBTITLE**
Therapeutic Targeting of Immune Dysfunction in Langerhans Cell Histiocytosis

**5a. CONTRACT NUMBER**
W81XWH-19-1-0167

**5b. GRANT NUMBER**
CA181344

**5c. PROGRAM ELEMENT NUMBER**

**6. AUTHOR(S)**
Rikhia Chaudhury Chakraborty

E-Mail: rxchakra@txch.org

**5d. PROJECT NUMBER**
0011338275-0001

**5e. TASK NUMBER**

**5f. WORK UNIT NUMBER**

**7. PERFORMING ORGANIZATION NAME(S) AND ADDRESS(ES)**

Baylor College of Medicine
One Baylor Plaza
Houston, TX 77030

**8. PERFORMING ORGANIZATION REPORT NUMBER**

**9. SPONSORING / MONITORING AGENCY NAME(S) AND ADDRESS(ES)**

U.S. Army Medical Research and Development Command
Fort Detrick, Maryland 21702-5012

**10. SPONSOR/MONITOR'S ACRONYM(S)**

**11. SPONSOR/MONITOR'S REPORT NUMBER(S)**

**12. DISTRIBUTION / AVAILABILITY STATEMENT**

Approved for Public Release; Distribution Unlimited

**13. SUPPLEMENTARY NOTES**

**14. ABSTRACT**
Langerhans cell histiocytosis (LCH) is a myeloproliferative disorder with similar incidence and overall survival as pediatric Hodgkin's Lymphoma. The current therapeutic standard of care for patients with multi-focal disease remains empiric chemotherapy which fails in over 50% of patients, and treatment failure is associated with significant long-term morbidity and mortality. Translational research resources and efforts to study LCH have been relatively sparse due to challenging samples and the lack of reliable *pre-clinical* models. To address this issue the Histiocytosis Program at Texas Children's Cancer Center has developed an unprecedented research resource of ~1000 viably preserved LCH lesions and paired peripheral blood mononuclear cells, along with associated clinical data. In addition, we generated the first mouse models of LCH-like disease, allowing us to characterize the molecular mechanisms that drive LCH. LCH lesions histology reveals a universal feature of accumulation of Langerin-positive dendritic cells along with a large inflammatory infiltrate. Upon immune cell phenotyping of LCH microenvironment we found T lymphocytes are most abundant but are dysfunctional and express exhaustion markers on their surface. To improve outcomes for patients, we not only need to more completely define the mechanisms driving LCH, but also to translate these discoveries into improved therapeutic strategies. The objective of this proposal is to develop pre-clinical models to determine the most effective therapeutic strategies for patients with LCH. We hypothesize that combination therapeutic strategies targeting MAPK activation and dysfunctional T cells can overcome the immune suppressive microenvironment in LCH, leading to better clinical outcomes than chemotherapy or MAPK inhibition alone. Aim 1: To define the impact of specific MAPK pathway mutations on initial treatment failure and immune evasion in patients with LCH; Aim 2: To test novel therapeutic salvage strategies in mutation-specific in vitro and in vivo models of LCH.

**15. SUBJECT TERMS**
Langerhans cell histiocytosis, LCH, MAPK, T cells, exhausted T cells, dysfunctional T cells, somatic mutation, immunotherapy, MAPK inhibition, combination therapy, novel therapeutics

| 16. SECURITY CLASSIFICATION OF: | | | 17. LIMITATION OF ABSTRACT | 18. NUMBER OF PAGES | 19a. NAME OF RESPONSIBLE PERSON |
|---|---|---|---|---|---|
| a. REPORT | b. ABSTRACT | c. THIS PAGE | | | USAMRMC |
| Unclassified | Unclassified | Unclassified | Unclassified | | 19b. TELEPHONE NUMBER *(include area code)* |

## TABLE OF CONTENTS


| | Page |
|---|---|
| 1. Introduction | 4 |
| 2. Keywords | 4 |
| 3. Accomplishments | 4 |
| 4. Impact | 9 |
| 5. Changes/Problems | 10 |
| 6. Products | 11 |
| 7. Participants & Other Collaborating Organizations | 12 |
| 8. Special Reporting Requirements | 14 |
| 9. Appendices | 15 |

**1. INTRODUCTION:** *Narrative that briefly (one paragraph) describes the subject, purpose and scope of the research.*

Langerhans cell histiocytosis (LCH) is a myeloproliferative disorder with similar incidence and overall survival as pediatric Hodgkin's Lymphoma. The current therapeutic standard of care for patients with multi-focal disease remains empiric chemotherapy which fails in over 50% of patients, and treatment failure is associated with significant long-term morbidity and mortality. Translational research resources and efforts to study LCH have been relatively sparse due to challenging samples and the lack of reliable *pre-clinical* models. To address this issue the Histiocytosis Program at Texas Children's Cancer Center has developed an unprecedented research resource of ~1000 viably preserved LCH lesions and paired peripheral blood mononuclear cells, along with associated clinical data. In addition, we generated the first mouse models of LCH-like disease, allowing us to characterize the molecular mechanisms that drive LCH. LCH lesions histology reveals a universal feature of accumulation of Langerin-positive dendritic cells along with a large inflammatory infiltrate. Upon immune cell phenotyping of LCH microenvironment we found T lymphocytes are most abundant but are dysfunctional and express exhaustion markers on their surface. To improve outcomes for patients, we not only need to more completely define the mechanisms driving LCH, but also to translate these discoveries into improved therapeutic strategies. The **purpose** of this proposal is to develop pre-clinical models to determine the most effective therapeutic strategies for patients with LCH. We hypothesize that combination therapeutic strategies targeting MAPK activation and dysfunctional T cells can overcome the immune suppressive microenvironment in LCH, leading to better clinical outcomes than chemotherapy or MAPK inhibition alone. Aim 1: To define the impact of specific MAPK pathway mutations on initial treatment failure and immune evasion in patients with LCH; Aim 2: To test novel therapeutic salvage strategies in mutation-specific in vitro and in vivo models of LCH. The goal for the experiments in this proposal is to develop a rational approach to therapy for pediatric patients with LCH. We are using preclinical data to determine which patients are at highest risk for relapse based on mutation and cell of origin. Further, these experiments will provide the platform from which to consider and test specific targeted agents in LCH patients with specific mutations.

**2. KEYWORDS:** *Provide a brief list of keywords (limit to 20 words).*

Langerhans cell histiocytosis, LCH, MAPK, T cells, exhausted T cells, dysfunctional T cells, somatic mutation, immunotherapy, MAPK inhibition, combination therapy, novel therapeutics

**3. ACCOMPLISHMENTS:** *The PI is reminded that the recipient organization is required to obtain prior written approval from the awarding agency grants official whenever there are significant changes in the project or its direction.*

**What were the major goals of the project?**
*List the major goals of the project as stated in the approved SOW. If the application listed milestones/target dates for important activities or phases of the project, identify these dates and show actual completion dates or the percentage of completion.*

**A. Career Development-Specific Tasks:**
**Major Task 1: Training and educational development in pre-clinical and clinical translational research**

- **Subtask 1:** Participate and present research at the weekly Histiocytosis Program meetings at the Texas Medical Center (Months 1-36).
- **Subtask 2:** Participate in weekly meetings and present (once annually) at the Center for Cell and Gene Therapy, Baylor College of Medicine (Months 1-36).
- **Subtask 3:** Participate in weekly meetings with Dr. Carl E Allen (Months 1-36).
- **Subtask 4:** Organize and attend quarterly meetings with mentoring team (comprising Dr. Miriam Merad, Dr. Kenneth L McClain, Dr. Helen Heslop, and Dr. Carl E Allen) to discuss progress of proposed research and career development plans. I also plan to add, in consultation with the mentoring team, a Cancer Pharmacologist to the mentoring team within the first six months of the grant period (Months 1-36).
- **Subtask 5:** Attend scientific grant writing and other relevant workshops, which are routinely offered by the Career Development Center at Baylor College of Medicine (Months 1-24).
- **Subtask 6:** Attend and present research findings at annual national and international conferences, including the (i) Annual Meeting of the American Society of Hematology, (ii) Histiocyte Society Meeting, and (iii) relevant Keystone Symposia and Gordon Research Conferences (Months 1-36).

**B. Research-Specific Tasks:**

***Specific Aim 1: To define the impact of specific MAPK pathway mutations on initial treatment failure and immune evasion in patients with LCH.***
**Major Task 1: To determine the clinical significance of specific recurrent mutations in LCH.**

- **IRB/HRPO Approval** (Months 0-3)
- **Subtask 1:** Analysis of LCH specimens (lesions, correlated clinical data) from the Histiocytosis Program at Texas Children's Cancer Center (TXCC). Recurrent mutations will be analyzed with respect to clinical variables including age of onset of disease, gender, single vs multifocal lesions, and low-risk vs high risk lesions (Months 4-6).
- **Subtask 2:** Association between each characteristic and mutation status will be determined by calculating crude odds ratios (OR) and 95% confidence intervals using unconditional logistic regression analysis. Develop adjusted models based on variables identified in Subtask 1 with a significance level of $P < 0.05$ (Months 4-6).

- **Subtask 3:** Kaplan-Meier estimates will be used to calculate probability of treatment failure (event-free survival) and overall mortality for each mutation group (Months 7-8).
- **Subtask 4:** Analyze differences in clinical outcomes using Cox proportional hazards models to adjust for relevant covariates, including: age, gender, race/ethnicity, and treatment (Months 7-8).
- **Milestone(s) Achieved:** Define how specific activating MAPK gene pathway mutations affect LCH patients' response to initial therapy, the results of which will be incorporated into prioritization of agents/strategies tested in Aim 2.

**Major Task 2: To determine the impact of LCH-specific mutations on immune evasion.**

- **Subtask 1:** Perform mass cytometric analysis on a larger cohort with ~ 15 samples per mutation type) of LCH lesions harboring different MAPK pathway somatic mutations. Analyze inhibitory receptors' (PD-1, TIM-3, LAG-3) expression on CD3+ T cells, corresponding ligands for the inhibitory receptors on CD207+ cells (Months 3-12).
- **Subtask 2:** Perform transcriptomic analysis to identify the factors and signaling mechanisms that are promoting differential immune cell exhaustion marker expression in LCH based on specific MAPK pathway mutations (Months 9-15).

***Specific Aim 2: To test novel therapeutic salvage strategies in mutation-specific in vitro and in vivo models of LCH.***
**Major Task 3: Test the relative efficacy of myeloid-directed chemotherapy, MAPK pathway inhibition, and other targeted therapies on tumor progression and survival in mouse models of LCH.**

- **IACUC/ACURO approval** (Months 15-18)

**What was accomplished under these goals?**

*For this reporting period describe: 1) major activities; 2) specific objectives; 3) significant results or key outcomes, including major findings, developments, or conclusions (both positive and negative); and/or 4) other achievements. Include a discussion of stated goals not met. Description shall include pertinent data and graphs in sufficient detail to explain any significant results achieved. A succinct description of the methodology used shall be provided. As the project progresses to completion, the emphasis in reporting in this section should shift from reporting activities to reporting accomplishments.*

**ACCOMPLISHMENTS AND PROGRESS**

**A. Career Development-Specific Tasks:**

**Major Task 1: Training and educational development in pre-clinical and clinical translational research**

- **Subtask 1:** I have regularly participated in weekly Histiocytosis Program meetings at the Texas Medical Center.
- **Subtask 2:** I have participated in the weekly meeting of the Center for Cell and Gene Therapy, Baylor College of Medicine.
- **Subtask 3:** Dr. Allen and I had multiple meetings every week including a dedicated one-hour meeting where we discuss progress and expectations.
- **Subtask 4:** I had the quarterly meetings with Dr. Allen and Dr. Merad. Dr. McClain could attend only one of the meetings while Dr. Heslop could not attain these meetings as her workload as considerably increased over the last year. I have also added Dr. Greg M. Delgoffe, a world renouned expert in tumor microenvironment, to my collaboration team. I have also discussed my goals and progress with Dr. Martin Matzuk, Interim Chair of The Department of Pharmacology and Chemical Biology at Baylor College of Medicine and plan to formally request him to attend my subsequent meetings/presentations. I have also been added to the NACHO-LIBRE (North American Consortium for Histiocytosis–Registry Study of LCH and Related Disorders: Inhibition of MAPK Pathway Activation [RAS, BRAF, MEK, and ERK]) as a co-investigator which provides me direct access to experts in Cancer Pharmacology.
- **Subtask 5:** Professional educational development activities: Immuno-Oncology and Cancer Pathology using Mass Cytometry (October 2019), Clear Science Writing Workshop (September 2019), Grant Writing of Researchers NIH Process Workshop (January 2020).
- **Subtask 6:** I presented an invited seminar at the American Society of Hematology ASH-a-Palooza Blood Drops Session, Orlando, FL. I attended the 2019 Annual ASH meeting at Orlando, FL. I have now transitioned to a Senior Manager – Business Development (Immuno-Oncology) at Xilis, Inc., Durham, NC, which was a rational next step of my career advancement. Unfortunately, even though this move preclude me from finishing the experiments outlined for year-03 in the proposal, it did ensure I achieved the professional goals of this career development award from DoD.

**B. Research-Specific Tasks:**

***Specific Aim 1: To define the impact of specific MAPK pathway mutations on initial treatment failure and immune evasion in patients with LCH.***
**Major Task 1: To determine the clinical significance of specific recurrent mutations in LCH.**
**Major Task 2: To determine the impact of LCH-specific mutations on immune evasion.**

**Major Task 1 - Subtasks 1-4 & Major Task 2 - Subtasks 1-2:**

- **IRB/HRPO Approval** (Months 0-3): The HRPO approval was obtained on August 25, 2020 (HRPO Log Number E00845.1a). The delay was largely due to the requirement of having a stand-alone (pertaining to the goals of the DoD approved proposal) human subject protocol approved by the Institutional Review Board at Baylor College of Medicine.

Given the COVID-19 pandemic and the closures this protocol submission, review, and resubmissions took much longer than initially anticipated.

- Experiments proposed in Major Tasks 1 and 2 resulted in a publication in the journal *Blood*, citation of which is as follows:

  Sengal A, Velasquez J, Hahne M, Burke TM, Abhyankar H, Reyes R, Olea W, Scull B, Eckstein O, Bigenwald C, Bollard CM, Yu E, Merad M, McClain KL, Allen CE, **Chakraborty R**. Overcoming T cell exhaustion in LCH: PD-1 blockade and targeted MAPK inhibition are synergistic in a mouse model of LCH. *Blood* 137(13): 1777-1791.

- Our work was
  (a) highlighted in cover of *Blood* April 1, 2021
  (b) Discussed in *Blood* Podcast Season 2, Episode 13
  (c) Independent commentary about our work was published in *Blood* 137(13):1705-1706 (2021).
  (d) Our work was recommended in *Faculty Opinions* as being of *special significance* in its field.

- The major findings are summarized below and referenced to the actual *Blood* manuscript attached to this final report.

***A. Phenotypic analysis of LCH lesions***

We first analyzed the immune composition using mass cytometry by time-of-flight (CyTOF) of patient biopsies (n=15; *BRAF* WT (n=6) and *BRAF*V600E (n=9) and healthy skin controls (skin $CD207^+$ DCs (n=5)) (**Fig. 1A-C**; **Supplementary Figure 1A-D in *Blood* paper**). Immune infiltrate in LCH lesions varied between 50 and 70% with $CD3^+$ T cells and myeloid derived suppressor cells (MDSCs) ($CD11b^+CD14^+HLA\text{-}DR^{low/-}CD15^-$) as the most abundant populations. Overall, LCH lesion DCs ($HLA\text{-}DR^+CD1A^+$), T cells, and MDSCs accounted for 25.60% ± 10.72%, 28.20% ± 6.46% and 31.90% ± 4.02%, respectively. T cells were significantly more abundant in WT *BRAF* compared to *BRAF*V600E lesions, consistent with increased LCH DC ($HLA\text{-}DR^+CD1A^+$) in the *BRAF*V600E lesions (**Supplementary Figure 1A, B, D**; **Supplementary Table 3 in *Blood* paper**). By comparison, immune infiltrate in normal skin included 5.00% ± 1.00% LCs, 3.00%± 1.58% T cells and 13.60% ± 2.07% MDSC (**Fig. 1B, C**; **Supplementary Figure 1C, D in *Blood* paper**). The proportion of T cells compared to MDSC was significantly larger in the LCH lesions when compared to healthy skin (**Fig. 1A-C in *Blood* paper**).

The T cells were further characterized by automatic gating using FlowSOM that allows multivariate clustering of cells based on the self-organized map (SOM) algorithm and categorizes cells into relevant meta-clusters based on their surface markers (**Fig. 1D**, **Supplementary Figure 2A-C in *Blood* paper**). Within LCH lesions, $CD3^+CD4^+$ T cells (74.00% ± 12.26%) were significantly higher than effector $CD3^+CD8^+$ T cells (21.00% ± 5.61%) (**Fig. 1D, E in *Blood* paper**) as compared to tonsil control (41.20% ± 7.02% CD4 and 32.00% ± 4.64% CD8) (**Fig. 1E**, **Supplementary Figure 2A**), healthy skin (27.00% ± 13.23% CD4 and 63.67% ± 6.11%) (**Fig. 1E, Supplementary Figure 2B in *Blood* paper**), or lymph node with macrophage activation (Kikuchi lymphadenitis) (**Supplementary Figure 2C in *Blood* paper**). Among $CD4^+$ T cells, the fraction of Tregs was significantly greater in LCH lesions than in tonsil or skin controls (**Fig. 1F in *Blood* paper**). These results were independent of *BRAF* mutation status (**Supplementary Figure 1E, F in *Blood* paper**).

B. ***Infiltrating T cells are dysfunctional***

In many malignancies, tumor infiltrating $CD8^+$ T cells mediate adaptive immune response against tumor antigen. Indeed, frequency of tumor-infiltrating $CD8^+$ T cells has been widely shown to correlate with cancer-free survival time among patients with different tumor types. Given the presence of LCH-lesion infiltrating $CD8^+$ T cells, we next assessed their functional capacity and found that they demonstrated attenuated expression of Tc1/Tc2 cytokines, interferon gamma (IFN-$\gamma$), tumor necrosis factor alpha (TNFα), interleukin (IL)-17 or interleukin (IL)-10 in the native state, and after stimulation. By comparison, all 4 cytokines were robustly induced in T cells isolated from healthy tonsil (**Fig. 2A-D in *Blood* paper)**. Accordingly, $CD8^+$ T cells within the LCH lesions had impaired alloreactivity (**Fig. 2E in *Blood* paper**), consistent with altered effector function along with high CD44 expression and low/absent expression of CD127. In contrast, Tregs isolated from LCH lesions demonstrated intact suppressive activity (**Fig. 2F in *Blood* paper**).

C. ***Infiltrating T cells in LCH tumor microenvironment exhibit an 'exhausted' phenotype***

Increased expression of inhibitory immune receptors can raise the threshold for activation, resulting in suppressed immune responses and T cell exhaustion. Hence, to elucidate the mechanisms underlying T cell dysfunction within LCH lesions, we assessed expression of inhibitory receptors on $CD8^+$ and $CD4^+$ T cell subsets using FlowSOM. $CD8^+$ T cells residing in the LCH lesions showed higher expression of the inhibitory receptors programmed death receptor-1 (PD-1) (**Fig. 3A, B in *Blood* paper**), T cell immunoglobulin- and mucin domain-containing molecule (TIM-3) (**Fig. 3A**, **Supplementary Figure 3B in *Blood* paper**), and lymphocyte-activation gene 3 (LAG-3) (**Fig. 3A**, **Supplementary Figure 3C in *Blood* paper**), but not cytotoxic T lymphocyte antigen-4 (CTLA-4) (**Fig. 3A in *Blood* paper**), compared to peripheral $CD8^+$ T cells from the same patients, skin controls, or peripheral $CD8^+$ T cells from controls (**Fig. 3B**, **Supplementary Figure 3A-3C in *Blood* paper**). Compared to $CD8^+$ T cells from healthy skin tissues, the $CD8^+$ T cells from LCH lesions showed significantly higher numbers of $PD\text{-}1^+TIM\text{-}3^+$ and $PD\text{-}1^+TIM\text{-}3^+LAG\text{-}3^+$ cells, but not $PD\text{-}1^+LAG\text{-}3^+$ or $TIM\text{-}3^+LAG\text{-}3^+$ cell (**Fig. 3C in *Blood* paper**). $CD4^+$ T cells within the lesion also showed significantly higher expression of PD-1 and TIM-3 compared to peripheral $CD4^+$ T cells from the same patients, skin controls, or peripheral $CD4^+$ T cells from controls (**Supplementary Figure 3D, E in *Blood* paper**). However, there

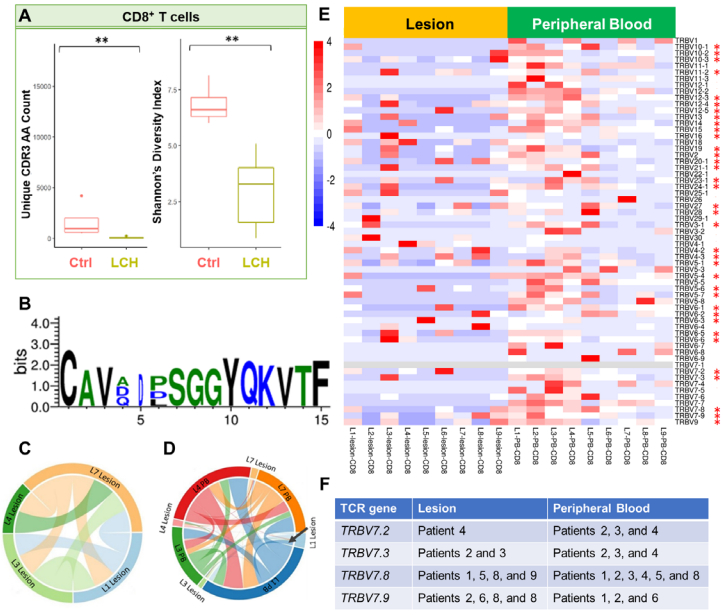
was no significant difference in the numbers of PD-1$^{+}$TIM-3$^{+}$, PD-1$^{+}$LAG-3$^{+}$, TIM-3$^{+}$LAG-3$^{+}$, or PD-1$^{+}$TIM-3$^{+}$LAG-3$^{+}$ CD4$^{+}$ T cells between LCH lesions and healthy skin tissues (**Supplementary Figure 3F in *Blood* paper**).

Compared to the PD-1$^{-}$TIM-3$^{-}$LAG-3$^{-}$CD8$^{+}$ T cells, the PD-1$^{+}$, TIM-3$^{+}$, LAG-3$^{+}$, PD-1$^{+}$TIM-3$^{+}$, and PD-1$^{+}$TIM-3$^{+}$LAG-3$^{+}$ CD8$^{+}$ T cells presented significantly decreased granzyme B and perforin secretion (**Fig. 3D in *Blood* paper**), indicating a whole-spectrum immunosuppression in these cells. The expression of PD-1 ligands PD-L1 and PD-L2 were significantly elevated in CD207$^{+}$ DCs from LCH lesions compared to healthy skin (**Fig. 3E**, **Supplementary Figure 3G in *Blood* paper**).

These results suggest that immobilized PD-L1 or PD-L2-expressing CD207$^{+}$ cells may engage the T cells due to their high PD-1, resulting in accumulation of exhausted T cells in the lesions. Alternatively, CD207 may induce T cells to express PD-1, in turn engaging them, and eventually preventing them from performing effector functions. Thus, we next evaluated if PD-1 blockade would restore T cell function in LCH lesions and found that treatment of patient-derived LCH lesion CD8+ T cells with anti-PD-1 antibody for 24 hours significantly rescued their effector functions (**Fig. 3F in *Blood* paper**). Taken together, these results suggested that PD-1 blockade could influence the immune dysfunction induced by LCH DC.

D. ***Distinct TCR repertoires in patients with LCH.***

One of our proposed sub-tasks was performing transcriptomic analysis of different LCH infiltrating T cell populations. Given that the functional state and clonality of tumor-infiltrating T lymphocytes are critical predictors of disease state and immunotherapy outcome, we performed TCR sequencing of CD4$^{+}$, CD8$^{+}$, and CD4+CD25$^{Bright}$ T cell subsets sorted from lesions and peripheral blood from 9 LCH patients (4 with WT *BRAF* and 5 with *BRAF*V600E mutation) and 4 controls. Compared with controls, the




| TCR gene | Lesion | Peripheral Blood |
|---|---|---|
| *TRBV7.2* | Patient 4 | Patients 2, 3, and 4 |
| *TRBV7.3* | Patients 2 and 3 | Patients 2, 3, and 4 |
| *TRBV7.8* | Patients 1, 5, 8, and 9 | Patients 1, 2, 3, 4, 5, and 8 |
| *TRBV7.9* | Patients 2, 6, 8, and 8 | Patients 1, 2, and 6 |

***Figure 1. LCH lesion-infiltrating T cells exhibit marked clonal expansion.*** (**A**) Box-plots showing the distribution of the total number of unique CDR3 clonotypes per sample in control (n=4) and LCH intralesional T cells (n=9) (CD8$^{+}$ *(left)* and Shannon's diversity index (*right*). (**B**) Shared amino acid motif analysis was performed by the CD-HIT analysis software to identify the common amino acid sequences. Shown is the top amino acid motif enriched for CD8$^{+}$ T cell. The cluster similarity cut-off set for the CD-HIT analysis was 0.9. (**C**) Graphical representation of the shared CDR3 clonotypes in intralesional CD8+ T cells between different patients, generated using VDJTools CalcPairwiseDistances. Each chord shows the connectivity or perfect match of the CDR3 amino acid sequences derived from TCRα/β chains between samples. Each arc (on the periphery of each diagram) represents a V or J segment and is scaled lengthwise according to the relative proportion at which the segment is represented in the dataset. Each chord (connecting the arcs) represents a set of clonotypes which include the indicated V-J combination and is weighted according to the relative abundance of that combination in the dataset. Overall, the data shows there were multiple patients that had perfectly matching CDR3 clonotypes found in the lesion infiltrating CD8$^{+}$ T cells. (**D**) Shared CDR3 clonotypes from CD8$^{+}$ T cells among lesion and peripheral blood (PB) repertoire for patients that showed relatedness in the clonotypes in their lesion shown in ***C***. One of the shared clonotypes derived from a patient lesion and the corresponding peripheral blood are highlighted by *black* arrow. This analysis showed that for CD8$^{+}$ T cells, there were a subset of CDR3 clonotypes shared between lesion and peripheral blood of multiple LCH patients. (**E**, **F**) Shared *TRBV* gene usage analysis. Clustering of the *TRBV* genes in patient lesions and peripheral blood for all the 9 patients to represent the shared *TRBV* gene usage. The z scores represent normalized frequency of each of the *TRBV* chains in each sample, wherein *blue* means that the V genes had a lower frequency and *red* represents high frequency. The shared TRAV and *TRBV* genes found at a high frequency in at least one patient and shared in the blood repertoire by one or more patients are highlighted by *red* asterisks (**E**). We note that there were several shared clonotypes for CD8$^{+}$ T cells, that were present at a high frequency in lesions and the peripheral blood (**F**). For **A-F**, similar observations were made for CD4$^{+}$ and Tregs *(data not shown due to space constraints).*

number of productive amino acid CDR3 clonotypes and repertoire diversity (Shannon's diversity index) for all three subsets were significantly less in patients (**Fig. 1A**), indicating marked clonal expansion of the TCR repertoire. Conserved amino acid motif analyses using CDR3 amino acid sequences in the TCR repertoire for all T cell compartments across all patient lesions revealed highly conserved motifs (**Fig. 5B**), indicating the presence of shared antigens. Pairwise sample relatedness analyses revealed shared CDR3 amino acid sequences in clonally amplified TCR chains in the repertoire of patient lesions (**Fig. 5C**) and between intralesional and peripheral T cells (**Fig. 5D**). Previous studies of tumor-infiltrating T lymphocyte clones suggest that the use of certain TRBV regions are predominant in tumor tissue, indicating LC-associated antigen-specific T cell responses[44]. Through statistical analysis and the frequencies of V gene usage, we identified the biased use of V gene segments in both LCH lesions (**Fig. 5E**) and peripheral blood compared with controls (data not shown). We found that in CD4$^{+}$ and CD8$^{+}$ T cells, some segments of the *TRBV7* gene, namely *TRBV7.2*, *TRBV7.3*, and *TRBV7.9,* were used more frequently in LCH lesions and peripheral blood than in controls (**Fig. 5F**), indicating **(a) that specific T cell clones are recruited from peripheral blood to the LCH tumor microenvironment and (b) a common antigen usage**.

***Specific Aim 2: To test novel therapeutic salvage strategies in mutation-specific in vitro and in vivo models of LCH.***

**Major Task 3: Test the relative efficacy of myeloid-directed chemotherapy, MAPK pathway inhibition, and other targeted therapies on tumor progression and survival in mouse models of LCH.**

- **IACUC/ACURO approval:** Even though this was scheduled for months 15-18, we went ahead and got the ACURO approval on July 31, 2020 (ACURO Log Number CA181344.e001).
- Me taking up a position at Xilis, Inc meant we did not have the time to fulfil the experiments outlined in the proposal. But in some preliminary experiments that were also published in the above referenced *Blood* paper, we have shown that the treatment of *BRAF*V600E$^{CD11c}$ LCH mice with anti-PD-1 or MAPK inhibitor reduced lesion size, but with distinct responses: whereas MAPK inhibitor treatment resulted in reduction of the myeloid compartment, anti-PD-1 treatment was associated

with reduction in the lymphoid compartment. Notably, combined treatment with MAPK inhibitor and anti-PD-1 significantly decreased both $CD8^+$ T cell and myeloid LCH cells in a synergistic fashion (***please refer to Fig. 5-7 and Supplementary Figures 4-8 in Blood paper***).

**What opportunities for training and professional development has the project provided?**
*If the project was not intended to provide training and professional development opportunities or there is nothing significant to report during this reporting period, state "Nothing to Report."*

*Describe opportunities for training and professional development provided to anyone who worked on the project or anyone who was involved in the activities supported by the project. "Training" activities are those in which individuals with advanced professional skills and experience assist others in attaining greater proficiency. Training activities may include, for example, courses or one-on-one work with a mentor. "Professional development" activities result in increased knowledge or skill in one's area of expertise and may include workshops, conferences, seminars, study groups, and individual study. Include participation in conferences, workshops, and seminars not listed under major activities.*

In addition to what is described above under accomplishments of Career Development Specific Tasks, this project provided me the following opportunities for training and professional development:

- Research personnel in my lab has presented posters and or talks at the 2019 Annual ASH meeting and the 2020 TXCH Symposium. My lab personnel also gave oral presentations at the 2020 Annual Histiocyte Society meeting. These has helped me in developing my mentoring and leadership skills.
- I have also served as a peer reviewer in the American Society of Hematology Research Training Award for Fellows Study Section, the American Society of Hematology Scholar Award Study Section, and the Histiocyte Society Research Grants Program Study Section. I was appointed as an Editorial Board Member of *IUBMB Life*, the flagship journal of the International Union of Biochemistry and Molecular Biology.
- I received the mentor award under the 2020 American Society of Hematology Minority Medical Student Award Program to mentor Omar A. Ramos-Mas, first year medical student at the Universidad Central del Caribe, Bayamón, Puerto Rico.
- I was awarded (a) a competitive Baylor College of Medicine – Pilot projects on COVID-19 research, titled "T-cell activation in COVID-19 for diagnostic and therapeutic insights", and (b) Children's Oncology Group - Solid Malignancies - Integrated Translational Science Center (SM-ITSC) award, titled "Analytical validation of plasma microRNA biomarker in pediatric osteosarcoma".
- Finally, I transitioned to a Senior Manager role in Xilis, Inc., Durham, NC.

**How were the results disseminated to communities of interest?**
*If there is nothing significant to report during this reporting period, state "Nothing to Report."*

*Describe how the results were disseminated to communities of interest. Include any outreach activities that were undertaken to reach members of communities who are not usually aware of these project activities, for the purpose of enhancing public understanding and increasing interest in learning and careers in science, technology, and the humanities.*

Nothing to Report.

**What do you plan to do during the next reporting period to accomplish the goals?**
*If this is the final report, state "Nothing to Report."*

*Describe briefly what you plan to do during the next reporting period to accomplish the goals and objectives.*

Nothing to Report.

**4. IMPACT:** D*escribe distinctive contributions, major accomplishments, innovations, successes, or any change in practice or behavior that has come about as a result of the project relative to:*

**What was the impact on the development of the principal discipline(s) of the project?**
*If there is nothing significant to report during this reporting period, state "Nothing to Report."*

*Describe how findings, results, techniques that were developed or extended, or other products from the project made an impact or are likely to make an impact on the base of knowledge, theory, and research in the principal disciplinary field(s) of the project. Summarize using language that an intelligent lay audience can understand (Scientific American style).*

Our experimental results are consistent with a model that MAPK hyperactivation in myeloid LCH cells drives recruitment of functionally exhausted T cells within the LCH microenvironment and highlight combined MAPK and checkpoint inhibition as a potential therapeutic strategy. The past decade has elucidated the broad strokes of LCH pathogenesis: MAPK activation in differentiating myeloid precursors. However, the mechanisms that regulate recruitment, retention, and activation of immune cells to lesions is not known, and the role of inflammation in pathogenesis is undefined. To identify optimal curative therapies for patients for LCH, various strategies may first be tested in pre-clinical models to prioritize for testing in clinical trials. The results from our study provide novel insights into the character and function of lesion infiltrating T cells in LCH. Given that neither character and function of lesion infiltrating T cells in LCH nor MEK inhibition is dependent on MAPK pathway mutations, the synergistic impact of combined MEK inhibition and checkpoint blockade represent a novel therapeutic strategy that merits clinical development. The findings of this study demonstrate activity of checkpoint inhibition against LCH, supporting further investigation to refine optimal agents, dosing, and combinations to be tested in clinical trials. The revised conceptualization of LCH as an inflammatory myeloid neoplastic disorder driven by pathologic MAPK activation in myeloid precursor cells coupled with the findings that combination therapy provides synergistic effect on disease outcome offers an opportunity to move treatment for LCH beyond empiricism to rational, risk-based strategies.

**What was the impact on other disciplines?**
*If there is nothing significant to report during this reporting period, state "Nothing to Report."*

*Describe how the findings, results, or techniques that were developed or improved, or other products from the project made an impact or are likely to make an impact on other disciplines.*

Nothing to report

**What was the impact on technology transfer?**
*If there is nothing significant to report during this reporting period, state "Nothing to Report."*

*Describe ways in which the project made an impact, or is likely to make an impact, on commercial technology or public use, including:*

- *transfer of results to entities in government or industry;*
- *instances where the research has led to the initiation of a start-up company; or*
- *adoption of new practices.*

Nothing to report

**What was the impact on society beyond science and technology?**
*If there is nothing significant to report during this reporting period, state "Nothing to Report."*

*Describe how results from the project made an impact, or are likely to make an impact, beyond the bounds of science, engineering, and the academic world on areas such as:*

- *improving public knowledge, attitudes, skills, and abilities;*
- *changing behavior, practices, decision making, policies (including regulatory policies), or social actions; or*
- *improving social, economic, civic, or environmental conditions.*

Nothing to report

**5. CHANGES/PROBLEMS:** *The PD/PI is reminded that the recipient organization is required to obtain prior written approval from the awarding agency grants official whenever there are significant changes in the project or its direction. If not previously reported in writing, provide the following additional information or state, "Nothing to Report," if applicable:*

**Changes in approach and reasons for change**
*Describe any changes in approach during the reporting period and reasons for these changes. Remember that significant changes in objectives and scope require prior approval of the agency.*

There were no changes in approach.

**Actual or anticipated problems or delays and actions or plans to resolve them**
*Describe problems or delays encountered during the reporting period and actions or plans to resolve them.*

Nothing to report.

*Describe changes during the reporting period that may have had a significant impact on expenditures, for example, delays in hiring staff or favorable developments that enable meeting objectives at less cost than anticipated.*

Nothing to report.

**Significant changes in use or care of human subjects, vertebrate animals, biohazards, and/or select agents**
*Describe significant deviations, unexpected outcomes, or changes in approved protocols for the use or care of human subjects, vertebrate animals, biohazards, and/or select agents during the reporting period. If required, were these changes approved by the applicable institution committee (or equivalent) and reported to the agency? Also specify the applicable Institutional Review Board/Institutional Animal Care and Use Committee approval dates.*

**Significant changes in use or care of human subjects**

Nothing to report.

**Significant changes in use or care of vertebrate animals**

Nothing to report.

**Significant changes in use of biohazards and/or select agents**

Nothing to report.

**6. PRODUCTS:** *List any products resulting from the project during the reporting period. If there is nothing to report under a particular item, state "Nothing to Report."*

- **Publications, conference papers, and presentations**

*Report only the major publication(s) resulting from the work under this award.*

**Journal publications.** *List peer-reviewed articles or papers appearing in scientific, technical, or professional journals. Identify for each publication: Author(s); title; journal; volume: year; page numbers; status of publication (published; accepted, awaiting publication; submitted, under review; other); acknowledgement of federal support (yes/no).*

1. Sengal A, Velasquez J, Hahne M, Burke TM, Abhyankar H, Reyes R, Olea W, Scull B, Eckstein O, Bigenwald C, Bollard CM, Yu E, Merad M, McClain KL, Allen CE, Chakraborty R. Overcoming T cell exhaustion in LCH: PD-1 blockade and targeted MAPK inhibition are synergistic in a mouse model of LCH. ***Blood*** 137(13): 1777-1791 (2021).

2. Bigenwald C, Le Berichel J, Wilk M, Chakraborty R, Chen ST, Tanachnikova A, Mancusi R, Abhyankar HA, Cassnova-Acebes M, Laface I, Akturk G, Jobson J, Karoulia Z, Martin JC, Grout J, Rafiei A, Lin H, Manz M, Baccarini A, Poulikakos P, Brown B, Gnjatic S, Lukambio A, McClain KL, Picarsic J, Allen CR, Merad M. BRAFV600E-induced senescence drives Langerhans Cell Histiocytosis pathophysiology. ***Nature Medicine*** 27(5): 851-861 (2021).

3. Chakraborty R, Abdel-Wahab O, Durham B.H. MAP-Kinase-Driven Hematopoietic Neoplasms: A Decade of Progress in the Molecular Age. ***Cold Spring Harbor Perspective in Medicine*** 11(5): a034892 (2020).

**Books or other non-periodical, one-time publications.** *Report any book, monograph, dissertation, abstract, or the like published as or in a separate publication, rather than a periodical or series. Include any significant publication in the proceedings of a one-time conference or in the report of a one-time study, commission, or the like. Identify for each one-time publication: author(s); title; editor; title of collection, if applicable; bibliographic information; year; type of publication (e.g., book, thesis or dissertation); status of publication (published; accepted, awaiting publication; submitted, under review; other); acknowledgement of federal support (yes/no).*

None to Report

**Other publications, conference papers and presentations**. *Identify any other publications, conference papers and/or presentations not reported above. Specify the status of the publication as noted above. List presentations made during the last year (international, national, local societies, military meetings, etc.). Use an asterisk (*) if presentation produced a manuscript.*

None to Report

- **Website(s) or other Internet site(s)**

*List the URL for any Internet site(s) that disseminates the results of the research activities. A short description of each site should be provided. It is not necessary to include the publications already specified above in this section.*

None to Report

- **Technologies or techniques**

*Identify technologies or techniques that resulted from the research activities. Describe the technologies or techniques were shared.*

None to Report.

- **Inventions, patent applications, and/or licenses**

*Identify inventions, patent applications with date, and/or licenses that have resulted from the research. Submission of this information as part of an interim research performance progress report is not a substitute for any other invention reporting required under the terms and conditions of an award.*

None to Report.

- **Other Products**

*Identify any other reportable outcomes that were developed under this project. Reportable outcomes are defined as a research result that is or relates to a product, scientific advance, or research tool that makes a meaningful contribution toward the understanding, prevention, diagnosis, prognosis, treatment and /or rehabilitation of a disease, injury or condition, or to improve the quality of life. Examples include:*

- *data or databases;*
- *physical collections;*
- *audio or video products;*
- *software;*
- *models;*
- *educational aids or curricula;*
- *instruments or equipment;*
- *research material (e.g., Germplasm; cell lines, DNA probes, animal models);*
- *clinical interventions;*
- *new business creation; and*
- *other.*

None to Report

## 7. PARTICIPANTS & OTHER COLLABORATING ORGANIZATIONS

**What individuals have worked on the project?**

*Provide the following information for: (1) PDs/PIs; and (2) each person who has worked at least one person month per year on the project during the reporting period, regardless of the source of compensation (a person month equals approximately 160 hours of effort). If information is unchanged from a previous submission, provide the name only and indicate "no change".*

*Example:*

*Name:* *Mary Smith*

*Project Role:* *Graduate Student*
*Researcher Identifier (e.g. ORCID ID): 1234567*
*Nearest person month worked:* *5*

*Contribution to Project:* *Ms. Smith has performed work in the area of combined error-control and constrained coding.*
*Funding Support:* *The Ford Foundation (Complete only if the funding support is provided from other than this award.)*

Name: Rikhia Chaudhury Chakraborty
Project Role: PI
Nearest person month worked: 3.6
Contribution to Project: Primarily responsible for the organization and operation of the project.
Funding Support: Children's Oncology Group, BCM Pilot COVID-19 Grant, National Cancer Institute.

Name: Carl E Allen
Project Role: Mentor
Nearest person month worked: 0.12
Contribution to Project: Weekly and quarterly meeting with PI to advise on progress and goals.
Funding Support: National Cancer Institute, Leukemia and Lymphoma Society, St. Baldrick's Foundation, Cookies for Cancer Research, Children's Oncology Group.

Name: Miriam Merad
Project Role: Mentor
Nearest person month worked: 0.12
Contribution to Project: Quarterly meeting with PI to advise on progress and goals.
Funding Support: National Cancer Institute, Boehringer Ingelheim, Regeneron.

Name: Jessica Velazquez
Project Role: Research Technician
Nearest person month worked: 6.0
Contribution to Project: Jessica is responsible for sorting cell populations and preparing for transcriptomic analysis.
Funding Support: National Cancer Institute, Children's Oncology Group.

Name: Ryan Fleischman
Project Role: Research Technician
Nearest person month worked: 0.12
Contribution to Project: Ryan is responsible for mass cytometry.
Funding Support: National Cancer Institute, Children's Oncology Group.

**Has there been a change in the active other support of the PD/PI(s) or senior/key personnel since the last reporting period?**
*If there is nothing significant to report during this reporting period, state "Nothing to Report."*

*If the active support has changed for the PD/PI(s) or senior/key personnel, then describe what the change has been. Changes may occur, for example, if a previously active grant has closed and/or if a previously pending grant is now active. Annotate this information so it is clear what has changed from the previous submission. Submission of other support information is not necessary for pending changes or for changes in the level of effort for active support reported previously. The awarding agency may require prior written approval if a change in active other support significantly impacts the effort on the project that is the subject of the project report.*

Nothing to Report.

**What other organizations were involved as partners?**
*If there is nothing significant to report during this reporting period, state "Nothing to Report."*

*Describe partner organizations – academic institutions, other nonprofits, industrial or commercial firms, state or local governments, schools or school systems, or other organizations (foreign or domestic) – that were involved with the project. Partner organizations may have provided financial or in-kind support, supplied facilities or equipment, collaborated in the research, exchanged personnel, or otherwise contributed.*

*Provide the following information for each partnership:*
*Organization Name:*
*Location of Organization: (if foreign location list country)*
*Partner's contribution to the project (identify one or more)*

- *Financial support;*
- *In-kind support (e.g., partner makes software, computers, equipment, etc., available to project staff);*
- *Facilities (e.g., project staff use the partner's facilities for project activities);*
- *Collaboration (e.g., partner's staff work with project staff on the project);*
- *Personnel exchanges (e.g., project staff and/or partner's staff use each other's facilities, work at each other's site); and*
- *Other.*

Nothing to Report.

## 8. SPECIAL REPORTING REQUIREMENTS

**COLLABORATIVE AWARDS:** *For collaborative awards, independent reports are required from BOTH the Initiating Principal Investigator (PI) and the Collaborating/Partnering PI. A duplicative report is acceptable; however, tasks shall be clearly marked with the responsible PI and research site. A report shall be submitted to* ***https://ers.amedd.army.mil*** *for each unique award.*

**QUAD CHARTS:** *If applicable, the Quad Chart (available on https://www.usamraa.army.mil) should be updated and submitted with attachments.*

Not applicable.

**9. APPENDICES:** *Attach all appendices that contain information that supplements, clarifies or supports the text. Examples include original copies of journal articles, reprints of manuscripts and abstracts, a curriculum vitae, patent applications, study questionnaires, and surveys, etc.*

blood®
Regular Article

Check for updates

MYELOID NEOPLASIA

# Overcoming T-cell exhaustion in LCH: PD-1 blockade and targeted MAPK inhibition are synergistic in a mouse model of LCH

Amel Sengal,[1,2] Jessica Velazquez,[1,2] Meryl Hahne,[1] Thomas M. Burke,[1-3] Harshal Abhyankar,[1] Robert Reyes,[1] Walter Olea,[1] Brooks Scull,[1] Olive S. Eckstein,[1] Camille Bigenwald,[4,5] Catherine M. Bollard,[6-8] Wendong Yu,[9] Miriam Merad,[4,5] Kenneth L. McClain,[1,2] Carl E. Allen,[1-3] and Rikhia Chakraborty[1,2]

[1]Texas Children's Cancer Center, Texas Children's Hospital, Houston, TX; [2]Division of Pediatric Hematology-Oncology, Department of Pediatrics and [3]Program in Translational Biology and Molecular Medicine, Baylor College of Medicine, Houston, TX; [4]Department of Oncological Sciences, Tisch Cancer Institute, and [5]Department of Dermatology, Icahn School of Medicine, New York, NY; [6]Center for Cancer and Immunology Research, Children's National Medical Center, Washington, DC; [7]Department of Pediatrics and [8]Department of Microbiology, Immunology and Tropical Medicine, The George Washington University, Washington, DC; and [9]Department of Pathology, Baylor College of Medicine, Houston, TX

KEY POINTS

- LCH lesions are infiltrated with exhausted and dysfunctional T cells.
- Immune checkpoint inhibition decreases disease burden in a preclinical mouse model of LCH and augments responses to MEK inhibition.

**Langerhans cell histiocytosis (LCH) is an inflammatory myeloid neoplasia characterized by granulomatous lesions containing pathological CD207$^+$ dendritic cells (DCs) with persistent MAPK pathway activation. Standard-of-care chemotherapies are inadequate for most patients with multisystem disease, and optimal strategies for relapsed and refractory disease are not defined. The mechanisms underlying development of inflammation in LCH lesions, the role of inflammation in pathogenesis, and the potential for immunotherapy are unknown. Analysis of the immune infiltrate in LCH lesions identified the most prominent immune cells as T lymphocytes. Both CD8$^+$ and CD4$^+$ T cells exhibited "exhausted" phenotypes with high expression of the immune checkpoint receptors. LCH DCs showed robust expression of ligands to checkpoint receptors. Intralesional CD8$^+$ T cells showed blunted expression of Tc1/Tc2 cytokines and impaired effector function. In contrast, intralesional regulatory T cells demonstrated intact suppressive activity. Treatment of *BRAFV600E*$^{CD11c}$ LCH mice with anti-PD-1 or MAPK inhibitor reduced lesion size, but with distinct responses. Whereas MAPK inhibitor treatment resulted in reduction of the myeloid compartment, anti-PD-1 treatment was associated with reduction in the lymphoid compartment. Notably, combined treatment with MAPK inhibitor and anti-PD-1 significantly decreased both CD8$^+$ T cells and myeloid LCH cells in a synergistic fashion. These results are consistent with a model that MAPK hyperactivation in myeloid LCH cells drives recruitment of functionally exhausted T cells within the LCH microenvironment, and they highlight combined MAPK and checkpoint inhibition as a potential therapeutic strategy. (*Blood*. 2021;137(13):1777-1791)**

## Introduction

Langerhans cell histiocytosis (LCH) is an inflammatory myeloid neoplastic disorder characterized by a variable number of myeloid cells with activating MAPK mutations and an inflammatory infiltrate.[1-4] The clinical extent of disease is associated with the differentiation capacity of the myeloid precursor cells, although LCH lesions from the spectrum of clinical presentations are histologically indistinguishable. LCH lesions are composed of Langerhans cells (LCs; CD207$^+$ dendritic cells; LCH DCs) and an inflammatory infiltrate that typically constitutes most of the cells.[5] The mechanisms that orchestrate recruitment and activation of the inflammatory infiltrate and the role of immune cells in LCH pathogenesis is not known.

A median of 8% of cells within LCH lesions are LCH DCs, and the remainder are inflammatory cells. Exuberant production of proinflammatory cytokines and chemokines has been described in LCH.[6] However, the etiology of the inflammatory infiltrate, its precise composition, and its contribution to pathogenesis have not been defined. Enrichment of regulatory T cells (Tregs) in LCH lesions, proximity of Tregs to LCH DCs, and increased PD-L1 expression on CD207$^+$ cells have been described.[6-13] However, the mechanisms that underlie Treg enrichment and expression of regulators of checkpoint expression in LCH lesions and the functional consequences of these observations have not been explored.

LCH remains a challenging clinical condition, for which current therapies remain suboptimal because of the rarity of the disorder and lack of understanding of pathogenic mechanisms. The current front-line standard of care is chemotherapy

Downloaded from http://ashpublications.org/blood/article-pdf/137/13/1777/1803993/bloodbld2020005867.pdf by Rikhia Chakraborty on 03 December 2021

© 2021 by The American Society of Hematology

(vinblastine/prednisone) for systemic disease; however, ~50% of patients with multisystem disease do not respond to the therapy,[14,15] and treatment failure is associated with significant long-term morbidity and mortality.[16] Salvage therapies with nucleoside analogues may be effective but are associated with considerable rates of treatment-related mortality.[17]

Single-agent MAPK inhibition experiments in early-phase studies in adults with LCH and related histiocytic disorders have yielded nearly universal responses in adult[18-21] and pediatric[22,23] early-phase trials and case series. However, the potential for this strategy to cure patients with LCH is uncertain. Cessation of MAPK inhibition is associated with rapid relapse in most cases,[22,24] and peripheral blood mononuclear cells (PBMCs) with LCH-associated mutations (eg, *BRAF*V600E) persist in patients treated with MAPK inhibition where the presumed precursor cells disappear from circulation with successful cytotoxic chemotherapy.[5,22,23]

A critical role of the immune system in regulating tumorigenesis is highlighted by the dramatic clinical effects of disinhibiting cytotoxic T cells in adult cancers.[25] However, the clinical potential for immune-directed therapies in LCH has not yet been investigated. This study therefore was conducted to characterize the composition and functional capacity of immune cells within the LCH lesions. Further, we tested the therapeutic potential of immune checkpoint inhibitors, alone or in combination with MAPK inhibition.

# Methods

## Study patients and human tissue samples

Biopsy specimens (from liver, bone, or spleen) and blood samples were collected from patients with LCH or control subjects under a protocol approved by the Baylor College of Medicine Institutional Review Board. Clinical data were recorded for each patient (supplemental Table 1, available on the *Blood* Web site). Samples used in mass cytometry were solid tissue cells obtained from biopsies (n = 6 *BRAF* WT; n = 9 *BRAF*V600E) and PBMCs (n = 6). Skin biopsy samples (n = 5), lymph nodes (n = 7), and PBMCs (n = 5) from healthy subjects were used as control samples. All samples, except for control skin tissue, were processed identically into single cells by mechanical disruption over 70-μm mesh (542070; Bio-One EASY strainer; Greiner), washed, and viably stored in aliquots in recovery-cell culture medium (12648-010; Gibco). Control skin tissues were incubated overnight at 37°C in PluriSTEM Dispase-II solution (1 mg/mL; SCM133; Sigma-Aldrich, St Louis, MO) before being stored in aliquots in recovery-cell culture medium. Where indicated, samples were stimulated by anti-CD3 (55329; clone: UCHT1, 1 μg/mL) and CD28 (555725; clone: CD28.2, 1 μg/mL; both from BD Biosciences) for 18 hours before acquisition for mass cytometry, but most samples were stained immediately upon thawing.

## Mouse model of LCH

The animal experiments performed in this study were approved by the Institutional Animal Care and Use Committee of Baylor College of Medicine. The animals were housed under pathogen-free conditions and euthanized at various time points. *BRAF*V600E$^{CD11c}$ mice were created as described previously[5,26] by crossing *BRAF*V600E$^{ca/wt}$ or *BRAF*V600E$^{ca/ca}$ mice[27] with mice expressing *cre* recombinase under the control of the *CD11c* promoter (C57BL/6 background; The Jackson Laboratory). A lethal LCH-like syndrome develops in *BRAF*V600E$^{CD11c}$ mice with 1 *BRAF*V600E$^{CA}$ allele and 1 *CD11c-Cre* allele.[5]

## Preclinical studies in the mouse model of LCH

Six-week-old LCH (*BRAF*V600E$^{CD11c}$) mice were randomly assigned to the following treatment groups (9 mice per group): no treatment, MAPK inhibitor (MEKi; trametinib; Selleckchem, Houston, TX), MAPK inhibitor vehicle (Veh MEKi), anti-PD-L1 blocking antibody (clone 10F.9G; BioXCell, West Lebanon, NH), PD-L1 isotype (Iso PD-L1, Clone LTF-2; BioXCell), anti-PD-1 antibody (Clone 29F.1A12, BioXCell), or PD-1 isotype (Iso PD-1; Clone LTF2; BioXCell). Mice in the anti-PD-L1, anti-PD-1 or isotype groups were injected intravenously at 20 mg/kg on days 0 and 2, whereas animals in the MEKi group received daily intraperitoneal injection of 3 mg/kg trametinib. The animals were monitored daily for body weight and clinical score, according to previously described parameters.[28,29] They were euthanized on day 14, and various tissues were harvested.

## Animal tissue processing

Single-cell suspension was obtained from liver and lung of mice after digestion with an Octamacs Tissue dissociator and liver dissociation kit (130-105-807; Miltenyi Biotech). Cells after dissociation were filtered using 100-, 70-, and 50-μm filters (BD Bioscience) and were processed for red blood cell lysis in ACK lysis buffer and then subjected to centrifugation at 1000*g* for 5 minutes. The cells were counted, aliquoted, and either frozen or used for downstream application. The cells were processed for identification of the markers, as described in "Mass cytometry and data analysis."

## Histology and immunohistochemistry

Histology and immunohistochemistry were performed as described previously.[26] Sections were stained with anti-CD4 (D7D2Z; 1:100 dilution) and anti-CD8α (D4W2Z; 1:400 dilution; both from Cell Signaling Technology, Danvers, MA) antibodies overnight at 4°C. The slides were evaluated by a pathologist blinded to the identity of the experimental groups and scored for disease burden. Disease burden was estimated based on the percentage of tumor area (both tumor cells and surrounding lymphocytes) on the entire histology section. Infiltrating CD4$^+$ and CD8$^+$ T cells were imaged with an Ni-E microscope (4×/0.20 Plan Apo λ OFN25 WD20; Nikon) and quantified with NISA image analysis software (Nikon). The region of interest was measured from 5 different random stained fields and then the H-score was calculated manually by averaging the object area fraction to calculate the amount of staining per image.

## Mass cytometry and data analysis

Cells were initially stained with cisplatin (DVS Sciences) to identify live and dead cells before incubation with metal-tagged antibodies followed by an intercalator (DVS Sciences). A panel of 50 antibodies for human samples and 19 antibodies for mouse samples that encompassed a broad range of immune subsets was used for time-of-flight mass cytometry (CyTOF) in different combinations (supplemental Table 2). All procedures were in accordance with the Maxpar cell-staining protocol (Fluidigm Corporation).[30] Samples were analyzed on a CyTOF-II mass cytometer (Fluidigm). Signal was bead normalized by using EQ

Downloaded from http://ashpublications.org/blood/article-pdf/137/13/1777/1803993/bloodbld2020005867.pdf by Rikhia Chakraborty on 03 December 2021

Four Element Calibration Beads (201078; Fluidigm), according to the manufacturer's instructions.[30] All data files were normalized before analysis and uploaded to cytobank.org in the form of .fcs files. All files were first gated for viability using a gate around the double-positive population on Ir191 vs Ir193. Specific populations were gated further to provide more accurate classification of cell type. After gating, dynamic down sampling and downstream analyses were run based on the CD markers that these populations expressed at high levels.

### Suppression assays

The in vitro suppressive capacity of human natural Tregs (positive control) from healthy donors or of Tregs isolated from LCH lesions (LCH-Treg) or control tonsils (Tonsil-Treg), and $CD25^-$ cells (negative control) from healthy donors was assessed in a carboxyfluorescein succinimidyl ester (CFSE)–based inhibition assay.[31,32] Tregs were isolated by positive selection as $CD3^+CD4^+CD25^{Bright}$. For the $CD25^-$ cells, $CD3^+CD4^+CD25^{Low}$ cells were collected by gating out undesired $CD3^+CD4^+CD25^{Intermediate}$ and $CD3^+CD4^+CD25^{Bright}$ populations. PBMCs were labeled with 1.5 M CFSE (ThermoFisher Scientific, Carlsbad, CA), according to the manufacturer's instructions, and then stimulated with irradiated (40 Gy) allogeneic PBMCs (at a 4:1 effector/feeder ratio) and OKT3 (0.5 μg/mL). To assess their suppressive capacity, Tregs and PBMCs were added to the culture at a 1:1 ratio. After 7 days, cells were labeled with PE-conjugated CD4 and APC-conjugated CD8 monoclonal antibodies, and CFSE dilution was analyzed on a FACSCalibur flow cytometer to measure cell proliferation. Suppression was expressed as the percentage of inhibition of T-cell proliferation in the presence of Tregs, compared with proliferation in the absence of any added Tregs.

### Mixed lymphocyte reaction assay

Freshly sorted $CD3^+CD8^+$ T cells (responders) were purified from LCH lesion biopsies and PBMCs from healthy donors (control) and stained with CFSE as for the suppression assays. Triplicate 10 000 CFSE-labeled responder $CD3^+CD8^+$ T cells were seeded in a round-bottomed 96-well plate in RPMI 10% AB serum, either alone or with irradiated (40 Gy) allogeneic PBMCs (stimulators) at 1:1, 2:1, and 5:1 ratios in the presence of $CD14^+$ antigen-presenting cells (isolated from healthy donors by positive selection; CD3/CD14 ratio, 1:5). The cultures were incubated for 3 days at 37°C and 5% $CO_2$. At the end of the incubation, the cells were stained with annexin V/7-AAD (BioLegend, San Diego, CA) according to the manufacturer's instructions to exclude any dead cells. T-cell proliferation was determined by analyzing CFSE dilution of the responders (annexin-V/7-$AAD^-$ population) by flow cytometry (FACSCalibur).

### T-cell activation

Tumor-infiltrating lymphocytes were stained with anti-CD3 and -CD8 and were sorted into a $CD3^+CD8^+$ population with a FACS-ARIA sorter (BD Biosciences). Recovered T cells were incubated in medium alone or stimulated with phorbol myristate acetate (PMA, 20 ng/mL) and ionomycin (1 μg/mL; both from Sigma-Aldrich). Interferon-γ (IFN-γ), interleukin-10 (IL-10), tumor necrosis factor-α (TNF-α), and IL-17α were measured by Luminex (T helper 1 [Th1]/Th2 custom; Millipore) in the supernatants collected before or 72 hours after T-cell activation.

### Statistical analysis

All data are expressed as the mean ± standard deviation (SD). Intergroup comparisons were performed using the unpaired, nonparametric Wilcoxon-Mann-Whitney (WMW) test or 1-way analysis of variance (ANOVA), followed by Tukey's post hoc test for multiple comparisons. A $P < .05$ was considered statistically significant.

## Results

### Phenotypic analysis of LCH lesions

We first analyzed the immune composition using time-of-flight mass cytometry (CyTOF) of patient tissue samples (n = 15; *BRAF* WT [n = 6] and *BRAF*V600E [n = 9]) and skin samples from healthy controls (skin $CD207^+$ DCs; n = 5) (Figure 1A-C; supplemental Figure 1A-D). The Immune infiltrate in LCH lesions varied between 50% and 70% with $CD3^+$ T cells and myeloid-derived suppressor cells (MDSCs; $CD11b^+CD14^+HLA\text{-}DR^{low/-}CD15^-$) as the most abundant populations. Overall, LCH lesion DCs ($HLA\text{-}DR^+CD1A^+$), T cells, and MDSCs accounted for 25.60% ± 10.72%, 28.20% ± 6.46%, and 31.90% ± 4.02%, respectively. T cells were significantly more abundant in WT *BRAF* compared with *BRAF*V600E lesions, consistent with increased LCH DCs ($HLA\text{-}DR^+CD1A^+$) in the *BRAF*V600E lesions (supplemental Figure 1A-B,D; supplemental Table 3). By comparison, immune infiltrate in normal skin included 5.00% ± 1.00% LCs, 3.00% ± 1.58% T cells, and 13.60% ± 2.07% MDSCs (Figure 1B-C; supplemental Figure 1C-D). The proportion of T cells compared with MDSCs was significantly larger in the LCH lesions when compared with healthy skin (Figure 1A-C).

The T cells were further characterized by automatic gating with the FlowSOM,[33] which allows for multivariate clustering of cells based on the self-organized map (SOM) algorithm and categorizes cells into relevant metaclusters based on their surface markers (Figure 1D, supplemental Figure 2A-C). Within LCH lesions, $CD3^+CD4^+$ T cells (74.00% ± 12.26%) were significantly higher than effector $CD3^+CD8^+$ T cells (21.00% ± 5.61%; Figure 1D-E) as compared with tonsil control (41.20% ± 7.02% CD4 and 32.00% ± 4.64% CD8; Figure 1E; supplemental Figure 2A), healthy skin (27.00% ± 13.23% CD4 and 63.67% ± 6.11%; Figure 1E; supplemental Figure 2B), or lymph node samples with macrophage activation (Kikuchi lymphadenitis; supplemental Figure 2C). Among $CD4^+$ T cells, the fraction of Tregs was significantly greater in LCH lesions than in the tonsil or skin control specimens (Figure 1F). These results were independent of *BRAF* mutation status (supplemental Figure 1E-F).

### Infiltrating T cells are dysfunctional

In many malignancies, tumor infiltrating $CD8^+$ T cells mediate adaptive immune response against tumor antigen.[34] Indeed, frequency of tumor-infiltrating $CD8^+$ T cells has been widely shown to correlate with cancer-free survival time among patients with different tumor types.[34] Given the presence of LCH lesion-infiltrating $CD8^+$ T cells, we next assessed their functional capacity and found that they demonstrated attenuated expression of Tc1/Tc2 cytokines, IFN-γ, TNFα, IL-17, or IL-10 in the native state, and after stimulation. By comparison, all 4 cytokines were robustly induced in T cells isolated from healthy tonsil sections (Figure 2A-D). Accordingly, $CD8^+$ T cells within the LCH lesions showed impaired alloreactivity (Figure 2E), consistent with altered

Downloaded from http://ashpublications.org/blood/article-pdf/137/13/1777/1803993/bloodbld2020005867.pdf by Rikhia Chakraborty on 03 December 2021

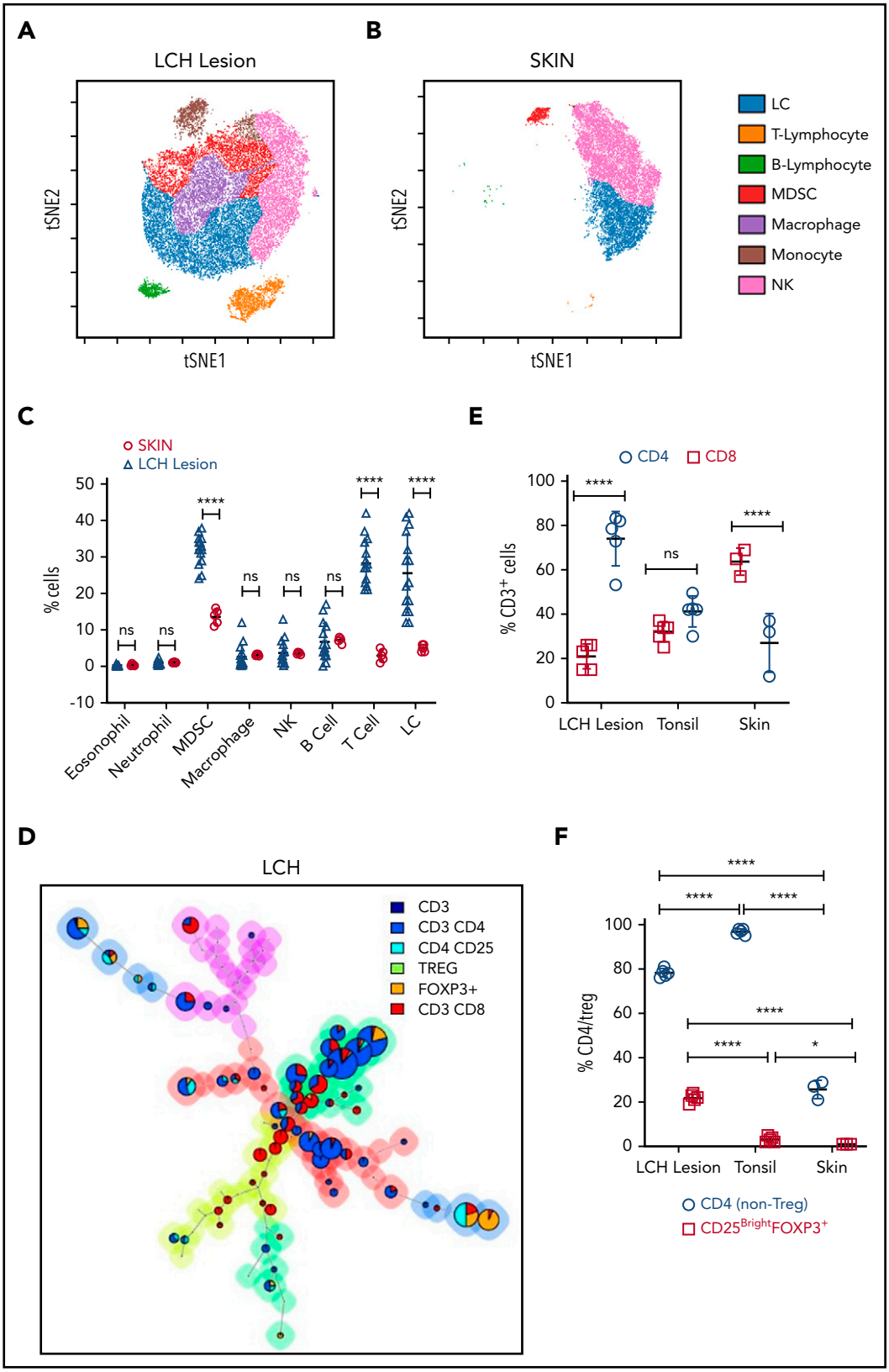



**Figure 1. T cells are the major components of the immune infiltrate in LCH lesions.** (A-B) viSNE plots of live CD45$^+$ cells from a representative sample of an LCH lesion (A) and a biopsy specimen of control healthy skin (B). Each dot in the viSNE plots represents a single cell, and the axes represent arbitrary units based on the *t* distributed SNE (*t* SNE) algorithm. The general phenotype in multidimensional space is represented by the relative position of a cell on the plot. (C) Quantification of LCH lesion-infiltrating cells shown in panel A (n = 15) in comparison with the normal skin specimens shown in panel B (n = 5). (D) Relative T-cell subtypes in LCH. Analyses of CyTOF data were performed with the FlowSOM algorithm and visualized as pie charts, showing the mean values for the indicated markers. The background colors of the nodes result from metaclustering corresponding to an automatic gating procedure to avoid bias in the analyses. The size of the nodes is relative to the percentage of cells present in each cluster. Shown are



Downloaded from http://ashpublications.org/blood/article-pdf/137/13/1777/1803993/bloodbld2020005867.pdf by Rikhia Chakraborty on 03 December 2021

effector function along with high CD44 expression and low-to-absent expression of CD127.[6] In contrast, Tregs isolated from LCH lesions demonstrated intact suppressive activity (Figure 2F).

## Infiltrating T cells in LCH tumor microenvironment exhibit an "exhausted" phenotype

Increased expression of inhibitory immune receptors can raise the threshold for activation, resulting in suppressed immune responses and T-cell exhaustion.[35] Hence, to elucidate the mechanisms underlying T-cell dysfunction within LCH lesions, we assessed expression of inhibitory receptors on $CD8^+$ and $CD4^+$ T-cell subsets by using the FlowSOM algorithm. $CD8^+$ T cells residing in the LCH lesions showed higher expression of the inhibitory PD-1 receptors (Figure 3A-B), a T-cell immunoglobulin- and mucin domain–containing molecule (TIM-3; Figure 3A; supplemental Figure 3B), and lymphocyte-activation gene 3 (LAG-3) (Figure 3A; supplemental Figure 3C), but not cytotoxic T-lymphocyte antigen-4 (CTLA-4) (Figure 3A), compared with peripheral $CD8^+$ T cells from the same patients, skin controls, or peripheral $CD8^+$ T cells from the controls (Figure 3B; supplemental Figure 3A-C). Compared with $CD8^+$ T cells from healthy skin tissues, the $CD8^+$ T cells from LCH lesions showed a significantly higher number of $PD\text{-}1^+TIM\text{-}3^+$ and $PD\text{-}1^+TIM\text{-}3^+LAG\text{-}3^+$ cells, but not $PD\text{-}1^+LAG\text{-}3^+$ or $TIM\text{-}3^+LAG\text{-}3^+$ cells (Figure 3C). $CD4^+$ T cells within the lesion also showed significantly higher expression of PD-1 and TIM-3 than did the peripheral $CD4^+$ T cells from the same patients, skin controls, or peripheral $CD4^+$ T cells from controls (supplemental Figure 3D-E). However, there was no significant difference in the number of $PD\text{-}1^+TIM\text{-}3^+$, $PD\text{-}1^+LAG\text{-}3^+$, $TIM\text{-}3^+LAG\text{-}3^+$, or $PD\text{-}1^+TIM\text{-}3^+LAG\text{-}3^+$ $CD4^+$ T cells between LCH lesions and healthy skin tissues (supplemental Figure 3F).

Compared with the $PD\text{-}1^-TIM\text{-}3^-LAG\text{-}3^-CD8^+$ T cells, the $PD\text{-}1^+$, $TIM\text{-}3^+$, $LAG\text{-}3^+$, $PD\text{-}1^+TIM\text{-}3^+$, and $PD\text{-}1^+TIM\text{-}3^+LAG\text{-}3^+$ $CD8^+$ T cells presented significantly decreased granzyme B and perforin secretion (Figure 3D), indicating a whole-spectrum immunosuppression in these cells. The expression of PD-1 ligands PD-L1 and PD-L2 were significantly elevated in $CD207^+$ DCs from LCH lesions compared with healthy skin (Figure 3E; supplemental Figure 3G).

These results suggest that immobilized PD-L1 or PD-L2-expressing $CD207^+$ cells may engage the T cells because of their high PD-1, resulting in accumulation of exhausted T cells in the lesions. Alternatively, CD207 may induce T cells to express PD-1, in turn engaging them and eventually preventing them from performing effector functions. Thus, we next evaluated whether PD-1 blockade would restore T-cell function in LCH lesions and found that treatment of patient-derived LCH lesion $CD8^+$ T cells with anti-PD-1 antibody for 24 hours significantly rescued their effector functions (Figure 3F). Taken together, these results suggested that PD-1 blockade could influence the immune dysfunction induced by LCH DCs.

## The tumor immune microenvironment in a mouse model of LCH is comparable to that in a human LCH lesion

To determine whether ex vivo observations would translate to decreased LCH disease burden in vivo, we used our previously characterized $BRAFV600E^{CD11c}$ multisystem LCH mouse model, which develops an aggressive, high-risk, LCH-like disease phenotype starting at 6 weeks of age. Broad destruction of tissue architecture appears by 16 to 18 weeks of age with 100% penetrance and decreased lifespan.[5] We sought initially to determine whether the LCH-like lesions in mice reflect the immune profile described earlier in human LCH. The most abundant cells in the immune infiltrate within LCH-like lung lesions were MDSCs and T cells (Figure 4A; supplemental Figure 4A). As in human lesion-infiltrating T cells, $CD3^+CD4^+$ T cells were more numerous than effector $CD3^+CD8^+$ T cells (Figure 4B; supplemental Figure 4B). Compared with $Cre^{-/-}$ littermate control mice there was a significantly higher number of $PD\text{-}1^+$ and $TIM\text{-}3^+$ $CD8^+$ T cells in lung lesions in $BRAFV600E^{CD11c}$ mice (Figure 4C-D). However, we did not observe a significant difference in the number of $PD\text{-}1^+TIM\text{-}3^+$ or $PD\text{-}1^+TIM\text{-}3^+LAG\text{-}3^+$ $CD8^+$ T cells between the $Cre^{-/-}$ littermate control and $BRAFV600E^{CD11c}$ mice (Figure 4D), as was observed in LCH lesion-infiltrating $CD8^+$ T cells (Figure 3C). A similar observation was made for the lesion-infiltrating $CD4^+$ T cells (Figure 4E-F). The expression of PD-L1 was significantly elevated in CD11C cells within lung lesions of $BRAFV600E^{CD11c}$ mice (Figure 4G). Lung-lesion–infiltrating $CD8^+$ T cells from $BRAFV600E^{CD11c}$ mice demonstrated attenuated expression of Tc1/Tc2 cytokines in the native state and after stimulation, in comparison with $Cre^{-/-}$ littermate control mice (supplemental Figure 4C). $CD8^+$ T cells within the lung lesion of $BRAFV600E^{CD11c}$ mice showed impaired alloreactivity (supplemental Figure 4D). Similar observations were made for lesions within liver and spleen (data not shown). Cumulatively, this finding indicated that both the lesion and the tumor-infiltrating cells in $BRAFV600E^{CD11c}$ mice have similar phenotypic and functional properties, as observed in samples of patients with LCH.

## Testing the impacts of checkpoint inhibition on LCH-like lesions and MAPK inhibition on immune infiltrate in vivo

Identifying PD-1 expression on infiltrating lymphocytes and PD-L1 on $CD11C^+$ cells in $BRAFV600E^{CD11c}$ mice prompted us to assess the impact of immune checkpoint inhibitors as a therapeutic option in the preclinical LCH model. $BRAFV600E^{CD11c}$ mice were treated with anti-PD-L1, anti-PD-1 antibody, or their respective isotype controls (Figure 5A). Treatment with anti-PD-1, but not anti-PD-L1 or the controls significantly decreased gross organ weight of lung (Figure 5B), liver (Figure 5C), and spleen (Figure 5D). Anti-PD-1, but not PD-L1 significantly decreased the disease burden in both lung (Figure 5E) and liver (Figure 5F). These outcomes were evidenced by decreased classic granulomatous tissue, including the multinucleated giant cell formation frequently observed in human LCH,[5,36] as well as reduced histiocytic

**Figure 1 (continued)** representative FlowSOM minimal spanning tree (MST) plots for the indicated T-cell types. (E) Quantification of the relative abundance of $CD4^+$ and $CD8^+$ T cells in the LCH lesion infiltrate (n = 5), healthy tonsil control (n = 5), or normal skin (n = 3). (F) CD4/Treg ($C25^+FOXP3^+$) ratios in the indicated specimens (n = 5 each for LCH and tonsil; n = 3 for skin control samples). For all panels, LCH lesions were derived from liver, bone, or spleen. For panels C, E, and F, data are mean ± SD. $^{**}P < .01$; $^{****}P < .0001$, ns, not significant ($P > .05$). WMW test in panel C, 1-way ANOVA with Tukey's post hoc test in panels E and F. NK cell, natural killer cell; SNE, stochastic neighbor embedding; viSNE, visualization of *t* distributed SNE.



Downloaded from http://ashpublications.org/blood/article-pdf/137/13/1777/1803993/bloodbld2020005867.pdf by Rikhia Chakraborty on 03 December 2021

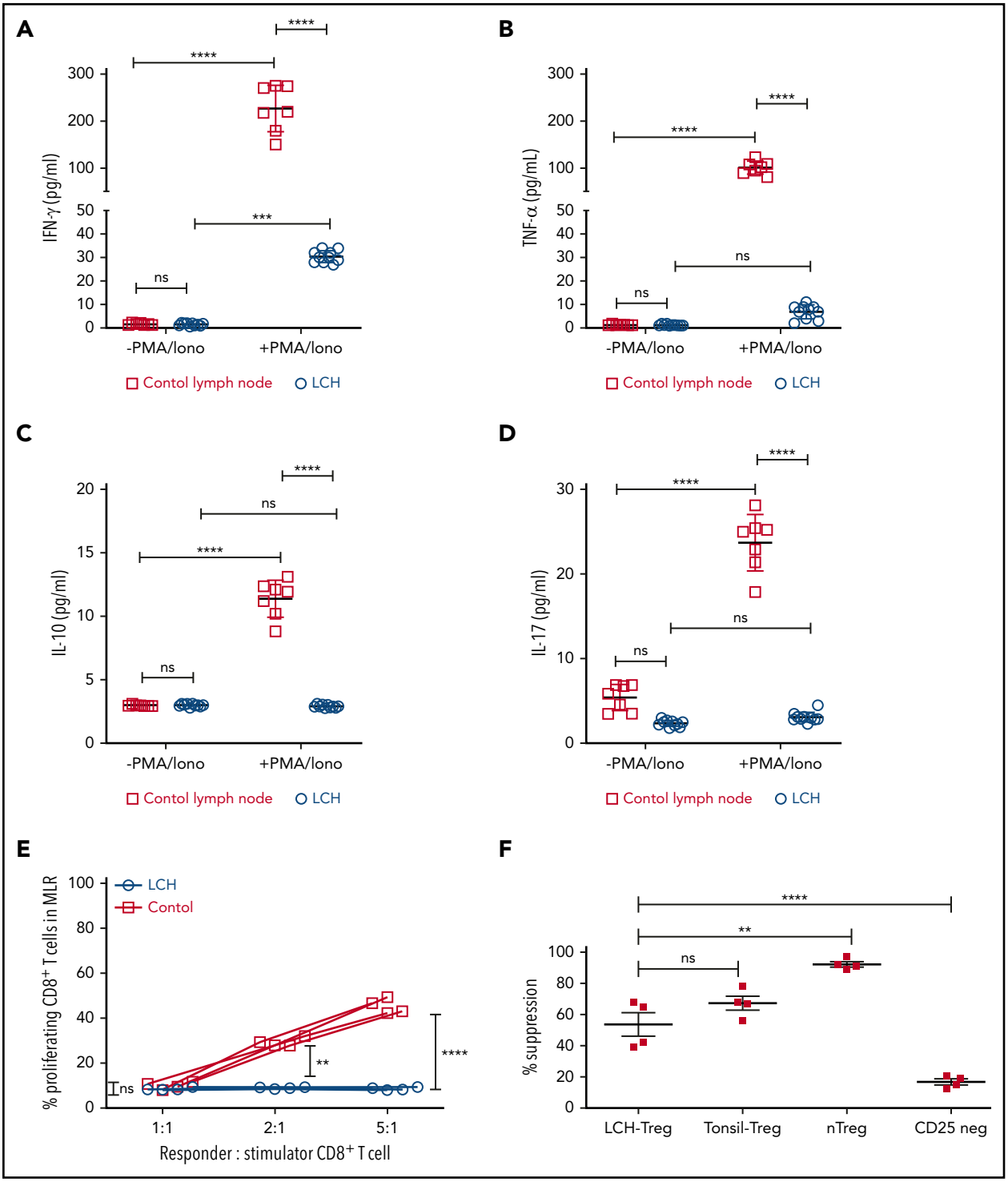



**Figure 2. Infiltrating T lymphocytes in the LCH tumor microenvironment are dysfunctional.** (A-D) Relative expression of the indicated cytokines in $CD8^+$ T cells isolated from LCH lesions (n = 10) and control lymph nodes from a tonsillectomy (n = 7) before and after activation with PMA and ionomycin (PMA/Iono). Data are means ± SD. (E) $CD8^+$ T cells isolated from LCH lesions, but not PBMCs from healthy donors (control), were dysfunctional, as determined by mixed lymphocyte reaction (MLR) assay. Data points represent averaged triplicate measures from cells isolated from 4 patients with LCH or controls. (F) The inhibitory activity of Tregs isolated from LCH lesions or freshly isolated "natural" Tregs (nTregs; $CD3^+CD4^+CD25^{Bright}$), which develop in the thymus during the course of positive and negative selection, Tregs isolated from tonsils obtained from a tonsillectomy, and $CD25^{Dep}$ ($CD3^+CD4^+CD25^{Low}$) cells (n = 4 each) were assessed in a CFSE-based suppression assay. Data are the mean ± SD. $^{**}P < .01$; $^{***}P < .001$; $^{****}P < .0001$, ns, not significant ($P > .05$), by 1-way ANOVA with Tukey's post hoc test.

infiltration of alveoli and peribronchiolar stroma in the lungs (Figure 5G) and significantly reduced sinusoidal distension and periportal cellular infiltration in the liver (Figure 5H).

Given that universal ERK activation is observed in patients with LCH and pharmacological MAPK inhibition restored migration and apoptosis potential in a mouse model of LCH,[26] 2 groups of

Downloaded from http://ashpublications.org/blood/article-pdf/137/13/1777/1803993/bloodbld2020005867.pdf by Rikhia Chakraborty on 03 December 2021

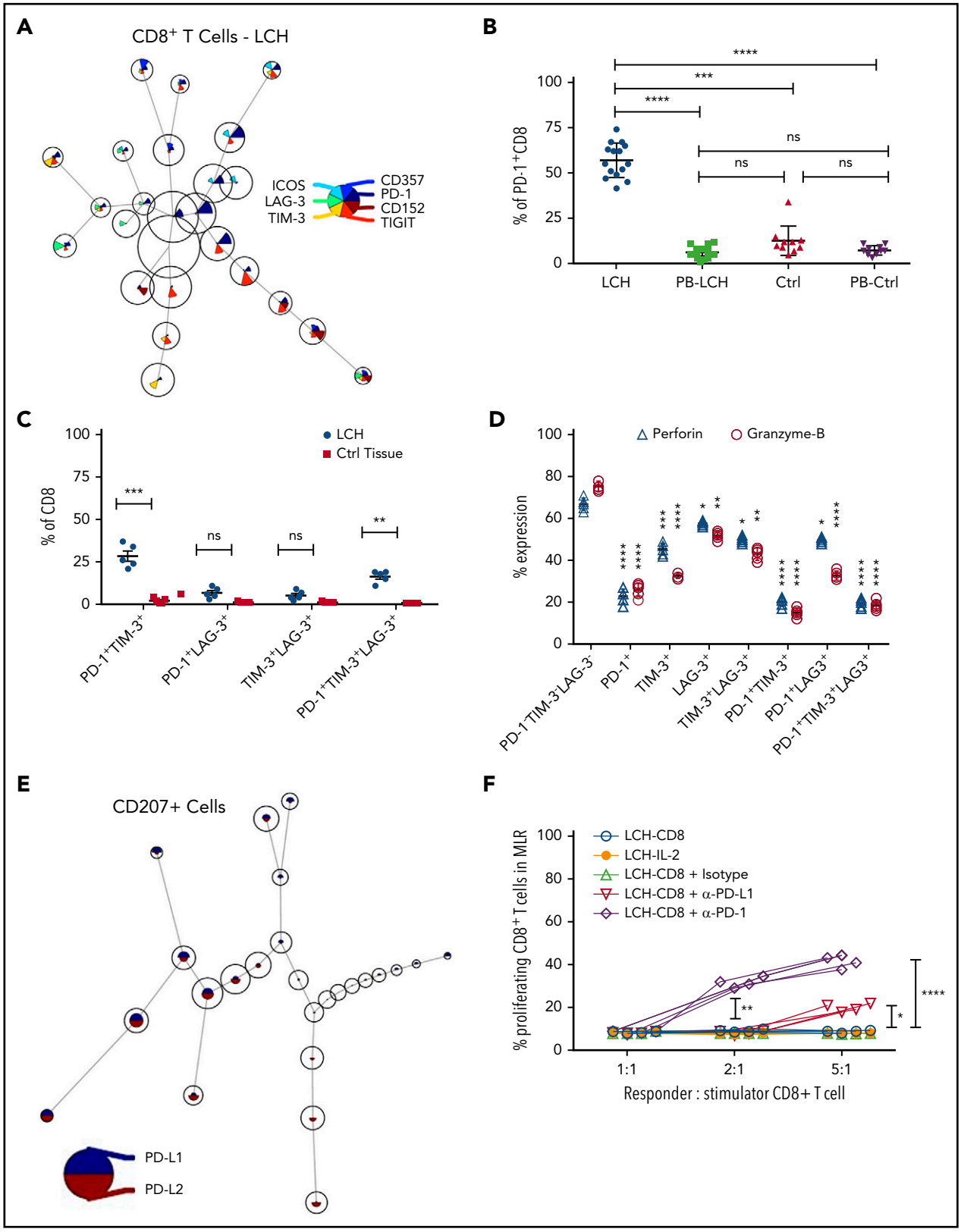



**Figure 3. Infiltrating T lymphocytes in the LCH tumor microenvironment exhibit an exhausted phenotype.** (A) Expression of different immune checkpoint receptors on LCH lesion-infiltrating CD8$^+$ T cells. Analyses of CyTOF data were performed using the FlowSOM algorithm and visualized as pie charts. (B-C) Quantification of relative expression of PD-1 (n = 15, LCH; n = 10, control) (B) and coexpression of immune checkpoint receptors (n = 5 each) (C) in CD8$^+$ T cells, as determined by CyTOF. Data are the means ± SD. (D) Relative expression of perforin and granzyme B in LCH lesion–infiltrating CD8$^+$ T cells not expressing PD-1, TIM-3, or LAG-3 or expressing 1 or more of the immune checkpoint receptors (n = 5). Data are the mean ± SD. (E) Pie chart representing FlowSOM algorithm–based assessment of PD-L1 and PD-L2 expression on CD207$^+$ gated cells. (F) Effector function of CD8$^+$ T cells was restored after treatment for 24 hours with anti-PD-1 but not with anti-PD-L1 antibody, as determined by mixed lymphocyte reaction (MLR) assay. Data points represent averaged triplicate measures from cells isolated from 4 patients with LCH. For all panels, LCH lesions were derived from liver, bone, or spleen. *$P < .05$, **$P < .01$, ***$P < .001$, ****$P < .0001$, ns, not significant ($P > .05$), by 1-way ANOVA with Tukey's post hoc test.

Downloaded from http://ashpublications.org/blood/article-pdf/137/13/1777/1803993/bloodbld2020005867.pdf by Rikhia Chakraborty on 03 December 2021

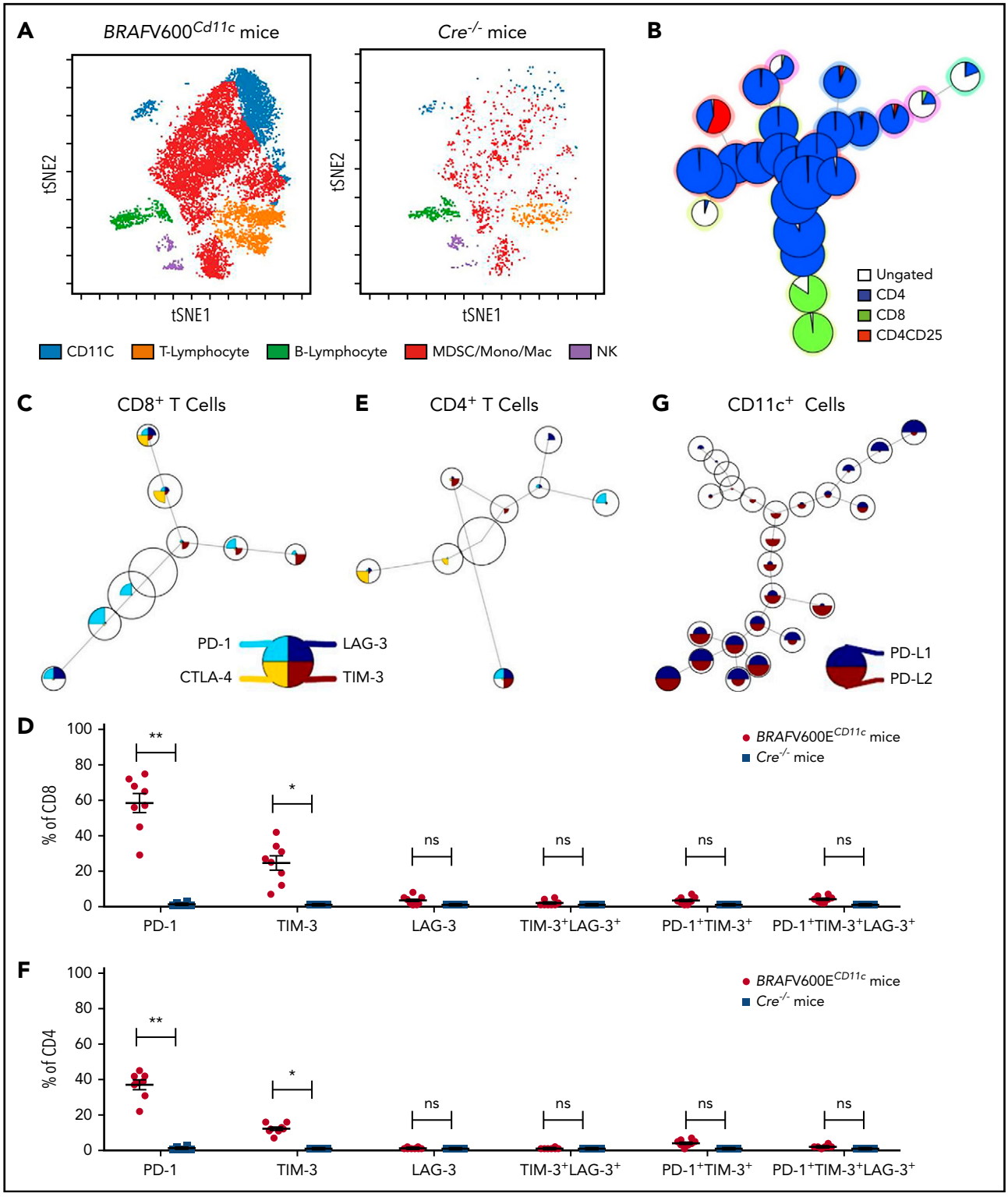



**Figure 4. High PD-1 and PD-L1 expression is conserved in lesion-infiltrating CD8⁺ T cells and Cd11b⁺ DCs in *BRAFV600E*$^{CD11c}$ multisystem LCH mice.** (A) viSNE plot of live cells from representative lesion biopsy specimens from lungs of *BRAFV600E*$^{CD11c}$ and *Cre*$^{-/-}$ littermate control mice. (B) Relative T-cell subtypes in lesion biopsy specimens from lung of *BRAFV600E*$^{CD11c}$ mice depicted by FlowSOM analysis. (C) Expression of different immune checkpoint receptors on lung lesion-infiltrating CD8$^+$ T cells was performed with FlowSOM analysis and visualized as pie charts. (D) Quantification of relative expression of immune checkpoint receptors in lesion-infiltrating CD8$^+$ T cells in *BRAFV600E*$^{CD11c}$ mice and *Cre*$^{-/-}$ littermate control mice (n = 8 each). *$P < .05$; **$P < .01$; ns, not significant ($P > .05$), by WMW test. (E-F) Same as panels C and D, respectively, but for CD4$^+$ T cells (n = 8 each). *$P < .05$; **$P < .01$; ns, not significant ($P > .05$), by the WMW test. (G) FlowSOM grid plots of CyTOF data of PD-L1 and PD-L2 expression on CD11C-gated cells.

Downloaded from http://ashpublications.org/blood/article-pdf/137/13/1777/1803993/bloodbld2020005867.pdf by Rikhia Chakraborty on 03 December 2021

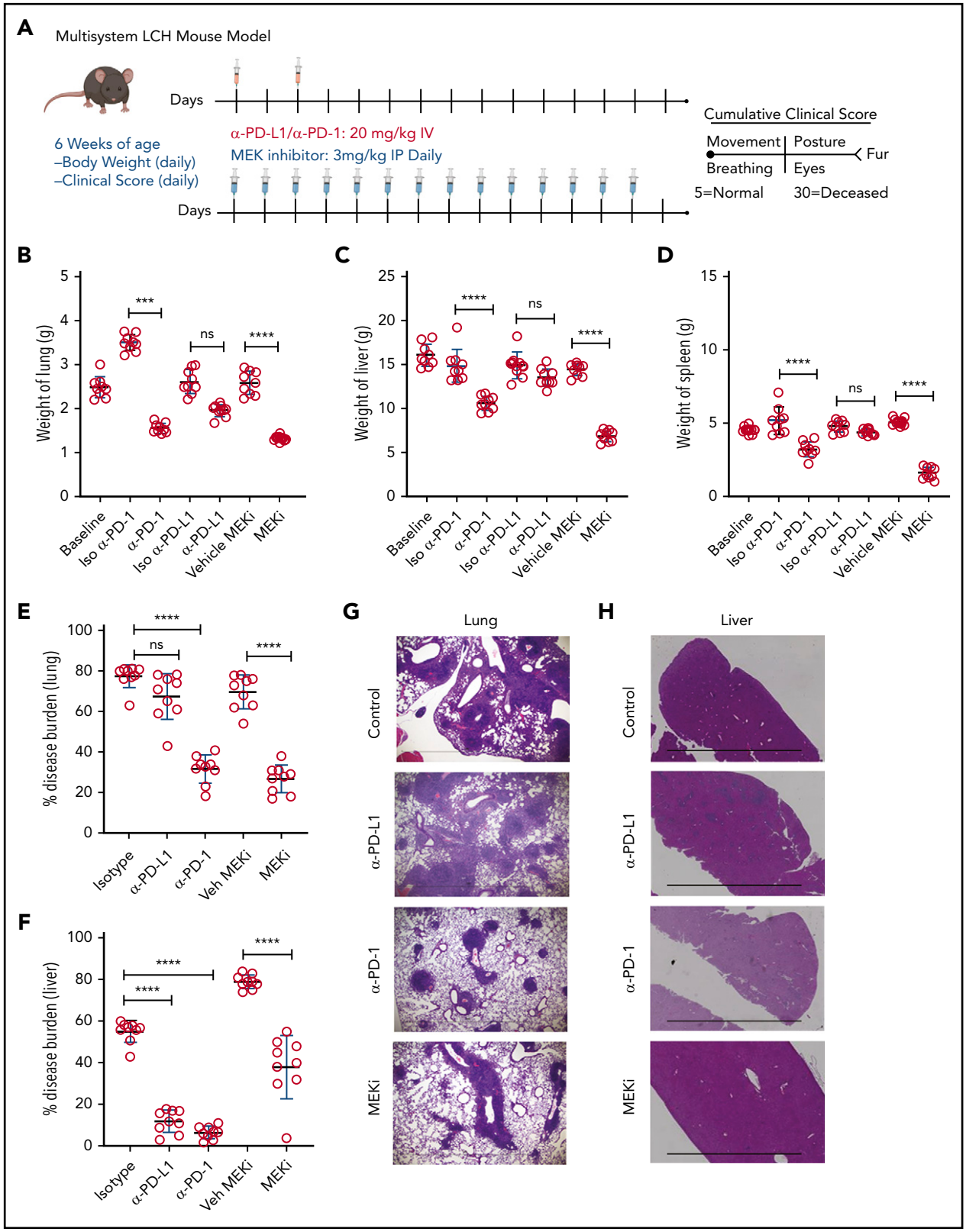



**Figure 5. Treatment with a MEK inhibitor or anti-PD-1 antibody decreases disease burden in a mouse model of LCH.** (A) Treatment and evaluation schema for intervention with PD-L1 or PD-1 blocking antibodies and anti-MEKi. (B-D) Organ weight of lung (B), liver (C), and spleen (D) from *BRAFV600E*$^{CD11c}$ mice treated with MEKi, vehicle control, isotype control, anti-PD-L1, or anti-PD-1. Data are the mean ± SD. ***$P < .001$, ****$P < .0001$, ns, not significant ($P > .05$), by WMW test. (E, F) Disease burden significantly decreased in lung (E) and liver (F) of *BRAFV600E*$^{CD11c}$ mice treated with MEKi or anti-PD-1, but not anti-PD-L1 antibody, compared with isotype control. Data are the mean ± SD. ***$P < .001$, ****$P < .0001$, ns, not significant ($P > .05$), by 1-way ANOVA with Tukey's post hoc test. (G, H) Hematoxylin and eosin–stained lung (G) and liver (H) specimens from *BRAFV600E*$^{CD11c}$ mice after treatment with MEKi or anti-PD-1, but not anti-PD-L1, compared with the corresponding isotype control groups. Bars represent 100 μm. For panels B-F, n = 9 mice per group.

Downloaded from http://ashpublications.org/blood/article-pdf/137/13/1777/1803993/bloodbld2020005867.pdf by Rikhia Chakraborty on 03 December 2021

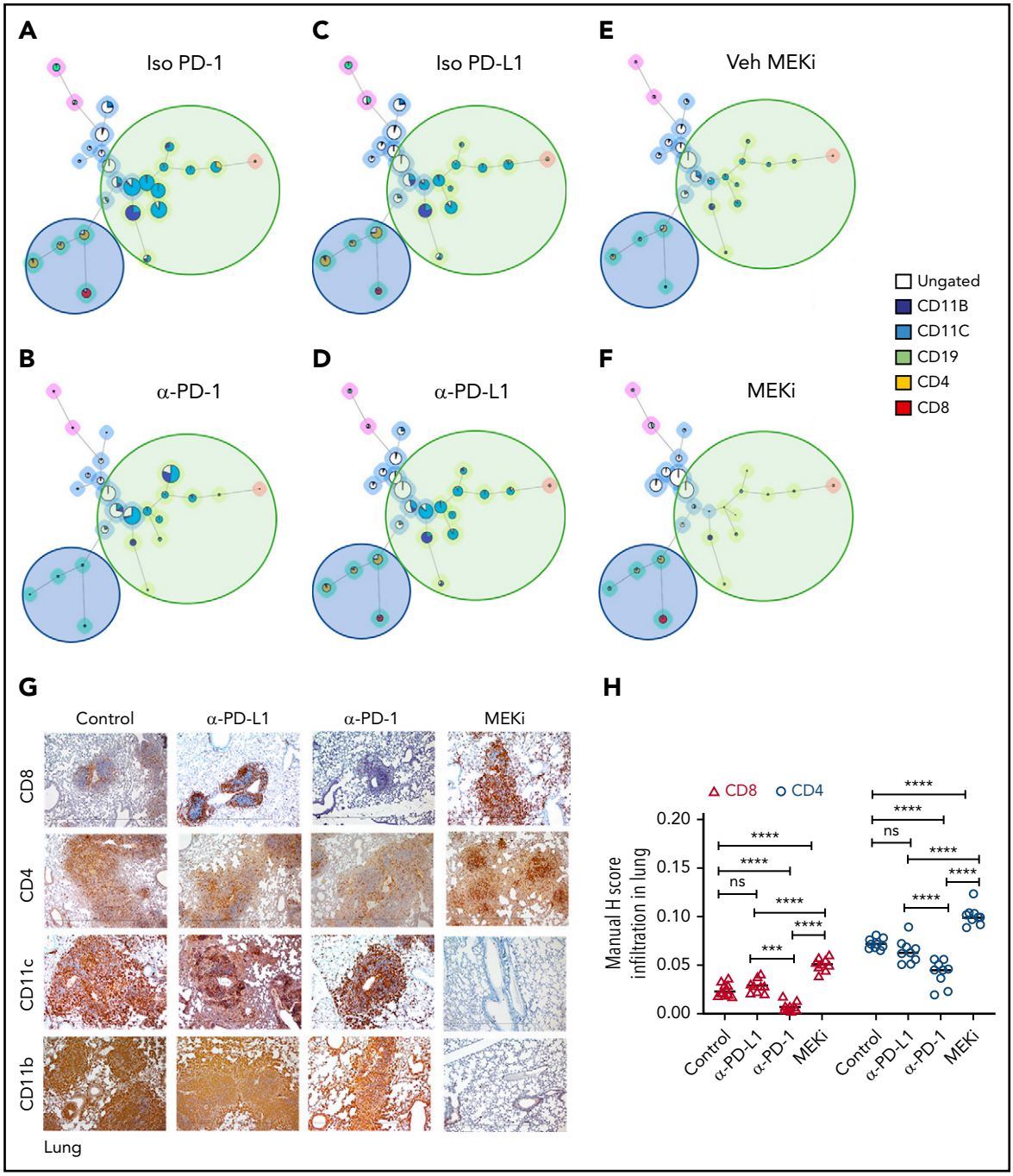



**Figure 6. Distinct effect of MEKi and anti-PD-1 on myeloid lesional cells and intralesional lymphoid cells.** (A-F) FlowSOM analysis of representative lesion biopsy specimens from lung of *BRAFV600E*$^{CD11c}$ mice in the indicated experimental groups. Green circle, myeloid compartment; blue circle, lymphoid compartment. (G) Representative immunohistochemistry images of infiltrating T cells (CD8$^+$ and CD4$^+$), and DCs (CD11b$^+$ and CD11c$^+$) in lungs of the different experimental groups. Bars represent 100 μm. (H) Quantification of lesion infiltrating CD8$^+$ and CD4$^+$ T cells in the indicated experimental groups. Data are the means ± SD (n = 9 mice per group); ***$P < .001$; ****$P < .0001$; ns, not significant ($P > .05$), by 1-way ANOVA with Tukey's post hoc test.

*BRAFV600E*$^{CD11c}$ mice were also treated with either the MAPK pathway inhibitor (MEKi, trametinib; Selleckchem, Houston, TX) or vehicle control (Figure 5A). Treatment with MEKi significantly decreased gross organ weight (Figure 5B-D), disease burden (Figure 5E-F), histiocytic infiltration of alveoli and peribronchiolar stroma in the lungs (Figure 5G), and sinusoidal distension and periportal cellular infiltration in the liver (Figure 5H). No difference in clinical score was observed among the different treatments (MEKi, anti-PD-L1, and anti-PD-1) groups (data not shown).

Analysis of the bulk lung lesions with the FlowSOM algorithm revealed that, compared with the isotype treatment, monotherapy with anti-PD-1 antibody significantly decreased infiltration of lymphoid cells while having a nominal effect on the myeloid compartment (Figure 6A-B). Monotherapy with anti-PD-L1 antibody did not decrease either the myeloid or lymphoid compartments (Figure 6C-D). On the other hand, MEKi treatment decreased the myeloid CD11b$^+$ population (myeloid DC precursors expressing *BRAFV600E*), but also resulted in an increased number



Downloaded from http://ashpublications.org/blood/article-pdf/137/13/1777/1803993/bloodbld2020005867.pdf by Rikhia Chakraborty on 03 December 2021

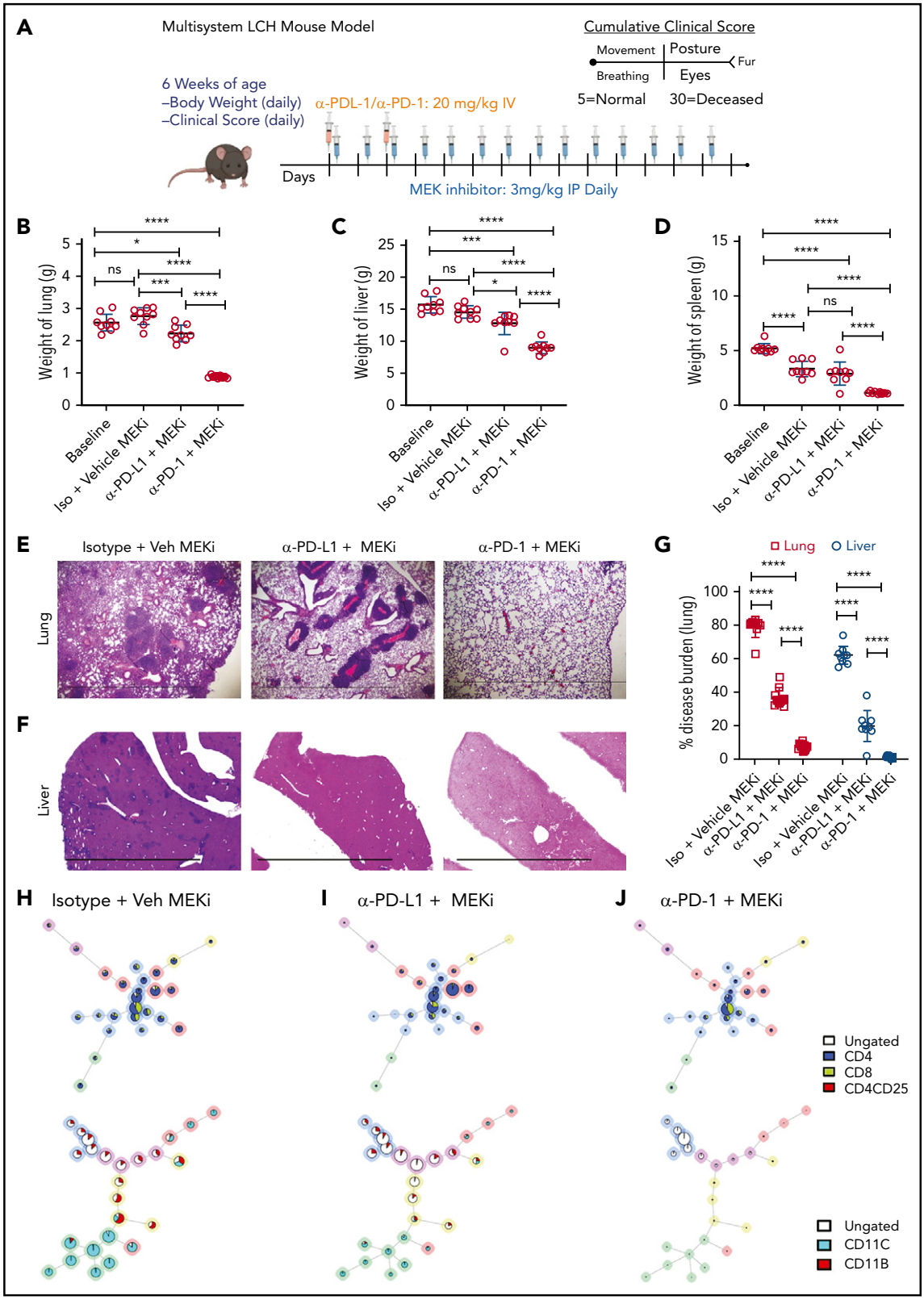



**Figure 7. Synergistic effect on disease outcome in a preclinical LCH model with combined PD-1 blockade and targeted MAPK inhibition.** (A) Treatment and evaluation schema for intervention with anti-MEKi, -PD-L1, and/or -PD-1 blocking antibodies. (B-D) Organ weight of lung (B), liver (C), and spleen (D) from *BRAFV600E*$^{CD11c}$ mice treated with the different combinations indicated. (E, F) Hematoxylin and eosin–stained lung (E) and liver (F) specimens from *BRAFV600E*$^{CD11c}$ mice after the indicated treatment regimens compared with the corresponding control groups. The disease burden significantly decreased in lung and liver of *BRAFV600E*$^{CD11c}$ mice cotreated with MEKi and anti-PD-1 compared with the other regimens (G). (H-J) FlowSOM minimal spanning tree (MST) plots of lymphoid (top) and myeloid (bottom) cells from representative lesion biopsy specimens of lung of *BRAFV600E*$^{CD11c}$ mice in isotype+vehicle MEKi (H), anti-PD-L1+MEKi (I), and anti-PD-1+MEKi (J) groups. For panels B-D and G, data are the means ± SD (n = 9 mice per group). *$P < .05$; ***$P < .001$, ****$P < .0001$, ns, not significant ($P > .05$), by 1-way ANOVA with Tukey's post hoc test.

Downloaded from http://ashpublications.org/blood/article-pdf/137/13/1777/1803993/bloodbld2020005867.pdf by Rikhia Chakraborty on 03 December 2021

of infiltrating CD4$^+$ and CD8$^+$ T cells (Figure 6E-F). Immunohistochemical analysis confirmed the CyTOF analysis in lungs (Figure 6G-H) and liver (supplemental Figure 5A-B). Collectively, these results indicate that an optimal outcome is not achieved with monotherapy with immune checkpoint inhibitor(s) or MEKi.

### Combined targeted therapy using MEKi and immunotherapy using anti-PD-1 are clinically synergistic in the LCH mouse model

Given our observations with MAPK inhibitor alone or anti-PD-L1 and anti-PD-1 monotherapies, we tested whether concomitant targeted immunotherapy with anti-PD-1 or anti-PD-L1 and inhibition of MAPK activation would improve clinical outcomes (Figure 7A). Combination of MEKi with anti-PD-1, but not with anti-PD-L1, had a synergetic effect on decreasing organ weight (Figure 7B-D) and disease burden in lung (Figure 7E,G) and liver (Figure 7F-G). No difference in clinical score was observed among the different combination groups (data not shown). In comparison to vehicle or combined MEKi and anti-PD-L1 therapy, combined MEKi and anti-PD-1 therapy significantly reduced infiltration of CD8$^+$ and CD4$^+$ T cells in lung (Figure 7H-J, top; supplemental Figure 6A-B) and liver lesions (supplemental Figure 6C- D), as well as tissue LCH DC accumulation (Figure 7H-J; bottom; supplemental Figure 6A,C). In addition, the combined MEKi and anti-PD-1 therapy significantly decreased the abundance of PD-1–expressing CD8$^+$ T cells (supplemental Figure 7A-D) and PD-L1 expression by lesional CD11c$^+$ cells (supplemental Figure 7E) and restored the function of the lesion-infiltrating CD8$^+$ cells, as assessed by expression of Tc1/Tc2 cytokines (supplemental Figure 8). Collectively, these results indicate that immune checkpoint inhibitor therapy with anti-PD-1 enhances clinical responses to inhibition of the MAPK pathway.

## Discussion

Current therapies for LCH are based on empiric chemotherapy, curing <50% of patients treated with front-line standard-of-care vinblastine/prednisone. Optimal salvage therapies have not been defined, and failure of treatment is associated with increased risks of morbidity and mortality. Much of the research focus on LCH in the past decade has been on origins and genetic alterations of the pathologic LCs, which constitute a minority population in the LCH lesion. This study focused on characterizing the composition and functional capacity of the immune infiltrate to enhance understanding of pathogenic mechanisms of LCH and to identify novel therapeutic opportunities.

Previous studies have described a lymphocyte-rich microenvironment in LCH lesions with an abundance of T cells and regulatory Th cells.[6,8,10-12] However, the function of these tumor-infiltrating lymphocytes and their contribution to pathogenesis is not known. In this study, LCH lesional CD207$^+$ cells had high expression of PD-L1 and the lesion-infiltrating T cells in human and mouse models of LCH expressed excess checkpoint inhibitor proteins and signaling molecules that inhibited T-cell function and negatively regulated normal T-cell responses. Indeed, the infiltrating CD8$^+$ T cells in LCH lesions were dysfunctional. This study provides preclinical evidence of a synergistic effect of MAPK inhibition and PD-1 blockade on LCH disease outcome and support a novel immunotherapeutic strategy for the treatment of LCH. However, it remains to be determined in future studies whether the lesion-infiltrating T cells in LCH are truly tumor reactive or merely bystanders. T cells may contribute to LCH pathogenesis, either through direct tissue damage or through modulation of the survival and function of *BRAF*V600E DCs or other myeloid cells that accumulate in LCH lesions and further promote tissue damage. In addition, the mechanisms underlying recruitment, activation, and expansion of T cells in LCH and how each of these is affected by the constitutive MAPK activation observed in the pathogenic CD207$^+$ DCs have to be defined.

The mechanisms of Treg-mediated immune suppression and checkpoint regulation in LCH may be distinct from cancer paradigms such as melanoma where tumor-directed lymphocytes are held at bay. This dissimilarity between LCH and other neoplastic disorders may be caused by their vast differences in mutational load and/or neoantigens, as well as the intrinsic nature of LCH cells.[4] In the case of LCH, the pathogenic myeloid cells with unopposed MAPK activation differentiate with features of a professional antigen-presenting cell.[37] The interactions between T cells and pathogenic DCs may therefore reflect distinct mechanisms of immune cell dysregulation. LCH is a unique neoplastic disorder, as the pathologic CD207$^+$ cell has features of a professional antigen-presenting cell. Naive (CD8$^+$) T cells require antigen binding by their T-cell receptor and costimulatory signals for activation. LCH lesional cells express the costimulatory receptors CD40,[38-40] CD80,[39,41,42] ICOS ligand,[10] and CD86.[39,40] LCH cells express similar levels of CD40, CD80, and CD86 messenger RNA, when compared with normal epidermal CD207$^+$ LCs,[43,44] and confer high expression of genes that are relevant to antigen presentation (including CD1E) and genes encoding members of the HLA complex.[45] Cumulatively, this finding suggests that LCH lesional DCs should impact T-cell responses. In fact, the results of this study show that the lesion-infiltrating T cells were exhausted and dysfunctional. It is plausible that the infiltrating T cells are exhausted by prolonged exposure to antigenic stimulation within the LCH lesion. However, alternate mechanisms such as an immunosuppressive cytokine environment[6,9-13,46] potentiated by the high number of lesion-infiltrating MDSCs and Tregs, as we observed, may also lead to exhausted T cells.

Clinical trials for PD-1 and PD-L1 blockade for patients with advanced melanoma and Hodgkin's lymphoma have demonstrated consistent therapeutic responses.[47-50] We have shown in previous studies that, in the absence of augmented proliferation, constitutive ERK activation results in accumulation and persistence of pathological DCs by downregulating expression of CCR7, effectively trapping the DCs at the site of disease, recruiting activated T cells, and together producing mediators of inflammation and tissue destruction.[6,26] In this study, treatment of *BRAF*V600E$^{CD11c}$ mice with anti-PD-1 decreased the number of infiltrating T cells. Nevertheless, the CD11c$^+$ *BRAF*V600E$^+$ DC population was not substantially altered, even though overall lesion size significantly decreased. This result suggests that the PD-L1/PD-1 interaction plays a role in the accumulation and activation of T cells that contribute to local and systemic pathologic inflammation. However, these results are less consistent with restoration of CD8$^+$ T cell antitumor (eg, anti-CD11c$^+$ DC) activity.

Single-agent MAPK inhibition studies in early phase studies in adults with LCH and related disorders have yielded nearly

Downloaded from http://ashpublications.org/blood/article-pdf/137/13/1777/1803993/bloodbld2020005867.pdf by Rikhia Chakraborty on 03 December 2021

universal clinical responses.[18-20,22,23,51] However, the potential for a durable "cure" is uncertain, as many patients have improved but persistent disease, and relapse almost always occurs after cessation of therapy.[24] In this study, MEK inhibition decreased the myeloid compartment but resulted in an increase of $CD8^+$ T cells. Although not an expected result, this phenomenon has been observed in other tumors. In pancreatic cancer, depletion of MDSC or macrophage subsets results in increased infiltration and activation of $CD8^+$ T cells.[52] In this context, it was reported that myeloid cells regulate expression of PD-L1 in tumor cells that then suppress antitumor immune responses mediated by $CD8^+$ cells and that treatment with MAPK inhibitors lowered the intratumoral expression of PD-L1, rendering the tumor susceptible to PD-1 blockade. Observations from this study support the potential for MAPK activation in LCH DCs, inducing expression of PD-L1. Therefore, in addition to affecting LCH DC migration and survival,[26] MEK inhibition may enhance $CD8^+$ T-cell function. This may be because of the increased transcription of genes involved in cellular activation and inflammatory cytokine production, as has been shown after a single cycle of combined checkpoint blockade in melanoma.[53]

The past decade has elucidated the broad strokes of LCH pathogenesis: MAPK activation in differentiating myeloid precursors. However, the mechanisms that regulate recruitment, retention, and activation of immune cells to lesions are not known, and the role of inflammation in pathogenesis is undefined. To identify optimal curative therapies for patients with LCH, various strategies may first have to be tested in preclinical models to prioritize for testing in clinical trials. The results of the present study provide novel insights into the character and function of lesion-infiltrating T cells in LCH. Given that neither character and function of lesion-infiltrating T cells in LCH nor MEK inhibition is dependent on MAPK pathway mutations,[18] the synergistic impact of combined MEK inhibition and checkpoint blockade represent a novel therapeutic strategy that merits clinical development. The findings of this study demonstrate the effect of checkpoint inhibition against LCH, supporting further investigation to refine optimal agents, dosing, and combinations to be tested in clinical trials. The revised conceptualization of LCH as an inflammatory myeloid neoplastic disorder driven by pathologic MAPK activation in myeloid precursor cells coupled with the findings that combination therapy exerts a synergistic effect on disease outcome offers an opportunity to move treatment of LCH beyond empiricism to rational, risk-based strategies.

## Acknowledgments

The authors thank Jared K. Burks (The University of Texas Anderson Cancer Center Flow Cytometry Core) and Joel Sederstorm (Baylor College of Medicine Flow Cytometry Core) for help with CyTOF and flow cytometry, respectively, and the research coordinators of the Histio/Lymphoma team at Texas Children's Cancer Center for help with patient sample collection. The TXCH (Texas Children's Hospital) Histiocytosis Program is supported by a research grant from the HistioCure Foundation.

This work was supported by the Department of Defense through the Peer Reviewed Cancer Research Program under Award W81XWH-19-1-0167 (R.C.), National Institutes of Health (NIH), National Cancer Institute (NCI) grants R01 CA154489 (M.M., C.E.A.), CA154947 (M.M., C.E.A.), NIH Specialized Program of Research Excellence (SPORE) in Lymphoma, NCI grant P50CA126752 (C.E.A.); an Alex's Lemonade Stand Foundation Young Investigator Grant (R.C.), the American Society of Hematology Scholar Award (R.C.), St. Baldrick's Foundation Innovation Award (C.E.A), the Leukemia and Lymphoma Society Translational Research Program (C.E.A.), and Cookies for Kids Cancer (C.E.A). This study was a collaborative project with support from St. Baldrick's Foundation, which sponsors the North American Consortium for Histiocytosis Research (M.M, K.L.M., C.E.A.).

## Authorship

Contribution: A.S. performed most of the CyTOF and mouse experiments and analyzed the data; J.V., M.H., T.M.B., H.A., R.R., W.O., and B.S. performed experiments and analyzed the data; W.Y. evaluated and scored the mouse histology sections in a blinded fashion; O.S.E., C.B., C.M.B., M.M., and K.L.M. contributed to the study design; R.C. conceived, designed, performed experiments, analyzed data, and wrote the manuscript; C.E.A. and R.C. supervised the project; and all authors reviewed the final manuscript.

Conflict-of-interest disclosure: The authors declare no competing financial interests.

ORCID profiles: T.M.B., 0000-0003-0942-7580; O.S.E., 0000-0002-1895-8810; K.L.M., 0000-0003-0725-6263.

Correspondence: Rikhia Chakraborty, Texas Medical Center, 1102 Bates St, Ste 1025.21, Houston, TX 77030; e-mail: rxchakra@txch.org; and Carl E. Allen, Texas Medical Center, 1102 Bates St, Ste 1025.21, Houston, TX 77030; e-mail: ceallen@txch.org.

## Footnotes

Submitted 17 March 2020; accepted 17 September 2020; prepublished online on *Blood* First Edition 19 October 2020. DOI 10.1182/blood.2020005867.

All data supporting the findings of this study that are not included in the manuscript are available upon request to the corresponding authors.

The online version of this article contains a data supplement.

There is a *Blood* Commentary on this article in this issue.

The publication costs of this article were defrayed in part by page charge payment. Therefore, and solely to indicate this fact, this article is hereby marked "advertisement" in accordance with 18 USC section 1734.

Downloaded from http://ashpublications.org/blood/article-pdf/137/13/1777/1803993/bloodbld2020005867.pdf by Rikhia Chakraborty on 03 December 2021

## REFERENCES

1. Allen CE, Merad M, McClain KL. Langerhans-Cell Histiocytosis. *N Engl J Med*. 2018;379(9):856-868.
2. Berres ML, Allen CE, Merad M. Pathological consequence of misguided dendritic cell differentiation in histiocytic diseases. *Adv Immunol*. 2013;120:127-161.
3. Chakraborty R, Burke TM, Hampton OA, et al. Alternative genetic mechanisms of BRAF activation in Langerhans cell histiocytosis. *Blood*. 2016;128(21):2533-2537.
4. Chakraborty R, Hampton OA, Shen X, et al. Mutually exclusive recurrent somatic mutations in MAP2K1 and BRAF support a central role for ERK activation in LCH pathogenesis. *Blood*. 2014;124(19):3007-3015.
5. Berres ML, Lim KP, Peters T, et al. BRAF-V600E expression in precursor versus differentiated de0ndritic cells defines clinically distinct LCH risk groups [published correction appears in *J Exp Med*. 2015;212(2):281]. *J Exp Med*. 2014;211(4):669-683.
6. Allen CE, Li L, Peters TL, et al. Cell-specific gene expression in Langerhans cell histiocytosis lesions reveals a distinct profile

compared with epidermal Langerhans cells. *J Immunol*. 2010;184(8):4557-4567.

7. Battistella M, Fraitag S, Teillac DH, Brousse N, de Prost Y, Bodemer C. Neonatal and early infantile cutaneous Langerhans cell histiocytosis: comparison of self-regressive and non-self-regressive forms. *Arch Dermatol*. 2010; 146(2):149-156.

8. Bechan GI, Egeler RM, Arceci RJ. Biology of Langerhans cells and Langerhans cell histiocytosis. *Int Rev Cytol*. 2006;254:1-43.

9. Gatalica Z, Bilalovic N, Palazzo JP, et al. Disseminated histiocytoses biomarkers beyond BRAFV600E: frequent expression of PD-L1. *Oncotarget*. 2015;6(23):19819-19825.

10. Quispel WT, Stegehuis-Kamp JA, Santos SJ, Egeler RM, van Halteren AG. Activated Conventional T-Cells Are Present in Langerhans Cell Histiocytosis Lesions Despite the Presence of Immune Suppressive Cytokines. *J Interferon Cytokine Res*. 2015;35(10): 831-839.

11. Senechal B, Elain G, Jeziorski E, et al. Expansion of regulatory T cells in patients with Langerhans cell histiocytosis. *PLoS Med*. 2007;4(8):e253.

12. Tong C, Jia X, Jia Y, He Y. Langerhans cell histiocytosis in Chinese adults: absence of BRAF mutations and increased FOXP3(+) regulatory T cells. *Int J Clin Exp Pathol*. 2014; 7(6):3166-3173.

13. Zeng K, Wang Z, Ohshima K, et al. BRAF V600E mutation correlates with suppressive tumor immune microenvironment and reduced disease-free survival in Langerhans cell histiocytosis. *OncoImmunology*. 2016;5(7): e1185582. org/10.1080/2162402X.2016. 1185582

14. Gadner H, Minkov M, Grois N, et al; Histiocyte Society. Therapy prolongation improves outcome in multisystem Langerhans cell histiocytosis. *Blood*. 2013;121(25):5006-5014.

15. Minkov M, Grois N, McClain K, et al Histiocyte Society evaluation and treatment guidelines. https://www2.hematologie-amc.nl/bestanden/hematologie/bijlagennietinDBS/SocietyLCHTreatmentGuidelines.PDF. Accessed 10 January 2020.

16. Haupt R, Nanduri V, Calevo MG, et al. Permanent consequences in Langerhans cell histiocytosis patients: a pilot study from the Histiocyte Society-Late Effects Study Group. *Pediatr Blood Cancer*. 2004;42(5):438-444.

17. Allen CE, Ladisch S, McClain KL. How I treat Langerhans cell histiocytosis. *Blood*. 2015; 126(1):26-35.

18. Diamond EL, Durham BH, Ulaner GA, et al. Efficacy of MEK inhibition in patients with histiocytic neoplasms. *Nature*. 2019; 567(7749):521-524.

19. Diamond EL, Subbiah V, Lockhart AC, et al. Vemurafenib for BRAF V600-Mutant Erdheim-Chester Disease and Langerhans Cell Histiocytosis: Analysis of Data From the Histology-Independent, Phase 2, Open-label VE-BASKET Study. *JAMA Oncol*. 2018;4(3):384-388.

20. Haroche J, Cohen-Aubart F, Emile JF, et al. Reproducible and sustained efficacy of targeted therapy with vemurafenib in patients with BRAF(V600E)-mutated Erdheim-Chester disease. *J Clin Oncol*. 2015;33(5):411-418.

21. Hyman DM, Puzanov I, Subbiah V, et al. Vemurafenib in Multiple Nonmelanoma Cancers with BRAF V600 Mutations [published correction appears in *N Engl J Med*. 2018; 379(16):1585]. *N Engl J Med*. 2015;373(8): 726-736.

22. Donadieu J, Larabi IA, Tardieu M, et al. Vemurafenib for Refractory Multisystem Langerhans Cell Histiocytosis in Children: An International Observational Study. *J Clin Oncol*. 2019;37(31):2857-2865.

23. Eckstein OS, Visser J, Rodriguez-Galindo C, Allen CE; NACHO-LIBRE Study Group. Clinical responses and persistent *BRAF* V600E$^+$ blood cells in children with LCH treated with MAPK pathway inhibition. *Blood*. 2019;133(15):1691-1694.

24. Cohen Aubart F, Emile JF, Carrat F, et al. Targeted therapies in 54 patients with Erdheim-Chester disease, including follow-up after interruption (the LOVE study). *Blood*. 2017;130(11):1377-1380.

25. Schiffer JT, Corey L. Rapid host immune response and viral dynamics in herpes simplex virus-2 infection. *Nat Med*. 2013;19(3): 280-290.

26. Hogstad B, Berres ML, Chakraborty R, et al. RAF/MEK/extracellular signal-related kinase pathway suppresses dendritic cell migration and traps dendritic cells in Langerhans cell histiocytosis lesions. *J Exp Med*. 2018;215(1): 319-336.

27. Dankort D, Filenova E, Collado M, Serrano M, Jones K, McMahon M. A new mouse model to explore the initiation, progression, and therapy of BRAFV600E-induced lung tumors. *Genes Dev*. 2007;21(4):379-384.

28. Nunamaker EA, Anderson RJ, Artwohl JE, Lyubimov AV, Fortman JD. Predictive observation-based endpoint criteria for mice receiving total body irradiation. *Comp Med*. 2013;63(4):313-322.

29. Shrum B, Anantha RV, Xu SX, et al. A robust scoring system to evaluate sepsis severity in an animal model. *BMC Res Notes*. 2014;7(1):233.

30. Finck R, Simonds EF, Jager A, et al. Normalization of mass cytometry data with bead standards. *Cytometry A*. 2013;83(5): 483-494.

31. Di Stasi A, De Angelis B, Rooney CM, et al. T lymphocytes coexpressing CCR4 and a chimeric antigen receptor targeting CD30 have improved homing and antitumor activity in a Hodgkin tumor model. *Blood*. 2009;113(25): 6392-6402.

32. Chakraborty R, Mahendravada A, Perna SK, et al. Robust and cost effective expansion of human regulatory T cells highly functional in a xenograft model of graft-versus-host disease. *Haematologica*. 2013;98(4):533-537.

33. Van Gassen S, Callebaut B, Van Helden MJ, et al. FlowSOM: Using self-organizing maps for visualization and interpretation of cytometry data. *Cytometry A*. 2015;87(7):636-645.

34. Reiser J, Banerjee A. Effector, Memory, and Dysfunctional CD8(+) T Cell Fates in the Antitumor Immune Response. *J Immunol Res*. 2016;2016:8941260.

35. Wherry EJ, Kurachi M. Molecular and cellular insights into T cell exhaustion. *Nat Rev Immunol*. 2015;15(8):486-499.

36. da Costa CE, Szuhai K, van Eijk R, et al. No genomic aberrations in Langerhans cell histiocytosis as assessed by diverse molecular technologies. *Genes Chromosomes Cancer*. 2009;48(3):239-249.

37. Collin M, Milne P. Langerhans cell origin and regulation. *Curr Opin Hematol*. 2016;23(1): 28-35.

38. Egeler RM, Favara BE, Laman JD, Claassen E. Abundant expression of CD40 and CD40-ligand (CD154) in paediatric Langerhans cell histiocytosis lesions. *Eur J Cancer*. 2000; 36(16):2105-2110.

39. Geissmann F, Lepelletier Y, Fraitag S, et al. Differentiation of Langerhans cells in Langerhans cell histiocytosis. *Blood*. 2001;97(5): 1241-1248.

40. Tazi A, Moreau J, Bergeron A, Dominique S, Hance AJ, Soler P. Evidence that Langerhans cells in adult pulmonary Langerhans cell histiocytosis are mature dendritic cells: importance of the cytokine microenvironment. *J Immunol*. 1999;163(6):3511-3515.

41. Emile JF, Fraitag S, Leborgne M, de Prost Y, Brousse N. Langerhans' cell histiocytosis cells are activated Langerhans' cells. *J Pathol*. 1994;174(2):71-76.

42. Sahm F, Capper D, Preusser M, et al. BRAFV600E mutant protein is expressed in cells of variable maturation in Langerhans cell histiocytosis. *Blood*. 2012;120(12):e28-e34.

43. Hutter C, Kauer M, Simonitsch-Klupp I, et al. Notch is active in Langerhans cell histiocytosis and confers pathognomonic features on dendritic cells. *Blood*. 2012;120(26): 5199-5208.

44. Allen CE, Flores R, Rauch R, et al. Neurodegenerative central nervous system Langerhans cell histiocytosis and coincident hydrocephalus treated with vincristine/cytosine arabinoside. *Pediatr Blood Cancer*. 2010; 54(3):416-423.

45. Halbritter F, Farlik M, Schwentner R, et al. Epigenomics and Single-Cell Sequencing Define a Developmental Hierarchy in Langerhans Cell Histiocytosis. *Cancer Discov*. 2019;9(10):1406-1421.

46. Mitchell JM, Berzins SP, Kannourakis G. A potentially important role for T cells and regulatory T cells in Langerhans cell histiocytosis. *Clin Immunol*. 2018;194:19-25.

47. Ansell SM, Lesokhin AM, Borrello I, et al. PD-1 blockade with nivolumab in relapsed or refractory Hodgkin's lymphoma. *N Engl J Med*. 2015;372(4):311-319.

48. Powles T, Eder JP, Fine GD, et al. MPDL3280A (anti-PD-L1) treatment leads to clinical activity in metastatic bladder cancer. *Nature*. 2014; 515(7528):558-562.

49. Rizvi NA, Mazières J, Planchard D, et al. Activity and safety of nivolumab, an anti-PD-1 immune checkpoint inhibitor, for patients with advanced, refractory squamous non-small-cell lung cancer (CheckMate 063): a phase 2, single-arm trial. *Lancet Oncol*. 2015;16(3): 257-265.

Downloaded from http://ashpublications.org/blood/article-pdf/137/13/1777/1803993/bloodbld2020005867.pdf by Rikhia Chakraborty on 03 December 2021

50. Topalian SL, Hodi FS, Brahmer JR, et al. Safety, activity, and immune correlates of anti-PD-1 antibody in cancer. *N Engl J Med*. 2012; 366(26):2443-2454.

51. Diamond EL, Durham BH, Haroche J, et al. Diverse and Targetable Kinase Alterations Drive Histiocytic Neoplasms. *Cancer Discov*. 2016;6(2):154-165.

52. Zhang Y, Velez-Delgado A, Mathew E, et al. Myeloid cells are required for PD-1/PD-L1 checkpoint activation and the establishment of an immunosuppressive environment in pancreatic cancer. *Gut*. 2017;66(1):124-136.

53. Das R, Bar N, Ferreira M, et al. Early B cell changes predict autoimmunity following combination immune checkpoint blockade. *J Clin Invest*. 2018;128(2):715-720.

Downloaded from http://ashpublications.org/blood/article-pdf/137/13/1777/1803993/bloodbld2020005867.pdf by Rikhia Chakraborty on 03 December 2021

**Supplementary File**

# Overcoming T cell exhaustion in Langerhans cell histiocytosis: PD-1 blockade and targeted MAPK inhibition are synergistic in a mouse model of LCH

**Running Title: Synergistic action of MAPK inhibition and PD-1 blockade in LCH**

Amel Sengal[1,2], Jessica Velazquez[1,2], Meryl Hahne[1], Thomas M Burke[1-3], Harshal Abhyankar[1], Robert Reyes[1], Walter Olea[1], Brooks Scull[1], Olive S. Eckstein[1], Camille Bigenwald[4,5], Catherine M Bollard[6,7], Wendong Yu[8], Miriam Merad[4,5], Kenneth L McClain[1,2], Carl E Allen[1-3,#] Rikhia Chakraborty[1,2,#]

[1]Texas Children's Cancer Center, Texas Children's Hospital, Houston, TX; [2]Division of Pediatric Hematology-Oncology, Department of Pediatrics, Baylor College of Medicine, Houston, TX; [3]Program in Translational Biology and Molecular Medicine, Baylor College of Medicine, Houston, TX; [4]Department of Oncological Sciences, Tisch Cancer Institute, and [5]Department of Dermatology, Icahn School of Medicine, New York, NY 10029; [6]Center for Cancer and Immunology Research, Departments of Pediatrics and Microbiology, Immunology and Tropical Medicine, Children's National Medical Center and [7]The George Washington University, Washington, District of Columbia; [8]Department of Pathology, Baylor College of Medicine, Houston, TX

**Supplementary Table 1-3**

**Supplementary Figure Legends**

**Supplementary Figure 1-8**

**Supplementary Table 1. LCH patient characteristics.** No skin limiting patient was included in this study.

| | Total n = 15 |
|---|---|
| Age (years) | |
| *Mean (SD)* | 6.73 |
| *Median (Range)* | 5 |
| Gender, n (%) | |
| *Male* | 7 (46.6) |
| *Female* | 8 (53.3) |
| Risk | |
| *Low* | 12 |
| *High* | 3 |
| Extent of Disease | |
| *Single* | 7 |
| *Multi* | 8 |
| *BRAF* mutation status | |
| *Wild type* | 6 |
| *BRAF*V600E | 9 |

**Supplementary Table 2. List of antibodies used in CyTOF.**

| HUMAN | | | |
|---|---|---|---|
| **Marker** | **Label** | **Source** | **Catalog #** |
| BATF | 154Sm | DVS-Fluidigm | 3154012A |
| CCR4 | 152Sm | R&D | MAB1567 |
| CD11a | 168Er | BioLegend | 301202 |
| CD11c | 147SM | DVS-Fluidigm | 3147008B |
| CD127, IL-7Ra | 176Yb | DVS-Fluidigm | 3176004B |
| CD152, CTLA-4 | 161Dy | DVS-Fluidigm | 3161004B |
| CD154 | 168Er | DVS-Fluidigm | 3168006B |
| CD197, CCR7 | 159Tb | DVS-Fluidigm | 3159003A |
| CD1a | 167Er | DVS-Fluidigm | 3167012B |
| CD207 | 175Lu | DVS-Fluidigm | 3175016B |
| CD223, LAG-3 | 149Sm | R&D | AF2319 |
| CD25 | 169Tm | DVS-Fluidigm | 3169003B |
| CD25 | 148Nd | BD | 555430 |
| CD27 | 167Er | DVS-Fluidigm | 3167002B |
| CD273, PD-L2 | 172Yb | DVS-Fluidigm | 3172014B |
| CD274, PD-L1 | 150Nd | BioLegend | 329702 |
| CD279, PD1 | 160Gd | Miltenyi | 130-096-168 |
| CD279, PD1 | 158Gd | Miltenyi | 130-096-168 |
| CD279, PD1 | 175Lu | MBL | D133-3 |
| CD3 | 151Eu | BioLegend | 300443 |
| CD3 | 154Sm | DVS-Fluidigm | 3154003B |
| CD3 | 170Er | DVS-Fluidigm | 3170001B |
| CD39 | 160Gd | DVS-Fluidigm | 3160004B |
| CD4 | 145Nd | DVS-Fluidigm | 3145001B |
| CD40 | 165Ho | DVS-Fluidigm | 3165005B |
| CD44 | 166Er | DVS-Fluidigm | 3166001B |
| CD45 | 154Sm | DVS-Fluidigm | 3154001B |
| CD45 | 141Pr | DVS-Toronto | 3141009B |
| CD45RA | 153Eu | DVS-Fluidigm | 3153001B |
| CD45RO | 165Ho | DVS-Fluidigm | 3165011B |
| CD49d | 141PR | DVS-Fluidigm | 3141004B |
| CD57 | 172Yb | DVS-Fluidigm | 3712009B |
| CD69 | 162Dy | DVS-Fluidigm | 3162001B |
| CD80 | 162Dy | DVS-Fluidigm | 3162010B |
| CD86 | 150Nd | DVS-Fluidigm | 3150020B |
| CD8a | 146Nd | DVS-Fluidigm | 3146001B |
| CD95 | 164Dy | DVS-Fluidigm | 3164008B |
| FoxP3 | 162DY | DVS-Fluidigm | 3162024A |
| Galectin-9 | 163Dy | DVS-Fluidigm | 3163002B |

| | | | |
|---|---|---|---|
| GITR | 143Nd | BioLegend | 311602 |
| HLA-DR | 174Yb | DVS-Fluidigm | 3174001B |
| ICOS | 155Gd | BioLegend | 313502 |
| IFNg | 165Ho | DVS-Fluidigm | 3165002B |
| IL-2 | 166Er | DVS-Fluidigm | 3166002B |
| Ki67 | 168ER | DVS-Fluidigm | 3168001B |
| OX40 | 148Nd | BioLegend | 350002 |
| TIGIT | 160Gd | eBioscience | 16-9500-82 |
| TIM-3 | 156Gd | BioLegend | 345002 |
| TNFa | 152Sm | DVS-Fluidigm | 3152002B |
| **MOUSE** | | | |
| **Marker** | **Label** | **Source** | **Catalog #** |
| CD11b | 148Nd | DVS-Fluidigm | 3148003B |
| CD11c | 142Nd | DVS-Fluidigm | 3142003B |
| CD14 | 169Tm | BioLegend | 123302 |
| CD16/32 | 144Nd | DVS-Fluidigm | 3144009B |
| CD223 LAG-3 | 163Dy | BioLegend | 125202 |
| CD274 PD-L1 | 154Sm | BioLegend | 124303 |
| CD279 PD1 | 159Tb | DVS-Fluidigm | 3159024B |
| CD3e | 152Sm | DVS-Fluidigm | 3152004B |
| CD4 | 172Yb | DVS-Fluidigm | 3172003B |
| CD45 | 147Sm | DVS-Fluidigm | 3147003B |
| CD49d | 153Eu | BioLegend | 103701 |
| CD62L | 160Gd | DVS-Fluidigm | 3160008B |
| CD64 | 151Eu | DVS-Fluidigm | 3151012B |
| CD69 | 156Gd | BioLegend | 104533 |
| CD71 | 139La | BioLegend | 113802 |
| CD8a | 168Er | DVS-Fluidigm | 3168003B |
| I-A/I-E (MHCII) | 174Yb | DVS-Fluidigm | 3174003B |
| Ly-6G/C Gr-1 | 175Lu | BioLegend | 108402 |
| Ter119 | 162Dy | DVS-Fluidigm | 3162003B |

**Supplementary Table 3. Quantification of LCs and infiltrating immune cells.** *LC*, Langerhans cells; *MDSC*, myeloid deriver suppressor cells. P-value - One-way ANOVA with Turey *post hoc* multiple comparison.

| | *BRAF*V600E (n = 9) | *BRAF* WT (n = 6) | Skin (n = 5) |
|---|---|---|---|
| $CD207^+$ LCs | 31.77% ± 9.09%; P = 0.0011 compared to *BRAF* WT; P = 0.0308 compared to skin control | 16.33% ± 4.23%; P<0.0001 compared to skin control | 5.00% ± 1.00% |
| T cells | 25.00% ± 3.39%; P = 0.0116 compared to *BRAF* WT; P<0.0001 compared to skin control | 33.00% ± 7.24%; P<0.0001 compared to skin control | 3.00% ± 1.58% |
| MDSCs | 33.00% ± 72.35%; P = 0.3576 compared to *BRAF* WT; P<0.0001 compared to skin control | 30.34% ± 5.61%; P<0.0001 compared to skin control | 13.60% ± 2.08% |

**Supplementary figure legends**

**Supplementary Figure 1.** (**A-C**) viSNE plots of live cells from representative LCH patient lesion biopsy with *BRAF*V600E (**A**), *BRAF* WT (**B**), and normal skin biopsy (**C**). (**D**) Quantification of lesion-infiltrating cells shown in **A-C** (n=6 *BRAF* WT; n=9 *BRAF*V600E) in comparison to normal skin biopsies (n=5). (**E**) Quantification of relative abundance of CD4 and CD8 T cells in LCH lesion infiltrate (n=5 each) or tonsil control (n=5). *P<0.05 for both $CD4^+$ and $CD8^+$ compared to tonsil control. (**F**) CD4/Treg (C25+FOXP3+) ratios in indicated samples (n=5 each). For ***D-F***, data are mean ± SD; *P<0.05; **P<0.01; ***P<0.001, ****P<0.0001, ns, not significant (P>0.05) – one-way ANOVA with Tukey's post hoc test. *LC*, Langerhans cells; *NK*, natural killer cell; *MDSC*, myeloid deriver suppressor cells.

**Supplementary Figure 2.** Relative T cell subtypes in tonsil (**A**), skin (**B**), and histiocytic neoplasm (**C**) assessed by FlowSOM) analysis and visualized as pie charts. Mean-marker value for indicated markers are shown in the pie charts. *HLH/MAS*, hemophagocytic lymphohistiocytosis/macrophage activation syndrome.

**Supplementary Figure 3.** (**A**) FlowSOM analysis of expression of different immune checkpoint receptors on $CD8^+$ T cells from skin control. (**B**, **C**) Quantification of relative expression of TIM-3 (**B**) and LAG-3 (**C**) in $CD8^+$ T cells as determined by CyTOF (n=5 each). (**D**) Expression of different immune checkpoint receptors on LCH lesion infiltrating $CD4^+$ T cells. Analysis of CyTOF data was done using FlowSOM and visualized as pie charts. (**E**, **F**) Quantification of relative expression of PD-1 (**E**) and co-expression of immune checkpoint receptors (**F**) in $CD4^+$ T cells as determined by CyTOF (n=5 each). (**F**) Quantification of PD-L1 and PD-L2 expression on CD207 gated cells obtained from LCH lesion and skin controls (n=5 each). For ***B***, ***C***, ***E-G***, data are mean ± SD. For ***B***, ***C***, and ***E***, *P<0.05; **P<0.01; ***P<0.001, ****P<0.0001, ns, not significant (P>0.05) – one-way ANOVA with Tukey's post hoc test. For ***F*** and ***G***, ns, not significant (P>0.05) – WMW test.

**Supplementary Figure 4.** (**A**) Quantification of lung lesion-infiltrating cells in *BRAF*V600E$^{Cd11c}$ mice (n=5) in comparison to *Cre*$^{-/-}$ littermate control mice (n=3) shown in **Figure 4A**. (**B**) Quantification of relative abundance of CD4 and CD8 T cells in lung lesion-infiltrating cells in *BRAF*V600E$^{Cd11c}$ (n=5) and *Cre*$^{-/-}$ littermate control mice (n=3). (**C**) Relative expression of indicated cytokines in $CD8^+$ T cells isolated from lung lesions of *BRAF*V600E$^{Cd11c}$ or *Cre*$^{-/-}$ littermate control mice (n=3 each), pre- and post-activation with PMA and Ionomycin (PMA/Iono). Data in ***A-C*** are mean ± SD. (**D**) $CD8^+$ T cells isolated from lung lesions of *BRAF*V600E$^{Cd11c}$, but not from *Cre*$^{-/-}$ littermate control mice (n=3 each), were dysfunctional as determined by mixed lymphocyte reaction (MLR) assay. Data points represent averaged triplicate measures from cells isolated from 4 LCH patients or controls. *P<0.05, **P<0.01, ***P<0.001, ****P<0.0001, ns, not significant (P>0.05) – WMW test for ***A*** and one-way ANOVA with Tukey's *post hoc* test for ***B-D***.

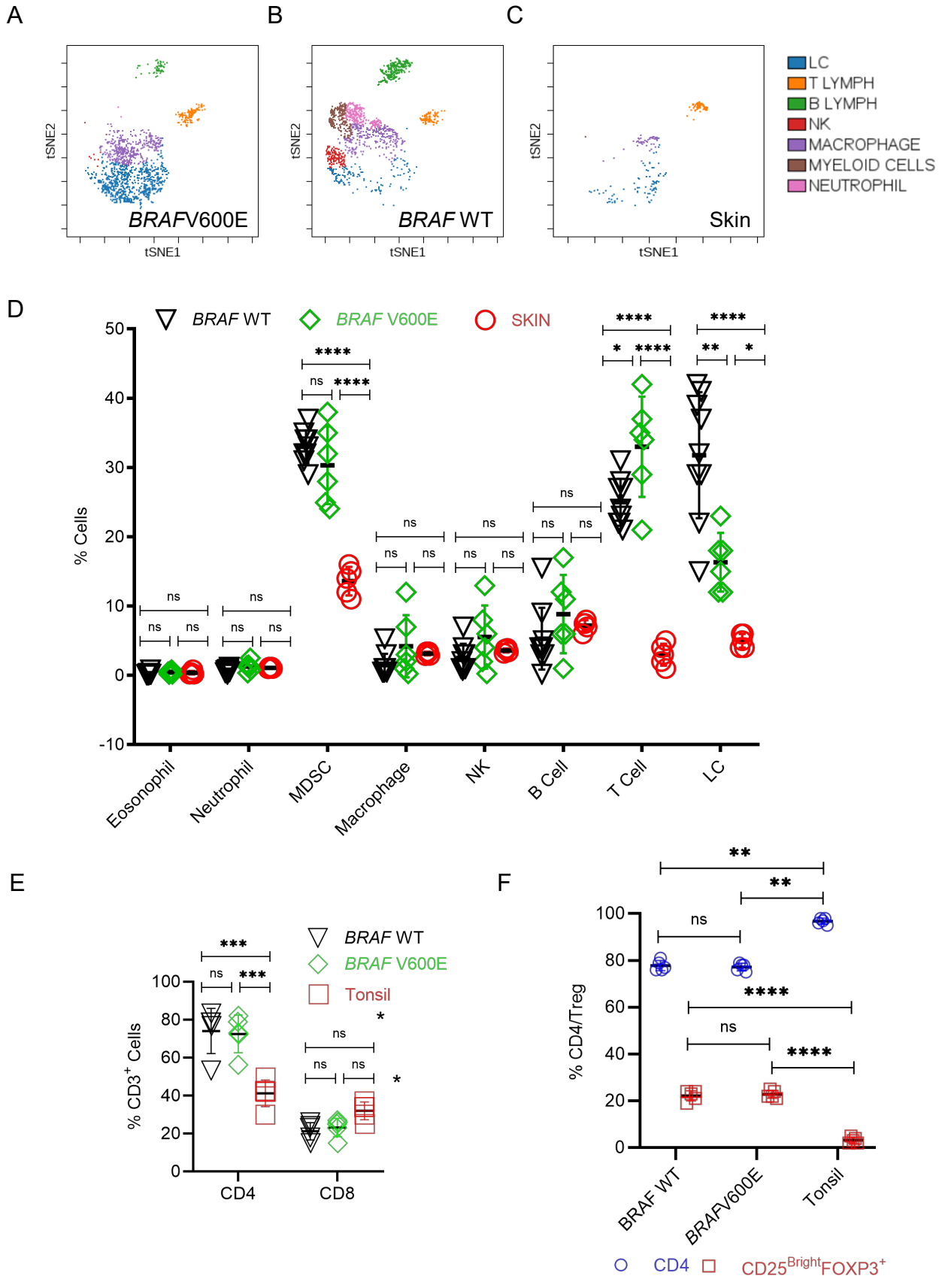
**Supplementary Figure 5.** (**A**) Representative immunohistochemistry images of infiltrating T cells ($CD8^+$ and $CD4^+$) and DCs ($CD11b^+$ and $CD11c^+$) in liver in the indicated experimental groups. Scale bar, 100 μm. (**B**) Quantification of relative liver lesion infiltrating $CD8^+$ and $CD4^+$ T cells in indicated experimental groups. Data are mean ± SD (n=9 mice per group); ***P<0.001, ****P<0.0001, ns, not significant (P>0.05) – one-way ANOVA with Tukey's *post hoc* test.

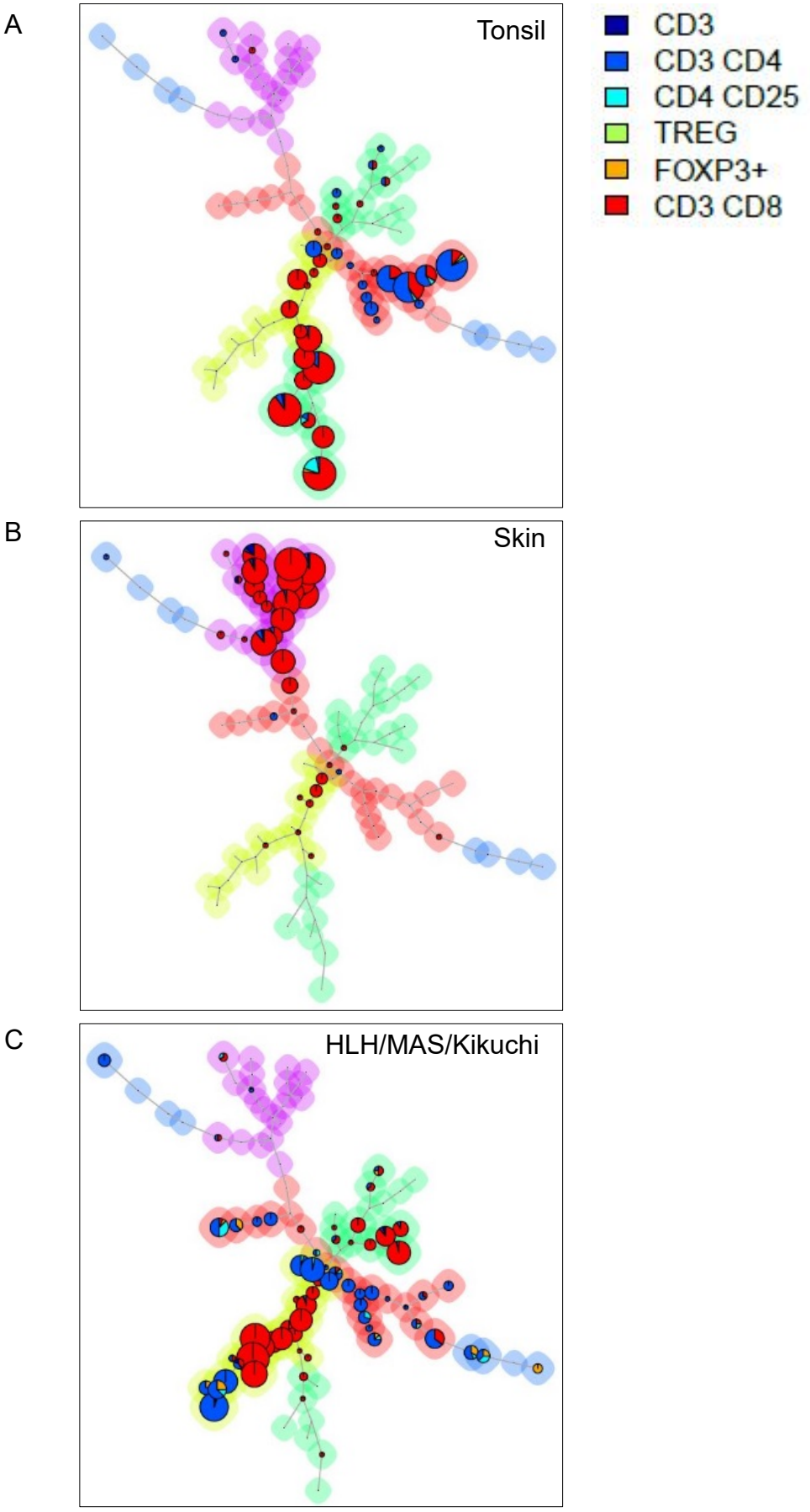
**Supplementary Figure 6.** (**A**, **C**) Representative immunohistochemistry images of infiltrating T cells ($CD8^+$ and $CD4^+$) and DCs ($CD11b^+$ and $CD11c^+$) in lung (**A**) and liver (**C**) in the indicated experimental groups. Scale bar, 100 μm. (**B**, **D**) Quantification of liver lesion infiltrating $CD8^+$ and $CD4^+$ T cells in the indicated experimental groups. Data are mean ± SD (n=9 mice per group);

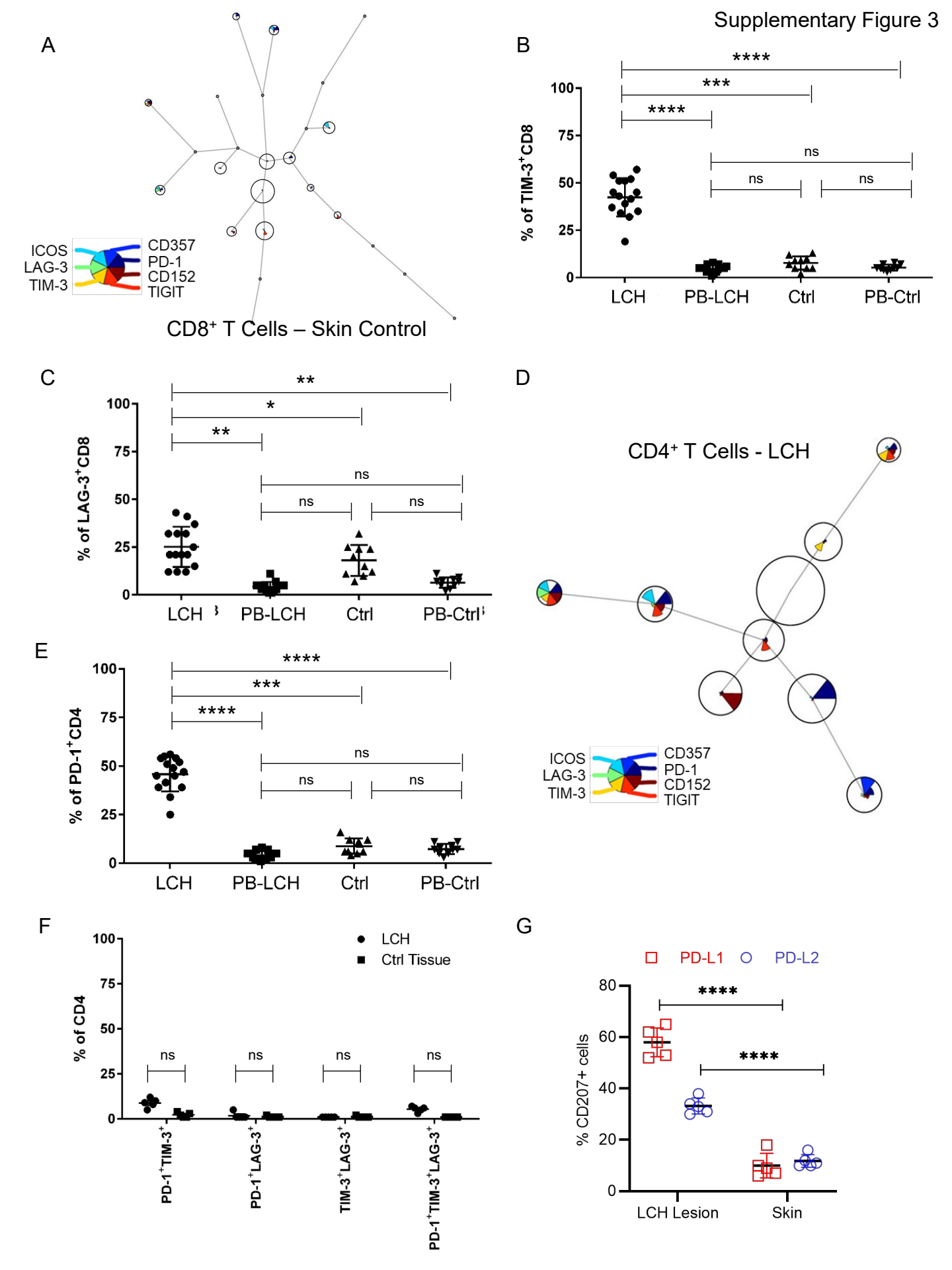
**P<0.01, ****P<0.0001, ns, not significant (P>0.05) – one-way ANOVA with Tukey's *post hoc* test.

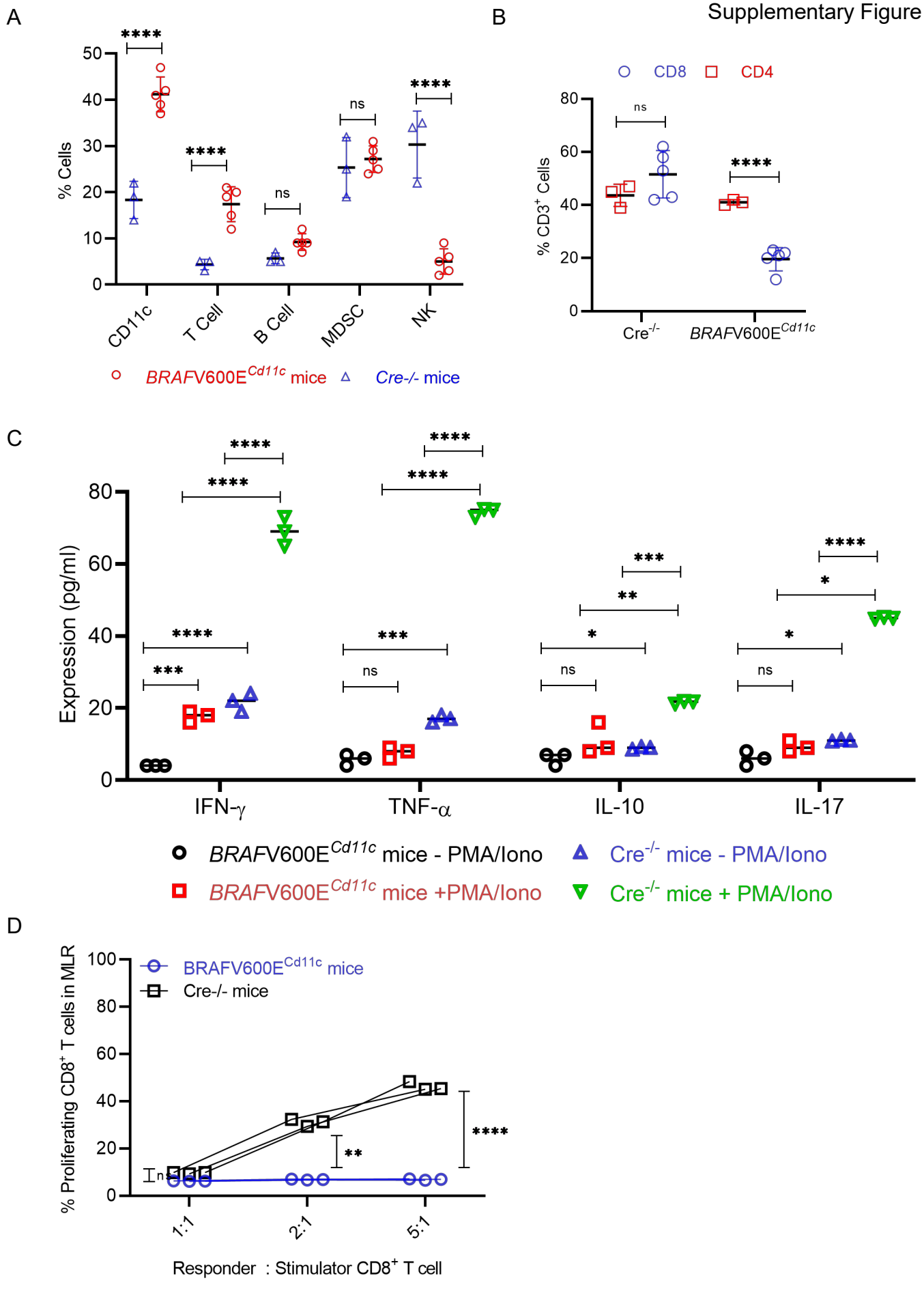
**Supplementary Figure 7.** (**A-C**) Expression of different immune checkpoint receptors on $CD8^+$ T cells isolated from lung lesions of *BRAF*V600E$^{Cd11c}$ mice treated with Isotype + Veh MEKi (**A**), α-PD-L1 + MEKi (**B**), and α-PD-1 + MEKi (**C**). Analysis of CyTOF data was done using self-organizing map (FlowSOM) and visualized as pie charts. (**D**) Quantification of relative expression of PD-1 in $CD8^+$ T cells isolated from lung lesions of *BRAF*V600E$^{Cd11c}$ mice from the indicated experimental groups as determined by CyTOF (n=5 each). (**E**) Quantification of PD-L1 and PD-L2 expression on $CD11c^+$ gated cells obtained from lung lesions of *BRAF*V600E$^{Cd11c}$ mice from the indicated experimental groups (n=5 each). Data in ***D, E*** are mean ± SD. *P<0.05; ****P<0.0001 – one-way ANOVA with Tukey's *post hoc* test.

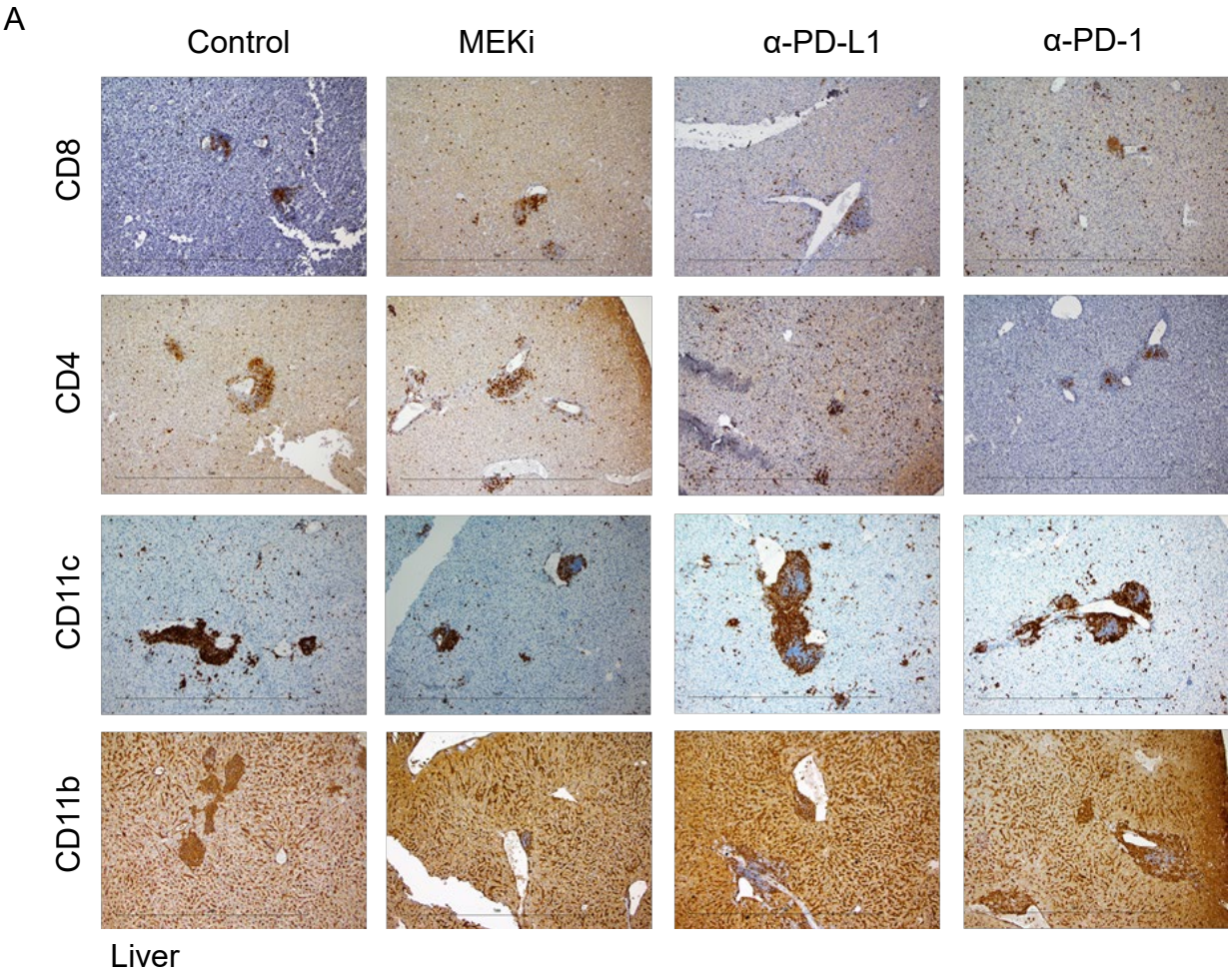
**Supplementary Figure 8.** Relative expression of indicated cytokines in $CD8^+$ T cells isolated from lung lesions of *BRAF*V600E$^{Cd11c}$ mice treated with Isotype + Veh MEKi, α-PD-L1 + MEKi, and α-PD-1 + MEKi (n=5 each), pre- and post-activation with PMA and Ionomycin (PMA/Iono). Data are mean ± SD. ****P<0.0001, ns, not significant (P>0.05) – one-way ANOVA with Tukey's *post hoc* test.

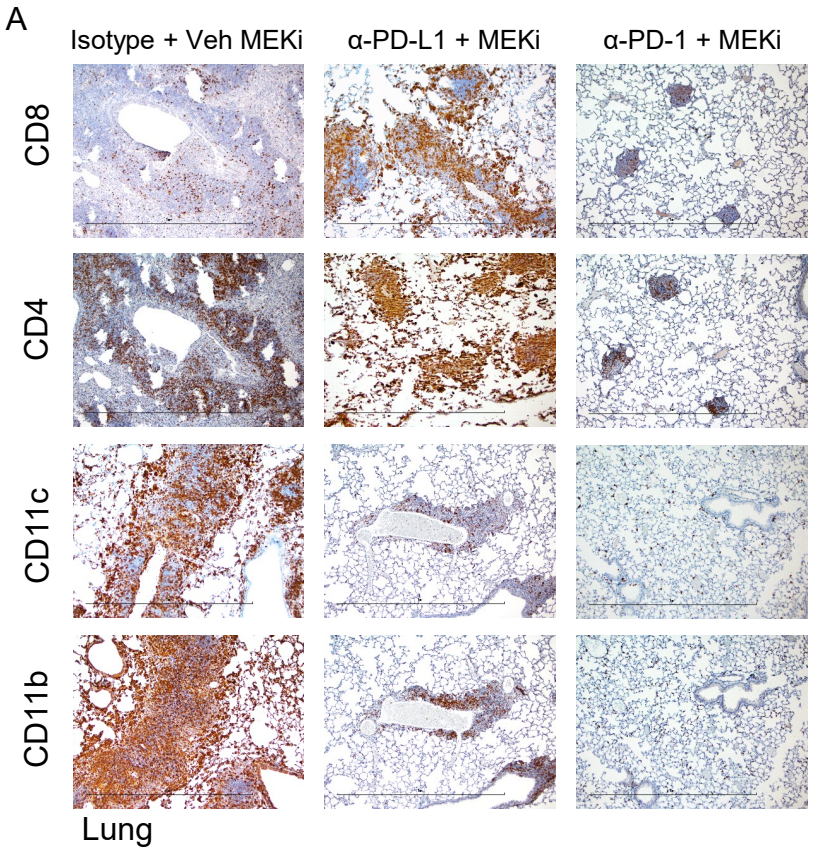

A
B
C
tSNE2
tSNE1
BRAFV600E
BRAF WT
Skin
LC
T LYMPH
B LYMPH
NK
MACROPHAGE
MYELOID CELLS
NEUTROPHIL
D
BRAF WT
BRAF V600E
SKIN
% Cells
Eosonophil
Neutrophil
MDSC
Macrophage
NK
B Cell
T Cell
LC
E
% CD3+ Cells
CD4
CD8
Tonsil
F
% CD4/Treg
BRAF WT
BRAFV600E
Tonsil
CD4
CD25BrightFOXP3+

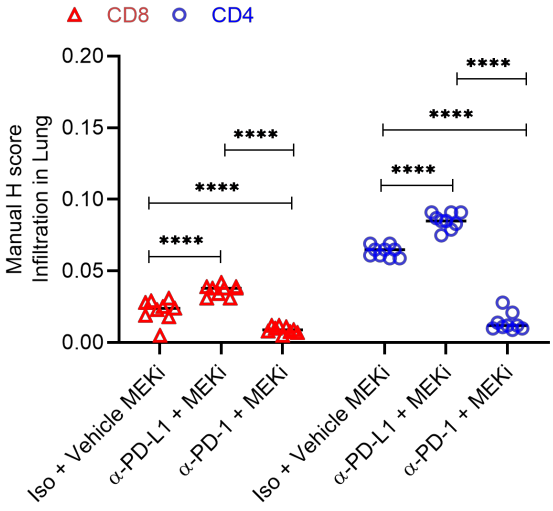

A
Tonsil
B
Skin
C
HLH/MAS/Kikuchi
CD3
CD3 CD4
CD4 CD25
TREG
FOXP3+
CD3 CD8

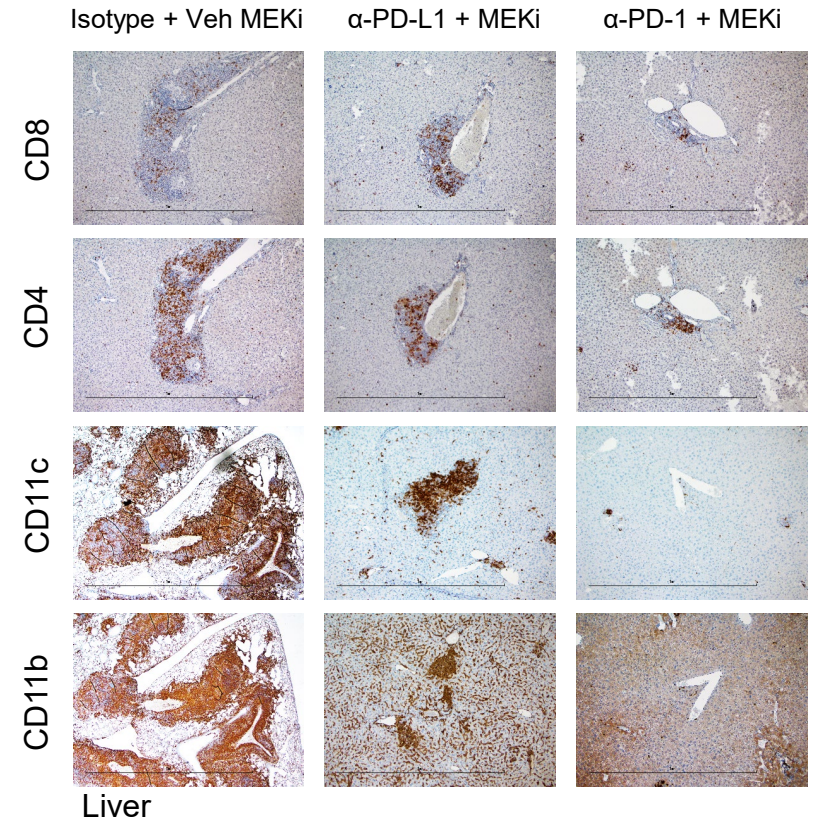

A
ICOS
LAG-3
TIM-3
CD357
PD-1
CD152
TIGIT
CD8⁺ T Cells – Skin Control
B
% of TIM-3⁺CD8
LCH
PB-LCH
Ctrl
PB-Ctrl
C
% of LAG-3⁺CD8
D
CD4⁺ T Cells - LCH
E
% of PD-1⁺CD4
F
% of CD4
LCH
Ctrl Tissue
PD-1⁺TIM-3⁺
PD-1⁺LAG-3⁺
TIM-3⁺LAG-3⁺
PD-1⁺TIM-3⁺LAG-3⁺
G
PD-L1
PD-L2
% CD207+ cells
LCH Lesion
Skin

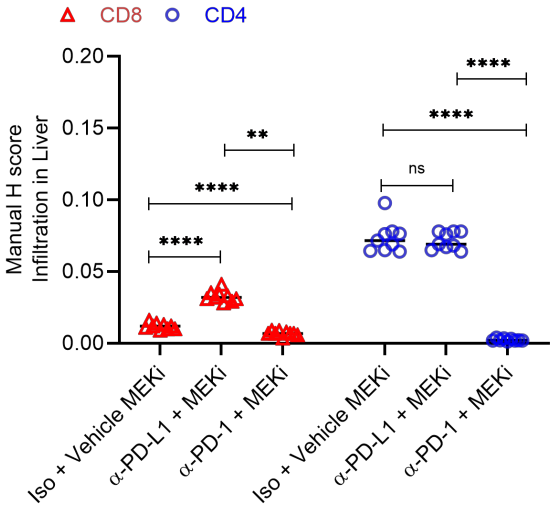

A
% Cells
CD11c
T Cell
B Cell
MDSC
NK
BRAFV600E Cd11c mice
Cre-/- mice
B
CD8
CD4
% CD3+ Cells
Cre-/-
BRAFV600E Cd11c
C
Expression (pg/ml)
IFN-γ
TNF-α
IL-10
IL-17
BRAFV600E Cd11c mice - PMA/Iono
Cre-/- mice - PMA/Iono
BRAFV600E Cd11c mice +PMA/Iono
Cre-/- mice + PMA/Iono
D
% Proliferating CD8+ T cells in MLR
BRAFV600E Cd11c mice
Cre-/- mice
1:1
2:1
5:1
Responder : Stimulator CD8+ T cell

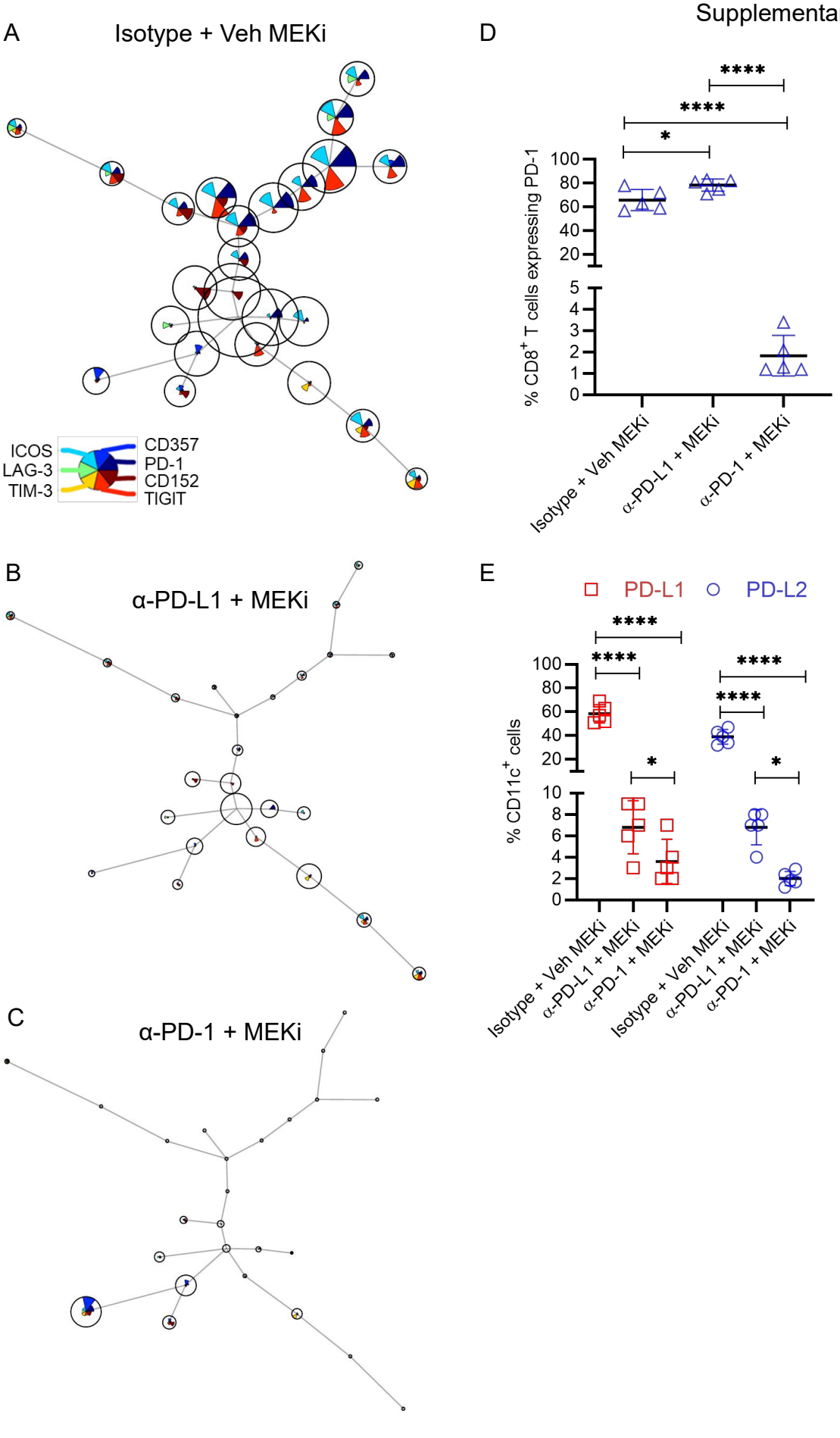

A
Control
MEKi
α-PD-L1
α-PD-1
CD8
CD4
CD11c
CD11b
Liver
B
CD8
CD4
Manual H score
Infiltration in Liver
0.20
0.15
0.10
0.05
0.00
****
****
****
****
****
ns
ns
****
****
****
***
Control
α-PD-L1
α-PD-1
MEKi
Control
α-PD-L1
α-PD-1
MEKi

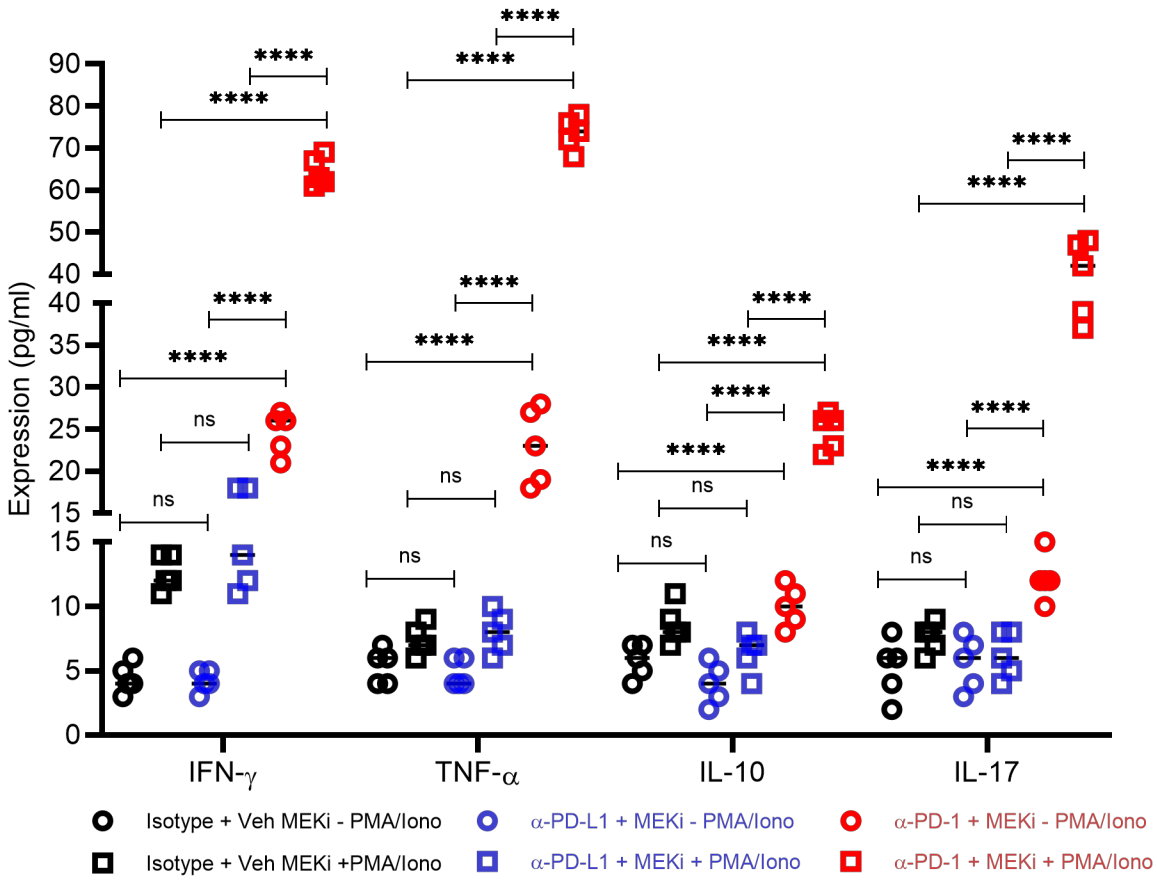

A
Isotype + Veh MEKi
α-PD-L1 + MEKi
α-PD-1 + MEKi
CD8
CD4
CD11c
CD11b
Lung


B
CD8
CD4
Manual H score
Infiltration in Lung
0.20
0.15
0.10
0.05
0.00
****
****
****
****
****
****
Iso + Vehicle MEKi
α-PD-L1 + MEKi
α-PD-1 + MEKi
Iso + Vehicle MEKi
α-PD-L1 + MEKi
α-PD-1 + MEKi


C
Isotype + Veh MEKi
α-PD-L1 + MEKi
α-PD-1 + MEKi
CD8
CD4
CD11c
CD11b
Liver


D
CD8
CD4
Manual H score
Infiltration in Liver
0.20
0.15
0.10
0.05
0.00
****
**
****
ns
****
****
Iso + Vehicle MEKi
α-PD-L1 + MEKi
α-PD-1 + MEKi
Iso + Vehicle MEKi
α-PD-L1 + MEKi
α-PD-1 + MEKi


A
Isotype + Veh MEKi
ICOS
LAG-3
TIM-3
CD357
PD-1
CD152
TIGIT
B
α-PD-L1 + MEKi
C
α-PD-1 + MEKi
D
% CD8+ T cells expressing PD-1
Isotype + Veh MEKi
α-PD-L1 + MEKi
α-PD-1 + MEKi
E
PD-L1
PD-L2
% CD11c+ cells
Isotype + Veh MEKi
α-PD-L1 + MEKi
α-PD-1 + MEKi


Expression (pg/ml)
90
80
70
60
50
40
40
35
30
25
20
15
15
10
5
0
****
ns
IFN-γ
TNF-α
IL-10
IL-17
Isotype + Veh MEKi - PMA/Iono
Isotype + Veh MEKi +PMA/Iono
α-PD-L1 + MEKi - PMA/Iono
α-PD-L1 + MEKi + PMA/Iono
α-PD-1 + MEKi - PMA/Iono
α-PD-1 + MEKi + PMA/Iono

nature medicine

ARTICLES

https://doi.org/10.1038/s41591-021-01304-x

Check for updates

# *BRAF*$^{V600E}$-induced senescence drives Langerhans cell histiocytosis pathophysiology

Camille Bigenwald[1,2,3], Jessica Le Berichel[1,2,3], C. Matthias Wilk[1,2,3,7], Rikhia Chakraborty[4,7], Steven T. Chen[1,2,3,7], Alexandra Tabachnikova[1,2,3], Rebecca Mancusi[2,3], Harshal Abhyankar[4], Maria Casanova-Acebes[1,2,3], Ilaria Laface[1,2,3], Guray Akturk[1,2,3], Jenielle Jobson[1,2,3], Zoi Karoulia[1,2,3], Jerome C. Martin[1,2,3], John Grout[1,2,3], Anahita Rafiei[5], Howard Lin[4], Markus G. Manz[5], Alessia Baccarini[1,2,3], Poulikos I. Poulikakos[2,3], Brian D. Brown[1,2,3], Sacha Gnjatic[1,2,3], Amaia Lujambio[1,2,3], Kenneth L. McClain[4], Jennifer Picarsic[6], Carl E. Allen[4,7] and Miriam Merad[1,2,3,7] ✉

**Langerhans cell histiocytosis (LCH) is a potentially fatal condition characterized by granulomatous lesions with characteristic clonal mononuclear phagocytes (MNPs) harboring activating somatic mutations in mitogen-activated protein kinase (MAPK) pathway genes, most notably *BRAF*$^{V600E}$. We recently discovered that the *BRAF*$^{V600E}$ mutation can also affect multipotent hematopoietic progenitor cells (HPCs) in multisystem LCH disease. How the *BRAF*$^{V600E}$ mutation in HPCs leads to LCH is not known. Here we show that enforced expression of the *BRAF*$^{V600E}$ mutation in early mouse and human multipotent HPCs induced a senescence program that led to HPC growth arrest, apoptosis resistance and a senescence-associated secretory phenotype (SASP). SASP, in turn, promoted HPC skewing toward the MNP lineage, leading to the accumulation of senescent MNPs in tissue and the formation of LCH lesions. Accordingly, elimination of senescent cells using *INK-ATTAC* transgenic mice, as well as pharmacologic blockade of SASP, improved LCH disease in mice. These results identify senescent cells as a new target for the treatment of LCH.**

Histiocytoses are a group of conditions characterized by the accumulation of histiocytes in various tissues. Histiocytes, now more commonly known as mononuclear phagocytes (MNPs), consist of heterogeneous cells of myeloid origin that include dendritic cells and macrophages. Specifically, LCH results from the accumulation of CD207$^{+}$CD1a$^{+}$ cells that resemble Langerhans cells[1]. LCH occurs mostly in children with an incidence of 8.9 in $10^{6}$ children per year, similar to pediatric Hodgkin's lymphoma[2]. LCH can arise in a variety of settings from single bone lesions to life-threatening disseminated disease that affects the spleen, liver and bone marrow (BM). Front-line chemotherapy fails in more than 50% of patients with multisystem disease, highlighting the need for new therapies for this group of patients[3].

Activating somatic mutations in MAPK pathway genes, most notably *BRAF*$^{V600E}$, have been identified in 85% cases of LCH, specifically in the pathogenic CD207$^{+}$ cells within LCH lesions[4–7]. Importantly, we and others[8–10] recently discovered that the *BRAF*$^{V600E}$ mutation can also be identified in CD34$^{+}$ BM HPCs in patients with systemic LCH disease, which led to the reclassification of multifocal LCH as a myeloid neoplasia[3,7,11]. These new results revealed a new conundrum in LCH pathophysiology: how does the somatic *BRAF*$^{V600E}$ mutation in multipotent progenitor (MPP) cells lead to LCH lesions?

Here we explored the mechanisms by which the *BRAF*$^{V600E}$ mutation could potentially drive a multipotent hematopoietic progenitor to give rise to LCH lesions. Strikingly, we found that enforced expression of the *BRAF*$^{V600E}$ mutation in early mouse and human multipotent HPCs induced a senescence program that led to HPC growth arrest, apoptosis resistance and SASP induction. This SASP, in turn, promoted multipotent HPC skewing toward the MNP lineage, away from other hematopoietic lineages. *BRAF*$^{V600E}$-induced senescence persisted in differentiated MNPs that accumulated in tissues, where SASP induction and sustained MNP survival contributed to the formation of LCH lesions. Accordingly, we found that genetic elimination of senescent cells using *INK-ATTAC* (*Ink4a*/*Arf* or *Cdkn2a*–apoptosis through targeted activation of caspase) transgenic mice, as well as pharmacologic blockade of SASP, improved LCH disease burden in mice. These results transform our understanding of LCH pathophysiology and identify senescent cells as a new target for the treatment of LCH.

## Results

**Expression of the *BRAF*$^{V600E}$ mutation in mouse multipotent HPCs is sufficient to drive to LCH lesion formation.** To examine whether *BRAF*-V600E$^{+}$ HPCs can drive LCH lesions, we enforced expression of the *BRAF*$^{V600E}$ mutation in cells expressing Scl (also

[1]Precision Immunology Institute, Icahn School of Medicine at Mount Sinai, New York, NY, USA. [2]Department of Oncological Sciences, Icahn School of Medicine at Mount Sinai, New York, NY, USA. [3]The Tisch Cancer Institute, Icahn School of Medicine at Mount Sinai, New York, NY, USA. [4]Texas Children's Cancer Center, Texas Children's Hospital, Baylor College of Medicine, Houston, TX, USA. [5]Department of Medical Oncology and Hematology, University Hospital Zurich, Comprehensive Cancer Center Zurich, Zurich, Switzerland. [6]Department of Pathology and Laboratory Medicine, Cincinnati Children's Hospital Medical Center, Cincinnati, OH, USA. [7]These authors contributed equally: C. Matthias Wilk, Rikhia Chakraborty, Steven T. Chen, Carl E. Allen, Miriam Merad. ✉e-mail: miriam.merad@mssm.edu

known as Tal1), a molecule expressed specifically in long-term and short-term hematopoietic stem cells (HSCs) in mice[12]. We genetically engineered somatic mosaicism for a *BRAF*$^{V600E}$ allele linked to a yellow fluorescent protein (YFP) in HSCs using tamoxifen-inducible targeting in *Scl-cre*$^{ER}$ mice, which we named *BRAF*-V600E$^{Scl+}$ and used *BRAF*-wild-type (WT)$^{Scl+}$ mice as control littermates (Fig. 1a). Thus, *Rosa*$^{YFP+}$ cells carried the *BRAF*$^{V600E}$ mutation in *BRAF*-V600E$^{Scl+}$ mice, whereas *Rosa*$^{YFP+}$ cells in *BRAF*-WT$^{Scl+}$ mice did not carry the mutation but underwent *Rosa26*-locus driven Cre recombination. Pulsed administration of tamoxifen led to YFP expression in 30% of HSCs, providing the opportunity to compare *BRAF*-V600E$^{+}$(YFP$^{+}$)$^{Scl+}$ cells to *BRAF*$^{WT}$(YFP$^{-}$)$^{Scl+}$ cells within the same mouse (Fig. 1b). Strikingly, *BRAF*-V600E$^{Scl+}$ mice developed substantial organomegaly, granulomatous bone lesions and BM aplasia within 4 weeks of tamoxifen administration, while *BRAF*-WT$^{Scl+}$ control littermates did not (Fig. 1c and Extended Data Fig. 1a–c). Histological analysis of hematoxylin and eosin (H&E)-stained formalin-fixed paraffin-embedded (FFPE) tissue sections revealed an accumulation of histiocytes within granulomatous lesions, multinucleated giant cells and an inflammatory infiltrate in the liver, lungs and dermises of *BRAF*-V600E$^{Scl+}$ mice (Fig. 1d and Extended Data Fig. 1d). Immunohistochemistry analysis revealed that many histiocytes expressed CD207 (Fig. 1d). Flow cytometry analysis confirmed the significant increase in immune cell infiltration and the expansion of the MNP compartment within the immune cell infiltrate (Fig. 1f and Extended Data Fig. 1e). Importantly, in the skin, MNPs mostly accumulated in the dermis and were absent from the epidermis (Fig. 1f), mimicking the dermotropism of the human disease. Flow cytometry analysis also revealed the preferential expansion of MNPs within the *BRAF*-V600E$^{YFP+}$ immune cell compartment in tissues known as targets of LCH lesions (Fig. 1e and Extended Data Fig. 1f).

**Humanized mice reconstituted with human CD34$^{+}$ HPCs expressing the *BRAF*$^{V600E}$ mutation develop LCH-like disease.** To determine whether expression of the *BRAF*$^{V600E}$ mutation in human HPCs could also lead to LCH disease, we generated a lentiviral vector expressing the GFP reporter together with the *BRAF*$^{V600E}$ mutation (*BRAF*-V600E$^{hu}$) or the *NGFR* truncated gene (nerve growth factor receptor (NGFR)$^{hu}$) under the *EF1A1* promoter (Extended Data Fig. 1g). HPC transduction efficiency, around 40%, led to sustained extracellular signal-regulated kinase (ERK) phosphorylation in *BRAF*-V600E$^{hu}$ but not in NGFR$^{hu}$ HPCs (Extended Data Fig. 1h,i). We reconstituted sublethally irradiated NOD-severe combined immunodeficient (SCID) gamma (NSG) mice with human CD34$^{+}$ cord blood HPCs transduced with this lentiviral vector (Fig. 1g). NSG mice deteriorated within 2 months following reconstitution with *BRAF*-V600E$^{hu}$CD34$^{+}$ HPCs but not NGFR$^{hu}$CD34$^{+}$ HPCs and developed an expansion of CD11c$^{+}$CD14$^{+}$ MNP cells circulating in the blood (Extended Data Fig. 1j), accompanied by an accumulation of CD1a$^{+}$CD207$^{+}$ cells in the liver, lung and spleen, pathognomonic of LCH disease (Fig. 1h). These results, together with our data showing that *BRAF*-V600E$^{Scl+}$ mice develop LCH-like lesions, establish that expression of the *BRAF*$^{V600E}$ mutation in mouse and human early HPCs is sufficient to drive LCH lesion formation.

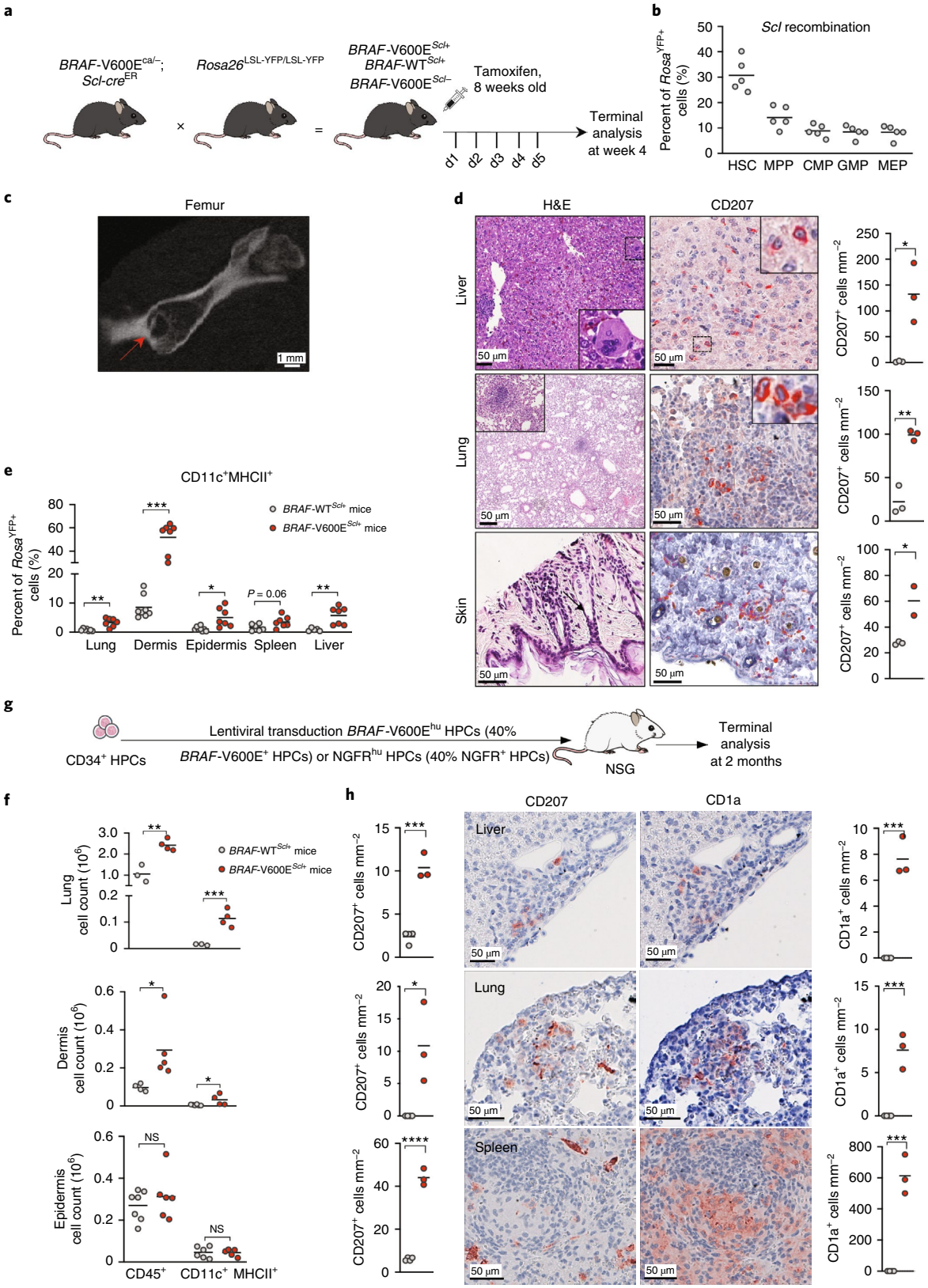
***BRAF*$^{V600E}$ HPCs differentiate predominantly toward the MNP lineage.** To explore how the *BRAF*$^{V600E}$ mutation in early HPCs drives the specific accumulation of MNPs in the periphery, we measured the differentiation potential of *BRAF*-V600E$^{+}$YFP$^{+}$ HPCs in *BRAF*-V600E$^{Scl+}$ mice. Strikingly, we found that levels of *BRAF*-V600E$^{+}$ HSCs and MPPs were reduced, while levels of *BRAF*-V600E$^{+}$ granulocyte–macrophage progenitors (GMPs) were significantly expanded in the BM compared to those in *BRAF*$^{WT}$ progenitors (Fig. 2a and Extended Data Fig. 2a), suggesting that the *BRAF*-V600E$^{+}$ HPCs failed to expand and were instead biased toward the myeloid lineage. The expansion of *BRAF*-V600E$^{+}$ GMPs was associated with a remarkable expansion of BM *BRAF*-V600E$^{+}$ monocytes, macrophages and dendritic cells, whereas BM *BRAF*-V600E$^{+}$ neutrophils did not expand (Fig. 2b and Extended Data Fig. 2b). To directly examine whether the *BRAF*$^{V600E}$ mutation skewed HPC commitment to the MNP lineage, we cultured purified HPCs from *BRAF*-V600E$^{Scl+}$ or *BRAF*-WT$^{Scl+}$ mice in methylcellulose and measured HPC progeny using a colony-forming unit (CFU) assay that reflects differentiation into committed progenitors. Consistent with the lineage bias observed in vivo, we found that *BRAF*$^{V600E}$ HPCs preferentially differentiated into CFUs consisting of macrophage progenitors (CFU-M), while numbers of granulocytic progenitors (CFU-G) and erythroid progenitors, also called burst-forming unit erythroids (BFU-E), were reduced (Fig. 2c).

We also examined whether the *BRAF*$^{V600E}$ mutation affected human HPC lineage commitment. Consistent with the results obtained from murine *BRAF*-V600E$^{Scl+}$ HPCs, we found that human *BRAF*-V600E$^{hu}$ HPCs preferentially differentiated into the MNP lineage (Fig. 2d). Remarkably, using the same CFU assay applied in mice, we found that human *BRAF*-V600E$^{+}$ HPCs differentiated preferentially into CFU-GM and CFU-M colonies but not into CFU-G colonies, whereas NGFR$^{+}$ HPCs retained a pluripotent differentiation potential (Fig. 2e and Extended Data Fig. 2c). Gene expression profiling of human *BRAF*-V600E$^{+}$GFP$^{+}$ and control NGFR$^{+}$GFP$^{+}$ HPCs 7 d after culture in stem cell medium revealed enrichment for an MNP signature in *BRAF*-V600E$^{+}$ HPCs that included the expression of classical dendritic cell genes (*BATF3*, *IRF4*, *CLEC10A*) as well as that of macrophage genes (*CSF1R*, *CD68*, *SPP1*), while HPC differentiation into granulocytes was strongly reduced compared to that in control NGFR$^{+}$ HPCs (Fig. 2f).

To further confirm the MNP skewing of *BRAF*-V600E$^{+}$ HPCs in patients with LCH, we performed RNA-seq of purified CD34$^{+}$ HPCs isolated from the BM of patients with LCH

**Fig. 1 | Expression of the *BRAF*$^{V600E}$ mutation in mouse and human multipotent HPCs is sufficient to lead to LCH lesions. a**, Cartoon shows the experimental breeding scheme used to generate *BRAF*-V600E$^{Scl+}$ mice and control littermates. d1–5 indicates day 1–5. **b**, Percentage of *Rosa*$^{YFP+}$ cells among purified hematopoietic progenitors in *BRAF*-WT$^{Scl+}$ mice 4 weeks after tamoxifen injections ($n=5$ mice). CMP, common myeloid progenitor; MEP, megakaryocytic erythroid progenitor. **c**, Representative computerized tomography image of a femur from a BRAF-V600E$^{Scl+}$ animal. The red arrow shows a pathognomonic granuloma. **d**, H&E staining and CD207 immunohistochemistry staining of tissues isolated from *BRAF*-V600E$^{Scl+}$ mice. We note the presence of multinucleated giant cells and granuloma-like lesions. The graph represents the number of CD207$^{+}$ cells per mm$^{2}$ in tissue sections isolated from animals ($n=3$ mice per group). **e**, Percentage of the CD11c$^{+}$MHCII$^{+}$ MNP population among *Rosa*$^{YFP+}$ cells in organs of *BRAF*-V600E$^{Scl+}$ mice and control littermates. Data are representative of three experiments ($n=7$ mice). **f**, Absolute numbers of total CD45$^{+}$ immune cells and CD11c$^{+}$MHCII$^{+}$ MNPs that populate the lung and the skin of *BRAF*-V600E$^{Scl+}$ mice and control littermates. Data are representative of three experiments ($n=3$–7 mice). NS, not significant. **g**, Cartoon shows the scheme used to generate the humanized LCH mouse. **h**, Liver, lung and spleen tissue sections isolated from humanized mice reconstituted with *BRAF*-V600E$^{hu}$ HPCs were stained with anti-CD207 and anti-CD1a antibodies. Graphs represent the number of CD207$^{+}$ or CD1a$^{+}$ cells per mm$^{2}$ in tissue sections isolated from animals ($n=3$–4 mice). Data are represented as mean ± s.e.m.; statistical significance was analyzed by unpaired two-sided *t*-tests and is indicated by $^{*}P<0.05$, $^{**}P<0.01$, $^{***}P<0.001$ and $^{****}P<0.0001$. These data are representative of three independent experiments.

(Supplementary Table 1). Similar to the signature of *BRAF*$^{V600E}$-transduced HPCs, CD34$^+$ HPCs isolated from patients with LCH showed reduced expression of genes associated with granulopoiesis (*ELANE*, *MPO*, *PRTN3*, *CSF3R*) and an increased expression of genes involved in dendritic cell–macrophage commitment (*BATF3*, *IRF4*, *CSF1R*, *CLEC10A*) compared to that in CD34$^+$ HPCs isolated from an age-matched individual (Fig. 2g). In sum, these data establish that the *BRAF*$^{V600E}$ mutation directs mouse and human HPCs to differentiate into the MNP lineage, away from the lymphoid and the granulocytic lineage.



**Skewing of *BRAF*-V600E$^+$ HPCs into the MNP lineage is driven by both cell-intrinsic and cell-extrinsic cues.** To examine whether the enhanced MNP differentiation of *BRAF*-V600E$^+$ HPCs was cell intrinsic or a result of external cues, we measured the expansion of *BRAF*-V600E$^+$ and *BRAF*$^{WT}$ HPCs within the same animal. Strikingly, while we failed to observe an expansion of GMPs in *BRAF*-WT$^{Scl+}$ mice, there was an expansion of *BRAF*-V600E$^+$ and *BRAF*$^{WT}$ GMPs within the same *BRAF*-V600E$^{Scl+}$ mice (Fig. 2h), associated with an increase in BM *BRAF*-V600E$^+$ and *BRAF*$^{WT}$ MNPs but not an increase in neutrophils (Fig. 2i). The expansion of BM *BRAF*$^{WT}$ MNPs in *BRAF*-V600E$^{Scl+}$ mice but not in *BRAF*-WT$^{Scl+}$ mice suggests that MNP skewing may not be driven only by cell-intrinsic cues.

To examine whether similar cell-extrinsic cues can also drive human HPC differentiation into MNPs, we took advantage of the fact that HPC transduction efficiency with *BRAF*$^{V600E}$ or NGFR lentiviral vectors did not exceed 40% (Extended Data Fig. 1g) to compare, within the same culture, the differentiation of *BRAF*-V600E$^+$GFP$^+$ and *BRAF*-V600E$^-$GFP$^-$ HPCs as well as that of NGFR$^+$GFP$^+$ and NGFR$^-$GFP$^-$ HPCs. Similar to our results in mice, *BRAF*-V600E$^-$GFP$^-$ cells co-cultured with *BRAF*-V600E$^+$GFP$^+$ cells had an enhanced MNP differentiation potential, although at a reduced scale compared to that of *BRAF*-V600E$^+$GFP$^+$ HPC counterparts (Fig. 2j). This contrasts with our earlier results showing that purified human *BRAF*-V600E$^-$GFP$^-$ HPCs cultured alone in CFU assays did not have an MNP differentiation advantage (Fig. 2e and Extended Data Fig. 2c). This suggests that secreted molecules produced by *BRAF*-V600E$^+$GFP$^+$ HPCs contributed to driving MNP differentiation of healthy HPCs. To directly measure whether the *BRAF*-V600E$^+$ HPC secretome skewed the differentiation of *BRAF*$^{WT}$ HPCs toward the MNP lineage, we cultured human CD34$^+$ HPCs in stem cell medium in the presence or absence of supernatant isolated from human *BRAF*-V600E$^+$ HPCs or NGFR$^+$ HPCs. Consistent with our hypothesis, we observed that healthy HPCs cultured in the presence of supernatant obtained from human *BRAF*-V600E$^+$ HPC cultures were more prone to differentiate into MNPs than healthy HPCs cultured in the presence of supernatant from NGFR$^+$ HPCs and that the enhanced MNP differentiation potential was dependent on the dose of supernatant from added *BRAF*-V600E$^+$ HPCs (Fig. 2k).

**The *BRAF*$^{V600E}$ mutation drives mouse and human hematopoietic progenitors into oncogene-induced senescence.** The realization that the *BRAF*$^{V600E}$ mutation limited the expansion of HSCs (Fig. 2a) prompted us to further assess the proliferation potential of *BRAF*$^{V600E}$-mutant HPCs using a competitive reconstitution assay in which purified *BRAF*-V600E$^+$ HPCs or *BRAF*$^{WT}$ HPCs (isolated from CD45.2$^+$ animals) were injected together with host HPCs (CD45.1$^+$) at a 2:1 ratio into sublethally irradiated CD45.1$^+$ recipients. Strikingly, we found that, at 4 and 8 weeks after transplantation, the number of engrafted *BRAF*-V600E$^+$ HPCs was strongly reduced compared to that of *BRAF*$^{WT}$ HPCs (Fig. 3a and Extended Data Fig. 3a), thus revealing a proliferative disadvantage of *BRAF*$^{V600E}$ HPCs compared to *BRAF*$^{WT}$ HPCs.

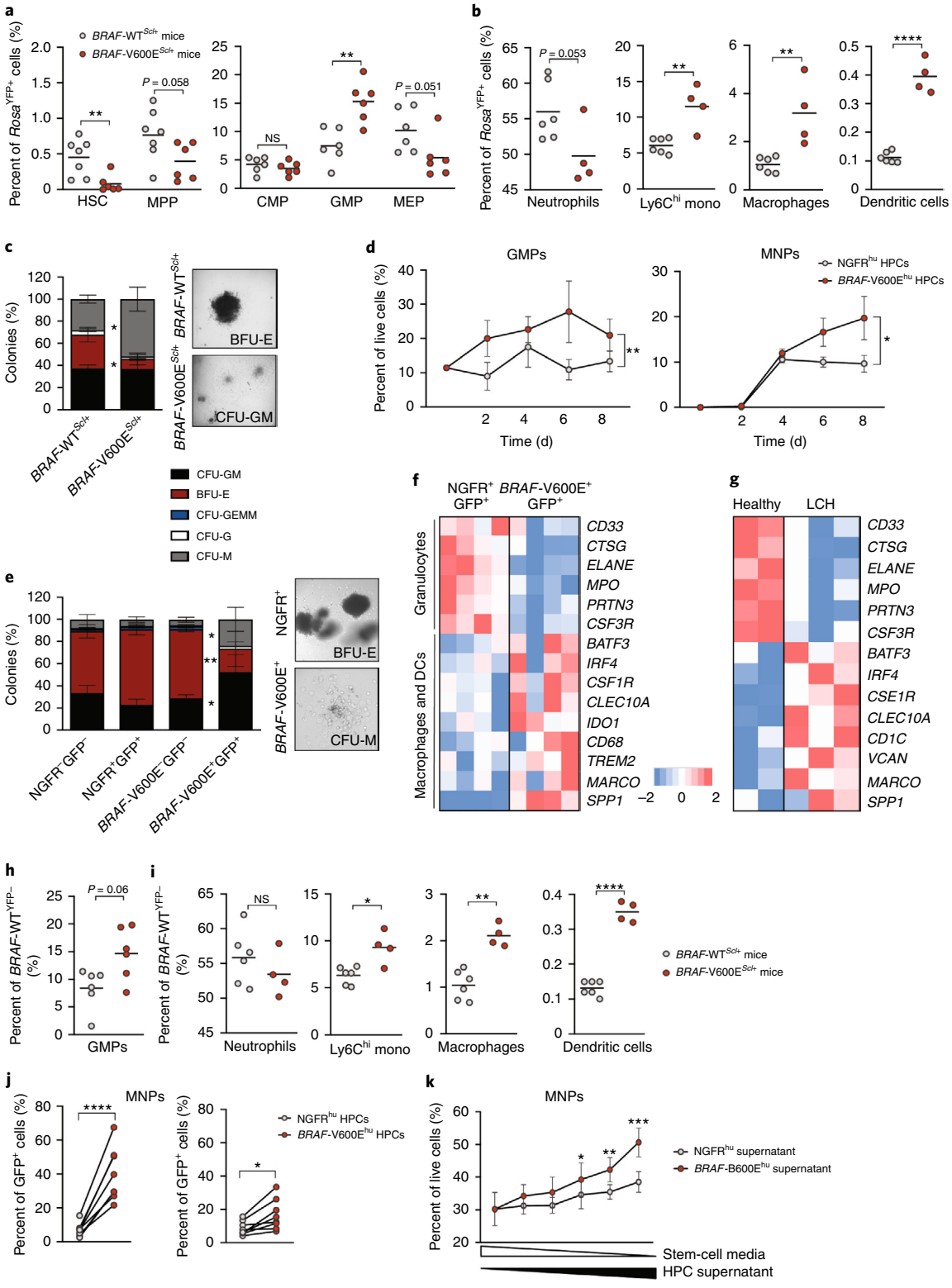
The *BRAF*$^{V600E}$ mutation was previously described to drive cellular senescence in human nevus lesions[13]. Cellular senescence classically occurs secondary to DNA damage or because of oncogene activation and results in cell cycle arrest driven by cell cycle regulators, such as p16$^{INK4a}$, and prolonged survival driven by the anti-apoptotic proteins BCL-xL and BCL-2. Senescent cells also form heterochromatin foci and express senescence-associated β-galactosidase (SAβGal), as well as exhibiting a SASP (reviewed in refs. [14,15]), which leads to the production of a wide range of inflammatory molecules such as interleukin (IL)-1, IL-6, IL-8 and several matrix metalloproteinases.

Strikingly, we found that *BRAF*-V600E$^{Scl+}$ HPCs were unable to cycle, as shown by the low BrdU incorporation potential, which likely accounts for their poor ability to engraft compared to that of HPCs from *BRAF*-WT$^{Scl+}$ mice in a competitive reconstitution assay (Fig. 3b). HPCs isolated from *BRAF*-V600E$^{Scl+}$ mice were also

**Fig. 2 | Expression of the *BRAF*$^{V600E}$ mutation in multipotent hematopoietic progenitors enforces their differentiation toward the MNP lineage.** **a**–**c**, *BRAF*-V600E$^{Scl+}$ mice were generated as described in Fig. 1a, and, in these mice, *Rosa*$^{YFP+}$ cells mark *BRAF*-V600E$^+$ cells, while *Rosa*$^{YFP-}$ cells mark *BRAF*-V600E$^-$ cells. In *BRAF*-WT$^{Scl+}$ control littermates, *Rosa*$^{YFP+}$ cells mark those that underwent a Cre recombination as well. **a**, Graphs show the percentage of HSCs, MPPs, common myeloid progenitors, granulocytic myeloid progenitors and megakaryocytic erythroid progenitors among *Rosa*$^{YFP+}$ cells in the BM of *BRAF*-V600E$^{Scl+}$ mice and *BRAF*-WT$^{Scl+}$ control littermates ($n=6$–7 mice). **b**, Percentages of neutrophils, Ly6C$^{hi}$ monocytes (mono), macrophages and dendritic cells among *Rosa*$^{YFP+}$ cells in the BM of *BRAF*-V600E$^{Scl+}$ mice and *BRAF*-WT$^{Scl+}$ control littermates ($n=4$–6 mice). **c**, CFU assays were performed on purified lineage-negative BM cells isolated from *BRAF*-V600E$^{Scl+}$ mice or *BRAF*-WT$^{Scl+}$ control littermates ($n=3$ mice) cultured in the presence of methylcellulose, with representative phase contrast photomicrographs of colonies. GEMM, granulocytes, erythrocytes, megakaryocytes, monocytes, megakaryocytes. **d**–**f**, Purified CD34$^+$ HPCs transduced with *BRAF*$^{V600E}$ (*BRAF*-V600E$^{hu}$) or NGFR control (NGFR$^{hu}$) lentiviral vectors were cultured in stem cell medium for 8 d. **d**, Graphs show the percentages of GMPs (defined as CD34$^+$CD38$^+$CD10$^-$CD123$^{hi/int}$CD45RA$^{+/-}$)[34] and the percentages of MNPs (defined as CD66b$^-$CD11c$^+$MHCII$^+$) among live cells ($n=3$ donors). **e**, CFU assays in methylcellulose performed on purified *BRAF*-V600E$^-$GFP$^-$ and *BRAF*-V600E$^+$GFP$^+$ cells isolated from HPCs transduced with the *BRAF*$^{V600E}$ lentiviral vector or purified NGFR$^+$GFP$^+$ or NGFR$^-$GFP$^-$ cells isolated from HPCs transduced with the NGFR lentiviral vector as described in Extended Data Fig. 3 ($n=6$ donors). Representative phase contrast photomicrographs of colonies are shown. **f**, Human CD34$^+$ HPCs transduced with *BRAF*$^{V600E}$ or the control NGFR lentiviral vector were cultured for 7 d in stem cell medium and analyzed using microarray sequencing. Heatmap representation of genes involved in granulopoiesis and the macrophage–dendritic cell (DC) lineage is shown ($n=4$ independent donors per group). **g**, Purified CD34$^+$ BM cells were isolated from a healthy pediatric donor (in duplicate) and from three patients with LCH and BM mononuclear cells known to be *BRAF*-V600E$^+$, and these cells were analyzed using bulk RNA-seq. Heatmap representation of genes involved in granulopoiesis and the macrophage–dendritic cell lineage is shown. **h**,**i**, *BRAF*-V600E$^{Scl+}$ mice and *BRAF*-WT$^{Scl+}$ control littermates were generated as described in Fig. 1a. The percentages of GMPs (**h**), neutrophils, Ly6C$^{hi}$ monocytes, macrophages and dendritic cells (**i**) among *BRAF*$^{WT}$;*Rosa*$^{YFP-}$ cells in the BM of *BRAF*-V600E$^{Scl+}$ mice and *BRAF*-WT$^{Scl+}$ control littermates is shown. **j**, Human CD34$^+$ HPCs were transduced with *BRAF*$^{V600E}$ or NGFR lentiviral constructs and cultured in stem cell medium. Seven days later, the percentages of CD11c$^+$ and/or CD14$^+$ MNP cells among *BRAF*$^{V600E}$ (GFP$^+$) or *BRAF*$^{WT}$ (GFP$^-$) cells were measured by flow cytometry. Because the transduction efficiency was around 40% for both vectors, GFP$^+$ cells mark *BRAF*-V600E$^+$ or NGFR$^+$ cells, while GFP$^-$ cells mark *BRAF*$^{WT}$ or NGFR$^-$ cells among HPCs transduced with the *BRAF*$^{V600E}$ or NGFR lentiviral construct, respectively ($n=8$ independent donors). **k**, Healthy human CD34$^+$ cord blood HPCs were cultured in stem cell medium (concentration is represented by the white triangle) in addition to supernatant isolated from HPCs transduced with the *BRAF*$^{V600E}$ lentiviral construct or the NGFR control (concentration is represented by the black triangle). The graph shows the percentage of HPC differentiation into CD14$^+$ MNPs analyzed by flow cytometry after 5 d of culture ($n=4$ independent donors), analyzed by paired *t*-tests. Data are represented as mean ± s.e.m.; $^*P<0.05$, $^{**}P<0.01$, $^{***}P<0.001$, $^{****}P<0.0001$ (unpaired two-sided *t*-tests, two-way ANOVA test for **d** and paired two-sided *t*-tests for **j**,**k**). Data are representative of at least three independent experiments.

enlarged compared to HPCs from *BRAF*-WT$^{Scl+}$ mice, a common feature of senescent cells (Extended Data Fig. 3b); expressed high levels of *Cdkn2a* transcripts, which code for the cell cycle regulator p16$^{INK4a}$ (Fig. 3c); were positive for SAβGal (Fig. 3d); and produced SASP-associated proteins (Fig. 3e), all features consistent with a senescent state. LCH cells isolated from peripheral tissues of *BRAF*-V600E$^{Scl+}$ mice were also in a senescent state, as shown by reduced Ki-67 expression (Fig. 3f), expression of *Cdkn2a* (Fig. 3g), SAβGal activity (Fig. 3h) and the production of SASP-associated proteins (Fig. 3i). These results suggest that the *BRAF*$^{V600E}$ mutation induced a senescence program in HPCs, which was maintained in differentiated LCH cells.

The *BRAF*$^{V600E}$ mutation in human HPCs led to an initial phase of proliferation (Extended Data Fig. 3c), followed by a marked cell



cycle arrest in vitro (Fig. 3j and Extended Data Fig. 3d). Human *BRAF*$^{V600E}$-transduced HPCs exhibited canonical markers of cellular senescence, including enlarged cellular size (Extended Data Fig. 3e), positivity for SAβGal staining (Fig. 3l), senescence-associated heterochromatin foci (Fig. 3m) and increased production of SASP cytokines (Fig. 3n and Extended Data Fig. 3f). Gene expression profiling of transduced human *BRAF*-V600E$^+$GFP$^+$ HPCs confirmed the senescence signature[16] (Fig. 3k), and LCH lesions that formed in humanized mice reconstituted with human *BRAF*$^{V600E}$ CD34$^+$ cells also had increased SAβGal activity and high p16$^{INK4a}$ levels (Extended Data Fig. 3g,h).

Importantly, CD34$^+$ BM cells isolated from patients with LCH also expressed a senescence signature, including increased expression of *CDKN2A*, *CDKN2C*, *CDKN2D*, *CD9*, *MDM2* and genes encoding matrix metalloproteinases, which was absent from CD34$^+$ BM cells isolated from age-matched healthy individuals (Fig. 4a and Extended Data Fig. 4a).

Purified CD207$^+$ cells from human LCH lesions expressed high levels of *CDKN2A*, *CDKN2B* and *CDKN2C* transcripts and high SASP transcript levels (*MMP1*, *MMP3*, *MMP9*, *MMP13*) (Fig. 4b). LCH cells from LCH lesions expressed low levels of or no Ki-67 (Fig. 4c), while they expressed high levels of p16$^{INK4a}$ protein and had high SAβGal activity (Fig. 4d,e and Extended Data Fig. 4b,c). In addition, we found high IL-6 and IL-8 cytokine levels in the plasma of patients with multisystem LCH disease (Fig. 4f).

A neurodegenerative syndrome (LCH-ND) characterized by progressive ataxia and learning and behavior difficulties arises in some patients with LCH and remains one of the most difficult-to-treat complications of LCH. We previously demonstrated the presence of *BRAF*-V600E$^+$ perivascular microglial-like cells along with *BRAF*-V600E$^+$ mononuclear cells circulating in the blood of patients with LCH-ND. To determine whether senescence could also contribute to LCH-ND pathophysiology, we examined brain autopsy sections of a patient with fatally progressive ND-LCH[17]. Strikingly, we found multifocal aggregates of enlarged *BRAF*-V600E$^+$ cells expressing monocyte–macrophage markers (CD14, CD163, CD33) and overexpressing the senescent marker p16$^{INK4a}$, aggregating in areas of the white matter (Extended Data Fig. 4d,e). These cells also lacked the microglial marker (P2RY12, Extended Data Fig. 4f) and accumulated in perivascular regions, suggesting that senescent circulating MNPs that were recruited from the blood to the brain parenchyma, rather than brain-resident microglial cells, might have contributed to neurodegeneration in this patient.

In sum, these data suggest that the *BRAF*$^{V600E}$ mutation induces a senescence program in HPCs that persisted in differentiated LCH cells that accumulate in the peripheral tissues and brain parenchyma.

**Pharmacological blockade of the mTOR pathway inhibits SASP induction and limits MNP differentiation of *BRAF*-V600E$^+$ HPCs.** Our results above, suggesting that the secretome produced by *BRAF*-V600E$^+$ HPCs contributed to the skewing of HPCs toward the MNP lineage, prompted us to examine whether SASP inhibition could help rescue HPC multilineage differentiation potential. The SASP includes a wide range of cytokines that can contribute to MNP skewing, and, therefore, targeting a specific cytokine might not be sufficient to obtain a therapeutic benefit. SASP induction in senescent cells is thought to be driven by the sustained activation of the mammalian target of rapamycin (mTOR) pathway[18,19]. Thus, we asked whether rapamycin, a potent mTOR inhibitor, could reduce MNP differentiation skewing of *BRAF*-V600E$^+$ senescent HPCs by its ability to blunt the pro-inflammatory phenotype of senescent cells.

We first confirmed that inhibition of the mTOR pathway was sufficient to reduce the production of inflammatory cytokines by *BRAF*-V600E$^+$ senescent HPCs in vitro (Fig. 5a). Importantly, and in line with our hypothesis, SASP inhibition significantly reduced *BRAF*-V600E$^+$ HPC skewing into MNPs in vitro (Fig. 5b). Rapamycin treatment also partially reduced excess MNP differentiation from *BRAF*-V600E$^-$GFP$^-$ HPCs co-cultured with senescent *BRAF*-V600E$^+$GFP$^+$ HPCs, further establishing that mTOR inhibition reduced the release of SASP-associated molecules driving HPC-sustained MNP differentiation potential (Fig. 5b). Of note, we did not observe any difference in expression of genes involved in the mTOR–phosphatidylinositol 3-kinase (PI3K) pathway (Extended Data Fig. 5a).

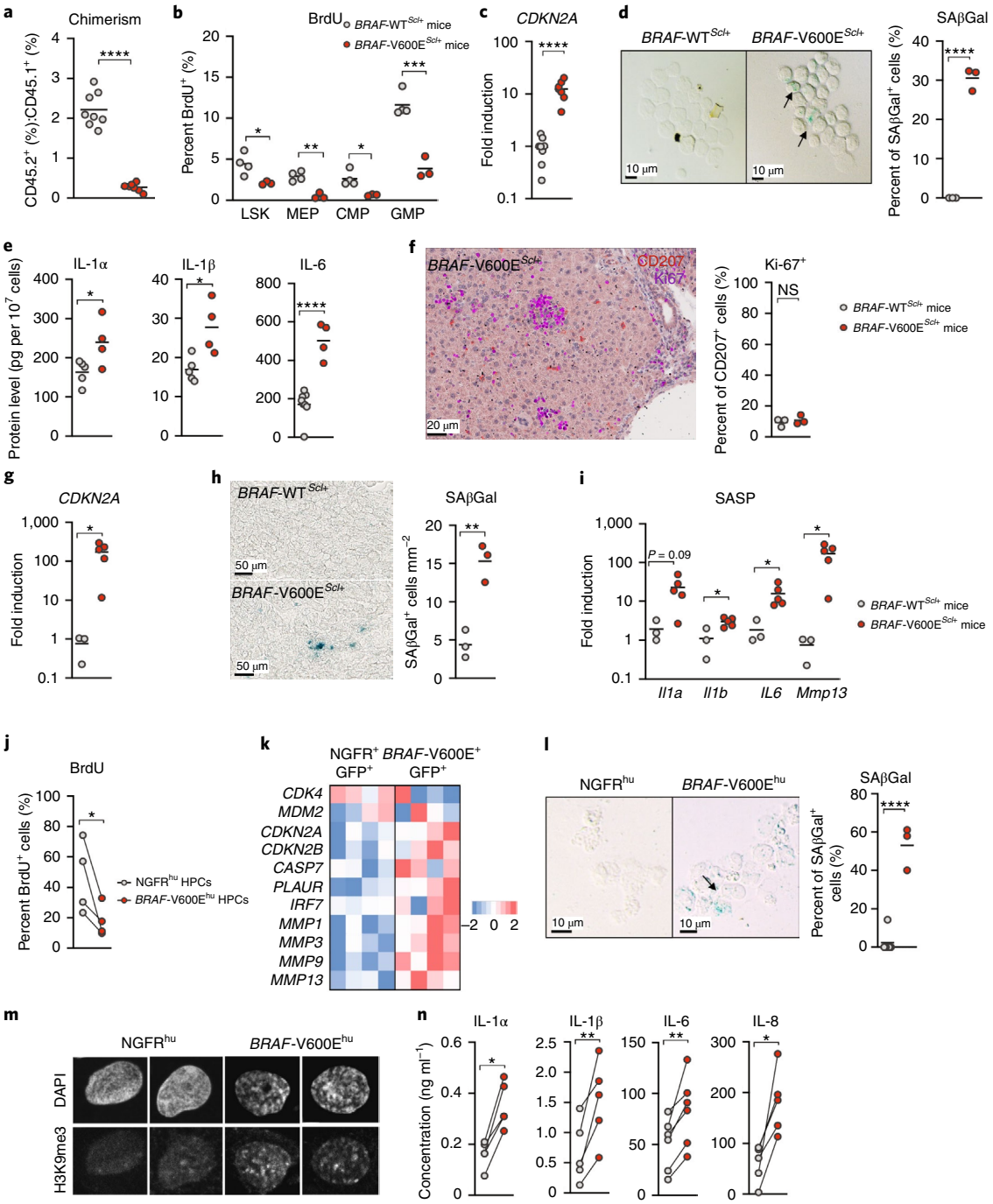
Importantly, administration of rapamycin to *BRAF*-V600E$^{Scl+}$ mice reduced the accumulation of BM GMPs and MNPs, while BM neutrophils were not affected by the treatment (Fig. 5c,d and Extended Data Fig. 5b). Rapamycin administration reduced organomegaly in *BRAF*-V600E$^{Scl+}$ animals (Fig. 5e) and the inflammatory infiltrate in tissues (Fig. 5f), improving LCH disease. Of note, rapamycin did not induce apoptosis of *BRAF*-V600E$^+$ cells (Extended Data Fig. 5c). While we cannot exclude the possibility that improved LCH disease symptoms in treated *BRAF*-V600E$^{Scl+}$ animals may also be linked to a direct effect of rapamycin on T cells infiltrating LCH lesions, the ability of rapamycin to inhibit

**Fig. 3 | The *BRAF*$^{V600E}$ mutation drives mouse and human hematopoietic progenitors into senescence. a**, Lineage-negative BM cells isolated from either *BRAF*-V600E$^{Scl+}$CD45.2$^+$ or *BRAF*-WT$^{Scl+}$CD45.2$^+$ mice were injected intravenously together with lineage-negative CD45.1$^+$ BM cells into lethally irradiated CD45.1$^+$ mice at a 2:1 ratio (CD45.2$^+$:CD45.1$^+$). Graph shows the ratio of CD45.2$^+$:CD45.1$^+$ cells circulating in the blood in each group, measured 4 weeks after transplantation using flow cytometry ($n=8$ animals). **b**–**e**, BM cells were isolated from *BRAF*-V600E$^{Scl+}$ and *BRAF*-WT$^{Scl+}$ control littermates and analyzed for the percentage of BrdU expression in lineage-negative Sca-1$^+$c-Kit$^+$ cells (LSK), megakaryocytic erythroid progenitors, common myeloid progenitors and GMPs after seven daily BrdU injections (1 mg per day) ($n=3$–4 mice) (**b**); *Cdkn2a* expression from purified lineage-negative BM cells measured by quantitative PCR with reverse transcription (RT-qPCR) (normalized to actin expression) ($n=8$ mice) (**c**); and SAβGal activity of purified lineage-negative BM cells (**d**). The graph shows the percentage of SAβGal$^+$ cells among total cells ($n=3$ mice per group). **e**, IL-1α, IL-1β and IL-6 protein levels in the BM supernatant, detected by ELISA, are shown ($n=4$–6 mice per group). **f**–**i**, Liver tissue sections were obtained from *BRAF*-V600E$^{Scl+}$ and *BRAF*-WT$^{Scl+}$ control littermates and analyzed for Ki-67$^+$ (violet) cells among liver infiltrating CD207$^+$ LCH cells (red) (**f**). Graphs show the percentage of Ki-67$^+$ cells among CD207$^+$ cells in liver sections ($n=3$ mice per group), *Cdkn2a* expression by RT-qPCR (normalized to actin expression) ($n=3$–5 mice per group) (**g**) and SAβGal activity (**h**). **i**, Graph shows the number of SAβGal$^+$ cells per mm$^2$ in liver sections ($n=3$ mice per group) and expression of *Il1a*, *Il1b*, *Il6* and *Mmp13* by RT-qPCR normalized to actin expression ($n=3$–5 per group). **j**–**n**, Human CD34$^+$ cord blood HPCs were transduced with *BRAF*$^{V600E}$ (*BRAF*-V600E$^{hu}$) or NGFR control (NGFR$^{hu}$) lentiviral vectors, cultured in stem cell medium and analyzed for BrdU expression after daily pulses of BrdU from day 10 to day 13 ($n=4$ different donors) (**j**), gene expression of senescence-associated genes using microarray expression profiling 7 d after transduction ($n=4$ donors) (**k**) and SAβGal activity 9 d after transduction (**l**). **l**, The percentage of SAβGal$^+$ cells among total cells is indicated ($n=4$ donors). **m**, Trimethylation at lysine 9 of histone 3 (H3K9me3) and 4,6-diamidino-2-phenylindole (DAPI) immunofluorescence co-staining of NGFR$^{hu}$ and *BRAF*-V600E$^{hu}$ HPCs 9 d after transduction; images are representative of senescence-associated-heterochromatin foci. **n**, IL-1α, IL-1β, IL-6 and IL-8 levels in the culture supernatant 7 d after HPC transduction ($n=4$–6 donors). Data are represented as mean ± s.e.m.; statistical significance analyzed by unpaired and paired (for **j**,**n**) two-sided *t*-tests is indicated by $^*P<0.05$, $^{**}P<0.01$, $^{***}P<0.001$ and $^{****}P<0.0001$. Data are representative of at least two independent experiments.

the release of inflammatory cytokines from *BRAF*$^{V600E}$ HPCs and the MNP skewing induced by secreted factors from *BRAF*-V600E$^{+}$ HPCs, in addition to rapamycin inhibition of GMP and MNP accumulation in the BM of *BRAF*-V600E$^{Scl+}$ animals, emphasize the strong contribution of mTOR-driven SASP to the increased MNP differentiation observed in mice and human *BRAF*$^{V600E}$ HPCs.

**Elimination of senescent cells improves the clinical outcome of LCH-bearing mice.** To measure the exact contribution of senescence to LCH pathogenesis, we took advantage of mice expressing the *INK-ATTAC* transgene that includes an open reading frame coding for enhanced GFP and the FK506-binding protein–caspase 8 (FKBP–Casp8) fusion protein, expressed under the promoter of the *Cdkn2a* gene, which encodes the p16$^{INK4a}$ protein[20]. These mice enable *Cdkn2a*-p16$^{INK4a+}$ senescent cells to be visualized based on GFP expression and conditionally deleted upon administration of AP20187 (AP), a synthetic drug that induces the dimerization of membrane-bound myristoylated FKBP–Casp8, leading to the apoptosis of Casp8-expressing cells.

*INK-ATTAC* mice were crossed with *BRAF*-V600E$^{ca/ca}$;*Scl-cre*$^{ER}$ (*BRAF*-V600E$^{Scl+}$;ATTAC$^{+}$) or *BRAF*-WT$^{ca/ca}$;*Scl-cre*$^{ER}$ mice (*BRAF*-WT$^{Scl+}$;ATTAC$^{+}$) as a control group. Both groups received tamoxifen for 5 d to induce LCH lesions, and we measured the accumulation and composition of senescent cells in the BM



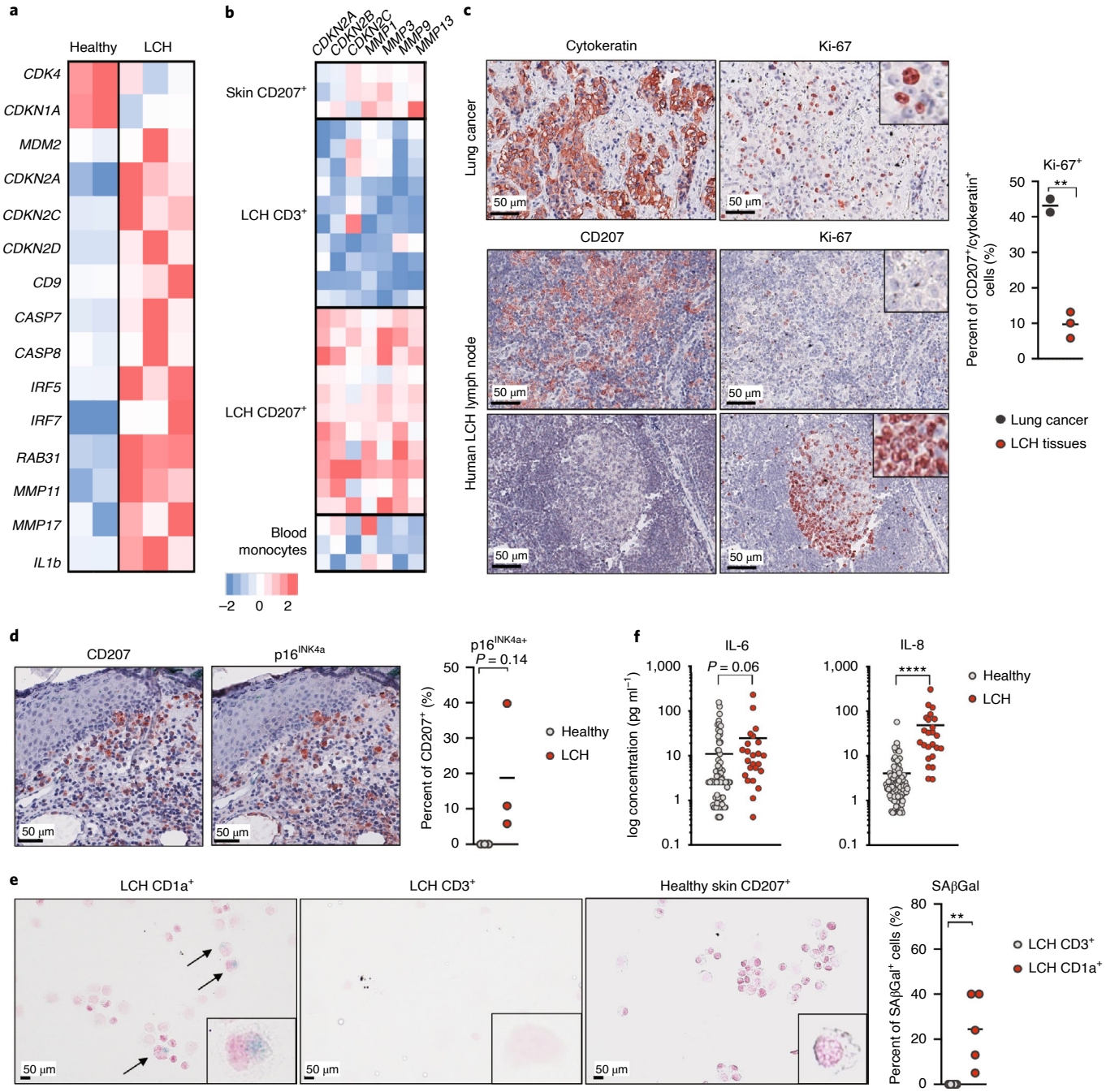



**Fig. 4 | The *BRAF*$^{V600E}$ mutation induces a senescence program in human LCH lesions. a**, Heatmap representation of senescence-associated gene expression, measured by RNA-seq in purified CD34$^+$ BM cells isolated from three patients with LCH and one pediatric healthy donor (performed in duplicate). **b**, Skin CD207$^+$ cells were isolated from healthy skin ($n=3$ patients), CD3$^+$ and CD207$^+$ cells were purified from LCH lesions ($n=11$ patients), and circulating CD14$^+$ cells were isolated from three healthy pediatric donors, and these cells were analyzed for gene expression profiles using microarrays. The expression profile of *CDKN2A*, *CDKN2B*, *CDKN2C*, *MMP1*, *MMP3*, *MMP9* and *MMP13* is shown. **c**, FFPE sections of LCH lymph node lesions from three different patients were immunostained for CD207 and Ki-67, and FFPE lung cancer sections ($n=2$ patients) were immunostained for cytokeratin and Ki-67. Images at the top show the high proliferation index of lung cancer. Images at the bottom show the same LCH donor with LCH in a lymph node. The middle panel shows a low proliferative index of the LCH as compared to that in the bottom panel of an uninvolved lymphoid follicle with its typical proliferative activity in the polarized germinal center. The graph represents the percent of Ki-67$^+$ cells among CD207$^+$ cells in LCH tissue or among cytokeratin-positive cells in lung cancers. **d**, Skin tissue sections isolated from patients with LCH and healthy age-matched donors were stained for CD207 and p16$^{INK4a}$ using immunohistochemistry. One representative image is shown. The graph shows the percentage of p16$^{INK4a}$-positive cells among CD207$^+$ cells ($n=3$ patients for each group). **e**, SAβGal activity in human LCH lesions. CD207$^+$ cells and CD3$^+$ cells were sorted from LCH lesions ($n=5$ patients), healthy skin and healthy tonsils, and these cells were stained for SAβGal activity. The graph shows the percent of SAβGal$^+$ cells among CD207$^+$ cells and CD3$^+$ cells, highlighting that the staining occurred mostly in LCH cells. **f,** Graphs show IL-6 and IL-8 protein levels in the plasma of patients with LCH and age-matched healthy donors ($n=24$ patients with multisystem LCH, $n=89$ healthy pediatric donors). Data are represented as mean ± s.e.m.; statistical significance analyzed by unpaired two-sided *t*-tests is indicated by $^*P<0.05$, $^{**}P<0.01$, $^{***}P<0.001$ and $^{****}P<0.0001$.

(Fig. 5g and Extended Data Fig. 5d). In line with our previous results, we observed an accumulation of GFP$^+$ senescent cells in the BM of *BRAF*-V600E$^{Scl+}$;ATTAC$^+$ animals compared to that in *BRAF*-WT$^{Scl+}$;ATTAC$^+$ control littermates (Fig. 5h). The majority of BM GFP$^+$ senescent cells were skewed toward the MNP lineage and led to enhanced accumulation of senescent macrophages and dendritic cells in *BRAF*-V600E$^{Scl+}$;ATTAC$^+$ mice compared to that in *BRAF*-WT$^{Scl+}$;ATTAC$^+$ mice (Fig. 5i). *BRAF*-V600E$^{Scl+}$;ATTAC$^+$ mice were then treated with AP to delete senescent cells for 3 weeks. AP treatment cleared GFP$^+$ cells from the BM of *BRAF*-V600E$^{Scl+}$;ATTAC$^+$ mice (Fig. 5j). Importantly, clearance of GFP$^+$ senescent cells from *BRAF*-V600E$^{Scl+}$;ATTAC$^+$ mice reduced organomegaly of LCH-bearing mice (Fig. 5k) and reduced the immune infiltrate in liver and lung tissues (Fig. 5l), showing that senescent cells are responsible for LCH pathophysiology.

Finally, to further examine whether pharmacological elimination of senescent cells can improve LCH outcome, we used ABT-263, an inhibitor of the anti-apoptotic proteins BCL-2 and BCL-xL, both of which are highly expressed in senescent cells. While not specific to senescent cells and potentially active in non-senescent neoplastic cells[21], ABT-263 was shown to improve the clinical outcome of several senescence-associated diseases[22–24]. We previously showed that inhibition of BCL-xL can efficiently eliminate LCH cells[25]. We administered ABT-263 to *BRAF*-V600E$^{Scl+}$ animals or *BRAF*-WT$^{Scl+}$ control littermates for 3 weeks (Extended Data Fig. 5e). The diluent for ABT-263 prevents its systemic administration, and gavage of both ABT-263 and the diluent control are quite toxic to mice, making it difficult to measure the beneficial outcome of ABT-263 in treated mice. Nonetheless, and in accordance with the ex vivo experiment, we found specific clearance of *BRAF*-V600E$^+$ cells (Extended Data Fig. 5f), reduced organomegaly (Extended Data Fig. 5g) and reduced immune lung infiltrate (Extended Data Fig. 5h) in *BRAF*-V600E$^{Scl+}$ mice treated with ABT-263 that survived. These results suggest that ABT-263 could provide a new clinical strategy to treat patients with LCH either alone or in combination with inhibitors of the BRAF kinase.

## Discussion

Using genetically engineered mouse models, we demonstrated that expression of the *BRAF*$^{V600E}$ mutation in mouse and human HPCs is sufficient to drive the formation of LCH lesions with a tissue distribution comparable to that of human systemic LCH. We also showed that mouse and human HPCs with enforced *BRAF*$^{V600E}$ mutation, as well as primary human CD34$^+$ hematopoietic progenitors isolated from patients with LCH, are in a senescent state and that *BRAF*$^{V600E}$-induced senescence in hematopoietic progenitors contributes to LCH pathophysiology. Finally, using the *INK-ATTAC* transgene, we confirmed the accumulation of senescent cells in the BM and demonstrated that depletion of senescent cells in LCH-bearing mice improves disease outcome.

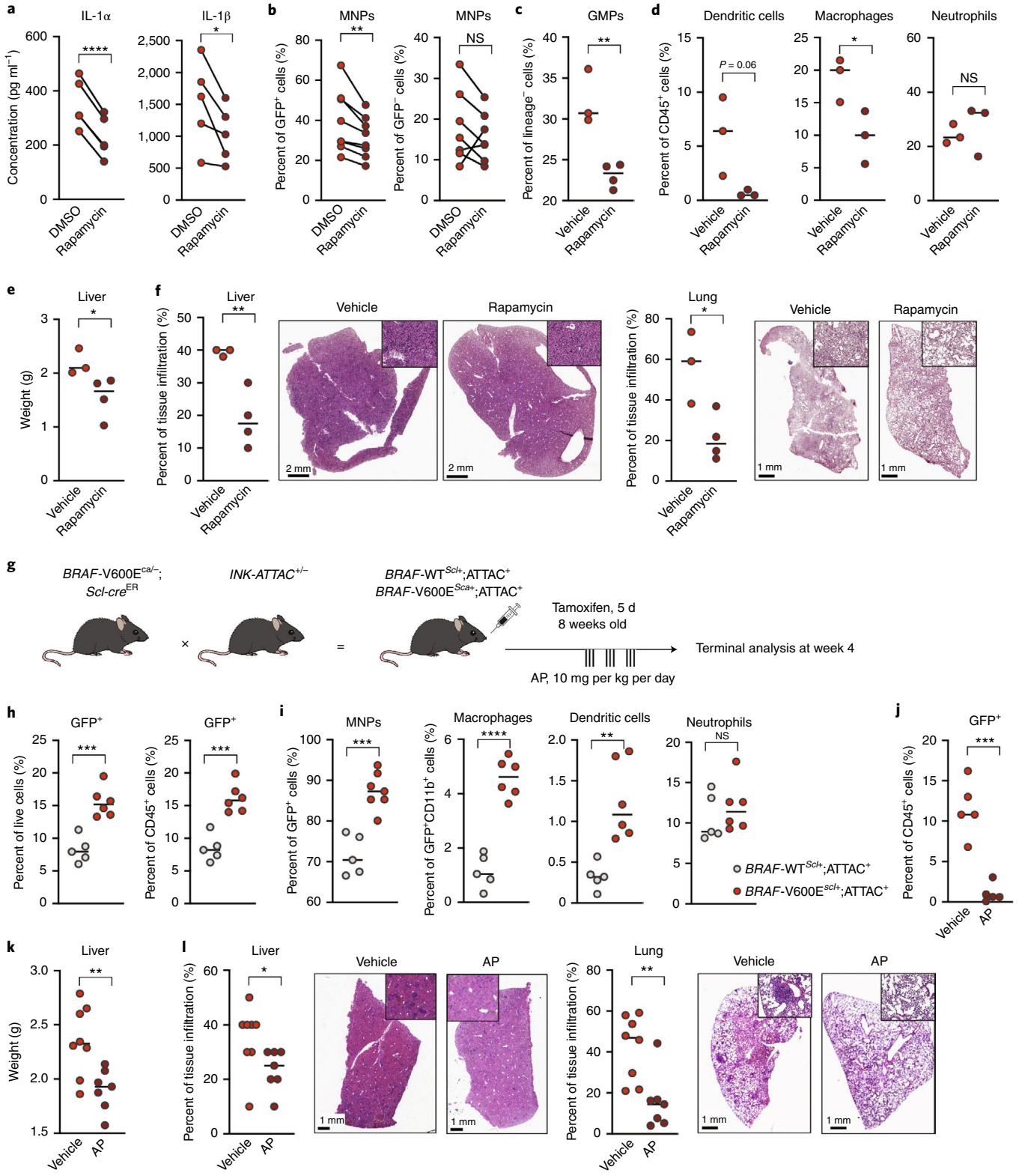
We previously generated a mouse model in which one allele of *BRAF*$^{V600E}$ was induced under the *Cd11c* (*Itgax*) promoter expressed by MNP progenitors and mature dendritic cells[8]. In that model, mice developed LCH-like disease in the spleen, lung and liver but only minimal disease in the skin and bones, which was surprising, as human LCH lesions frequently involve skin and bone tissues[8]. In the current study, we showed that, when the *BRAF*$^{V600E}$ mutation was expressed in pluripotent hematopoietic progenitors upstream of the MNP progenitors (*BRAF*-V600E$^{Scl+}$ mice), mice also developed skin lesions in the dermis that mimicked human LCH lesions, as well as granulomatous lesions, indicating that expression of the *BRAF*$^{V600E}$ mutation at the HSC level drives a more clinically relevant LCH phenotype than the disease that forms upon induction of the *BRAF*$^{V600E}$ mutation at the MNP progenitor stage.

We showed here that expression of the *BRAF*$^{V600E}$ oncogene in early hematopoietic progenitors promotes the induction of a senescence program and that senescence contributes to shaping the LCH phenotype. We also demonstrated that *BRAF*$^{V600E}$ HPCs have a much lower proliferative capacity in vitro and in vivo, which likely explains their decreased ability to engraft in competitive transplant assays when compared to WT HPCs (Fig. 3a). Instead, they are more prone to differentiate into pathogenic *BRAF*$^{V600E}$ senescent MNPs, which persist in tissues for prolonged periods of time, where they continue to release SASP-driven cytokines. The senescence program sheds light on key features of LCH disease, such as (1) the accumulation of poorly proliferative MNPs driven by the expression of the senescent-associated cell cycle inhibitor p16$^{INK4a}$ and (2) the large immune infiltrate, with subsequent fibrotic injuries (that is, to the central nervous system, including the pituitary gland and hepatic bile ducts) that accumulate in LCH lesions and lead to LCH

**Fig. 5 | SASP inhibition and eradication of senescent cells improve LCH outcome. a**,**b**, *BRAF*-V600E$^{hu}$-transduced CD34$^+$ HPCs were cultured in stem cell medium and treated at day 1 and day 4 with rapamycin (10 nM) or dimethylsulfoxide (DMSO). **a**, Graphs show IL-1α and IL-1β protein levels in the supernatant of CD34$^+$ HPCs 7 d after transduction ($n = 4$–5 independent donors). **b**, Percentages of MNPs (CD11c$^+$ and/or CD14$^+$) among total GFP$^+$*BRAF*-V600E$^+$ cells and among total GFP$^-$*BRAF*-V600E$^-$ cells within cultures of *BRAF*$^{V600E}$-transduced HPCs (*BRAF*-V600E$^{hu}$) that were treated with rapamycin or DMSO diluent were quantified by flow cytometry after 7 d of culture ($n = 7$ donors). **c**–**e**, *BRAF*-V600E$^{Scl+}$ mice were treated with rapamycin (0.5 mg per kg of body weight per day) or vehicle control for 10 d. Percentage of GMPs (defined as DAPI$^-$lineage$^-$c-Kit$^+$Sca$^-$CD16/CD32$^+$CD34$^{hi/int}$) among lineage-negative BM cells (**c**) and percentages of dendritic cells, macrophages and neutrophils among total CD45$^+$ BM cells were measured using flow cytometry ($n = 3$–4 mice) (**d**). **e**, Liver weight in each group ($n = 3$–4 mice). Data are representative of two experiments. **f**, The percentage of tissue infiltration in the liver and lung is shown with representative images of H&E staining of tissues isolated from *BRAF*-V600E$^{Scl+}$ mice. **g**, Cartoon shows the experimental breeding scheme and treatment strategy used to generate *BRAF*-V600E$^{Scl+}$;ATTAC$^+$ mice and control littermates. **h**,**i**, *BRAF*-V600E$^{Scl+}$;ATTAC$^+$ mice and *BRAF*-WT$^{Scl+}$;ATTAC$^+$ control littermates were treated with tamoxifen for 5 d and sacrificed 4 weeks later. **h**, The percentage of senescent p16$^{INK4a}$-overexpressing cells was assessed by flow cytometry in the BM from *BRAF*-V600E$^{Scl+}$;ATTAC$^+$ mice and control mice ($n = 5$–6 mice). Graphs show the percentage of GFP$^+$ cells among live cells and among CD45$^+$ cells, suggesting that senescent cells were exclusively hematopoietic cells. **i**, The nature of senescent p16$^{INK4a}$-positive cells was assessed by flow cytometry. Graphs show the percentage of CD11b$^+$ myeloid cells among GFP$^+$ senescent cells and the percentage of macrophages, dendritic cells and neutrophils among GFP$^+$CD11b$^+$ myeloid senescent cells in *BRAF*-V600E$^{Scl+}$;ATTAC$^+$ mice and control animals, highlighting that senescent cells in *BRAF*-V600E$^{Scl+}$;ATTAC$^+$ mice are almost exclusively myeloid cells and that among them there is an accumulation of macrophages and dendritic cells, rather than neutrophils ($n = 5$–6 mice). **j**–**l**, Following tamoxifen injections, *BRAF*-V600E$^{Scl+}$;ATTAC$^+$ mice and *BRAF*-WT$^{Scl+}$;ATTAC$^+$ control littermates were treated with AP or vehicle for 3 weeks and sacrificed 4 weeks after tamoxifen injections. **j**, The percentage of senescent p16$^{INK4a}$-overexpressing cells in the BM from untreated and treated *BRAF*-V600E$^{Scl+}$;ATTAC$^+$ mice ($n = 5$) was assessed by flow cytometry. The graph shows the percentage of GFP$^+$ cells among CD45$^+$ cells. **k**, Liver weight in each group ($n = 8$). **l**, Percentages of tissue infiltration in the liver and lung are shown with representative images of H&E staining of tissues isolated from untreated and treated *BRAF*-V600E$^{Scl+}$;ATTAC$^+$ mice ($n = 8$). Data are representative of three experiments and are represented as mean ± s.e.m.; statistical significance analyzed by unpaired and paired (for **a**,**b**) two-sided *t*-tests is indicated by $^*P < 0.05$, $^{**}P < 0.01$, $^{***}P < 0.001$ and $^{****}P < 0.0001$. Data are representative of at least two independent experiments.

morbidities, which we show are driven by SASP+ senescent LCH cells. In addition to inducing senescence, our previous findings, that *BRAF*$^{V600E}$ expression downregulates C–C motif chemokine receptor (CCR)7 expression in LCH cells and traps them in peripheral tissues, may further contribute to local pathogenic LCH cell accumulation[25].

While deletion of *CDKN2A* or *CDKN2B* has not been described in LCH lesions, clonal deletion of *CDKN2A* or *CDKN2B* was described in Langerhans cell sarcoma[26], a rare and highly aggressive disease defined by potent histiocyte proliferation with cytologic atypia and increased mitotic index. These results suggest that *BRAF*$^{V600E}$-induced senescence likely protects LCH cells from



malignant transformation, similar to what was observed in melanocytic nevi.

The nature of the inflammatory infiltrate in LCH lesions, while well known and widely described[27], has remained poorly understood, prompting several groups to search for a microbial origin of LCH[28,29]. Here we showed that it is instead the SASP program that drives the release of inflammatory cytokines in BM HPCs and differentiated cells in the periphery. We also showed that senescence-driven cytokine release by BM HPCs drives the induction of an MNP differentiation program. The release of inflammatory cytokines not only promotes the differentiation of HPCs into MNP cells but also likely contributes to the development of granulomatous lesions in peripheral tissues, common in LCH lesions, and subsequent fibrotic injury. mTOR inhibition by rapamycin was shown to reduce SASP expression[18,19]. In accordance with these studies, we found that mTOR inhibition reduced HPC skewing toward the MNP lineage and improved disease phenotype in vivo. Altogether, our results showing that SASP contributes to enhanced myeloid cell differentiation in the BM could explain the myeloid-biased hematopoiesis observed in aged patients (reviewed in ref. [30]) and, if confirmed, could suggest that mTOR inhibition in HPCs could help restore immune balance and homeostasis in older patients.

Systemic LCH remains a difficult-to-treat condition; BRAF or MEK kinase inhibition therapies can improve clinical outcome, although this approach is not curative in most cases, as most patients recur upon treatment interruption[31–33]. Our study strongly suggests that mTOR inhibitors and senolytics may provide a critical alternative to cytotoxic chemotherapy and chronic MAPK pathway inhibition for the treatment of patients with LCH, including those with LCH-ND.

Altogether, these results reveal the contribution of *BRAF*$^{V600E}$-driven senescence to LCH pathophysiology and identify senescent cells as an important target for the treatment of systemic LCH.

## Online content

Any methods, additional references, Nature Research reporting summaries, source data, extended data, supplementary information, acknowledgements, peer review information; details of author contributions and competing interests; and statements of data and code availability are available at https://doi.org/10.1038/s41591-021-01304-x.

Received: 29 May 2019; Accepted: 2 March 2021;
Published online: 06 May 2021

## References

1. Merad, M., Ginhoux, F. & Collin, M. Origin, homeostasis and function of Langerhans cells and other langerin-expressing dendritic cells. *Nat. Rev. Immunol.* **8**, 935–947 (2008).
2. Stålemark, H. et al. Incidence of Langerhans cell histiocytosis in children: a population-based study. *Pediatr. Blood Cancer* **51**, 76–81 (2008).
3. Allen, C. E., Merad, M. & McClain, K. L. Langerhans-cell histiocytosis. *N. Engl. J. Med.* **379**, 856–868 (2018).
4. Badalian-Very, G. et al. Recurrent *BRAF* mutations in Langerhans cell histiocytosis. *Blood* **116**, 1919–1923 (2010).
5. Chakraborty, R. et al. Mutually exclusive recurrent somatic mutations in *MAP2K1* and *BRAF* support a central role for ERK activation in LCH pathogenesis. *Blood* **124**, 3007–3015 (2014).
6. Chakraborty, R. et al. Alternative genetic mechanisms of BRAF activation in Langerhans cell histiocytosis. *Blood* **128**, 2533–2537 (2016).
7. Lim, K. P. H. et al. Circulating CD1c$^{+}$ myeloid dendritic cells are potential precursors to LCH lesion CD1a$^{+}$CD207$^{+}$ cells. *Blood Adv.* **4**, 87–99 (2020).
8. Berres, M.-L. et al. *BRAF*-V600E expression in precursor versus differentiated dendritic cells defines clinically distinct LCH risk groups. *J. Exp. Med.* **211**, 669–683 (2014).
9. Durham, B. H. et al. Functional evidence for derivation of systemic histiocytic neoplasms from hematopoietic stem/progenitor cells. *Blood* **130**, 176–180 (2017).
10. Milne, P. et al. Hematopoietic origin of Langerhans cell histiocytosis and Erdheim–Chester disease in adults. *Blood* **130**, 167–175 (2017).
11. Berres, M.-L., Merad, M. & Allen, C. E. Progress in understanding the pathogenesis of Langerhans cell histiocytosis: back to Histiocytosis X? *Br. J. Haematol.* **169**, 3–13 (2015).
12. Göthert, J. R. et al. In vivo fate-tracing studies using the *Scl* stem cell enhancer: embryonic hematopoietic stem cells significantly contribute to adult hematopoiesis. *Blood* **105**, 2724–2732 (2005).
13. Michaloglou, C. et al. BRAF$^{E600}$-associated senescence-like cell cycle arrest of human naevi. *Nature* **436**, 720–724 (2005).
14. Hernandez-Segura, A., Nehme, J. & Demaria, M. Hallmarks of cellular senescence. *Trends Cell Biol.* **28**, 436–453 (2018).
15. Muñoz-Espín, D. & Serrano, M. Cellular senescence: from physiology to pathology. *Nat. Rev. Mol. Cell Biol.* **15**, 482–496 (2014).
16. Kuilman, T. et al. Oncogene-induced senescence relayed by an interleukin-dependent inflammatory network. *Cell* **133**, 1019–1031 (2008).
17. McClain, K. L. et al. CNS Langerhans cell histiocytosis: common hematopoietic origin for LCH-associated neurodegeneration and mass lesions. *Cancer* **124**, 2607–2620 (2018).
18. Herranz, N. et al. mTOR regulates MAPKAPK2 translation to control the senescence-associated secretory phenotype. *Nat. Cell Biol.* **17**, 1205–1217 (2015).
19. Laberge, R.-M. et al. MTOR regulates the pro-tumorigenic senescence-associated secretory phenotype by promoting IL1A translation. *Nat. Cell Biol.* **17**, 1049–1061 (2015).
20. Baker, D. J. et al. Clearance of p16$^{Ink4a}$-positive senescent cells delays ageing-associated disorders. *Nature* **479**, 232–236 (2011).
21. Wilson, W. H. et al. Navitoclax, a targeted high-affinity inhibitor of BCL-2, in lymphoid malignancies: a phase 1 dose-escalation study of safety, pharmacokinetics, pharmacodynamics, and antitumour activity. *Lancet. Oncol.* **11**, 1149–1159 (2010).
22. Bussian, T. J. et al. Clearance of senescent glial cells prevents tau-dependent pathology and cognitive decline. *Nature* **562**, 578–582 (2018).
23. Chang, J. et al. Clearance of senescent cells by ABT263 rejuvenates aged hematopoietic stem cells in mice. *Nat. Med.* **22**, 78–83 (2016).
24. Jeon, O. H. et al. Local clearance of senescent cells attenuates the development of post-traumatic osteoarthritis and creates a pro-regenerative environment. *Nat. Med.* **23**, 775–781 (2017).
25. Hogstad, B. et al. RAF/MEK/extracellular signal-related kinase pathway suppresses dendritic cell migration and traps dendritic cells in Langerhans cell histiocytosis lesions. *J. Exp. Med.* **215**, 319–336 (2018).
26. Xerri, L. et al. *CDKN2A/B* deletion and double-hit mutations of the MAPK pathway underlie the aggressive behavior of Langerhans cell tumors. *Am. J. Surg. Pathol.* **42**, 150–159 (2018).
27. Picarsic, J. & Jaffe, R. Nosology and pathology of Langerhans cell histiocytosis. *Hematol. Oncol. Clin. North Am.* **29**, 799–823 (2015).
28. McClain, K., Jin, H., Gresik, V. & Favara, B. Langerhans cell histiocytosis: lack of a viral etiology. *Am. J. Hematol.* **47**, 16–20 (1994).
29. Jenson, H. B., McClain, K. L., Leach, C. T., Deng, J. H. & Gao, S. J. Evaluation of human herpesvirus type 8 infection in childhood Langerhans cell histiocytosis. *Am. J. Hematol.* **64**, 237–241 (2000).
30. Montecino-Rodriguez, E., Berent-Maoz, B. & Dorshkind, K. Causes, consequences, and reversal of immune system aging. *J. Clin. Invest.* **123**, 958–965 (2013).
31. Cohen Aubart, F. et al. Targeted therapies in 54 patients with Erdheim–Chester disease, including follow-up after interruption (the LOVE study). *Blood* **130**, 1377–1380 (2017).
32. Diamond, E. L. et al. Efficacy of MEK inhibition in patients with histiocytic neoplasms. *Nature* **567**, 521–524 (2019).
33. Eckstein, O. S., Visser, J., Rodriguez-Galindo, C. & Allen, C. E. Clinical responses and persistent *BRAF* V600E$^{+}$ blood cells in children with LCH treated with MAPK pathway inhibition. *Blood* **133**, 1691–1694 (2019).
34. Lee, J. et al. Lineage specification of human dendritic cells is marked by IRF8 expression in hematopoietic stem cells and multipotent progenitors. *Nat. Immunol.* **18**, 877–888 (2017).

**Publisher's note** Springer Nature remains neutral with regard to jurisdictional claims in published maps and institutional affiliations.

© The Author(s), under exclusive licence to Springer Nature America, Inc. 2021

## Methods

**Animal experiments.** All animal experiments performed in this study were approved by the Institutional Animal Care and Use Committee at the Icahn School of Medicine at Mount Sinai. *BRAF*-V600E$^{Scl+}$, *BRAF*-WT$^{Scl+}$, *BRAF*-V600E$^{Scl-}$ and *BRAF*-WT$^{Scl-}$ mice were created by crossing *BRAF*-V600E$^{ca/ca}$ mice (provided by M.W. Bosenberg, Yale University[35]) with mice expressing an inducible Cre recombinase under the control of the *Scl* promoter (provided by Y. Fujiwara, Harvard Medical School, Howard Hughes Medical Institute[12]). *BRAF*-V600E$^{ca/-}$; *Scl-cre*$^{ER}$ mice were then crossed with *Rosa26*$^{YFP/YFP}$ mice (C57BL/6 background; Jackson Laboratory). To induce the Cre recombinase, *BRAF*-V600E$^{Scl+}$, *BRAF*-WT$^{Scl+}$ or *BRAF*-V600E$^{Scl-}$ control littermates were injected intraperitoneally with tamoxifen for 5 consecutive days (5 mg, day 1; 2 mg, days 2 and 3; 1 mg, days 4 and 5). All animals were housed under specific pathogen-free conditions and sacrificed at the indicated time points. All experiments were controlled using Cre-positive littermates negative for the *BRAF*$^{V600E}$ construct or littermates negative for the Cre recombinase transgene construct. *BRAF*$^{V600E}$ or *BRAF*$^{WT}$ chimeras were generated by transplantation of 1–3 million whole BM cells flushed from the femurs of 8-week-old *BRAF*-V600E$^{Scl+}$ or *BRAF*-WT$^{Scl+}$ mice following tamoxifen injections into lethally irradiated (650 cGy × 2) CD45.1 mice aged 8–12 weeks (C57BL/6 background, Charles River Laboratories). Mice were kept on sulfamethoxazole–trimethoprim (STI Pharma) for 3 weeks. Mice were allowed to recover for 2 weeks after transplantation, before initiation of drug treatments.

*BRAF*-V600E$^{Scl+}$;ATTAC$^{+}$ and *BRAF*-WT$^{Scl+}$;ATTAC$^{+}$ mice were generated by crossing litters from *BRAF*-V600E$^{ca/ca}$;*Scl-cre*$^{ER}$ mice with ATTAC$^{+/-}$ mice (kindly provided by L. Galuzzi, Weill Cornell Medical College University). The Cre recombinase was induced as described earlier.

NSG mice were purchased from Jackson Laboratory (BALB/c background) and were housed under specific pathogen-free conditions. Humanized mice were generated by transplanting 200,000 human CD34$^{+}$ cells previously transduced for 16–24 h with the *BRAF*$^{V600E}$ or NGFR lentiviral vector into 8-week-old NSG mice sublethally irradiated with 250 cGy.

**Human specimens.** Human tissues used in these studies were collected, stored and processed according to protocols approved by the Baylor College of Medicine Institutional Review Board. Healthy control tissues were obtained from the Biorepository and Pathology CoRE facility (K. Donovan) at Mount Sinai School of Medicine. Cord blood was obtained from the New York Blood Center, National Cord Blood Program.

**Lentiviral vector construction.** *BRAF*$^{V600E}$ and *NGFR* transgenes were cloned into lentiviral expression vectors upstream of a 2A peptide linked to GFP for in vivo and in vitro analysis of transduced cells using standard cloning procedures. Briefly, PCR products were amplified from the pcDNA3 plasmid (provided by P.I.P.) using high-fidelity Taq polymerase. PCR products were purified using the QIAquick PCR purification kit (Qiagen), and restriction enzymes SalI and XbaI were used to digest the vector and PCR products. PCR products were ligated with the expression vector using NEB Quick Ligase, and plasmids were verified by Sanger sequencing.

**Lentiviral vector production and titration.** Lentiviral vectors were produced as previously described[36]. Briefly, 293T cells were seeded approximately 24 h before transfection in a 15-cm plate and incubated at 37 °C with 5% $CO_2$. The following day, cells were transfected with a third-generation packaging system (pVSV, pMDLg/pRRE, pRSV-REV) and the appropriate transfer plasmid using calcium phosphate. The medium was changed 14 h later. Another 30 h later, the supernatant containing the vector was collected, passed through a 0.22-µm filter and ultracentrifuged (20,000 r.p.m. for 2 h) to concentrate the vector 300–500-fold. The vector particles were resuspended in sterile PBS, aliquoted and stored at −80 °C. Vector titration was performed on 293T cells using the limiting dilution method.

**Cord blood processing and transduction.** Mononuclear cells from cord blood were isolated via a Ficoll-Paque PLUS (GE Healthcare) gradient. Mononuclear cells were washed and resuspended in FACS buffer (PBS without $Ca^{2+}$ and $Mg^{2+}$, supplemented with 2% heat-inactivated FBS and 5 mM EDTA). CD34$^{+}$ cells were purified using a Human CD34 MicroBead kit from Miltenyi Biotec (130-100-453).

CD34$^{+}$ human HPCs were resuspended at a concentration of 1 million cells per ml in StemSpan medium SFEM II (Stemcell Technologies, 09605) supplemented with 100 ng ml$^{-1}$ SCF, 100 ng ml$^{-1}$ FLT3L and 50 ng ml$^{-1}$ TPO (so-called stem cell medium). Two hundred thousand cells were plated in a 48-well plate, and 5 µl lentiviral construct (either *BRAF*$^{V600E}$ or NGFR) was added to the medium at an MOI of 50. Cells were incubated at 37 °C with 5% $CO_2$. Supplemented StemSpan medium was added 24 h after the initiation of transduction, and cells were kept in culture for up to 14 d. GFP-transduced cells were analyzed for myeloid and lymphoid surface marker expression (see antibody list) starting 2 d after transduction.

**Flow cytometry.** Adult skin (from the ears), lung, liver, spleen and femurs were dissected from mice at the age of 12–16 weeks. Adult skin was first incubated overnight at 4 °C in Dispase II solution (Roche) (2.5 mg ml$^{-1}$ in PBS) with the dermal side facing down. The dermis was separated mechanically from the epidermis, and both tissues were digested in a solution of collagenase D (Roche) (1 mg ml$^{-1}$) and DNase I (Roche) (1 mg ml$^{-1}$) in RPMI (Corning) with 10% FBS for 1 h at 37 °C. After digestion, the dermis and epidermis were homogenized using an 18G needle. The cell suspension was filtered through a 70-µm cell strainer into a flow cytometry tube.

For the spleen and the lung, tissues were enzymatically digested in a solution of collagenase D (Roche) (1 mg ml$^{-1}$) and DNase I (Roche) (1 mg ml$^{-1}$) in HBSS (Corning) for 30 min at 37 °C, followed by mechanical trituration with an 18G blunt-tipped syringe and filtration through a 70-µm filter.

Single-cell suspensions from livers were obtained after digestion with collagenase IV (C5138, Sigma) in HBSS (Corning) at 37 °C for 45 min. Non-parenchymal cells were enriched by centrifugation in 35% Percoll (17-0891-01, GE Healthcare) for 30 min at 1,300 r.c.f.

BM single-cell suspensions were obtained after flushing out the BM from the femur using a 27G needle and then were incubated with ACK lysis buffer (420301, BioLegend) for 3 min at room temperature. Blood was drawn from the liver sinus and treated twice with ACK lysis buffer for 5 min at room temperature.

For flow cytometry, cells were stained in FACS buffer with flow cytometry monoclonal antibodies for 20 min at 4 °C.

Murine HPCs were sorted as DAPI$^{-}$lineage$^{-}$c-Kit$^{+}$Sca1$^{-}$ singlets, and murine LSK$^{+}$ cells were sorted as DAPI$^{-}$lineage$^{-}$c-Kit$^{+}$Sca1$^{+}$ singlets. Human transduced HPCs were sorted as DAPI$^{-}$, GFP$^{+}$ or GFP$^{-}$ singlets.

Flow cytometry was performed using a Fortessa analyzer (BD), and sorting was performed using a FACSAria II (BD) or an LSR II (BD). Flow cytometry data analysis was performed using FlowJo (TreeStar) software. Antibodies used are listed in Table 1.

**Table 1 | Primary antibodies used for flow cytometry**

| Markers | Reactivity | Clone | Company | Dilution |
|---|---|---|---|---|
| CD16/CD32 | Mouse | 93 | eBioscience | 1:200 |
| Sca1 | Mouse | D7 | eBioscience | 1:200 |
| c-Kit | Mouse | 2B8 | eBioscience | 1:200 |
| FLT3L | Mouse | A2F10 | eBioscience | 1:100 |
| CD34 | Mouse | RAM34 | eBioscience | 1:100 |
| CD11b | Mouse | M1/70 | eBioscience | 1:100 |
| Ter119 | Mouse | TER-119 | eBioscience | 1:200 |
| Gr1 | Mouse | RB6-8C5 | eBioscience | 1:200 |
| B220 | Mouse | RA3-6B2 | eBioscience | 1:200 |
| CD115 | Mouse | AFS98 | eBioscience | 1:200 |
| CD45 | Mouse | 30-F11 | BioLegend | 1:200 |
| Ly6G | Mouse | 1A8 | BioLegend | 1:200 |
| MHCII | Mouse | M5/114.15.2 | eBioscience | 1:200 |
| CD11c | Mouse | N418 | Invitrogen | 1:200 |
| Ly6C | Mouse | A2-21 | eBioscience | 1:200 |
| F4/80 | Mouse | BM8 | BioLegend | 1:200 |
| Siglec F | Mouse | E50:2440 | BD Biosciences | 1:200 |
| CD24 | Mouse | M1/69 | BD Biosciences | 1:200 |
| CD103 | Mouse | 2E7 | BioLegend | 1:200 |
| EpCAM | Mouse | G8.8 | eBioscience | 1:200 |
| CD4 | Mouse | RM4.5 | eBioscience | 1:200 |
| CD8 | Mouse | 5H10 | Invitrogen | 1:200 |
| CD3 | Mouse | 145-2C11 | BD Biosciences | 1:200 |
| NK1.1 | Mouse | PK136 | eBioscience | 1:200 |
| CD45 | Human | 2D1 | eBioscience | 1:200 |
| CD34 | Human | 581 | BioLegend | 5:100 |
| CD38 | Human | HIT2 | BD Biosciences | 3:100 |
| CD123 (IL3Rα 6) | Human | 6H6 | BioLegend | 1:100 |
| CD11c | Human | B-ly6 | BD Horizon | 1:100 |
| CD1a | Human | HI149 | BioLegend | 1:100 |
| CD14 | Human | MHCD1405 | Invitrogen | 1:100 |
| CD207 | Human | IM3577 | Beckman Coulter | 1:100 |

**Table 2 | Primary antibodies used for multiplexed immunohistochemical consecutive staining**

| Marker | Reactivity | Reference | Clone | Antigen retrieval | Dilution | Incubation |
|---|---|---|---|---|---|---|
| Langerin | Human | Novocastra | 12D6 | pH 9 | 1:50 | 1 h at RT |
| CD1a | Human | Dako | O10 | pH 6 | 1:50 | 1 h at RT |
| Ki-67 | Human | Ventana | 30-09 | pH 9 | RTU | 1 h at RT |
| CD207 | Mouse | eBioscience | eBioRMUL.2 | pH 9 | 1:200 | Overnight at 4 °C |
| Ki-67 | Mouse | Bethyl | IHC-00375 | pH 9 | 1:250 | Overnight at 4 °C |
| $p16^{INK4a}$ | Human | Santa Cruz Biotechnology | Sc-759 | pH 9 | 1:50 | 1 h at RT |
| $p16^{INK4a}$ | Human | Ventana | BioHistomarker | CC1 | N/A | |
| CD33 | Human | Leica | PWS44 | CC1 | 1:100 | |
| CD163 | Human | Novocastra | 10D6 | CC1 | 1:200 | |
| CD14 | Human | Abcam | 7 | CC1 | 1:10 | |
| $BRAF^{V600E}$ | Human | Ventana | VE1 | CC1 | 1:50 | |
| P2RY12 | Human | Sigma | N/A | Target Retrieval Solution (Dako) | 1:1,000 | |

CC1, cell conditioning 1; N/A, not available; RT, room temperature; RTU, ready to use.

**Table 3 | Primers used for qPCR**

| Primer | Sequence |
|---|---|
| 5′-actin (*Actb*) | CTAAGGCCAACCGTGAAA |
| 3′-actin | ACCAGAGGCATACAGGGA |
| 5′-*Cdkn2a* | CCCAACGCCCCGAACT |
| 3′-*Cdkn2a* | GCAGAAGAGCTGCTACGTGAA |
| 5′-*Il1a* | CCATAACCCATGATCTGGAAGAGAC |
| 3′-*Il1a* | GTCCACATCCTGATATATAGTTTG |
| 5′-*Il1b* | TGGCAACTGTTCCTGAAC |
| 3′-*Il1b* | GGGTCCGTCAACTTCAAA |
| 5′-*Il6* | GCTACCAAACTGGATATA |
| 3′-*Il6* | CCAGGTAGCTATGGTACT |
| 5′-*Mmp13* | GGAGCCCTGATGTTTCCCAT |
| 3′-*Mmp13* | GTCTTCATCGCCTGGACCATA |

**Multiplexed immunohistochemical consecutive staining on a single slide.** Tissues were fixed with 4% formaldehyde for 24 h and embedded in paraffin. Five-mm-thick FFPE tissue sections on glass slides were baked at 37 °C overnight, deparaffinized in xylene and rehydrated in decreasing concentrations of ethanol. Next, tissue sections were incubated in retrieval solution (pH 6 or 9) for antigen retrieval at 95 °C for 30 min. Tissue sections were incubated in 3% hydrogen peroxide and in serum-free protein block solution (Dako, X0909) before adding the primary antibody for 1 h at room temperature. After signal amplification using the EnVison+ System HRP Labeled Polymer anti-mouse (Dako, K4001) or anti-rabbit (Dako, K4003) antibodies, chromogenic revelation was performed using 3-amino-9-ethylcarbazole (Vector Laboratories, SK4200). Slides were counterstained with hematoxylin, mounted with a glycerol-based mounting medium (Dako, C0563) and scanned for digital imaging (Hamamatsu NanoZoomer S60 Whole Slide Scanner). Next, the same slides were successively stained as described previously[37]. Primary antibodies used are listed in Table 2.

Images were analyzed (automatic analysis) using QuPath software (https://qupath.github.io/).

**Senescence-associated β-galactosidase staining.** Cells or frozen tissues were stained for SAβGal using the Senescence Detection kit (BioVision, K320-250) according to the manufacturer's instructions. Senescent cells were identified as blue-stained cells by light microscopy. Images were taken using a Hamamatsu NanoZoomer S60 Whole Slide Scanner. Images were analyzed using QuPath software (https://qupath.github.io/).

**Western blot.** Cells were lysed with lysis buffer (50 mM Tris, pH 7.5, 1% NP-40, 150 mM NaCl, 10% glycerol, 1 mM EDTA, supplemented with protease inhibitor cocktail tablets (Roche)). After a 5-min incubation on ice, lysates were centrifuged at 15,000 r.p.m. for 10 min, and supernatants were collected. Protein concentrations were quantified using BCA (Pierce). Proteins were separated with NuPAGE 4–12% Bis-Tris gels (Novex) and transferred to nitrocellulose membranes (10600006, Amersham) according to standard protocols. Membranes were immunoblotted overnight with primary antibodies against pERK (4370L, Cell Signaling), BRAF (9002, Santa Cruz) and β-actin (5125S, Cell Signaling), followed by secondary anti-rabbit IgG antibody (7074S, Cell Signaling). Chemiluminescent signals were detected on X-ray film.

**Methylcellulose assays.** To determine the differentiation potential of murine progenitors, femurs from *BRAF*-$V600E^{Scl+}$ or *BRAF*-$WT^{Scl+}$ control littermates were collected. Lineage-negative BM cells were obtained with a lineage cell depletion kit (MACS, Miltenyi Biotec, 130-090-858). One thousand lineage-negative BM cells (or sorted lineage-negative $Rosa^{YFP+}$ BM cells, depending on the experiment) were resuspended in IMDM (Gibco) supplemented with 2% FBS, plated in 1 ml methylcellulose medium (MethoCult M3434, Stemcell Technologies) and kept in culture for 14 d. Numbers and types of CFUs were assessed at day 14.

To determine the differentiation potential of human progenitors, 500 transduced $CD34^+$ HPCs were sorted according to GFP expression levels 3 d after transduction, resuspended in IMDM (Gibco) supplemented with 2% FBS and plated in 1 ml methylcellulose medium (MethoCult H4434, Stemcell Technologies) for 14 d. Numbers and types of CFUs were assessed at day 14.

**Gene expression profiling using microarrays and RNA-seq.** One hundred thousand human transduced HPCs were sorted according to GFP expression levels directly into Arcturus PicoPure Extraction Buffer (Applied Biosystems, 12317-03) 7 d after transduction with $BRAF^{V600E}$ or NGFR lentiviral constructs. Total RNA was processed from the sorted cells according to the PicoPure RNA Isolation kit protocol (Molecular Devices). RNA concentration and quality were verified using the 6000 Pico Chip (Agilent) at the Baylor College of Medicine Microarray Facility. cDNA amplification was performed with the WT-Ovation Pico System, according to the manufacturer's protocol (NuGen). Fragmented and biotinylated cDNA samples for the gene chip studies were generated using the FL-Ovation cDNA Biotin Module version 2 (NuGEN).

For Fig. 4b, total RNA was isolated from sorted subpopulations from peripheral blood and lesion specimens according to the Arcturus PicoPure RNA Isolation kit protocol (Applied Biosystems). RNA quality was verified using the Pico Chip at the Baylor College of Medicine Microarray Facility (all RIN > 6). cDNA amplification was performed using the Ovation Pico WTA version 2 system according to the manufacturer's protocol (NuGEN). Fragmented and biotinylated cDNA was hybridized to the GeneChip Human Transcriptome Array 2.0 according to the manufacturer's procedures (Affymetrix). Raw data from all samples were normalized using the SST-RMA algorithm implemented in the Affymetrix Expression Console. Differentially expressed genes were identified using BRB-ArrayTools version 4.5 (version 4.5, Biometric Research Branch, NCI) with a multivariate permutation test with a confidence level of false discovery rate assessment at 80% and the maximum allowed proportion of false-positive proteins at 0.1.

Human $CD34^+$ BM cells from patients with LCH were sorted directly into TRIzol LS Reagent (Ambion, Life Technologies, 10296028) and stored at −80 °C. RNA was extracted according to the RNeasy Mini kit protocol (Qiagen). RNA (1 ng) was converted to cDNA using the SMART-Seq version 4 Ultra Low Input RNA kit (Clontech). RNA-seq libraries were prepared using the Low Input Library Prep kit version 2 (Clontech). Sequencing was performed using the Illumina

NextSeq 500 system. Transcript abundance was quantified with the Ensembl GRCh38 cDNA reference using Kallisto version 0.43.0.

**Quantitative PCR.** Conventional reverse transcription was performed using the RNA to cDNA EcoDry Premix (639548, Takara Bio) in accordance with the manufacturer's instructions. qPCR was performed on a CFX384 Touch Real-Time PCR detection system (Bio-Rad) using EXPRESS SYBR GreenER master mix (11784200, Invitrogen) as follows: one cycle at 95 °C (10 min) and 40 cycles of 95 °C (15 s) and 58 °C (1 min). The expression of actin was used to normalize expression. The average threshold cycle number for each tested mRNA was used to quantify the relative expression: $2^{(Ct(Actb)-Ct(Cdkn2a))}$. Primers are listed below in Table 3.

**Proliferation assays.** For in vivo assay, *BRAF*-V600E$^{Scl+}$ or control littermate mice aged 8 weeks were injected intraperitoneally with 1 mg BrdU for 7 consecutive days. Femurs were collected 24 h after the last injection and processed into single-cell suspensions for BrdU incorporation by flow cytometry analysis. Tissue preparation and BrdU staining were performed according to the APC BrdU Flow kit protocol (BD PharMingen, 557892).

For in vitro assays, *BRAF*$^{V600E}$- or *NGFR*-transduced CD34$^+$ HPCs were kept in culture in StemSpan SFEM II medium (Stemcell Technologies). Transduced CD34$^+$ HPCs were incubated from day 10 to day 13 with 10 µM BrdU supplemented daily in cell culture medium. Transduced HPCs were collected at day 1 and analyzed for BrdU incorporation by flow cytometry using the same kit used for the in vivo experiment.

*Cell Trace Violet.* Transduced CD34$^+$ HPCs were labeled with 1 µM CFSE (Life Technologies) in PBS with 0.1% BSA for 10 min at 37 °C. Cells were analyzed 92 h after treatment with Cell Trace Violet.

**Competitive transplantation assays.** Femurs from 12-week-old *BRAF*-V600E$^{Scl+}$ or *BRAF*-WT$^{Scl+}$ mice were collected 4 weeks after tamoxifen injections. Lineage-negative BM cells from either *BRAF*-V600E$^{Scl+}$ or *BRAF*-WT$^{Scl+}$ mice (both CD45.2$^+$) were obtained using a MACS mouse lineage cell depletion kit (Miltenyi Biotec) and were injected intravenously together with lineage-negative BM cells of the host type (CD45.1$^+$) into lethally irradiated CD45.1$^+$ mice (1,200 rad delivered in two doses of 600 rad each, 3 h apart) at a ratio of 2:1 (200,000 CD45.2$^+$ cells:100,000 CD45.1$^+$ cells). Levels of blood donor chimerism were analyzed by measuring the percentage of CD45.2$^+$ cells among CD45$^+$ cells 4 and 8 weeks after transplantation.

**Enzyme-linked immunosorbent assay.** BM was prepared by flushing two femurs with 500 µl PBS. After pelleting the cells, supernatants were used for BM extra-fluid measurements and stored at −80 °C. For detecting and quantifying proteins, commercially available ELISA kits for IL-1α (R&D Systems, DY400), IL-1β (R&D Systems, DY401) and IL-6 (R&D Systems, DY406) were used.

Supernatants from transduced CD34$^+$ HPCs were collected at different time points (days 7, 9 and 14) and stored at −80 °C. For measurement of proteins levels, commercially available ELISA kits for IL-1α (BioLegend, 445807), IL-1β (BioLegend, 437007), IL-6 (BioLegend, 430507) and IL-8 (BioLegend, 431507) were used.

For human plasma specimens, blood was collected from pre-therapy pediatric patients with multisystem LCH and healthy pediatric controls in EDTA tubes and centrifuged at 400*g* for 30 min over a Ficoll gradient, and then the plasma supernatant was collected and recentrifuged for 5 min, and then purified supernatant was stored at −80 °C. None of the plasma samples analyzed underwent more than two freeze–thaw cycles. Protein levels were determined using the MAGPIX instrument (Luminex). The concentration of each analyte was measured by comparison to the protein standards. Levels of IL-6 and IL-8 were measured with the Millipore Human Cytokine/Chemokine Panel I (1:2 dilution).

**Therapeutic trials.** *Rapamycin in vitro.* Rapamycin (InvivoGen, tlrl-rap) was added at a concentration of 10 nM at day 1 and day 4 following transduction of CD34$^+$ HPCs. DMSO was used as a mock treatment. GFP-transduced cells were analyzed for myeloid surface marker expression (see antibody list) at day 8 post-transduction.

*Rapamycin in vivo.* Mice were treated with rapamycin or vehicle via intraperitoneal injection (diluted in 200 µl PBS per mouse) at 0.5 mg per kg of body weight per day for 10 consecutive days, starting 15 d after the generation of *BRAF*-WT$^{Scl+}$ or *BRAF*-V600E$^{Scl+}$ BM chimera. Mice were sacrificed at day 30.

*AP20187 in vivo.* Mice were treated with vehicle (4% ethanol:10% polyethylene glycol 400:2% Tween-20 in distilled water) or AP (purchased from Takara Bio (635069) and diluted in 4% ethanol:10% polyethylene glycol 400:2% Tween-20 in distilled water). AP or diluent was administered every Monday, Wednesday and Friday (triweekly) for 3 consecutive weeks by gavage at 10 mg per kg of body weight per day, following tamoxifen injections.

*ABT-263 (navitoclax) in vivo.* Mice were treated with diluent (10% ethanol:30% polyethylene glycol 400:60% Phosal 50 PG) or ABT-263 (diluted in 10% ethanol:30% polyethylene glycol 400:60% Phosal 50 PG). ABT-263 and vehicle were administered to mice by gavage at 50 mg per kg of body weight per day for 3 consecutive weeks.

**Reporting Summary.** Further information on research design is available in the Nature Research Reporting Summary linked to this article.

## Data availability

Datasets supporting the findings presented in this study are available from the corresponding author upon reasonable request. Any data that can be shared will be released via a material transfer agreement. Microarray sequencing data obtained from CD34$^+$ BM cells transduced with *BRAF*$^{V600E}$ or control NGFR lentiviral vector are listed in Supplementary Table 3. RNA-seq data obtained from CD34$^+$ cells purified from the BM of patients with LCH and healthy donors are listed in Supplementary Table 4. Source data are provided with this paper.

## References

35. Dankort, D. et al. A new mouse model to explore the initiation, progression, and therapy of *BRAF*$^{V600E}$-induced lung tumors. *Genes Dev.* **21**, 379–384 (2007).
36. Baccarini, A. et al. Kinetic analysis reveals the fate of a microRNA following target regulation in mammalian cells. *Curr. Biol.* **21**, 369–376 (2011).
37. Remark, R. et al. In-depth tissue profiling using multiplexed immunohistochemical consecutive staining on single slide. *Sci. Immunol.* **1**, aaf6925 (2016).

## Acknowledgements

We thank the Biorepository and Pathology Core and the Flow Cytometry Core Facilities at the Icahn School of Medicine at Mount Sinai for their technical expertise. We also thank K. Phaik Har Lim, T.-K. Man, T. Burke and B. Scull for their help with the generation of microarray sequencing data. We thank J. Kofler for kindly providing LCH-ND pictures and performing immunostaining. We thank L. Troncoso for her help. We thank C. Woods, image application specialist, Cincinnati Children's Hospital Medical Center, for figure preparation for human studies (Fig. 4g) and J. Kofler, UPMC Division of Neuropathology, for creating Extended Data Fig. 4e. M.M. received funding from the National Institute of Health (R01 CA154947 and R01 CA190400). C.B. received fellowships from the Fondation pour la Recherche Médicale (FDM20170638478), from l'Institut Servier and from Assistance Publique Hôpitaux de Paris (Année Recherche). C.M.W. is supported by the Swiss National Science Foundation (SNSF PostDoc Mobility Fellowship P400PM_186740) and by the Swiss Cancer League (grant for bursaries BIL KFS 4724-02-2019). We thank the research coordinators of the Histio–Lymphoma team at Texas Children's Cancer Center for their help with patient sample collection. The TXCH Histiocytosis Program is supported by a research grant from the HistioCure Foundation. This work was supported by the Department of Defense through the Peer Reviewed Cancer Research Program under award no. W81XWH-19-1-0167 (R.C.).

## Author contributions

C.B., J.L.B., C.M.W., R.C., S.T.C., A.T., R.M., H.A., J.J., I.L., M.C.-A., J.C.M., J.G., J.P. and H.A. designed and carried out experiments. A.B., P.I.P., A.L., S.G., K.L.M., J.P., C.E.A. and M.M. supervised experiments and analyzed and interpreted data. C.B., C.E.A. and M.M. drafted the manuscript. C.E.A. and M.M. designed the study, supervised experimental data collection and coordinated integration of collaboration between all participating laboratories. All authors critically reviewed and edited the final version of the manuscript.

## Competing interests

The authors declare no competing interests.

## Additional information

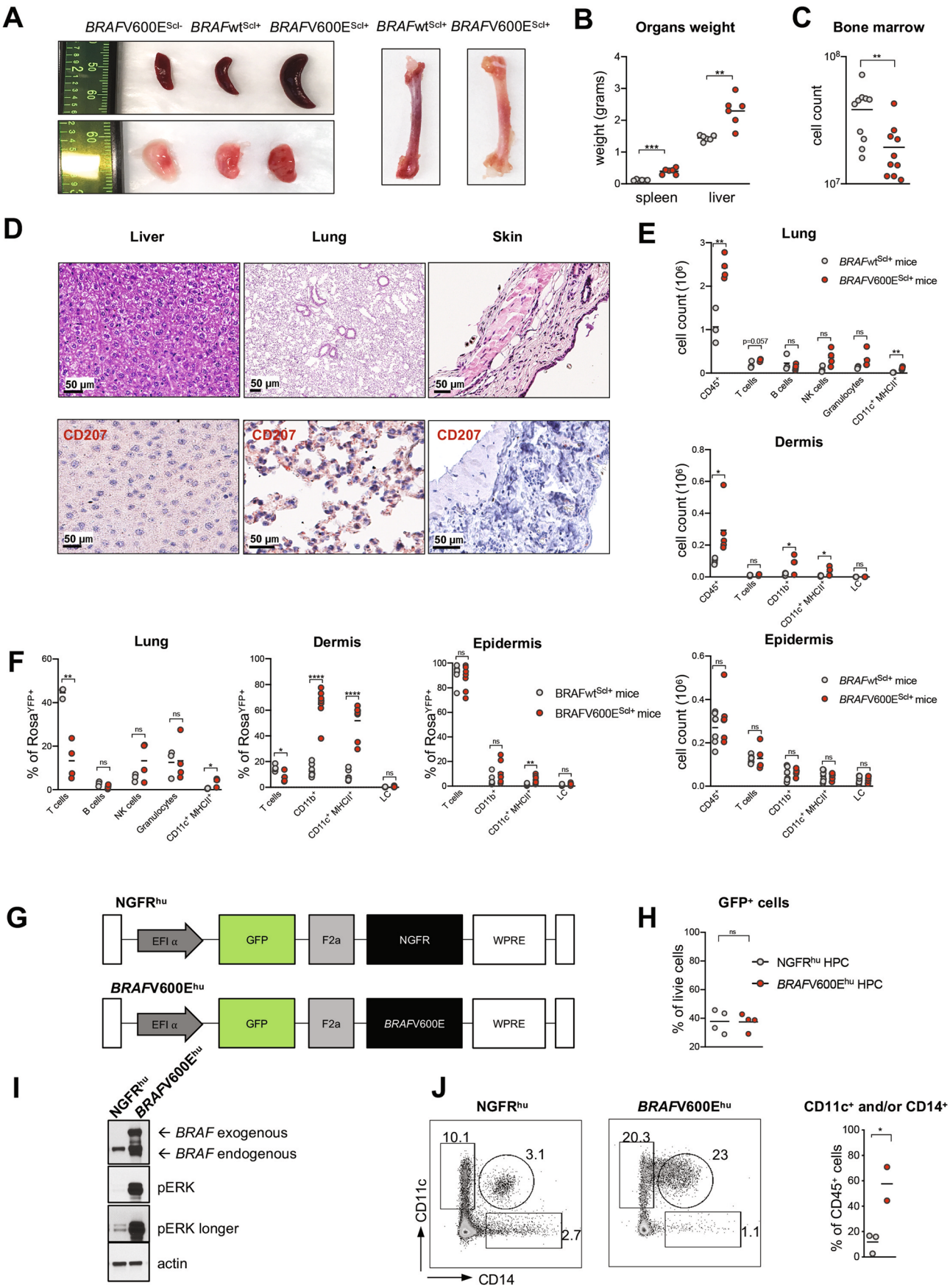
**Extended data** is available for this paper at https://doi.org/10.1038/s41591-021-01304-x.

**Supplementary information** The online version contains supplementary material available at https://doi.org/10.1038/s41591-021-01304-x.

**Correspondence and requests for materials** should be addressed to M.M.

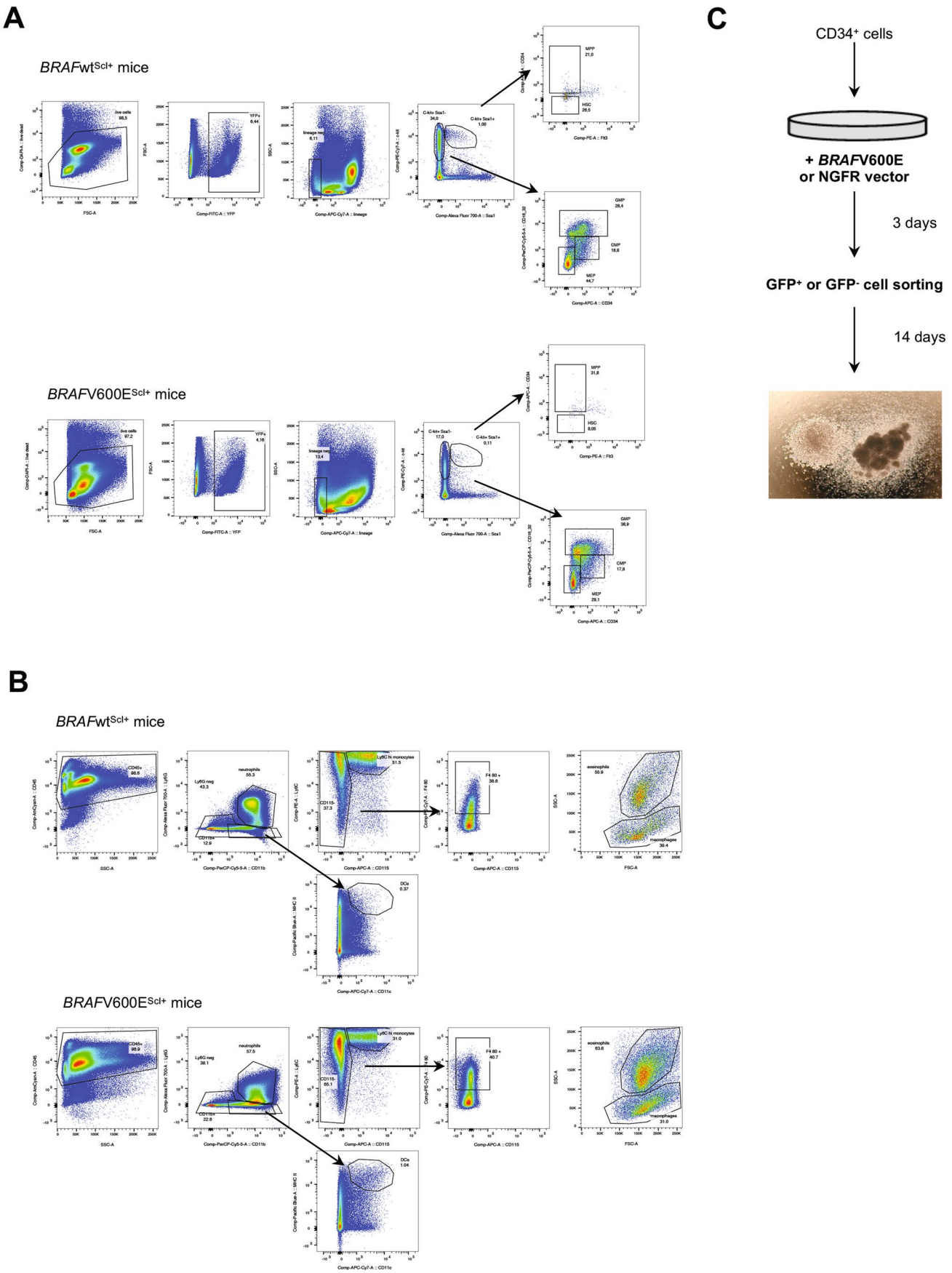
**Peer review information** *Nature Medicine* thanks the anonymous reviewers for their contribution to the peer review of this work. Joao Monteiro was the primary editor on this article and managed its editorial process and peer review in collaboration with the rest of the editorial team.

**Reprints and permissions information** is available at www.nature.com/reprints.



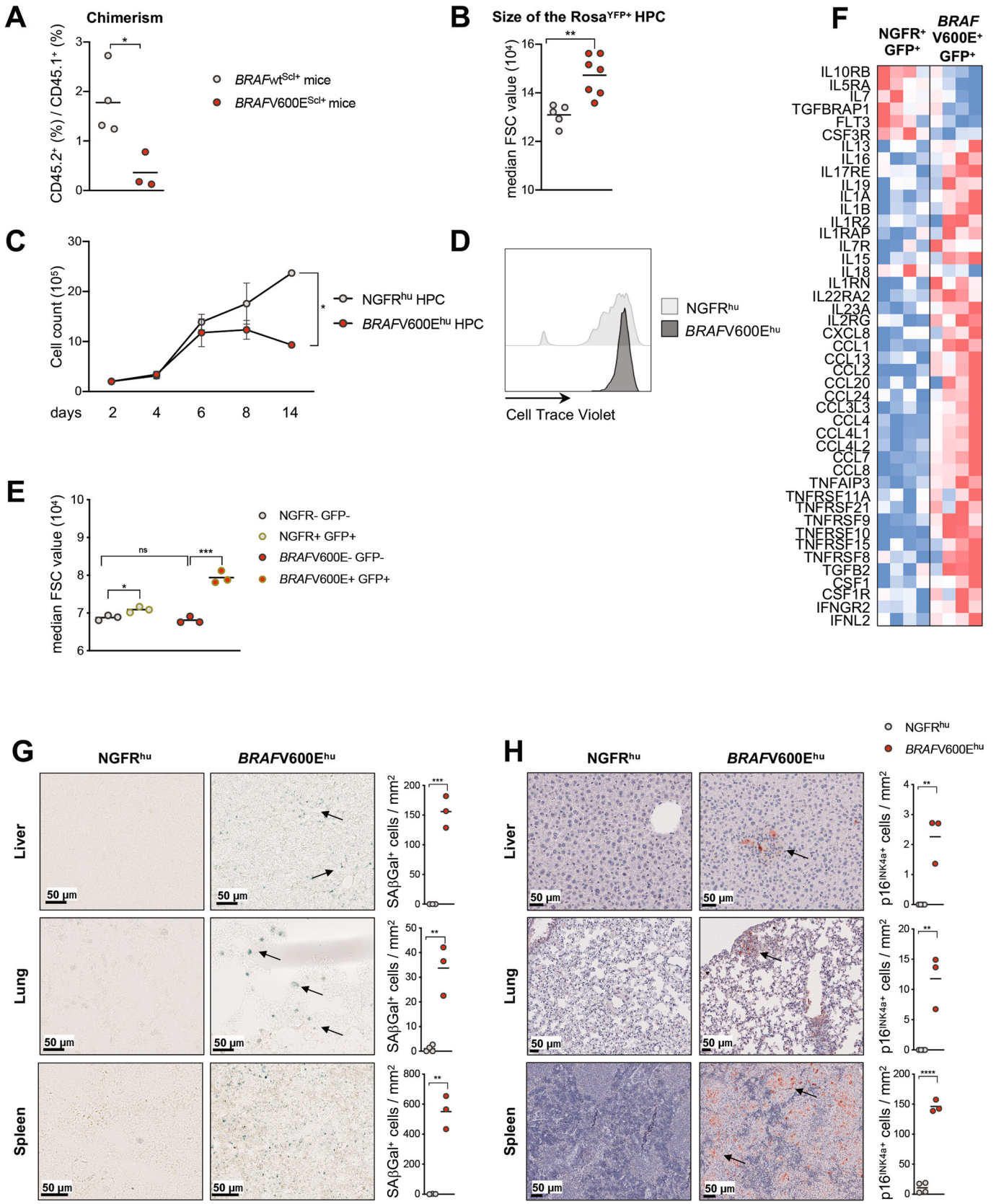

**Extended Data Fig. 1 | See next page for caption.**

**Extended Data Fig. 1 | Langerhans Cell Histiocytosis mouse models. a-f**, *BRAF*V600E$^{Scl+}$ mice and *BRAF*wt$^{Scl+}$ mice were generated as described in Fig. 1a. **a**, Representative images of spleen, lung, and femurs at 4 weeks post tamoxifen injections. **b**, Liver and spleen weights. **c**, Absolute number of BM cells in *BRAF*V600E$^{Scl+}$ mice and control littermates (n = 10 mice per group). **d**, Hematoxylin and eosin staining and CD207 immunohistochemistry staining of tissues isolated from *BRAF*wt$^{Scl+}$ mice (n = 2–3 mice per group). **e**, Absolute numbers of lung, dermal and epidermal immune cells in *BRAF*V600E$^{Scl+}$ mice and control littermates. Data are representative of 3 experiments (n = 3–8). **f**, Percentage of immune cell populations among lung and skin infiltrating Rosa$^{YFP+}$ cells in *BRAF*V600E$^{Scl+}$ mice and control littermates. Data are representative of 3 experiments (n = 3–8). **g**, Scheme of the lentiviral vector constructs used to transduce human CD34$^+$ HPC. **h**, Graph shows that the transduction efficiency of *BRAF*V600E and NGFR lentiviral constructs in human CD34$^+$ HPC does not exceed 40 %. **i**, Western blot of *BRAF* and phospho-ERK performed on purified *BRAF*V600E$^{hu}$ and NGFR$^{hu}$ human CD34$^+$ HPC 7 days after transduction. **j**, Representative flow plot showing the percentage of CD11c$^+$ CD14$^+$ MNP among circulating blood cells in NSG mice reconstituted with *BRAF*V600E$^{hu}$ and NGFR$^{hu}$ HPC. Graph represents the percentage of CD11c and or CD14$^+$ cells among human CD45$^+$ cells from NSG circulating blood (n = 2–3 mice per group). Data are represented as mean ± s.e.m; statistical significance analyzed by an unpaired two-sided t-test is indicated by *$p < 0.05$; **$p < 0.01$; ***$p < 0.001$; ****$p < 0.0001$.



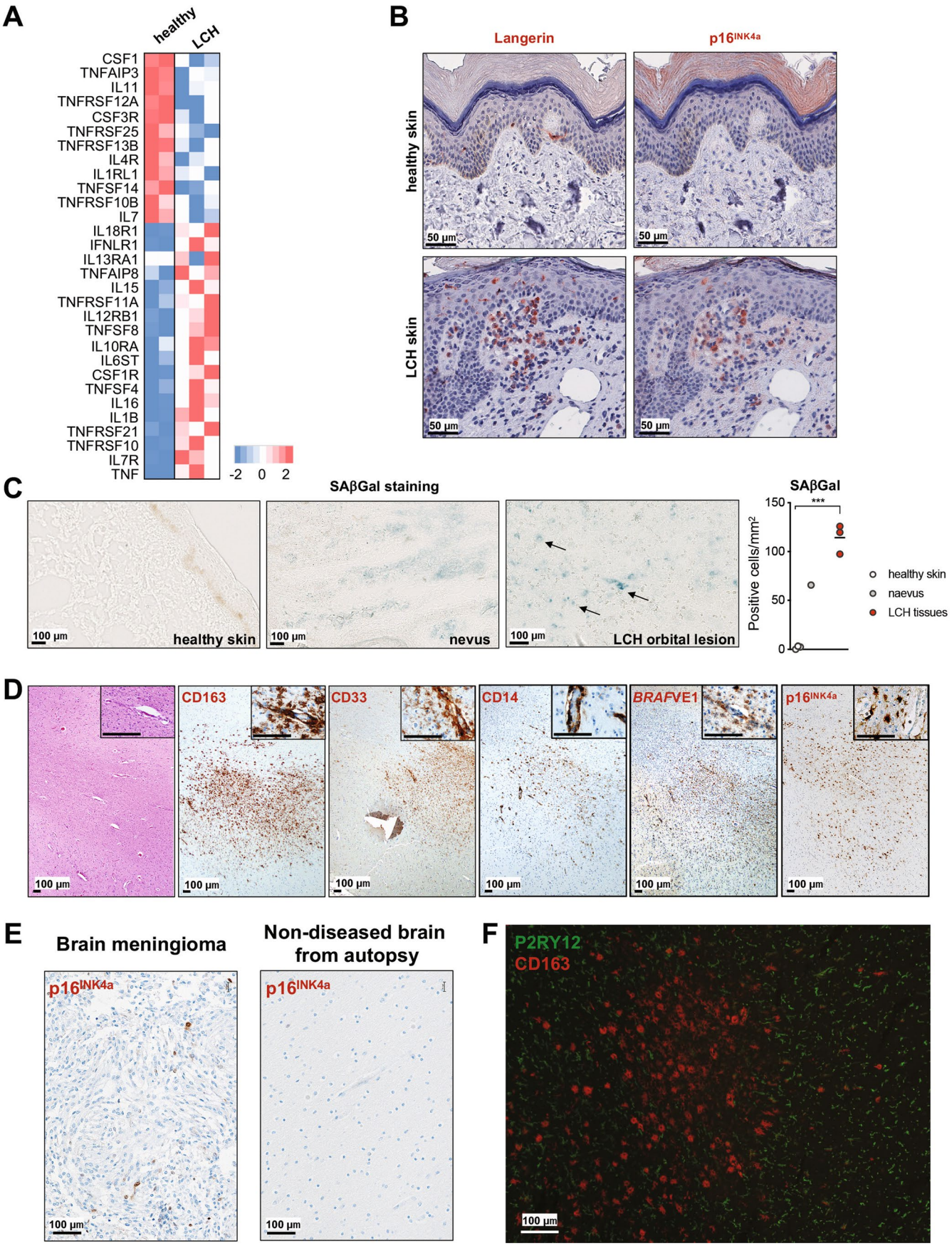

**Extended Data Fig. 2 | See next page for caption.**

**Extended Data Fig. 2 | Myeloid skewing of *BRAF*V600E$^{+}$ hematopoietic progenitors. a**, Flow cytometry gating strategy for hematopoietic progenitors (HSC: hematopoietic stem cell, MPP: multipotent progenitors, GMP: Granulocyte-macrophage progenitors, CMP: common myeloid progenitors, MEP: megakaryocyte-erythroid progenitors) in *BRAF*wt$^{Scl+}$ and *BRAF*V600E$^{Scl+}$ animals. **b**, Flow cytometry gating strategy for bone marrow myeloid cells in *BRAF*wt$^{Scl+}$ and *BRAF*V600E$^{Scl+}$ animals. **c**, Experimental design of the CFU assays performed in Fig. 2e is shown.



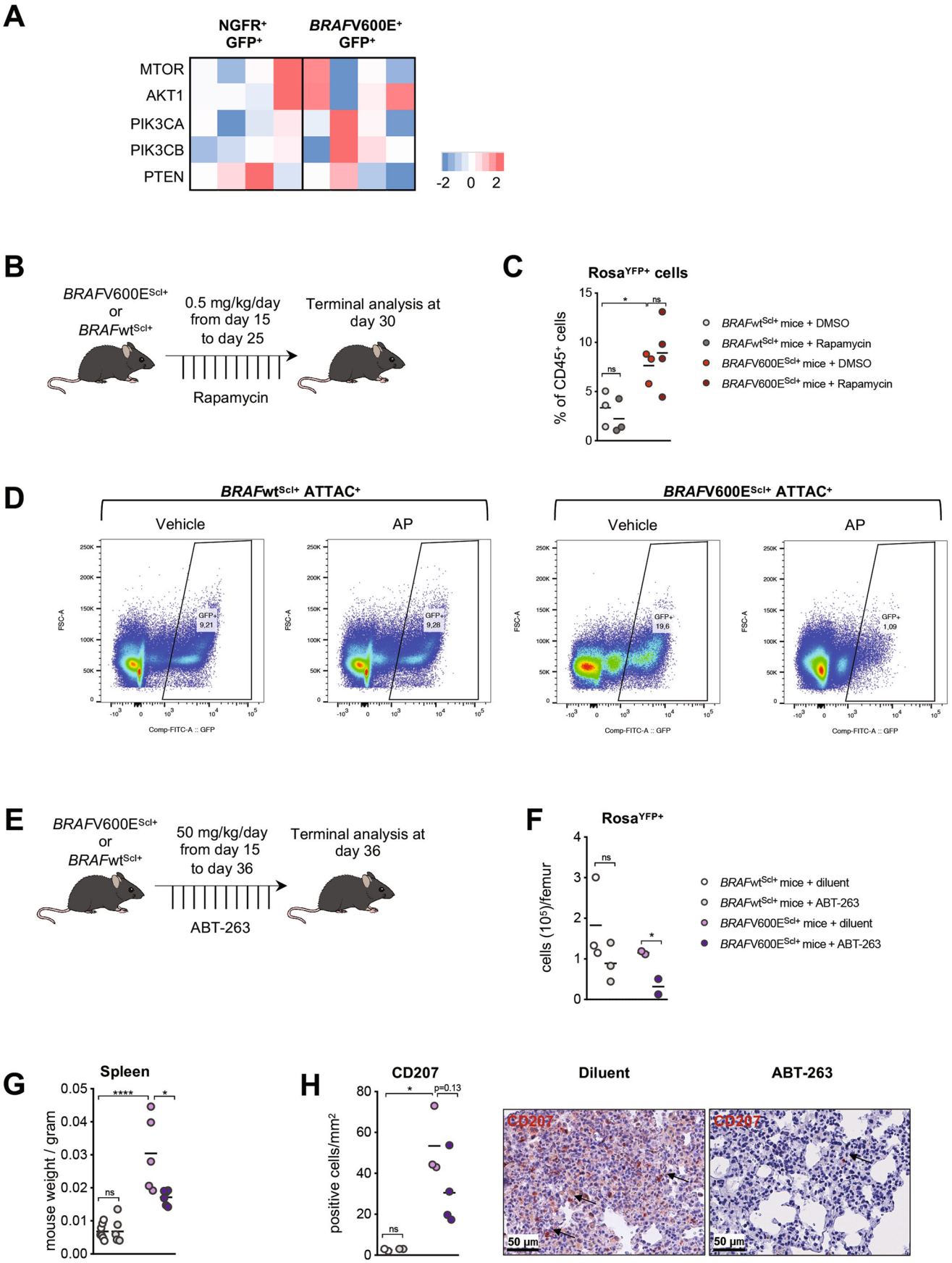

**Extended Data Fig. 3 | See next page for caption.**

**Extended Data Fig. 3 | Senescence program in different LCH models. a**, Lineage negative BM cells isolated from either *BRAF*V600E$^{Scl+}$ CD45.2$^+$ or *BRAF*wt$^{Scl+}$ CD45.2$^+$ mice were injected intravenously together with lineage negative CD45.1$^+$ BM cells into lethally irradiated CD45.1$^+$ mice at a 2:1 ratio (CD45.2$^+$: CD45.1$^+$). Graph shows the ratio of CD45.2$^+$ / CD45.1$^+$ in blood circulation in each group measured 8 weeks after transplantation using flow cytometry (n = 8). **b**, Forward scatter measurement of lineage negative Rosa$^{YFP+}$ cells in the BM from *BRAF*V600E$^{Scl+}$ mice and *BRAF*wt$^{Scl+}$ control littermates (n = 5–7 mice per group). **c**, Expansion of human CD34$^+$ cord blood HPC transduced with NGFR (NGFR$^{hu}$) or *BRAF*V600E (*BRAF*V600E$^{hu}$) lentiviral constructs and cultured in stem-cell media. Data are representative of at least 3 experiments (n = 3 donors). **d**, Proliferation capacity of NGFR$^{hu}$ and *BRAF*V600E$^{hu}$ HPC analyzed by Cell Trace Violet dilution, 92 hours after staining. **e**, Forward scatter measurement of NGFR$^{hu}$ and *BRAF*V600E$^{hu}$ HPC (n = 3 different donors) **f**, Heat map representation of SASP genes analyzed by microarray expression profiling of *BRAF*V600E$^+$ GFP$^+$ HPC and NGFR$^+$ GFP$^+$ HPC 7 days after transduction (n = 4 different donors). **g-h**, Frozen or FFPE tissue sections isolated from humanized mice reconstituted with *BRAF*V600E$^{hu}$ and NGFR$^{hu}$ HPC and stained for **g**, SAβGal activity or (**h**) p16$^{INK4a}$. Graph shows the number of positive cells per mm$^2$. Data are represented as mean ± s.e.m; *p < 0.05; **p < 0.01; ***p < 0.001; ****p < 0.0001 (unpaired two-sided t-tests, two-way ANOVA test for Extended Data Fig. 2c).




**Extended Data Fig. 4 | See next page for caption.**

**Extended Data Fig. 4 | Human LCH lesions show features of senescence. a**, Heat map representation of SASP associated gene expression measured by RNA sequencing in purified CD34$^+$ BM cells isolated from three LCH patients and one age-matched healthy donor (performed as duplicates). **b**, Skin from LCH patient and healthy age-matched donor were stained for CD207 and p16$^{INK4a}$ by immunohistochemistry. **c**, SAβGal activity of human tissues and LCH lesions. One representative image of healthy skin, naevus and LCH lesion are shown. Graph shows the number of SAβGal positive cells per mm$^2$ in healthy skins (n = 3), naevus (n = 1) and LCH lesions (n = 3). **d**, Autopsy brain sections from a patient with neurodegenerative-LCH and circulating *BRAF*V600E$^+$ peripheral blood cells. The H&E image shows a temporal lobe white matter injury with increased numbers of infiltrating plump cells. The immunohistochemical characterization of the enlarged plump cells shows a positivity for CD163, CD33, CD14, *BRAF*VE1 and p16$^{INK4a}$. (*indicates perivascular space). **e**, Control tissue with rare p16$^{INK4a}$ positivity by immunohistochemistry in meningioma and no appreciable staining in human brain (non-diseased from autopsy). **f**, Brain section from human patient with neurodegenerative-LCH (see Fig. 4g) dual-stained for P2RY12 (green) and CD163 (red). Spindled P2RY12$^+$ microglial cells surround the aggregates of plump activated CD163$^+$ macrophages. There is no dual staining. There is diminished P2RY12 staining within the CD163$^+$ macrophage rich aggregate. Image courtesy of Dr. Julia Kofler, MD UPMC Division of Neuropathology. Data are represented as mean ± s.e.m; statistical significance analyzed by an unpaired two-sided t-test is indicated by *$p < 0.05$; **$p < 0.01$; ***$p < 0.001$; ****$p < 0.0001$.




**Extended Data Fig. 5 | See next page for caption.**

**Extended Data Fig. 5 | Rapamycin and senolytic treatments improve LCH outcome. a**, Human CD34$^+$ cord blood HPC were transduced with *BRAF*V600E (*BRAF*V600E$^{hu}$) or NGFR control (NGFR$^{hu}$) lentiviral vectors, cultured in stem-cell media and analyzed for gene expression of PI3K pathway genes using microarray expression profiling 7 days after transduction (n = 4 donors); **b-c**, *BRAF*V600E$^{Scl+}$ mice and *BRAF*wt$^{Scl+}$ control littermates were treated with rapamycin (0.5 mg/ kg body weight/ day) or DMSO for 10 days. **b**, Cartoon shows the experimental design to test the clinical benefit of rapamycin on LCH in mice. **b**, Graph shows the percentage of Rosa$^{YFP+}$ cells among CD45$^+$ BM cells (n = 3–4 mice per group). **d**, *BRAF*V600E$^{Scl+}$ ATTAC$^+$ mice and *BRAF*wt$^{Scl+}$ ATTAC$^+$ control littermates were treated by tamoxifen for five days. Following tamoxifen injections, *BRAF*V600E$^{Scl+}$ ATTAC$^+$ mice and *BRAF*wt$^{Scl+}$ ATTAC$^+$ control littermates were treated by AP or vehicle during three weeks and sacrificed 4 weeks after tamoxifen injections. Representative flow plot showing the percentage of GFP$^+$ cells among CD45$^+$ live cells in the bone marrow from *BRAF*V600E$^{Scl+}$ ATTAC$^+$ mice and *BRAF*wt$^{Scl+}$ ATTAC$^+$ control littermates. **e-h**, *BRAF*V600E$^{Scl+}$ mice and *BRAF*wt$^{Scl+}$ control littermates were treated with ABT-263 (50 mg/ kg body weight/ day) or diluent for 21 days. **e**, Cartoon shows the experimental design to test the clinical benefit of ABT-263 on LCH in mice. **f**, Graph shows the absolute numbers of bone marrow Rosa$^{YFP+}$ cells (n = 2–3) **g**, Spleen weight and (**h**) lung infiltrating CD207$^+$ cells isolated from mice treated with ABT-263 or diluent (n = 3–4) with representative images of lung tissue sections isolated from mice treated with ABT-263 or diluent and stained with CD207. Data are representative of 2 experiments (n = 3–4). Data are represented as mean ± s.e.m; statistical significance analyzed by an unpaired two-sided t-test is indicated by *$p < 0.05$; **$p < 0.01$; ***$p < 0.001$; ****$p < 0.0001$.

nature research

Corresponding author(s): Miriam Merad

Last updated by author(s): 01/28/2021

# Reporting Summary

Nature Research wishes to improve the reproducibility of the work that we publish. This form provides structure for consistency and transparency in reporting. For further information on Nature Research policies, see Authors & Referees and the Editorial Policy Checklist.

## Statistics

For all statistical analyses, confirm that the following items are present in the figure legend, table legend, main text, or Methods section.

| n/a | Confirmed | |
|---|---|---|
| ☐ | ☒ | The exact sample size (*n*) for each experimental group/condition, given as a discrete number and unit of measurement |
| ☐ | ☒ | A statement on whether measurements were taken from distinct samples or whether the same sample was measured repeatedly |
| ☐ | ☒ | The statistical test(s) used AND whether they are one- or two-sided<br>*Only common tests should be described solely by name; describe more complex techniques in the Methods section.* |
| ☒ | ☐ | A description of all covariates tested |
| ☒ | ☐ | A description of any assumptions or corrections, such as tests of normality and adjustment for multiple comparisons |
| ☐ | ☒ | A full description of the statistical parameters including central tendency (e.g. means) or other basic estimates (e.g. regression coefficient) AND variation (e.g. standard deviation) or associated estimates of uncertainty (e.g. confidence intervals) |
| ☐ | ☒ | For null hypothesis testing, the test statistic (e.g. *F*, *t*, *r*) with confidence intervals, effect sizes, degrees of freedom and *P* value noted<br>*Give P values as exact values whenever suitable.* |
| ☒ | ☐ | For Bayesian analysis, information on the choice of priors and Markov chain Monte Carlo settings |
| ☒ | ☐ | For hierarchical and complex designs, identification of the appropriate level for tests and full reporting of outcomes |
| ☒ | ☐ | Estimates of effect sizes (e.g. Cohen's *d*, Pearson's *r*), indicating how they were calculated |

*Our web collection on statistics for biologists contains articles on many of the points above.*

## Software and code

Policy information about availability of computer code

| | |
|---|---|
| Data collection | FACS Diva software version 7(BD), QuPath (version 0.1.2) |
| Data analysis | FlowJo v10.0.6 (Tree Star Inc.), GraphPad Prism v8.0e (GraphPad Software Inc.), QuPath v0.1.2, ImageJ v1.52, RStudio v1.2, R v3.5.3, R packages: matrixStats, Matrix.utils, mixtools, matrix. tglkmeans (https://tanaylab.bitbucket.io/tglkmeans/). |

For manuscripts utilizing custom algorithms or software that are central to the research but not yet described in published literature, software must be made available to editors/reviewers. We strongly encourage code deposition in a community repository (e.g. GitHub). See the Nature Research guidelines for submitting code & software for further information.

## Data

Policy information about availability of data

All manuscripts must include a data availability statement. This statement should provide the following information, where applicable:

- Accession codes, unique identifiers, or web links for publicly available datasets
- A list of figures that have associated raw data
- A description of any restrictions on data availability

The dataset supporting the findings presented in this study are available from the corresponding author upon reasonable request. Any data that can be shared will be released via a material transfer agreement. Micro-array sequencing data obtained from CD34+ bone marrow cells transduced with BRAFV600E or control NGFR lentiviral vector are listed in Extended Data Table 3. RNA sequencing data obtained from bone marrow purified CD34+ cells from LCH patients and healthy donor are listed in Extended data table 4.

# Field-specific reporting

Please select the one below that is the best fit for your research. If you are not sure, read the appropriate sections before making your selection.

☒ Life sciences ☐ Behavioural & social sciences ☐ Ecological, evolutionary & environmental sciences

For a reference copy of the document with all sections, see nature.com/documents/nr-reporting-summary-flat.pdf

# Life sciences study design

All studies must disclose on these points even when the disclosure is negative.

| | |
|---|---|
| Sample size | No statistical methods were used to predetermine sample size. The phenotype had a robust penetrance (100% genotype to phenotype) so each experiment was done with a sample size of 3-8 mice per group. |
| Data exclusions | No data was excluded |
| Replication | All experiments were reproduced at least once. All attempts for replication were successfull. |
| Randomization | Mice were allocated to study groups randomly. |
| Blinding | Quantification of immune infiltration was blinded by de-identifying samples. |

# Reporting for specific materials, systems and methods

We require information from authors about some types of materials, experimental systems and methods used in many studies. Here, indicate whether each material, system or method listed is relevant to your study. If you are not sure if a list item applies to your research, read the appropriate section before selecting a response.

## Materials & experimental systems

| n/a | Involved in the study |
|---|---|
| ☐ | ☒ Antibodies |
| ☐ | ☒ Eukaryotic cell lines |
| ☒ | ☐ Palaeontology |
| ☐ | ☒ Animals and other organisms |
| ☐ | ☒ Human research participants |
| ☒ | ☐ Clinical data |

## Methods

| n/a | Involved in the study |
|---|---|
| ☒ | ☐ ChIP-seq |
| ☐ | ☒ Flow cytometry |
| ☒ | ☐ MRI-based neuroimaging |

## Antibodies

Antibodies used

Antibodies used for immuno-histochemistry (IHC):
Langerin Human Novocastra 12D6
CD1a Human Dako O10
Ki67 Human Ventana 30-09
CD207 Mouse eBioscience eBioRMUL.2
Ki67 Mouse Bethyl IHC-00375
CDKN2A Human Santa Cruz Biotechnology Sc-759

Antibodies used for flow cytometry and FACS:
CD16/32 mouse 93 eBioscience
Sca1 mouse D7 eBioscience
c-kit mouse 2B8 eBioscience
FLT3L mouse A2F10 eBioscience
CD34 mouse RAM34 eBioscience
CD11b mouse M1/70 eBioscience
Ter119 mouse TER-119 eBioscience
Gr1 mouse RB6-8C5 eBioscience
B220 mouse RA3-6B2 eBioscience
CD115 mouse AFS98 eBioscience
CD45 mouse 30-F11 Biolegend
Ly6G mouse 1A8 Biolegend
MHC II mouse M5/114.15.2 eBioscience
CD11c mouse N418 Invitrogen
Ly6C mouse A2-21 eBioscience
F4/80 mouse BM8 Biolegend

Siglec F mouse E50:2440 BD bioscience
CD24 mouse M1/69 BD bioscience
CD103 mouse 2E7 Biolegend
EpCAM mouse G8.8 eBioscience
CD4 mouse RM4.5 eBioscience
CD8 mouse 5H10 Invitrogen
CD3 mouse 145-2C11 BD bioscience
NK1.1 mouse PK136 eBioscience
CD45 human 2D1 eBioscience
CD34 human 581 Biolegend
CD38 human HIT2 BD bioscience
CD123= IL3R□ 6 human 6H6 Biolegend
CD11c human B-ly6 BD Horizon
CD1a human HI149 Biolegend
CD14 human MHCD1405 Invitrogen
CD33 human
CD207 human IM3577 Beckman Coulter.
All flow cytometry antibody were used at 1/200 dilution.

Validation

All primary anti-mouse and anti-human antibodies were validated for flow cytometry by the manufacturers.

## Eukaryotic cell lines

Policy information about cell lines

Cell line source(s)

293T cells were used for lentiviral construct production. They were received from Brian Brown Lab (Icahn School of Medecine at Mount Sinai).

Authentication

The cell line was not authenticated. However, these cells were 100% transfected and were able to produce lentiviral construct, so they can possibly be only 293T cells.

Mycoplasma contamination

293T cell line was tested negative for mycoplasma.

Commonly misidentified lines
(See ICLAC register)

No misidentified cell lines were used in the study.

## Animals and other organisms

Policy information about studies involving animals; ARRIVE guidelines recommended for reporting animal research

Laboratory animals

Both male and female mice were used, the phenotypes observed were not depended on sex.
C57BL/6 and BALB/c mice were used for experiments. The tamoxifen treatment was initiated between 8 weeks old and 12 weeks old. Mice were housed in the animal facility at Mount Sinai Hospital.

Wild animals

The study did not involve wild animals.

Field-collected samples

The study did not involve field-collected samples.

Ethics oversight

Ethical approval for mouse experiments was obtained by the IACUC at Mount Sinai Hospital.

Note that full information on the approval of the study protocol must also be provided in the manuscript.

## Human research participants

Policy information about studies involving human research participants

Population characteristics

The study involves staining on OCT embedded tissues and on paraffin embedded tissues from LCH patients followed at the Texas Children's Hospital. The study involves also bulk RNAseq of hematopoietic progenitors from bone marrow of LCH patients followed at the Texas Children's Hospital in Houston. Patients clinical characteritics are detailed in Extended Data Table 2.

Recruitment

For the bulk RNAseq of hematopoietic progenitors, patients were selected according to the % of BRAFV600E + cells detected in their bone marrow. We selected the three patients with the highest %. We could obtained bone marrow from one healthy infants. FFPE skin sections and OCT sections from LCH patients were selected according to their availability. There was no other criteria of selection.

Ethics oversight

Human tissues used in these studies were collected, stored, and processed according to protocols approved by the Baylor College of Medicine Institutional Review Board.

Note that full information on the approval of the study protocol must also be provided in the manuscript.

# Flow Cytometry

## Plots

Confirm that:

☒ The axis labels state the marker and fluorochrome used (e.g. CD4-FITC).

☒ The axis scales are clearly visible. Include numbers along axes only for bottom left plot of group (a 'group' is an analysis of identical markers).

☒ All plots are contour plots with outliers or pseudocolor plots.

☒ A numerical value for number of cells or percentage (with statistics) is provided.

## Methodology

| | |
|---|---|
| Sample preparation | Adult skin (from the ears), lung, liver, spleen, and femurs were dissected from mice at 12-16 weeks old (4 weeks after tamoxifen injections). Adult skin was first incubated overnight at 4° in dispase II solution (Roche) (2.5mg/mL in PBS) with the dermal side facing down. The dermis was separated mechanically from the epidermis and both tissues were digested in a solution of collagenase D (Roche) (1 mg/mL) and DNase I (Roche) (1 mg/mL) in RPMI (Corning) +10% FBS for one hour at 37°C. After digestion, the dermis and epidermis were homogenized using a 18G needle. The cell suspension was filtered through a 70 um cell strainer into a flow cytometry tube.<br>For the spleen and the lung, tissues were enzymatically digested in a solution of collagenase D (Roche) (1 mg/mL) and DNase I (Roche) (1 mg/mL) in HBSS (Corning) for 30 minutes at 37°C, followed by mechanical trituration with an 18G blunt tipped syringe and filtration through a 70 um filter.<br>Single cell suspensions from liver were obtained after digestion with collagenase IV (C5138, Sigma) in HBSS (Corning) at 37°C for 45 minutes. Nonparenchymal cells were enriched by centrifugation in 35% Percoll (17-0891-01, GE Healthcare) for 30 min at 1,300 rcf.<br>BM single cell suspensions were obtained after flushing out the BM from the femur using a 27G needle and then were incubated with ACK lysing buffer (420301, BioLegend) for 3 minutes at room temperature.<br>For flow cytometry, cells were stained in FACS buffer (PBS without Ca2+ and Mg2+ supplemented with 2% heat inactivated FBS and 5mM EDTA) with flow cytometry monoclonal antibodies for 20 minutes at 4°C. |
| Instrument | BD LSRFortessa |
| Software | FACS Diva software version 7 (BD). |
| Cell population abundance | Mostly GFP+ cells from transduced cord blood were FACS-sorted. Purity of sorted populations was ~97% in all samples and was assessed by flow cytometry. |
| Gating strategy | All gating strategy started by:<br>1. Gate on fsc-a vs. ssc-a was set to include all cell populations, but excluding debris<br>2. Gate on fsc-a vs. fsc-w was set to exclude doublets.<br>3. Gate on ssc-a vs. ssc-w was set to exclude doublets.<br>4. Gate on fsc-a vs. DAPI was set to exclude dead cells (DAPI+)<br><br>Gating for HSC (hematopoietic stem cells):<br>5. Gate on ssc-a vs. lineage to include lineage negative cells<br>6. Gate on c-kit+ Sca1+<br>7. Gate on CD34- Flt3-<br>Gating for MPP (mutipotent progenitors ):<br>5. Gate on ssc-a vs. lineage to include lineage negative cells<br>6. Gate on c-kit+ Sca1+<br>7. Gate on CD34+ Flt3-/+<br>Gating for MEP (megakaryocyte erythroid progenitors):<br>5. Gate on ssc-a vs. lineage to include lineage negative cells<br>6. Gate on c-kit+ Sca1-<br>7. Gate on CD34- CD16/32-<br>Gating for CMP (common myeloid progenitors):<br>5. Gate on ssc-a vs. lineage to include lineage negative cells<br>6. Gate on c-kit+ Sca1-<br>7. Gate on CD34+ CD16/32int<br>Gating for GMP (granulocyte macrophage progenitors):<br>5. Gate on ssc-a vs. lineage to include lineage negative cells<br>6. Gate on c-kit+ Sca1-<br>7. Gate on CD34+ CD16/32high<br><br>Gating for bone marrow neutrophils:<br>5. Gate on CD45 vs. fsc-a was set to exclude CD45- cells<br>6. Gate on CD11b+ Ly6G+<br>Gating for bone marrow dendritic cells:<br>5. Gate on CD45 vs. fsc-a was set to exclude CD45- cells<br>6. Gate on Ly6G vs CD11b to exclude Ly6G high cells<br>7. Gate on MHC II+ CD11c+ |

Gating for bone marrow monocytes
5. Gate on CD45 vs. fsc-a was set to exclude CD45- cells
6. Gate on CD11b vs Ly6G was set to include CD11b+ Ly6G- cells
7. Gate on Ly6C vs. CD115 was set to include Ly6C high CD115 negative as monocytes.
Gating for bone marrow macrophages:
5. Gate on CD45 vs. fsc-a was set to exclude CD45- cells
6. Gate on CD11b vs Ly6G was set to include CD11b+ Ly6G- cells
7. Gate on CD115 vs. LY6C to exclude CD115+ cells
8. Gate on F4/80 vs. CD115 to include F4/80+ cells
9. Gate on ssc-a vs. fsc-a, macrophages are fsc-a high but ssc-a low.

☒ Tick this box to confirm that a figure exemplifying the gating strategy is provided in the Supplementary Information.

Downloaded from http://perspectivesinmedicine.cshlp.org/ on September 20, 2020 - Published by Cold Spring Harbor Laboratory Press

Cold Spring Harbor Perspectives in Medicine
www.perspectivesinmedicine.org

# MAP-Kinase-Driven Hematopoietic Neoplasms: A Decade of Progress in the Molecular Age

**Rikhia Chakraborty,[1,2] Omar Abdel-Wahab,[3,4] and Benjamin H. Durham[3,5]**

[1]Texas Children's Cancer Center, Texas Children's Hospital, Houston, Texas 77030, USA

[2]Department of Pediatrics, Division of Pediatric Hematology-Oncology, Baylor College of Medicine, Houston, Texas 77030, USA

[3]Human Oncology and Pathogenesis Program, Department of Medicine, [4]Leukemia Service, Department of Medicine, [5]Department of Pathology, Memorial Sloan Kettering Cancer Center, New York, New York 10065, USA

*Correspondence:* abdelwao@mskcc.org, durhamb@mskcc.org

Mutations in members of the mitogen-activated protein kinase (MAPK) pathway are extensively studied in epithelial malignancies, with *BRAF* mutations being one of the most common alterations activating this pathway. However, *BRAF* mutations are overall quite rare in hematological malignancies. Studies over the past decade have identified high-frequency $BRAF^{V600E}$, *MAP2K1*, and other kinase alterations in two groups of MAPK-driven hematopoietic neoplasms: hairy cell leukemia (HCL) and the systemic histiocytoses. Despite HCL and histiocytoses sharing common molecular alterations, these are phenotypically distinct malignancies that differ in respect to clinical presentation and suspected cell of origin. The purpose of this review is to highlight the molecular advancements over the last decade in the histiocytic neoplasms and HCL and discuss the impact these insights have had on our understanding of the molecular pathophysiology, cellular origins, and therapy of these enigmatic diseases as well as perspectives for future research directions.

The mitogen-activated protein kinase (MAPK) pathway has a long association with human neoplasia. A key member in this pathway is the BRAF serine/threonine kinase belonging to the RAF family of serine/threonine kinases, which also includes ARAF and RAF1. RAF kinases transduce mitogenic signals from the cell membrane to the nucleus and regulate MEK-ERK signaling. Of the RAF kinases, BRAF is most frequently mutated in cancer with $BRAF^{V600E}$ accounting for 90% of activating mutations (Wellbrock et al. 2004). Similarly, the neoplastic cells of the systemic histiocytoses (SHs) and hairy cell leukemia (HCL) have nearly universal ERK overexpression suggesting constitutive activation of MAPK signaling in these distinct hematological neoplasms (Fig. 1; Badalian-Very et al. 2010; Tiacci et al. 2011; Haroche et al. 2012).

Although quite rare in hematological disorders overall, *BRAF* mutations are strikingly enriched in two sets of diseases: classical HCL

Editors: Michael G. Kharas, Ross L. Levine, and Ari M. Melnick
Additional Perspectives on Leukemia and Lymphoma: Molecular and Therapeutic Insights available at www.perspectivesinmedicine.org

Copyright © 2020 Cold Spring Harbor Laboratory Press; all rights reserved
Advanced Online Article. Cite this article as *Cold Spring Harb Perspect Med* doi: 10.1101/cshperspect.a034892

Downloaded from http://perspectivesinmedicine.cshlp.org/ on September 20, 2020 - Published by Cold Spring Harbor Laboratory Press

Cold Spring Harbor Perspectives in Medicine
www.perspectivesinmedicine.org

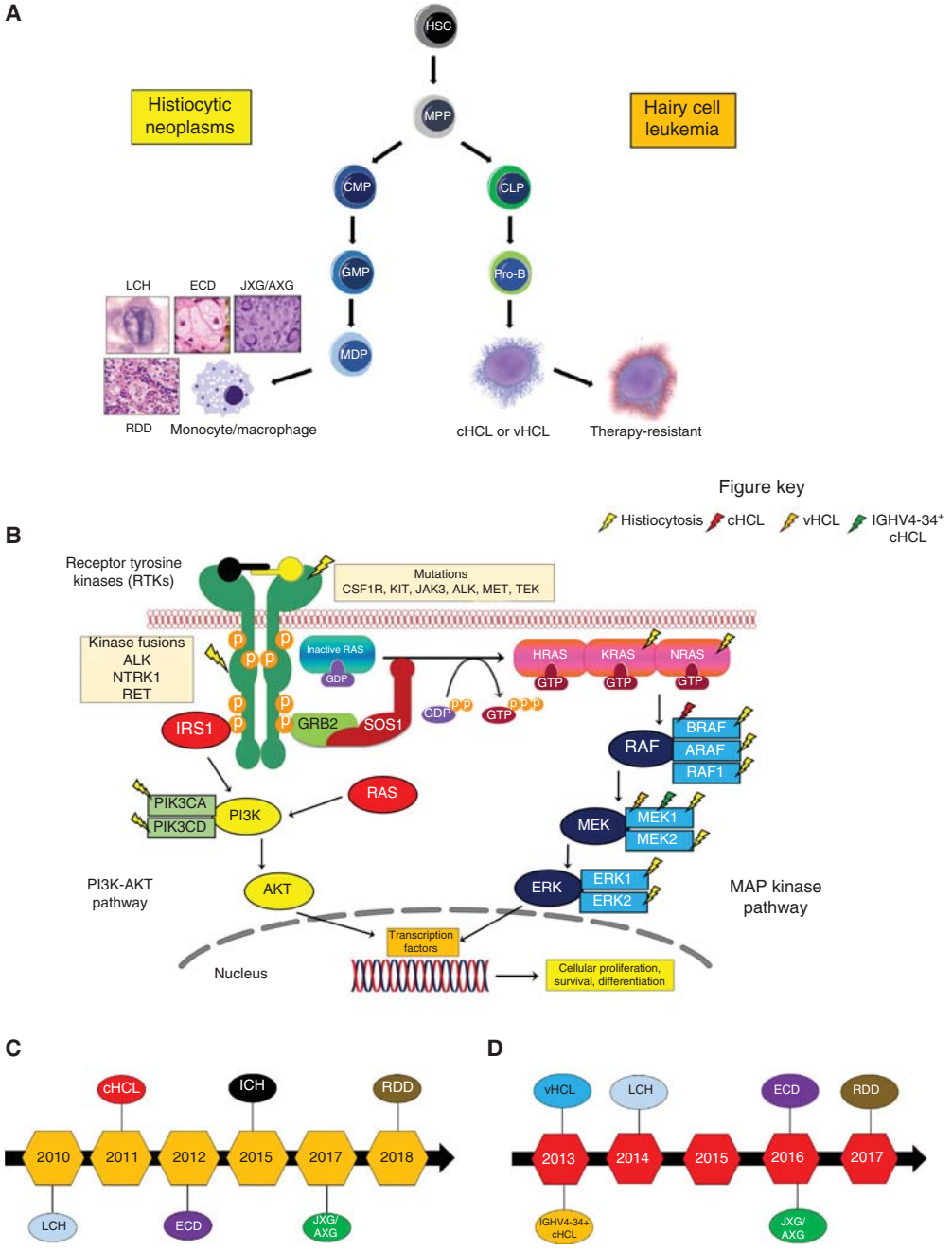



**Figure 1.** Overview of the mitogen-activated protein kinase (MAPK)-driven hematopoietic neoplasms with common molecular alterations but divergent phenotypes. (*A*) Diagram demonstrating the divergent hematopoietic development of histiocytic neoplasms and hairy cell leukemia. (*B*) Diagram of the MAPK and PI3K-AKT signaling pathways with description of the activation of the RAS proteins (HRAS, KRAS, and NRAS) with annotation of the signaling proteins affected by genetic alterations in the histiocytic neoplasms, classical hairy cell leukemia, IGHV4-34$^{+}$ classical hairy cell leukemia, and hairy cell leukemia variant. (*C*) Timeline of the discovery of recurrent *BRAF*$^{V600E}$ mutations in the MAPK-driven hematological neoplasms. (*D*) Timeline of the discovery of recurrent *MAP2K1* mutations in the MAPK-driven hematological neoplasms. LCH, Langerhans cell histiocytosis; ECD, Erdheim–Chester disease; JXG/AXG, juvenile xanthogranuloma/adult xanthogranuloma; RDD, Rosai–Dorfman–Destombes disease; ICH, indeterminate cell histiocytosis; cHCL, classical hairy cell leukemia; vHCL, hairy cell leukemia variant; *IGHV*, immunoglobulin heavy chain variable; HSC, hematopoietic stem cell; MPP, multipotent progenitor; CMP, common myeloid progenitor; GMP, granulocyte–monocyte progenitor; MDP, monocyte–dendritic cell progenitor; CLP, common lymphoid progenitor; Pro-B, pro-B-lymphocyte; RTK, receptor tyrosine kinase.

Downloaded from http://perspectivesinmedicine.cshlp.org/ on September 20, 2020 - Published by Cold Spring Harbor Laboratory Press



Cold Spring Harbor Perspectives in Medicine
www.perspectivesinmedicine.org



(cHCL) (Tiacci et al. 2011; Arcaini et al. 2012; Swerdlow et al. 2017) and SH—Langerhans cell histiocytosis (LCH) (Badalian-Very et al. 2010) and Erdheim–Chester disease (ECD) (Haroche et al. 2012). Furthermore, additional sequencing efforts identified recurrent mutations in *MAP2K1* (MEK1) in variant HCL (vHCL) (Waterfall et al. 2014), LCH (Brown et al. 2014; Chakraborty et al. 2014), ECD, and other non-LCH neoplasms (Diamond et al. 2016; Durham et al. 2016). Interestingly, $BRAF^{V600E}$ is frequently present in cHCL (~100%) (Tiacci et al. 2011) and LCH and ECD (50%–60%) (Badalian-Very et al. 2010; Haroche et al. 2012); meanwhile, *MAP2K1* mutations are present in vHCL (~50%) (Waterfall et al. 2014; Durham et al. 2017a) and SH (~25%) (Figs. 1–5; Brown et al. 2014; Chakraborty et al. 2014; Diamond et al. 2016; Durham et al. 2016). However, despite their common molecular alterations, these are distinct malignancies with different clinical presentations and biology. Nonetheless, the discovery of recurrent $BRAF^{V600E}$ and *MAP2K1* mutations in both malignancies has guided new therapeutic approaches, as well as an opportunity to explore how a common genetic event gives rise to these enigmatic diseases (Fig. 1; Haroche et al. 2013; Hyman et al. 2015; Tiacci et al. 2015; Diamond et al. 2016, 2018, 2019; Durham et al. 2019). This review discusses the amalgamation of diverse kinase alterations uncovered in SH and HCL during the last decade and underscore how new insights have refined our understanding of these disorders as clonal neoplasms with constitutive MAPK and PI3K-AKT activation. We will also highlight how our concepts of the cellular origins of the MAPK-driven hematological neoplasms and molecular therapeutics have started evolving.

## OVERVIEW OF HISTIOCYTIC NEOPLASMS

Histiocytic neoplasms are a heterogeneous group of disorders broadly classified as LCH and non-LCH that share the common pathological features of infiltration and accumulation of neoplastic histiocytes in tissues with nearly universal ERK activation and an accompanying inflammatory milieu (Badalian-Very et al. 2010; Haroche et al. 2012; Swerdlow et al. 2017; Ozkaya et al. 2018). However, a revised classification recategorized LCH and non-LCH into the following: "L" Langerhans group [LCH, ECD, disseminated juvenile/adult xanthogranuloma (JXG/AXG), and indeterminate cell histiocytosis (ICH)]; "C" group (cutaneous JXG/AXG and Rosai–Dorfman–Destombes disease [RDD]); "R" group (noncutaneous RDD) (Table 1; Emile et al. 2016).

## LANGERHANS CELL HISTIOCYTOSIS

### Historical Perspective

The first historical descriptions of LCH patients occurred in case series. Hippocrates reported a patient with a nonfatal disease with painful skull lesions ~400 BC, a presentation that could be consistent with LCH (Donadieu and Pritchard 1999). Later, Hand–Schüller–Christian described patients with rash, lytic bone lesions, and diabetes insipidus (DI) and Letterer–Siwe discussed a fatal disseminated disease (Hand 1893; Schüller 1915; Christian 1919; Letterer 1924; Siwe 1933). Afterward, Farber characterized single lytic bone lesions as "eosinophilic granulomas" (Farber 1941). However, Lichtenstein noted a similar histology in these clinically diverse descriptions and posited they constitute a common syndrome he called "histiocytosis X," with the "X" indicating uncertain cellular origin (Lichtenstein 1953). Eventually, Nezelof utilized electron microscopy and reported Birbeck granules in both LCH lesions and epidermal Langerhans cells (LCs), leading to the hypothesis that LCH arises from pathologically activated LCs (Nezelof et al. 1973; Lampert 1998; Arceci 1999).

### Clinical Presentation

LCH has diverse manifestations from self-resolving, single-organ lesions to multi-organ disease, which is associated with 10%–20% mortality (Arceci 1999; McClain et al. 2004). Bone (75%) and skin (34%) are the most commonly involved organs with lytic bone lesions frequently involving the skull (Table 1; Guyot-Goubin

Downloaded from http://perspectivesinmedicine.cshlp.org/ on September 20, 2020 - Published by Cold Spring Harbor Laboratory Press



Cold Spring Harbor Perspectives in Medicine
www.perspectivesinmedicine.org

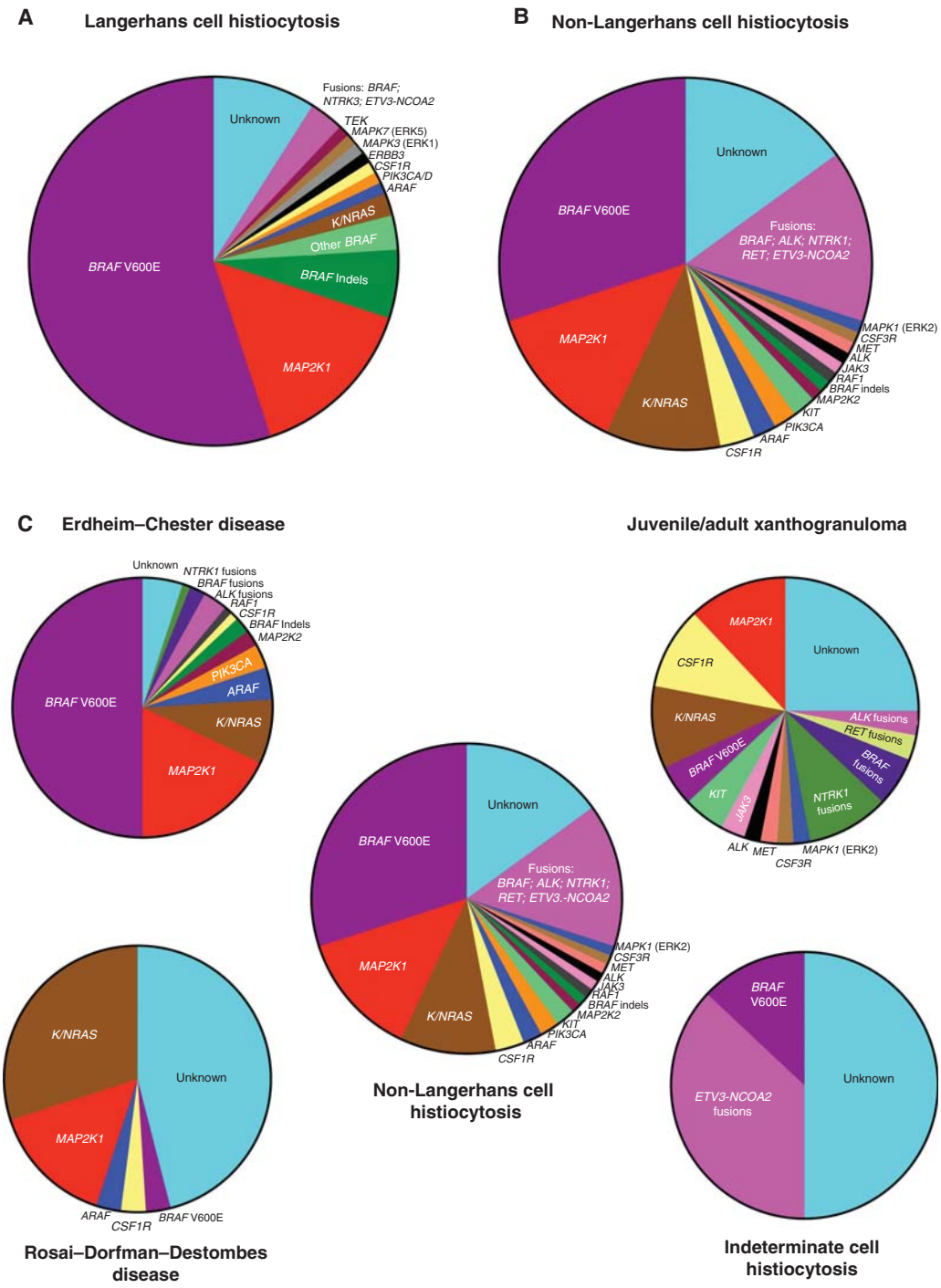



**Figure 2.** Summary of diverse kinase alterations discovered in the histiocytic neoplasms. (*A*) Pie chart illustrating a composite of the known kinase alterations in Langerhans cell histiocytosis. (*B*) Pie chart showing a composite of the known kinase alterations in non-Langerhans cell histiocytoses. (*C*) Pie charts demonstrating the published kinase alterations in the four discussed subcategories of the non-Langerhans cell histiocytic neoplasms.

Downloaded from http://perspectivesinmedicine.cshlp.org/ on September 20, 2020 - Published by Cold Spring Harbor Laboratory Press

Cold Spring Harbor Perspectives in Medicine
www.perspectivesinmedicine.org

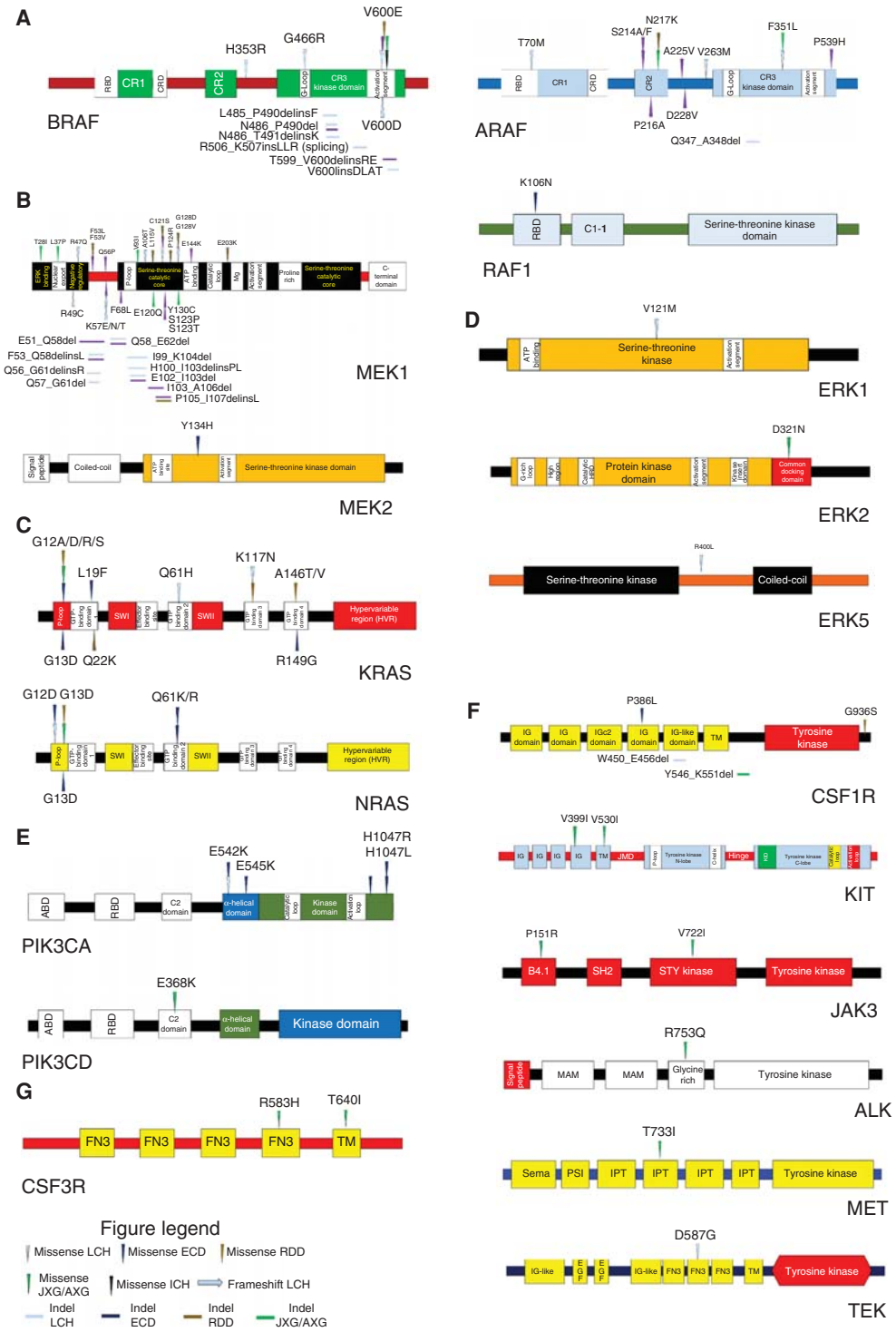



**Figure 3.** Summary of the diverse kinase mutations in histiocytic neoplasms. (*A*) Protein diagrams cataloging the published somatic mutations described in the RAF isoforms (BRAF, ARAF, and RAF1 [CRAF]). (*B*) Protein diagrams cataloging the somatic mutations discovered in MEK1 and MEK2. (*C*) Protein diagrams cataloging the somatic mutations uncovered in the RAS isoforms (KRAS and NRAS). (*D*) Protein diagrams cataloging somatic mutations described in ERK1, ERK2, and ERK5. (*E*) Protein diagrams cataloging somatic mutations involving the PI3K isoforms (PIK3CA and PIK3CD). (*F*) Protein diagrams documenting somatic mutations recently discovered in the receptor tyrosine kinases. (*G*) Protein diagram cataloging somatic mutations in CSF3R. LCH, Langerhans cell histiocytosis; ECD, Erdheim–Chester disease; JXG/AXG, juvenile xanthogranuloma/adult xanthogranuloma; RDD, Rosai–Dorfman–Destombes disease; ICH, indeterminate cell histiocytosis.

Downloaded from http://perspectivesinmedicine.cshlp.org/ on September 20, 2020 - Published by Cold Spring Harbor Laboratory Press



Cold Spring Harbor Perspectives in Medicine
www.perspectivesinmedicine.org

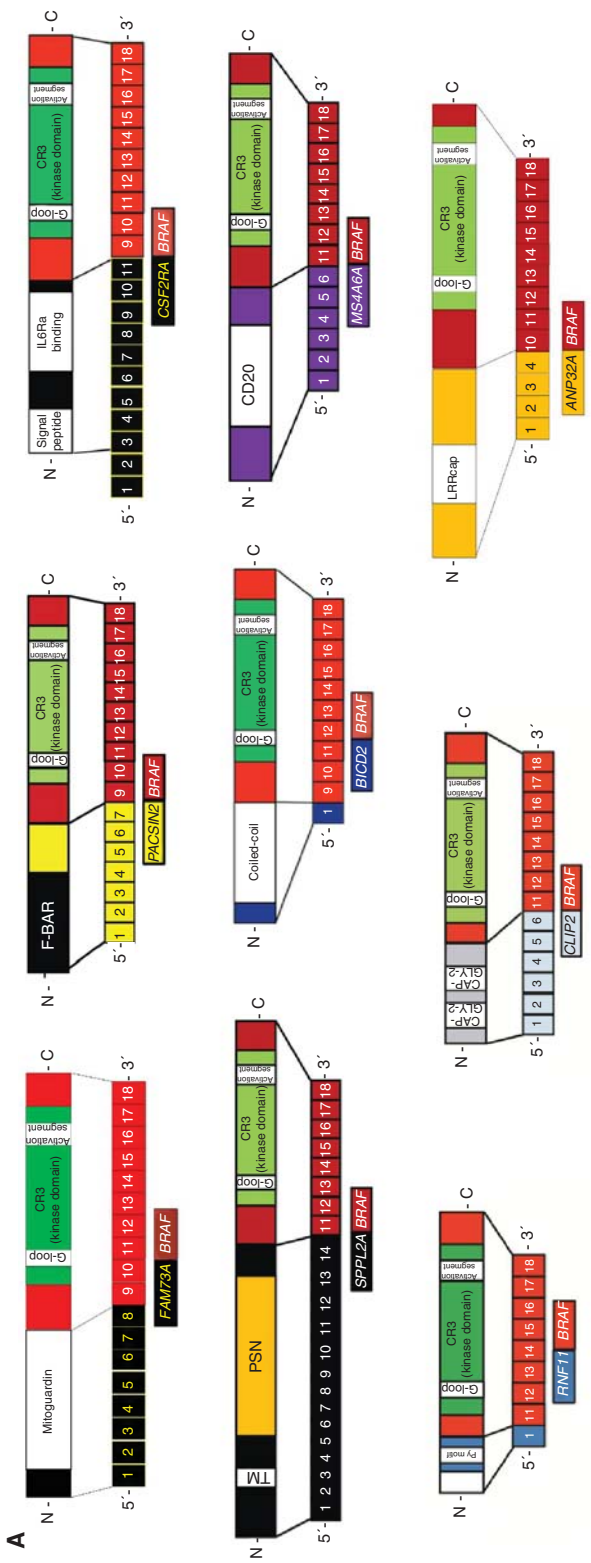



Figure 4. Summary of the diverse kinase fusions in histiocytic neoplasms. (*A*) Illustrations of recurrent *BRAF* fusions discovered in the histiocytic neoplasms. (*B*) Illustrations of the recurrent *NTRK1* fusions uncovered in non-Langerhans cell histiocytoses and an *NTRK3* fusion in Langerhans cell histiocytosis. (*C*) Illustrations of recurrent *ALK* fusions described in the non-Langerhans cell histiocytic neoplasms. (*D*) Illustration of the recurrent *ETV3-NCOA2* fusion discovered in both Langerhans cell histiocytosis and non-Langerhans cell histiocytosis. (*E*) Illustration of the recurrent *NCOA4-RET* fusion recently discovered in non-Langerhans cell histiocytosis.

Downloaded from http://perspectivesinmedicine.cshlp.org/ on September 20, 2020 - Published by Cold Spring Harbor Laboratory Press



Cold Spring Harbor Perspectives in Medicine
www.perspectivesinmedicine.org

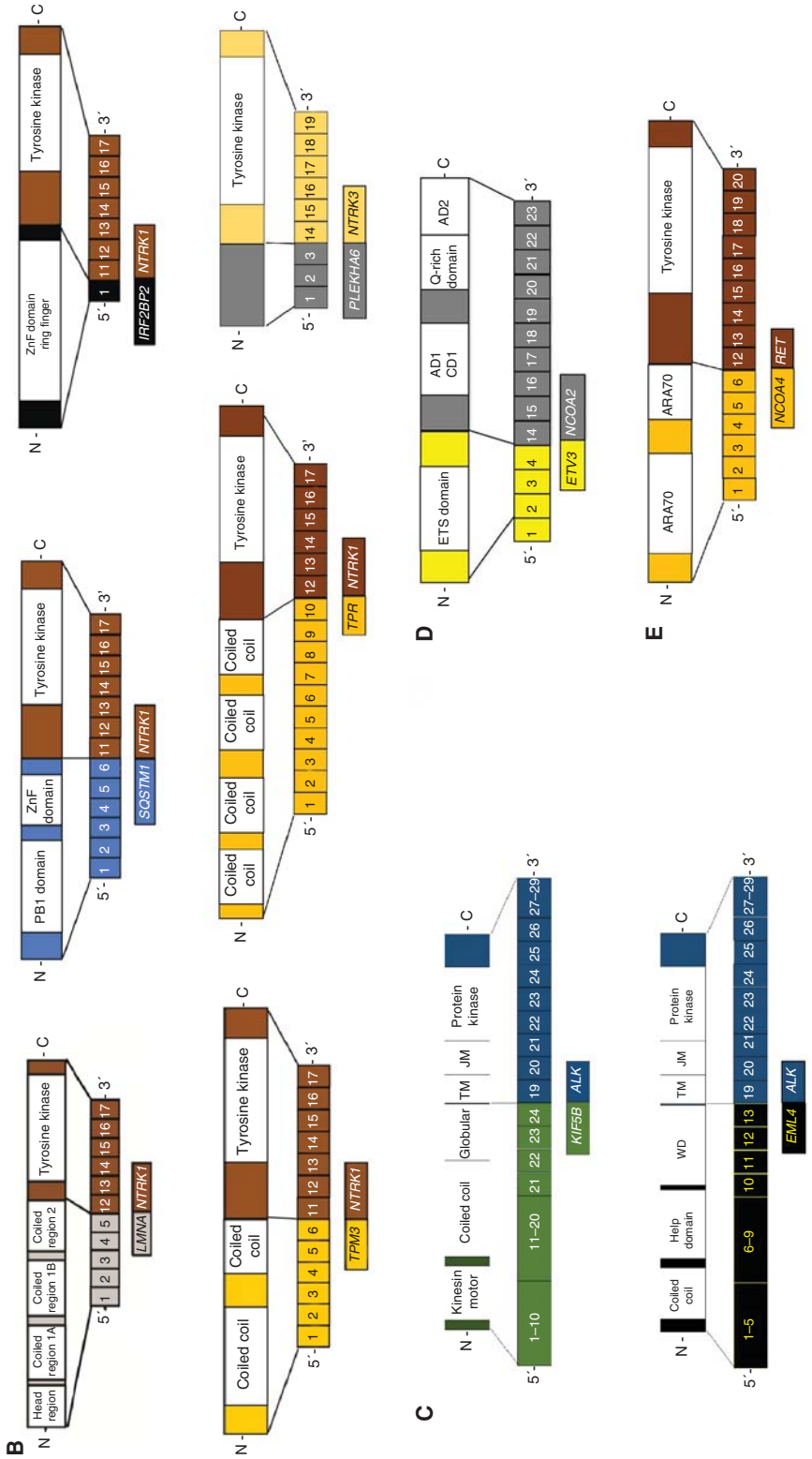



**Figure 4.** (*Continued.*)

Downloaded from http://perspectivesinmedicine.cshlp.org/ on September 20, 2020 - Published by Cold Spring Harbor Laboratory Press



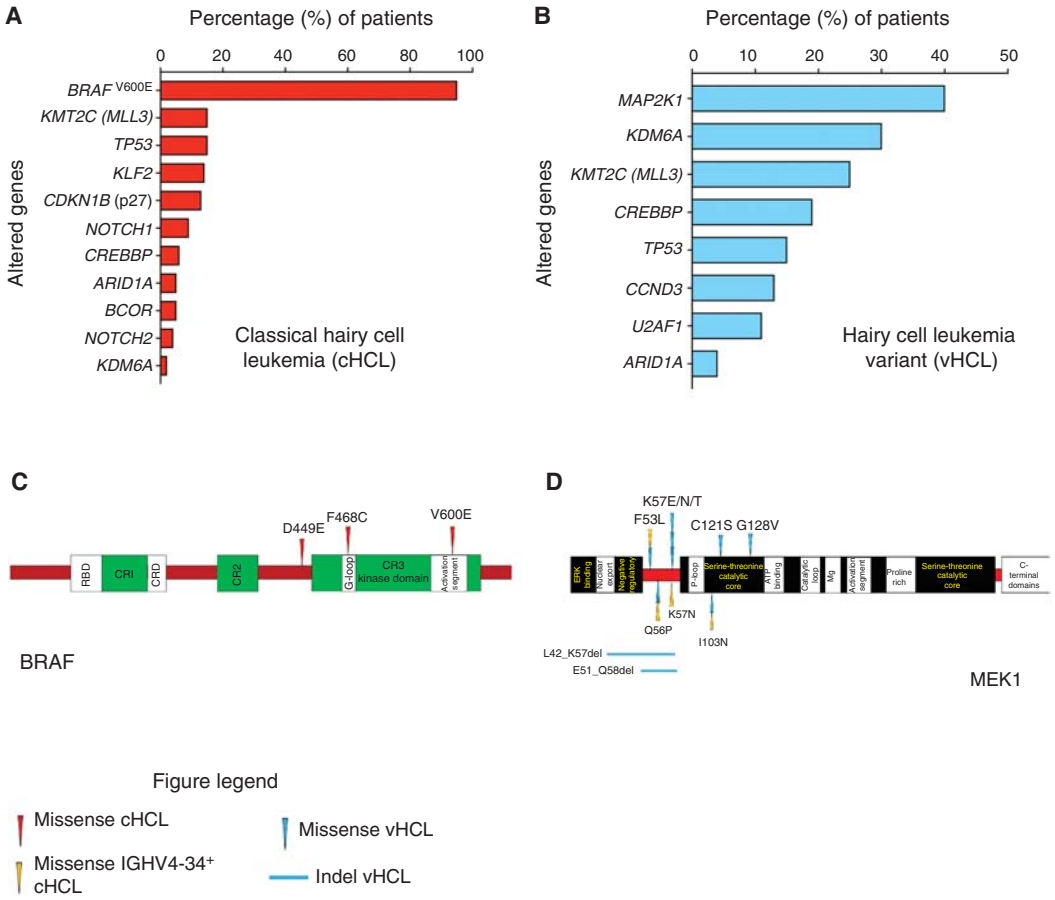



**Figure 5.** Summary of genetic alterations in hairy cell leukemia. (*A*) Histogram of driver and co-occurring mutations reported in classical hairy cell leukemia. (*B*) Histogram of driver and co-occurring mutations described in hairy cell leukemia variant. (*C*) Protein diagram mapping somatic mutations involving BRAF that have been uncovered in classical hairy cell leukemia. (*D*) Protein diagram mapping somatic mutations in MEK1 discovered in hairy cell leukemia variant and *IGHV4-34*$^{+}$ classical hairy cell leukemia. cHCL, Classical hairy cell leukemia; vHCL, hairy cell leukemia variant; *IGHV*, immunoglobulin heavy chain variable.

et al. 2008; Stålemark et al. 2008). Besides skin, LCH may arise in any mucosal tissue (gingiva, gastrointestinal tract) (Broadbent et al. 1994; Guyot-Goubin et al. 2008). "High-risk" LCH includes diffuse infiltration or focal lesions of spleen, liver, or bone marrow with a 5-yr survival rate of 84% compared to 99% in "low-risk" LCH (Gadner et al. 2013). LCH may also involve the central nervous system (LCH-CNS), presenting with mass lesions, diabetes insipidus, or progressive neurodegenerative symptoms (LCH-ND) arising decades after initial presentation (Grois et al. 1998, 2010; Héritier et al. 2018).

Pathologically, LCH is characterized by lesions composed of clonal, pathological "histiocytes" with reniform (coffee-bean-shaped) nuclei and abundant, pink cytoplasm with immunoreactivity for CD1a and langerin (CD207) and pathognomonic Birbeck granules (Table 1; Nezelof et al. 1973; Favara et al. 1997; Chikwava and Jaffe 2004; Swerdlow et al. 2017). Histology also shows a milieu of pathologic dendritic cells (DCs) and recruited inflammatory cells (lymphocytes, eosinophils, and macrophages) (Laman et al. 2003; Senechal et al. 2007; Allen et al. 2010; Berres et al. 2014).

Cold Spring Harbor Perspectives in Medicine
www.perspectivesinmedicine.org

Downloaded from http://perspectivesinmedicine.cshlp.org/ on September 20, 2020 - Published by Cold Spring Harbor Laboratory Press



Cold Spring Harbor Perspectives in Medicine
www.perspectivesinmedicine.org



**Table 1.** Summary of the classification, pathological, and radiological features of the histiocytic neoplasms.

| Disease | LCH | ECD | JXG/AXG | RDD | ICH |
|---|---|---|---|---|---|
| Broad classification | LCH | Non-LCH | Non-LCH | Non-LCH | Non-LCH |
| Revised classification groupings | L | L | L (extracutaneous) and C (cutaneous) | C (cutaneous) and R (other RDD) | L |
| **Immunophenotypic features** | | | | | |
| CD68 | + | ++ | ++ | ++ | + |
| CD163 | – | ++ | ++ | ++ | – |
| CD14 | – | ++ | ++ | ++ | – |
| CD1a | ++ | – | – | – | ++ |
| CD207 (Langerin) | ++ | – | – | – | – |
| S100 | + | –/+ | –/+ | + | + |
| Factor XIIIa | – | + | + | + | – |
| CD45 | + | + | + | + | + |
| **Histological features** | | | | | |
| Birbeck granules | Yes | No | No | No | No |
| Xanthomatous histiocytes | No | Yes | Yes | No | No |
| Touton giant cells | No | Yes | Yes | No | No |
| Emperipolesis (intractyoplasmic lymphocytes) | No | Occasional | Occasional | Abundant | No |
| **Radiological features** | | | | | |
| Bilateral, symmetric osteosclerosis involving meta-diaphysis of femur, tibia, and fibula | Rare | Frequent, pathognomonic | No | No | No |
| Lytic, "punched-out" lesions of skull and axial skeleton | Frequent | Rare | No | No | No |
| Infiltrative, perinephric soft tissue thickening ("hairy kidney") | No | Frequent | Rare | No | No |

LCH, Langerhans cell histiocytosis; ECD, Erdheim–Chester disease; JXG, juvenile xanthogranuloma; AXG, adult xanthogranuloma; RDD, Rosai–Dorfman–Destombes disease; ICH, indeterminate cell histiocytosis; L group, Langerhans-related; C group, cutaneous and mucocutaneous; R group, Rosai–Dorfman–Destombes disease; +, low expression; ++, high expression; –, no expression.

## JUVENILE/ADULT XANTHOGRANULOMA

### Clinical Presentation

JXG/AXG was originally described in the early 1900s and was believed to be endothelium derived and was named "nevoxanthoendothelioma" (McDonagh and McDonagh 1912). JXG/AXG is usually self-limiting with dermal lesions in most patients; but 4% present with disseminated disease (Weitzman and Jaffe 2005; Allen and Parsons 2015). Histologically, JXG/AXG shows xanthomatous histiocytes with admixed multinucleated and Touton giant cells that are immunoreactive for CD68, CD163, CD14, fascin, and Factor XIIIa with variable positivity for S100 and no immunoreactivity for CD1a or CD207 (Table 1; Weitzman and Jaffe 2005; Diamond et al. 2014; Haroche and Abla 2015; Swerdlow et al. 2017).

Downloaded from http://perspectivesinmedicine.cshlp.org/ on September 20, 2020 - Published by Cold Spring Harbor Laboratory Press



Cold Spring Harbor Perspectives in Medicine
www.perspectivesinmedicine.org

## ERDHEIM–CHESTER DISEASE

### Clinical Presentation

ECD is a rare, systemic, non-LCH disease with around 800 reported cases in the literature that was first described as a "lipoid granulomatosis" in 1930 by Erdheim and Chester. ECD has diverse clinical manifestations ranging from localized presentations (bone-only disease) to multisystem disease that are extensively discussed elsewhere (Chester 1930; Weitzman and Jaffe 2005; Diamond et al. 2014; Haroche and Abla 2015; Estrada-Veras et al. 2017; Haroche et al. 2017; Cohen-Aubart et al. 2018). The diagnosis of ECD requires combining the histological criteria and the appropriate clinical and radiological setting (Weitzman and Jaffe 2005; Diamond et al. 2014; Haroche and Abla 2015; Swerdlow et al. 2017). Radiographically, bilateral and symmetric diaphyseal and metaphyseal osteosclerosis of the legs is observed in most patients. Histologically, ECD shows xanthomatous histiocytes with surrounding fibrosis, as well as admixed multinucleated giant cells with immunoreactivity for CD68, CD163, CD14, fascin, and Factor XIIIa and negativity for CD1a and CD207 (Table 1; Weitzman and Jaffe 2005; Diamond et al. 2014; Haroche and Abla 2015; Swerdlow et al. 2017).

## ROSAI–DORFMAN–DESTOMBES DISEASE

### Clinical Presentation

RDD is a rare, non-LCH hematological disorder known as "sinus histiocytosis with massive lymphadenopathy" that was first described by Destombes, Rosai, and Dorfman (Destombes 1965; Rosai and Dorfman 1969, 1972; Haroche and Abla 2015). RDD has heterogeneous clinical manifestations and can occur as an isolated disorder or in association with hereditary, autoimmune, or neoplastic conditions. The majority of RDD patients present with classical (nodal) RDD that primarily manifests as bilateral, massive, and painless cervical lymphadenopathy with or without fever, night sweats, and weight loss. However, 43% of patients develop extranodal RDD with 19% showing multisystem RDD, and prognosis has been correlated with the number of extranodal systems affected with a detailed clinical discussion reviewed elsewhere (Haroche and Abla 2015; Abla et al. 2018). Histologically, the abnormal, xanthomatous histiocytes of RDD demonstrate abundant emperipolesis of erythrocytes, lymphocytes, and plasma cells. The abnormal histiocytes are immunoreactive for CD14, CD68, CD163, and S100 with negativity for CD1a and CD207 (Table 1; Weitzman and Jaffe 2005; Haroche and Abla 2015; Swerdlow et al. 2017; Durham 2019).

## INDETERMINANT CELL HISTIOCYTOSIS

### Clinical Presentation

ICH is a rare, non-LCH neoplasm first described in 1985 that predominantly involves the skin and is characterized by the presence of dendritic cells that are morphologically and immunophenotypically like LCH. However, ICH shows a dense dermal infiltration of neoplastic histiocytes admixed with lymphocytes without significant eosinophilic infiltration and is immunoreactive for CD68, S100, and CD1a but not for CD163 and CD207. Therefore, unlike LCH, ICH lacks CD207 and Birbeck granules (Table 1; Wood et al. 1985; Rezk et al. 2008).

## MOLECULAR PATHOPHYSIOLOGY OF HISTIOCYTIC NEOPLASMS

Prior to the molecular era, the determination of whether SHs were reactive or neoplastic was unclear and constituted a historical debate (Arceci et al. 1998; Degar and Rollins 2009). Furthermore, the cellular heterogeneity of histiocytoses and the limitations of molecular technology precluded classification of SHs as neoplasms (Merad et al. 2002; Senechal et al. 2007; da Costa et al. 2009). However, the dawning of the molecular era revealed a series of activating kinase alterations involved in MAPK, PI3K-AKT, and RTK signaling within the SHs (Figs. 2–4).

### RAF Isoforms

The discovery of *BRAF* mutations in the histiocytoses occurred after $BRAF^{V600E}$ was reported

Downloaded from http://perspectivesinmedicine.cshlp.org/ on September 20, 2020 - Published by Cold Spring Harbor Laboratory Press



Cold Spring Harbor Perspectives in Medicine
www.perspectivesinmedicine.org



in 57% of LCH (Badalian-Very et al. 2010) and 54% of ECD (Haroche et al. 2012). Later studies uncovered *BRAF*$^{V600E}$ in JXG/AXG, RDD, and ICH but were not prevalent in SHs other than LCH and ECD (O'Malley et al. 2015; Techavichit et al. 2017; Fatobene et al. 2018; Durham et al. 2019). Besides *BRAF*$^{V600E}$, SH case reports have revealed other activation segment *BRAF* mutations (*BRAF*$^{V600D}$; *BRAF*$^{V600insDLAT}$) (Satoh et al. 2012; Kansal et al. 2013). Additionally, a *BRAF* splicing mutation (*BRAF* c.1511_1517+2 duplication) was reported (Héritier et al. 2017). Furthermore, activating, in-frame deletions in *BRAF* exon 12 (encodes the β3-αC loop critical for kinase activation) and numerous *BRAF* fusions have been described in SHs (Figs. 2, 3A, 4A; Chakraborty et al. 2016; Lee et al. 2017; Zarnegar et al. 2018; Durham et al. 2019). Other whole-exome sequencing (WES) studies have revealed activating *ARAF* mutations in LCH (Nelson et al. 2014) and non-LCH (ECD; JXG/AXG; RDD) along with *RAF1* mutations in ECD (Figs. 2, 3A; Diamond et al. 2016, 2019; Durham et al. 2019).

## MAP2K1/MAP2K2

In *BRAF*$^{V600E}$-negative histiocytoses, NGS studies found *MAP2K1* to be a second recurrently mutated gene locus in LCH (Brown et al. 2014; Chakraborty et al. 2014) and non-LCH (ECD, JXG/AXG, and RDD) (Diamond et al. 2016; Garces et al. 2017). Functionally, the *MAP2K1* mutations occurred within mutational hotspots and clustered in the amino-terminal regulatory domain (exon 2) and amino-terminal kinase domain (exon 3) resulting in MAPK activation (Chakraborty et al. 2014; Nelson et al. 2015; Diamond et al. 2016; Garces et al. 2017). Additionally, ECD sequencing found recurrent *MAP2K2*$^{Y134H}$ in the MEK2 kinase domain that activated MAPK signaling (Figs. 2, 3B; Diamond et al. 2019; Durham et al. 2019).

## RAS Isoforms

The RAS isoforms encode small GTPases that regulate the MAPK and PI3K-AKT signaling pathways. First, *NRAS* mutations were found in single cases of LCH and ECD (Ozono et al. 2011; Diamond et al. 2013). Afterward, studies confirmed that *NRAS*/*KRAS* mutations are recurrent in SH and affected the GTP-binding domains leading to constitutive MAPK activation (Figs. 2, 3C; Emile et al. 2014; Diamond et al. 2016; Shanmugam et al. 2016; Garces et al. 2017; Lee et al. 2017; Durham et al. 2019).

## Extracellular-Signal-Regulated Kinases (ERK) Isoforms

As the molecular age continued to interrogate *BRAF*$^{V600}$-negative histiocytoses, rare mutations started to emerge in the ERK isoforms. An activating *MAPK1*$^{D321N}$ affecting the ERK2 carboxy-terminal-docking domain surfaced in JXG and showed in vitro sensitivity to ERK inhibition but not RAF or MEK inhibition (Chakraborty et al. 2017). Another WES study of LCH found *MAPK3*$^{V121M}$ in the ERK1 kinase domain and *MAPK7*$^{R400L}$ affecting the ERK5 carboxy-terminal domain with both mutations influencing MAPK signaling (Figs. 2, 3D; Durham et al. 2019).

## PI3K Isoforms

The PI3K isoforms include phosphatidylinositol-4,5-bisphosphate-3-kinase catalytic subunit alpha (*PIK3CA*) and catalytic subunit delta (*PIK3CD*), members of the PI3K-AKT signaling pathway. Recurrent *PIK3CA* mutations were first revealed in ECD (Emile et al. 2014) and then in LCH (Héritier et al. 2015). Later studies primarily identified *PIK3CA* mutations as recurrent events in ECD with rare *PIK3CD* mutations in JXG and LCH. *PIK3CA* mutations clustered in the α-helical and kinase domains leading to PI3K-AKT activation (Figs. 2, 3E; Chakraborty et al. 2014; Diamond et al. 2016; Durham et al. 2019).

## Receptor Tyrosine Kinases

Continued sequencing of histiocytoses implicated the RTKs. A WES study found a case of *ERBB3*-mutated LCH (Chakraborty et al. 2014). Later studies uncovered recurrent *ALK* and

Downloaded from http://perspectivesinmedicine.cshlp.org/ on September 20, 2020 - Published by Cold Spring Harbor Laboratory Press



Cold Spring Harbor Perspectives in Medicine
www.perspectivesinmedicine.org



*NTRK1* fusions in ECD and JXG/AXG (Diamond et al. 2016; Lee et al. 2017). Then, a large WES/NGS study evaluated 270 histiocytoses patients and discovered recurrent, activating mutations in *CSF1R*, the RTK critical for monocyte and macrophage development, which was enriched in JXG/AXG but found across histiocytoses; and this study was really the first time that activating *CSF1R* mutations have been implicated in cancer. Additionally, other RTK alterations were uncovered in JXG/AXG (*KIT*, *JAK3*, *ALK*, *MET*, and *CSF3R*) and in LCH (TEK), as well as the first *RET* and *NTRK3* fusions in the histiocytoses (Figs. 2, 3F–G, 4; Cai et al. 2019; Durham et al. 2019).

### ETV3-NCOA2 Fusions

*ETV3-NCOA2* fusions were described in ICH and then reported in one LCH case (Brown et al. 2015; Lee et al. 2017). These fusions involve exons 1–4 of *ETV3* and exons 14–23 of *NCOA2*. This leads to the preservation and fusion of the carboxy-terminal transcriptional activation domains of NCOA2 to the amino-terminal ETS domain of ETV3 (Fig. 4D; Wang et al. 2012; Mesquita et al. 2013; Brown et al. 2015), and prior studies of *NCOA2* gene fusions have demonstrated that the AD1 and CID domains in the carboxyl terminus are required for the transformation of NCOA2 fusion proteins (Figs. 2, 4D; Carapeti et al. 1998; Deguchi et al. 2003; Strehl et al. 2008; Sumegi et al. 2010; Wang et al. 2012; Brown et al. 2015; Durham 2019). However, extensive functional characterization of the role of the *ETV3-NCOA2* fusion in SH pathogenesis is warranted.

Overall, the molecular age demonstrates most SH patients harbor diverse alterations in MAPK, PI3K-AKT, and RTK pathway genes supporting that histiocytoses are clonal, hematopoietic neoplasms with many molecularly directed therapeutic targets.

## CELLULAR-ORIGIN STUDIES IN HISTIOCYTOSES

Identification of MAPK mutations has provided a molecular etiology for the SHs and a tool to trace potential precursor cells in these neoplasms. Thus, there has been an accumulation of evidence building on Nezelof's historical proposal of a pathological hematopoietic precursor for LCH ("pathological LCs") that has initiated new cellular origin studies into the SHs (Nezelof and Basset 2001). Gene expression studies in LCH and non-LCH have documented SH lesions have expression profiles of myeloid-derived precursors and not epidermal LCs (Allen et al. 2010; Diamond et al. 2016). Additionally, $BRAF^{V600E}$ was traced to $CD34^{+}$ hematopoietic stem/progenitor cells (HSPCs) in studies of high-risk pediatric and adult multisystem LCH and ECD patients but not in patients with single-system or low-risk, multifocal LCH (Berres et al. 2014; Milne et al. 2017; Durham et al. 2017b).

Furthermore, several groups have generated murine models with enforced $BRAF^{V600E}$-expression in $langerin^{+}$ cells resulting in formation of localized LCH-like lesions and in $CD11c^{+}$ cells resulting in a more aggressive phenotype similar to high-risk LCH (Berres et al. 2014; Mass et al. 2017). Notably, xenotransplantation studies using $CD34^{+}$ HSPCs from histiocytosis patients gave rise to genetically and phenotypically accurate xenografts, which provided functional evidence of the self-renewal capacity of kinase-altered HSPCs in SH patients (Durham et al. 2017b). Cumulatively, current evidence led to the proposal of a revised model of histiocytosis pathogenesis, the misguided myeloid differentiation model, in which the developmental stage at which an ERK-activating alteration arises determines the clinical manifestations. Thus, the cell of origin of at least a proportion of SH patients resides in the HSPC compartment prior to committed monocyte or dendritic cell differentiation (Milne et al. 2017; Durham et al. 2017b).

Additional murine studies into alternate cells of origin demonstrated that mosaic expression of $Braf^{V600E}$ in yolk sac–derived, erythro-myeloid progenitors (EMPs), the cell of origin of murine tissue–resident macrophages (e.g., microglia and Kupffer cells), led to clonal expansion and the accumulation of ERK-activated microglia in the CNS of these models. These

Downloaded from http://perspectivesinmedicine.cshlp.org/ on September 20, 2020 - Published by Cold Spring Harbor Laboratory Press





mice developed a severe, late-onset neurodegenerative disorder but lacked the systemic accumulation of histiocytes outside the CNS as was seen in models with *Braf*$^{V600E}$ expression in HSC-derived cells. Therefore, these results illustrate yolk sac–derived EMPs can be a potential cell of origin in the histiocytoses (Gomez Perdiguero et al. 2015; Mass et al. 2017). Thus, more than one immediate cellular precursor and the potential for alternate cells-of-origin exist for SHs. However, more investigation is required.

## MOLECULARLY BASED HISTIOCYTOSIS THERAPY

Over the past 5 years, SH therapy has dramatically changed with the emergence of targeted therapy and the first U.S. Food and Drug Administration (FDA)-approved SH treatment (Fig. 6A,B) resulting in an improved prognosis for ECD (5-yr survival of 43% in 1996 but 83% currently) (Veyssier-Belot et al. 1996; Cohen-Aubart et al. 2018).

Because 50%–60% of SH patients harbor *BRAF*$^{V600E}$ (Badalian-Very et al. 2010; Haroche et al. 2012), a vemurafenib phase II clinical trial studied *BRAF*$^{V600}$-mutated ECD and LCH and demonstrated a nearly 100% metabolic response rate, as did several case series. As a result, the U.S. FDA–approved vemurafenib for use in *BRAF*$^{V600}$-mutated ECD in November 2017 (Fig. 6A; Haroche et al. 2013, 2015; Cohen-Aubart et al. 2014; Hyman et al. 2015; Borys et al. 2016; Bhatia et al. 2018; Diamond et al. 2018). Although BRAF inhibition generally achieves robust and durable responses in *BRAF*$^{V600}$-mutated histiocytoses, the LOVE study showed 75% of patients who discontinued vemurafenib relapsed in 6 mo but were able to recapture their prior responses when restarted on BRAF inhibitors (vemurafenib; dabrafenib) (Cohen Aubart et al. 2017; Vaglio and Diamond 2017). Additionally, BRAF inhibitor resistance in the SH is rare and has only been reported in one instance where a dabrafenib-treated *BRAF*$^{V600E}$-mutated ECD patient acquired a *KRAS* mutation, which responded to trametinib (Nordmann et al. 2017).

It is important to note that the extreme sensitivity and durability of response of SH to vemurafenib are quite unique across cancers. Although *BRAF*$^{V600E}$ mutations are seen in ~8% of all cancer types overall, very few cancers have been shown to have high response rates to BRAF inhibitors as single agents as has been seen in SHs (for review, see Holderfield et al. 2014; Crispo et al. 2019). The largest experience with BRAF inhibition has been in the setting of *BRAF*$^{V600E}$-mutant metastatic melanoma in which BRAF inhibition is most commonly combined with MEK inhibition to improve efficacy and durability of response and reduce side effects from single-agent BRAF inhibition. But even with this approach, although 63%–76% of all patients with advanced *BRAF*$^{V600E}$-mutant melanoma derive clinical benefit from combined BRAF/MEK inhibition, median progression-free survival lasts only about 9 mo and 90% of patients develop resistance within 1 yr (for review, see Crispo et al. 2019). Currently, BRAF inhibitors are FDA-approved for the therapy of *BRAF*$^{V600E}$-mutant metastatic melanoma, either alone or in combination with MEK inhibitors, and there are three BRAF/MEK inhibitors approved for this setting (vemurafenib/debrafinib, dabrafenib and trametinib, and encorafenib plus binimetinib). In addition, BRAF inhibitors are approved in three specific settings for thyroid cancers: (1) vemurafenib for *BRAF*$^{V600E}$-mutant advanced radioactive iodine-refractory thyroid cancer, (2) dabrafenib for *BRAF*$^{V600E}$-mutated metastatic papillary thyroid cancer, and (3) debrafenib plus trametinib for the treatment of locally advanced or metastatic anaplastic thyroid cancer with a *BRAF*$^{V600E}$ mutation and no satisfactory locoregional treatment options.

Accumulating molecular knowledge in *BRAF*$^{V600}$-negative SH led to investigations into MEK inhibitors (cobimetinib; trametinib) (Diamond et al. 2016, 2019; Cohen Aubart et al. 2017, 2018) with the cobimetinib phase II clinical trial showing an 89% overall response rate (ORR) by positron emission tomography (PET)-computed tomography (CT) with fluorodeoxyglucose (FDG) tracer irrespective of disease site. As a result, the U.S. FDA granted

Downloaded from http://perspectivesinmedicine.cshlp.org/ on September 20, 2020 - Published by Cold Spring Harbor Laboratory Press



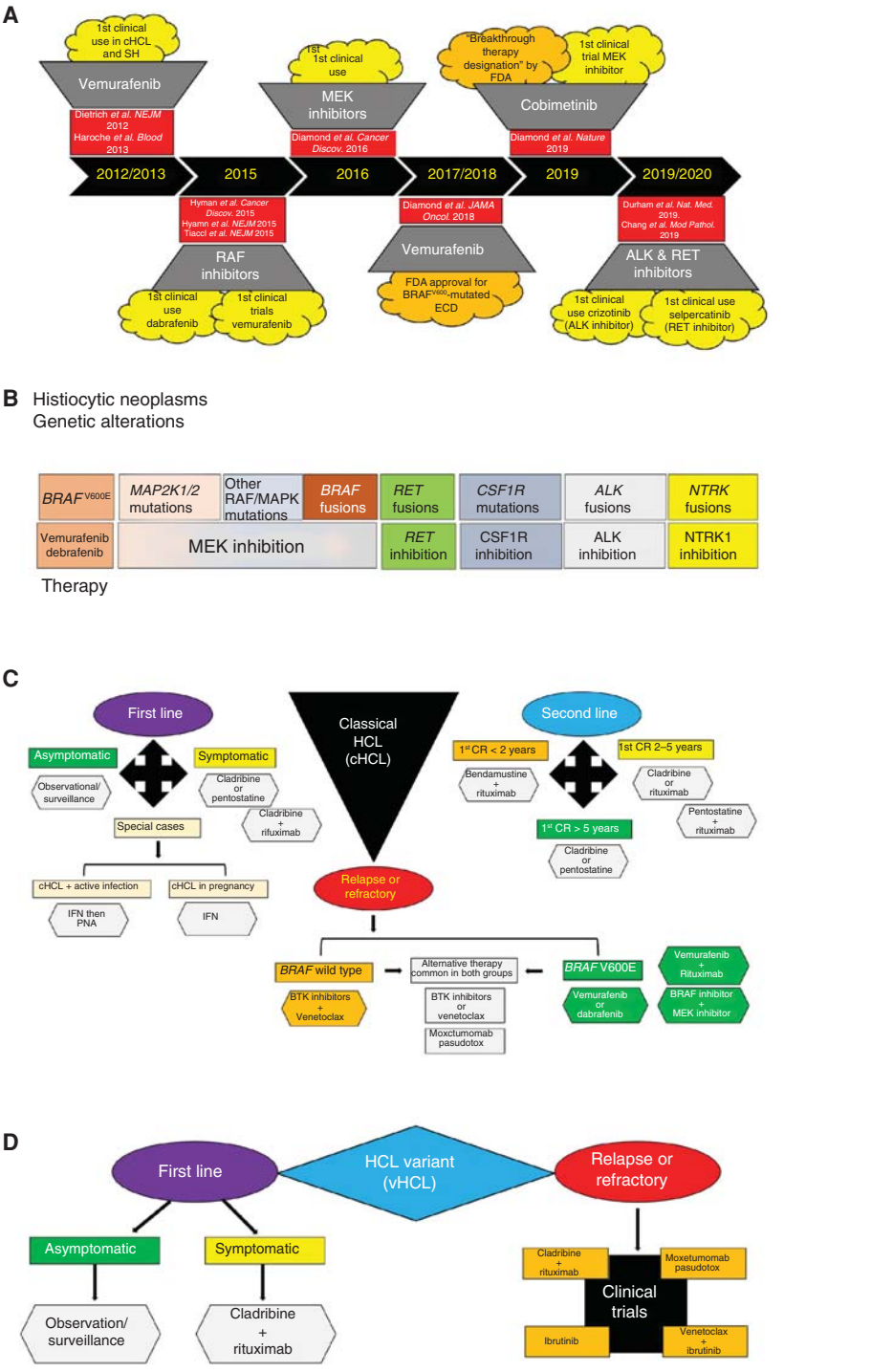



**Figure 6.** Therapeutic advancements achieved during a progressive molecular age for MAPK-driven hematopoietic neoplasms. (*A*) Timeline documenting the targeted therapeutic achievements in the histiocytic neoplasms and hairy cell leukemia over the past decade. (*B*) Diagram summarizing the molecular targeted therapies that have or may demonstrate clinical efficacy in the histiocytic neoplasms. (*C*) Diagram of a composite therapeutic algorithm for the first-line, second-line, and relapsed/refractory treatment of classical hairy cell leukemia based on current advancements during the molecular age. (*D*) Diagram of a composite therapeutic algorithm for the first-line and relapsed/refractory treatment of hairy cell leukemia variant founded on current molecular progress. SH, Systemic histiocytoses; ECD, Erdheim–Chester disease; cHCL, classical hairy cell leukemia; vHCL, hairy cell leukemia variant; FDA, Food and Drug Administration; PNA, purine analog; IFN, interferon; BTK, Bruton tyrosine kinase; CR, complete response.

Downloaded from http://perspectivesinmedicine.cshlp.org/ on September 20, 2020 - Published by Cold Spring Harbor Laboratory Press





"Breakthrough Therapy Designation" to cobimetinib in the treatment of *BRAF*$^{V600}$-negative histiocytoses (Fig. 6A; Diamond et al. 2019).

Moreover, molecular discovery of *ALK*, *NTRK1*, and *RET* fusions, as well as *CSF1R* mutations in diverse histioctyoses, have stimulated investigations into other targeted therapies. These studies have provided in vitro functional data or clinical reports supporting the use of ALK inhibitors (crizotinib; alectinib), the RET-specific inhibitor selpercatinib, NTRK inhibitors, and *CSF1R*-inhibitors (pexidartinib) in SHs (Fig. 6B; Diamond et al. 2016; Lee et al. 2017; Taylor et al. 2018; Chang et al. 2019; Durham et al. 2019). Therefore, the molecular age has provided many exciting therapeutic options for SH patients, but molecularly targeted therapies beyond BRAF and MEK inhibitors need to be scrutinized in future clinical trials. Also, questions about the optimal dosing, treatment duration, and therapy response assessments require further study, especially in pediatric SH patients.

## HAIRY CELL LEUKEMIA

### Clinical Presentation

HCL was originally named "leukemic reticuloendotheliosis" and described based on the existence of numerous "hairy" surface projections (Bouroncle et al. 1958). Classical HCL is a rare, mature B-lymphocytic neoplasm comprising 2% of lymphoid leukemias. Meanwhile, vHCL is a similar mature B-lymphocytic neoplasm with variant clinical, cytological, and immunophenotypical features and is 10% as common as cHCL (Swerdlow et al. 2017; Maitre et al. 2019).

Patients with HCL commonly present with weakness, fatigue, bleeding, and fever, and the immunophenotypical profile has emerged as the key component to distinguish cHCL and vHCL. Therefore, HCL is a group of hematological malignancies consisting of cHCL, *IGHV4-34*$^{+}$ cHCL, and vHCL that are morphologically similar with subtle pathological differences but have distinct clinical and laboratory features, immunophenotypes, and molecular characteristics that are compared in Table 2 (Tiacci et al. 2011; Waterfall et al. 2014; Dietrich et al. 2015; Falini et al. 2016; Swerdlow et al. 2017; Thompson and Ravandi 2017; Durham et al. 2017a; Maitre et al. 2019). Furthermore, newly discovered molecular features (Fig. 5; Table 2) assist in further characterization of the pathophysiology and therapeutic options for cHCL and vHCL and have been correlated with other HCL risk stratification parameters as detailed in Table 3 (Arons et al. 2009; Forconi et al. 2009; Xi et al. 2012; Poret et al. 2015; Falini et al. 2016; Swerdlow et al. 2017; Durham et al. 2017a; Maitre et al. 2019).

### Pathophysiology

#### *Genomic Profiling*

In 2011, WES of cHCL uncovered *BRAF*$^{V600E}$ as the driving genetic event in ~97% of cHCL (Tiacci et al. 2011; Waterfall et al. 2014; Dietrich et al. 2015; Durham et al. 2017a). Occasional *BRAF*$^{V600E}$-negative cHCL patients were shown to have *BRAF* exon 11 mutations (*BRAF*$^{D449E}$; *BRAF*$^{F468C}$) (Figs. 1C, 5) that were predicted but not proven to be activating (Tschernitz et al. 2014). Meanwhile, another WES study evaluated vHCL and *IGHV4-34*$^{+}$ cHCL and found activating *MAP2K1* mutations in ~50% of these cases (Figs. 1D, 5; Waterfall et al. 2014; Dietrich et al. 2015; Durham et al. 2017a). Therefore, through MAPK pathway activation by *BRAF* and *MAP2K1* mutations, the neoplastic hairy cells demonstrate increased proliferation and survival (Tiacci et al. 2011; Waterfall et al. 2014; Dietrich et al. 2015; Durham et al. 2017a).

Recently, the discovery of co-occurring genetic alterations that may cooperate with *BRAF*$^{V600E}$ in cHCL and *MAP2K1* mutations in vHCL have provided further insights into their pathogenesis. Alterations in genes involved in cell cycle regulation (*CCND1*; *CDKN1B/p27*; *CCND3*), NF-κB pathway and B-lymphocyte differentiation (*KLF2*), the spliceosome (*U2AF1*), and epigenetic regulation (*KMT2C/MLL3*, *KDM6A*, *CREBBP*, *ARID1A*) are potentially key players in the pathophysiology of cHCL or vHCL but will require further study to elucidate their mechanistic roles (Fig. 5A,B;

Downloaded from http://perspectivesinmedicine.cshlp.org/ on September 20, 2020 - Published by Cold Spring Harbor Laboratory Press



**Table 2.** Summary of the characteristic features of classical hairy cell leukemia and hairy cell leukemia variant

| Characteristic Features | IGHV4-34- cHCL | IGHV4-34$^{+}$ cHCL | vHCL |
|---|---|---|---|
| **Laboratory parameters** | | | |
| Pancytopenia | Present | Absent | Absent |
| Monocytopenia | Present | Absent | Absent |
| Absolute neutrophil count | Decreased | Normal | Normal |
| Leukocytosis | Absent | Present | Present |
| Soluble IL2 receptor (plasma) | Elevated | Unknown | Normal |
| Bone marrow aspiration | Dry tap | Easily aspirated | Easily aspirated |
| Immunophenotypic profile | | | |
| CD19 | ++ | ++ | ++ |
| CD20 | ++ | ++ | ++ |
| CD22 | ++ | ++ | ++ |
| FMC7 | + | + | + |
| CD11c | ++ | ++ | ++ |
| CD103 | + | + | + |
| CD25 | + | + | −− |
| CD123 | + | + | −− |
| CD200 | + | + | −− |
| Annexin A1 | + | + | −− |
| **Histological features** | | | |
| Nucleus (Wright–Giemsa) | Oval/kidney-shaped | Oval/kidney-shaped | Round/oval |
| Nucleolus (Wright–Giemsa) | Absent | Absent | Prominent |
| Cytoplasm (Wright–Giemsa) | Abundant, pale | Abundant, pale | Abundant, pale |
| Cellular surface | Thin, often long circumferential projections | Thin, often long circumferential projections | Thin, often long circumferential projections |
| Infiltration pattern (bone marrow) | Diffuse and/or interstitial | Diffuse and/or interstitial | Diffuse, intrasinusoidal, and/or interstitial |
| Infiltration pattern (spleen) | Red pulp with effacement of white pulp | Red pulp with effacement of white pulp | Red pulp |
| TRAP immunocytochemistry | + | + | −− |
| Annexin A1 immunohistochemistry | + | + | −− |
| *BRAF*$^{V600E}$ immunohistochemistry | + | −− | −− |
| **Molecular features** | | | |
| *BRAF*$^{V600E}$ mutations | Present (~97%) | Absent | Absent |
| *MAP2K1* alterations | Absent | Present | Present (~50%) |
| *IGHV* somatic hypermutation | Frequent | Absent | Rare |
| *IGHV4-34* usage | Absent | Present | Frequent |
| *CDKN1B* (p27) co-occurring mutations | Present | Unknown | Absent |
| *KLF2* co-occurring mutations | Present | Unknown | Absent |

*Continued*

Cold Spring Harbor Perspectives in Medicine
www.perspectivesinmedicine.org

Downloaded from http://perspectivesinmedicine.cshlp.org/ on September 20, 2020 - Published by Cold Spring Harbor Laboratory Press



**Table 2.** *Continued*

| Characteristic Features | IGHV4-34- cHCL | IGHV4-34$^+$ cHCL | vHCL |
|---|---|---|---|
| *NOTCH1* co-occurring mutations | Rare | Unknown | Absent |
| *NOTCH2* co-occurring mutations | Rare | Unknown | Absent |
| *BCOR* co-occurring mutations | Rare | Unknown | Absent |
| *KDM6A* co-occurring mutations | Rare | Unknown | Frequent |
| *CREBBP* co-occurring mutations | Rare | Unknown | Frequent |
| *CCND3* co-occurring mutations | Absent | Unknown | Present |
| *U2AF1* co-occurring mutations | Absent | Unknown | Present |

cHCL, Classical hairy cell leukemia; vHCL, hairy cell leukemia variant; IL2, interleukin 2; CD, cluster of differentiation; *IGHV*, immunoglobulin heavy chain variable; +, low expression; ++, high expression; –, not detected.

Cold Spring Harbor Perspectives in Medicine
www.perspectivesinmedicine.org



(Waterfall et al. 2014; Clipson et al. 2015; Dietrich et al. 2015; Piva et al. 2015; Falini et al. 2016; Jallades et al. 2017; Durham et al. 2017a; Maitre et al. 2018, 2019).

### Gene Expression and Methylation Profiling

The molecular era has refined epigenetic advancements, which has yielded new insights into the peculiar clinical-pathological features of cHCL, whereas few notable studies have investigated *IGHV4-34*$^+$ cHCL or vHCL. The methylation and gene expression profiles in cHCL supported the constitutive activation of the MAPK pathway. Also, hypomethylation and overexpression of genes that inhibit matrix metalloproteinase activity and hypermethylation and underexpression of chemokine receptors critical for B-lymphocyte migration to peripheral lymphoid organ follicles result in neoplastic hairy cells homing to bone marrow, splenic red pulp, and hepatic sinusoids rather than splenic white pulp and lymph nodes. Additionally, cHCL showed hypomethylation and overexpression of genes that stimulate fibronectin production and may contribute to the bone marrow reticulin fibrosis and poor bone marrow aspiration in cHCL (Basso et al. 2004; Arribas et al. 2019). Furthermore, overexpression of *TGFB1*, which stimulates neoplastic hairy cells to produce TGF-β, has been posited as a reason for the inhibition of normal hematopoiesis in cHCL (leukopenia; monocytopenia) (Basso et al. 2004; Swerdlow et al. 2017). Meanwhile, other studies support *LST1* (leukocyte transcript 1) and *ACTB* (actin β) genes are enriched in and important for the formation of actin-containing, circumferential "hairy" membrane projections characteristic of HCL (Pettirossi et al. 2015; Falini et al. 2016).

### Cellular Origins of cHCL

Through the discovery of *BRAF*$^{V600E}$ in cHCL, a biomarker for the evaluation of the cell of origin of cHCL appeared. Although epigenetic profiling suggests cHCL is derived from transformed, postgerminal center B-lymphocytes (Basso et al. 2004; Falini et al. 2016; Arribas et al. 2019), recent cellular-origin studies reported that the HSCs in cHCL harbor the *BRAF*$^{V600E}$ mutation. Furthermore, xenografting of purified, *BRAF*$^{V600E}$-mutated HSCs into immunodeficient mice resulted in stable engraftment, which functionally demonstrated the self-renewal capacity of *BRAF*$^{V600E}$-mutant HSCs in cHCL. However, the transplanted mice did not develop the complete cHCL phenotype, and this

Downloaded from http://perspectivesinmedicine.cshlp.org/ on September 20, 2020 - Published by Cold Spring Harbor Laboratory Press



**Table 3.** Summary of risk-stratification parameters in hairy cell leukemia that predict a poor prognosis and resistance to purine analogs

| Parameters | Measurement |
|---|---|
| Clinical | |
| Splenomegaly | >3 cm below the costal margin |
| Laboratory | |
| Leukocytosis | $>1 \times 10^9$ cells/L |
| Hairy cells in peripheral blood | >5 g/L |
| Beta-2 microglobulin level | >2× the upper limit of normal (High) |
| CD38 by immunophenotype | Present |
| Molecular features | |
| *BRAF*$^{V600E}$ | Absent |
| *IGHV* mutational status | Unmutated |
| *IGHV4-34* rearrangement | Present |
| Telomere length | Short |

cHCL, Classical hairy cell leukemia; vHCL, hairy cell leukemia variant; CD, cluster of differentiation; *IGHV*, immunoglobulin heavy chain variable

Cold Spring Harbor Perspectives in Medicine
www.perspectivesinmedicine.org
CSH PERSPECTIVES

raises the question as to whether or not a permissive epigenetic background and acquisition of cooperating genetic alterations are required for phenotypically accurate cHCL (Chung et al. 2014; Falini et al. 2016). Therefore, more functional studies and murine modeling are required to attain a faithful cHCL animal model.

## TREATMENT

HCL patients should be treated when symptomatic or when presenting with one of these hematological parameters: hemoglobin <11 g/dL; platelet count <100,000/μL; or ANC <1,000 cells/μL. Meanwhile, asymptomatic cHCL patients are to be managed with observation/surveillance (Grever et al. 2017; Andrasiak et al. 2018; Maitre et al. 2019).

### Chemotherapy

First-line treatment in cHCL patients involves purine analog (PNA) monotherapy (cladribine or pentostatin) because large studies have shown 76%–83% of patients achieved a complete response (CR) and 31%–33% a partial response (PR) (Dearden et al. 2011; Cornet et al. 2014; Else et al. 2015; Maitre et al. 2019). Additionally, a phase II trial of chemoimmunotherapy with cladribine followed by rituximab demonstrated a CR of 100% and has high efficacy as a first-line therapy. However, special cases do arise and include patients with symptomatic cHCL and a febrile infection requiring infection management prior to PNA treatment (INF-α before PNA). Also, pregnant cHCL patients should be treated with interferon (IFN) (Fig. 6C; Maitre et al. 2019).

Second-line chemotherapy is necessary for the 50% of cHCL patients who relapse during the first 5 yr following first-line chemotherapy, and the consensus on treatment options is stratified based on duration of the first CR (CR > 5 yr; CR = 2–5 yr; CR < 2 yr) (Fig. 6C; Else et al. 2011, 2015; Burotto et al. 2013; Cornet et al. 2014; Chihara et al. 2016; Sadeghi and Li 2018; Maitre et al. 2019).

First-line chemotherapy in symptomatic vHCL patients has no current consensus; however, a combination of cladribine/rituximab is the common treatment used when managing vHCL (Fig. 6D; Kreitman et al. 2013; Maitre et al. 2019).

### Targeted Therapy

The molecular era spawned the discovery of *BRAF*$^{V600E}$ in >97% of cHCL and the first molecular target in these neoplasms (Fig. 6A; Tiacci et al. 2011; Dietrich et al. 2012; Falini et al. 2016). The first clinical trials of vemurafenib in re-

Downloaded from http://perspectivesinmedicine.cshlp.org/ on September 20, 2020 - Published by Cold Spring Harbor Laboratory Press



Cold Spring Harbor Perspectives in Medicine
www.perspectivesinmedicine.org



lapsed/refractory cHCL showed an ORR approaching 100% with 35%–40% CRs, and the median relapse-free survival was ~19 mo (CR patients) and 6 mo (PR patients) (Tiacci et al. 2015; Falini et al. 2016; Maitre et al. 2019). Thus, the most promising therapeutic options for relapsed/refractory cHCL include targeted therapeutics: BRAF inhibitors in *BRAF*$^{V600E}$-mutated cHCL (Hyman et al. 2015; Tiacci et al. 2015); BRAF/MEK inhibitor combinations in *BRAF*$^{V600E}$-mutated cHCL; recombinant immunoconjugates targeting CD22 (moxetumomab pasudotox), which has promising preliminary results in a phase I clinical trial (91% ORR, including 59% with CRs) (Kreitman et al. 2018; Maitre et al. 2019); and the first-in-class Bruton tyrosine kinase (BTK) inhibitor ibrutinib approved for treating relapsed/refractory B-cell malignancies (e.g., chronic lymphocytic leukemia [CLL]/small lymphocytic leukemia [SLL]) (Fig. 6C; Byrd et al. 2015; Sarvaria et al. 2016; Maitre et al. 2019). Furthermore, clinical trials utilizing moxetumomab pasudotox, ibrutinib, and ibrutinib/venetoclax are suggested for the treatment of relapsed/refractory vHCL (Fig. 6D; Bohn et al. 2017; Maitre et al. 2019). Future directions for molecular treatments in HCL should include trials combining BRAF/MEK inhibitors in cHCL, MEK inhibitors in vHCL and *IGHV4-34*$^{+}$ cHCL, CDK4/6 inhibitors in *CCND3*-mutated vHCL, and ibrutinib in both cHCL and vHCL (Maitre et al. 2019).

## Mechanisms of Vemurafenib Resistance

As in metastatic melanoma, the dramatic clinical efficacy of vemurafenib in refractory/relapsed cHCL has now shown relapse, which suggests the development of resistance mechanisms (Tiacci et al. 2015; Falini et al. 2016). However, knowledge of the vemurafenib resistance mechanisms in cHCL has just begun to emerge. For example, resistance in two patients treated in a phase II cHCL clinical trial was secondary to acquired mutations in *KRAS/NRAS* following treatment with vemurafenib, which induce reactivation of the MAPK pathway through *RAF1* (Trunzer et al. 2013; Tiacci et al. 2015; Durham et al. 2017a). Another patient experienced complete, de novo vemurafenib resistance, and genomic analysis of his pretreatment sample revealed a gain-of-function mutation in *IRS1* (*IRS1*$^{P1201S}$) that functionally activated PI3K-AKT signaling. Furthermore, this patient had heterozygous deletions of *NF1* and *NF2* that functionally induced vemurafenib resistance in vitro (Whittaker et al. 2013; Shalem et al. 2014; Durham et al. 2017a). Nonetheless, more functional and sequencing studies are required to better elucidate and catalog cHCL vemurafenib-resistance mechanisms.

## Frequency and Implication of BRAF Mutations in Hematologic Malignancies outside of HCL and SH

In contrast to the very high frequency of *BRAF*$^{V600E}$ mutations in HCL and SH, BRAF mutations are far rarer in more common hematologic malignancies. Outside of HCL and SH, recurrent BRAF mutations have been reported in 4%–10% of multiple myeloma (Andrulis et al. 2013; Lohr et al. 2014), 2%–5% of patients with CLL (Jebaraj et al. 2013; Leeksma et al. 2019), and 1%–2% patients with acute myeloid leukemia (AML) (Papaemmanuil et al. 2016). To date, the only formal evaluation of the use of BRAF inhibition in BRAF-mutant hematologic malignancies outside of HCL and SH was the use of vemurafenib for nine patients with *BRAF*$^{V600E}$-mutant multiple myeloma as part of the VE-BASKET Study (Raje et al. 2018). The best confirmed overall response rate in this cohort was 33% with two patients achieving partial remissions. In the single published report of an AML patient treated with a BRAF inhibitor, a refractory AML patient was treated with combined dabrafenib/trametinib with only a very transient response (Wander et al. 2017). It is important to note that in CLL and myeloma, *BRAF* mutations are often subclonal. Moreover, in CLL, *BRAF* mutations frequently occur outside of the V600 residue (most commonly at the G466, D594, and K601 residues). Given the use of vemurafenib and dabrafenib for *BRAF*$^{V600E}$/K-mutant diseases specifically, the therapeutic implications of BRAF inhibition with approved

Downloaded from http://perspectivesinmedicine.cshlp.org/ on September 20, 2020 - Published by Cold Spring Harbor Laboratory Press



Cold Spring Harbor Perspectives in Medicine
www.perspectivesinmedicine.org



BRAF inhibitors has an unclear role in CLL and has never been evaluated.

## CONCLUDING REMARKS

Molecular advancements over the past decade helped unravel the molecular pathophysiology, cellular origins, and therapeutic targets in the MAPK-driven hematological neoplasms. Since the description of *BRAF*$^{V600E}$ in SH and cHCL (Badalian-Very et al. 2010; Tiacci et al. 2011; Haroche et al. 2012), there has been an onslaught of molecular progress linking diverse kinase alterations activating MAPK, PI3K-AKT, and RTK signaling to the histiocytic neoplasms, as well as *MAP2K1* mutations in *IGHV4-34*$^{+}$ cHCL and vHCL (Figs. 1–5). These recent discoveries have refined the current pathological understanding of the histiocytoses as clonal, myeloid neoplasms with constitutive activation of MAPK and PI3K-AKT signaling and confirm HCL belongs to the MAPK-driven, hematological neoplasms. Furthermore, molecular progress has re-imagined therapeutic options for patients with these disorders (Fig. 6). Additionally, many biomarkers are now available that have enhanced our biological understanding of the cellular pathogenesis and ontogeny of the SH and HCL. However, our functional genomic conceptualization of the molecular pathogenesis and histogenesis of SH and HCL are just emerging with many aspects still enshrouded in mystery requiring systematic dissection with studies employing single-cell molecular and epigenetic analyses, as well as preclinical models. Finally, as the molecular era continues to unfold, future studies to elucidate why HCL and SH share common MAPK alterations but are phenotypically distinct neoplasms with differing clinical presentations, pathophysiology, and suspected cellular origins are a desperately needed dimension of investigation.

## ACKNOWLEDGMENTS

O.A.-W. is supported by 1 R01 CA201247-01A1 from the National Cancer Institute (NCI) of the National Institutes of Health (NIH). B.H.D. is supported by the Fellow Scholar Award in Basic/Translational Research from the American Society of Hematology (ASH), a grant from the Erdheim–Chester Disease Global Alliance Foundation, and K08 CA218901 from the NCI/NIH. R.C. is supported by U.S. Department of Defense Peer Reviewed Cancer Research Program Career Development Award W81XWH1910167.

## REFERENCES

Abla O, Jacobsen E, Picarsic J, Krenova Z, Jaffe R, Emile JF, Durham BH, Braier J, Charlotte F, Donadieu J, et al. 2018. Consensus recommendations for the diagnosis and clinical management of Rosai–Dorfman–Destombes disease. *Blood* **131:** 2877–2890. doi:10.1182/blood-2018-03-839753

Allen CE, Parsons DW. 2015. Biological and clinical significance of somatic mutations in Langerhans cell histiocytosis and related histiocytic neoplastic disorders. *Hematology Am Soc Hematol Educ Program* **2015:** 559–564. doi:10.1182/asheducation-2015.1.559

Allen CE, Li L, Peters TL, Leung HC, Yu A, Man TK, Gurusiddappa S, Phillips MT, Hicks MJ, Gaikwad A, et al. 2010. Cell-specific gene expression in Langerhans cell histiocytosis lesions reveals a distinct profile compared with epidermal Langerhans cells. *J Immunol* **184:** 4557–4567. doi:10.4049/jimmunol.0902336

Andrasiak I, Rybka J, Wrobel T. 2018. Response to the therapy in hairy cell leukemia: Systematic review and meta-analysis. *Clin Lymphoma Myeloma Leuk* **18:** 392–399.e3. doi:10.1016/j.clml.2018.03.011

Andrulis M, Lehners N, Capper D, Penzel R, Heining C, Huellein J, Zenz T, von Deimling A, Schirmacher P, Ho AD, et al. 2013. Targeting the *BRAF* V600E mutation in multiple myeloma. *Cancer Discov* **3:** 862–869. doi:10.1158/2159-8290.CD-13-0014

Arcaini L, Zibellini S, Boveri E, Riboni R, Rattotti S, Varettoni M, Guerrera ML, Lucioni M, Tenore A, Merli M, et al. 2012. The *BRAF* V600E mutation in hairy cell leukemia and other mature B-cell neoplasms. *Blood* **119:** 188–191. doi:10.1182/blood-2011-08-368209

Arceci RJ. 1999. The histiocytoses: The fall of the Tower of Babel. *Eur J Cancer* **35:** 747–767; discussion 767–749. doi:10.1016/S0959-8049(99)00039-8

Arceci RJ, Brenner MK, Pritchard J. 1998. Controversies and new approaches to treatment of Langerhans cell histiocytosis. *Hematol Oncol Clin North Am* **12:** 339–357. doi:10.1016/S0889-8588(05)70514-1

Arons E, Suntum T, Stetler-Stevenson M, Kreitman RJ. 2009. VH4-34$^{+}$ hairy cell leukemia, a new variant with poor prognosis despite standard therapy. *Blood* **114:** 4687–4695. doi:10.1182/blood-2009-01-201731

Arribas AJ, Rinaldi A, Chiodin G, Kwee I, Mensah AA, Cascione L, Rossi D, Kanduri M, Rosenquist R, Zucca E, et al. 2019. Genome-wide promoter methylation of hairy cell leukemia. *Blood Adv* **3:** 384–396. doi:10.1182/bloodadvances.2018024059

Badalian-Very G, Vergilio JA, Degar BA, MacConaill LE, Brandner B, Calicchio ML, Kuo FC, Ligon AH, Stevenson

Downloaded from http://perspectivesinmedicine.cshlp.org/ on September 20, 2020 - Published by Cold Spring Harbor Laboratory Press



Cold Spring Harbor Perspectives in Medicine
www.perspectivesinmedicine.org



KE, Kehoe SM, et al. 2010. Recurrent *BRAF* mutations in Langerhans cell histiocytosis. *Blood* **116:** 1919–1923. doi:10.1182/blood-2010-04-279083

Basso K, Liso A, Tiacci E, Benedetti R, Pulsoni A, Foa R, Di Raimondo F, Ambrosetti A, Califano A, Klein U, et al. 2004. Gene expression profiling of hairy cell leukemia reveals a phenotype related to memory B cells with altered expression of chemokine and adhesion receptors. *J Exp Med* **199:** 59–68. doi:10.1084/jem.20031175

Berres ML, Lim KP, Peters T, Price J, Takizawa H, Salmon H, Idoyaga J, Ruzo A, Lupo PJ, Hicks MJ, et al. 2014. *BRAF*-V600E expression in precursor versus differentiated dendritic cells defines clinically distinct LCH risk groups. *J Exp Med* **211:** 669–683. doi:10.1084/jem.20130977

Bhatia A, Ulaner G, Rampal R, Hyman DM, Abdel-Wahab O, Durham BH, Dogan A, Ozkaya N, Lacouture ME, Hajdenberg J, et al. 2018. Single-agent dabrafenib for $BRAF^{V600E}$-mutated histiocytosis. *Haematologica* **103:** e177–e180. doi:10.3324/haematol.2017.185298

Bohn JP, Wanner D, Steurer M. 2017. Ibrutinib for relapsed refractory hairy cell leukemia variant. *Leuk Lymphoma* **58:** 1224–1226. doi:10.1080/10428194.2016.1239262

Borys D, Nystrom L, Song A, Lomasney LM. 2016. Erdheim–Chester disease with appendicular skeletal, renal and pleural involvement responding to Zelboraf (*BRAF* inhibitor) treatment: Case report. *Skeletal Radiol* **45:** 1397–1402. doi:10.1007/s00256-016-2431-6

Bouroncle BA, Wiseman BK, Doan CA. 1958. Leukemic reticuloendotheliosis. *Blood* **13:** 609–630. doi:10.1182/blood.V13.7.609.609

Broadbent V, Egeler RM, Nesbit ME Jr. 1994. Langerhans cell histiocytosis—Clinical and epidemiological aspects. *Br J Cancer Suppl* **23:** S11–S16.

Brown NA, Furtado LV, Betz BL, Kiel MJ, Weigelin HC, Lim MS, Elenitoba-Johnson KS. 2014. High prevalence of somatic *MAP2K1* mutations in *BRAF* V600E-negative Langerhans cell histiocytosis. *Blood* **124:** 1655–1658. doi:10.1182/blood-2014-05-577361

Brown RA, Kwong BY, McCalmont TH, Ragsdale B, Ma L, Cheung C, Rieger KE, Arber DA, Kim J. 2015. *ETV3-NCOA2* in indeterminate cell histiocytosis: Clonal translocation supports sui generis. *Blood* **126:** 2344–2345. doi:10.1182/blood-2015-07-655530

Burotto M, Stetler-Stevenson M, Arons E, Zhou H, Wilson W, Kreitman RJ. 2013. Bendamustine and rituximab in relapsed and refractory hairy cell leukemia. *Clin Cancer Res* **19:** 6313–6321. doi:10.1158/1078-0432.CCR-13-1848

Byrd JC, Furman RR, Coutre SE, Burger JA, Blum KA, Coleman M, Wierda WG, Jones JA, Zhao W, Heerema NA, et al. 2015. Three-year follow-up of treatment-naive and previously treated patients with CLL and SLL receiving single-agent ibrutinib. *Blood* **125:** 2497–2506. doi:10.1182/blood-2014-10-606038

Cai J, Huang X, Yin M, Pan C, Song L, Zhan Z, Chen J, Gao Y, Tang J, Li Y, et al. 2019. A novel fusion gene PLEKHA6-NTRK3 in Langerhans cell histiocytosis. *Int J Cancer* **144:** 117–124. doi:10.1002/ijc.31636

Carapeti M, Aguiar RC, Goldman JM, Cross NC. 1998. A novel fusion between MOZ and the nuclear receptor coactivator TIF2 in acute myeloid leukemia. *Blood* **91:** 3127–3133. doi:10.1182/blood.V91.9.3127

Chakraborty R, Hampton OA, Shen X, Simko SJ, Shih A, Abhyankar H, Lim KP, Covington KR, Trevino L, Dewal N, et al. 2014. Mutually exclusive recurrent somatic mutations in *MAP2K1* and *BRAF* support a central role for ERK activation in LCH pathogenesis. *Blood* **124:** 3007–3015. doi:10.1182/blood-2014-05-577825

Chakraborty R, Burke TM, Hampton OA, Zinn DJ, Lim KP, Abhyankar H, Scull B, Kumar V, Kakkar N, Wheeler DA, et al. 2016. Alternative genetic mechanisms of *BRAF* activation in Langerhans cell histiocytosis. *Blood* **128:** 2533–2537. doi:10.1182/blood-2016-08-733790

Chakraborty R, Hampton OA, Abhyankar H, Zinn DJ, Grimes A, Skull B, Eckstein O, Mahmood N, Wheeler DA, Lopez-Terrada D, et al. 2017. Activating *MAPK1* (ERK2) mutation in an aggressive case of disseminated juvenile xanthogranuloma. *Oncotarget* **8:** 46065–46070. doi:10.18632/oncotarget.17521

Chang KTE, Tay AZE, Kuick CH, Chen H, Algar E, Taubenheim N, Campbell J, Mechinaud F, Campbell M, Super L, et al. 2019. ALK-positive histiocytosis: An expanded clinicopathologic spectrum and frequent presence of *KIF5B-ALK* fusion. *Mod Pathol* **32:** 598–608. doi:10.1038/s41379-018-0168-6

Chester W. 1930. Über lipoidgranulomatose. *Virchows Arch Pathol Anat Physiol Klin Med* **279:** 561–602. doi:10.1007/BF01942684

Chihara D, Kantarjian H, O'Brien S, Jorgensen J, Pierce S, Faderl S, Ferrajoli A, Poku R, Jain P, Thompson P, et al. 2016. Long-term durable remission by cladribine followed by rituximab in patients with hairy cell leukaemia: Update of a phase II trial. *Br J Haematol* **174:** 760–766. doi:10.1111/bjh.14129

Chikwava K, Jaffe R. 2004. Langerin (CD207) staining in normal pediatric tissues, reactive lymph nodes, and childhood histiocytic disorders. *Pediatr Dev Pathol* **7:** 607–614. doi:10.1007/s10024-004-3027-z

Christian HA. 1919. Defects in membranous bones, exophthalmos and diabetes insipidus. An unusual syndrome of dyspituitarism—A clinical study. *Contrib Med Biol Res* **1:** 390.

Chung SS, Kim E, Park JH, Chung YR, Lito P, Teruya-Feldstein J, Hu W, Beguelin W, Monette S, Duy C, et al. 2014. Hematopoietic stem cell origin of *BRAF*V600E mutations in hairy cell leukemia. *Sci Transl Med* **6:** 238ra271.

Clipson A, Wang M, de Leval L, Ashton-Key M, Wotherspoon A, Vassiliou G, Bolli N, Grove C, Moody S, Escudero-Ibarz L, et al. 2015. *KLF2* mutation is the most frequent somatic change in splenic marginal zone lymphoma and identifies a subset with distinct genotype. *Leukemia* **29:** 1177–1185. doi:10.1038/leu.2014.330

Cohen-Aubart F, Emile JF, Maksud P, Galanaud D, Idbaih A, Chauvet D, Amar Y, Benameur N, Amoura Z, Haroche J. 2014. Marked efficacy of vemurafenib in suprasellar Erdheim–Chester disease. *Neurology* **83:** 1294–1296. doi:10.1212/WNL.0000000000000832

Cohen Aubart F, Emile JF, Carrat F, Charlotte F, Benameur N, Donadieu J, Maksud P, Idbaih A, Barete S, Hoang-Xuan K, et al. 2017. Targeted therapies in 54 patients with Erdheim–Chester disease, including follow-up after interruption (the LOVE study). *Blood* **130:** 1377–1380. doi:10.1182/blood-2017-03-771873

Downloaded from http://perspectivesinmedicine.cshlp.org/ on September 20, 2020 - Published by Cold Spring Harbor Laboratory Press



Cohen Aubart F, Emile JF, Maksud P, Galanaud D, Cluzel P, Benameur N, Aumaitre O, Amoura Z, Haroche J. 2018. Efficacy of the MEK inhibitor cobimetinib for wild-type *BRAF* Erdheim–Chester disease. *Br J Haematol* **180:** 150–153. doi:10.1111/bjh.14284

Cohen-Aubart F, Emile JF, Carrat F, Helias-Rodzewicz Z, Taly V, Charlotte F, Cluzel P, Donadieu J, Idbaih A, Barete S, et al. 2018. Phenotypes and survival in Erdheim–Chester disease: Results from a 165-patient cohort. *Am J Hematol* **93:** E114–E117. doi:10.1002/ajh.25055

Cornet E, Delmer A, Feugier P, Garnache-Ottou F, Ghez D, Leblond V, Levy V, Maloisel F, Re D, Zini JM, et al. 2014. Recommendations of the SFH (French Society of Haematology) for the diagnosis, treatment and follow-up of hairy cell leukaemia. *Ann Hematol* **93:** 1977–1983. doi:10.1007/s00277-014-2140-y

Crispo F, Notarangelo T, Pietrafesa M, Lettini G, Storto G, Sgambato A, Maddalena F, Landriscina M. 2019. *BRAF* inhibitors in thyroid cancer: Clinical impact, mechanisms of resistance and future perspectives. *Cancers (Basel)* **11:** 1388. doi:10.3390/cancers11091388

da Costa CE, Szuhai K, van Eijk R, Hoogeboom M, Sciot R, Mertens F, Björgvinsdóttir H, Debiec-Rychter M, de Krijger RR, Hogendoorn PC, et al. 2009. No genomic aberrations in Langerhans cell histiocytosis as assessed by diverse molecular technologies. *Genes Chromosomes Cancer* **48:** 239–249. doi:10.1002/gcc.20634

Dearden CE, Else M, Catovsky D. 2011. Long-term results for pentostatin and cladribine treatment of hairy cell leukemia. *Leuk Lymphoma* **52** (Suppl 2)**:** 21–24. doi:10.3109/10428194.2011.565093

Degar BA, Rollins BJ. 2009. Langerhans cell histiocytosis: Malignancy or inflammatory disorder doing a great job of imitating one? *Dis Model Mech* **2:** 436–439. doi:10.1242/dmm.004010

Deguchi K, Ayton PM, Carapeti M, Kutok JL, Snyder CS, Williams IR, Cross NC, Glass CK, Cleary ML, Gilliland DG. 2003. MOZ-TIF2-induced acute myeloid leukemia requires the MOZ nucleosome binding motif and TIF2-mediated recruitment of CBP. *Cancer Cell* **3:** 259–271. doi:10.1016/S1535-6108(03)00051-5

Destombes P. 1965. [Adenitis with lipid excess, in children or young adults, seen in the Antilles and in Mali. (4 cases)]. *Bull Soc Pathol Exot Filiales* **58:** 1169–1175.

Diamond EL, Abdel-Wahab O, Pentsova E, Borsu L, Chiu A, Teruya-Feldstein J, Hyman DM, Rosenblum M. 2013. Detection of an *NRAS* mutation in Erdheim–Chester disease. *Blood* **122:** 1089–1091. doi:10.1182/blood-2013-02-482984

Diamond EL, Dagna L, Hyman DM, Cavalli G, Janku F, Estrada-Veras J, Ferrarini M, Abdel-Wahab O, Heaney ML, Scheel PJ, et al. 2014. Consensus guidelines for the diagnosis and clinical management of Erdheim–Chester disease. *Blood* **124:** 483–492. doi:10.1182/blood-2014-03-561381

Diamond EL, Durham BH, Haroche J, Yao Z, Ma J, Parikh SA, Wang Z, Choi J, Kim E, Cohen-Aubart F, et al. 2016. Diverse and targetable kinase alterations drive histiocytic neoplasms. *Cancer Discov* **6:** 154–165. doi:10.1158/2159-8290.CD-15-0913

Diamond EL, Subbiah V, Lockhart AC, Blay JY, Puzanov I, Chau I, Raje NS, Wolf J, Erinjeri JP, Torrisi J, et al. 2018. Vemurafenib for *BRAF* V600–mutant Erdheim–Chester disease and Langerhans cell histiocytosis: Analysis of data from the histology-independent, phase 2, open-label VE-BASKET study. *JAMA Oncol* **4:** 384–388. doi:10.1001/jamaoncol.2017.5029

Diamond EL, Durham BH, Ulaner GA, Drill E, Buthorn J, Ki M, Bitner L, Cho H, Young RJ, Francis JH, et al. 2019. Efficacy of MEK inhibition in patients with histiocytic neoplasms. *Nature* **567:** 521–524. doi:10.1038/s41586-019-1012-y

Dietrich S, Glimm H, Andrulis M, von Kalle C, Ho AD, Zenz T. 2012. *BRAF* inhibition in refractory hairy-cell leukemia. *N Engl J Med* **366:** 2038–2040. doi:10.1056/NEJMc1202124

Dietrich S, Hüllein J, Lee SC, Hutter B, Gonzalez D, Jayne S, Dyer MJ, Oleś M, Else M, Liu X, et al. 2015. Recurrent *CDKN1B* (p27) mutations in hairy cell leukemia. *Blood* **126:** 1005–1008. doi:10.1182/blood-2015-04-643361

Donadieu J, Pritchard J. 1999. Langerhans cell histiocytosis-400 BC. *Med Pediatr Oncol* **33:** 520.

Durham BH. 2019. Molecular characterization of the histiocytoses: Neoplasia of dendritic cells and macrophages. *Semin Cell Dev Biol* **86:** 62–76. doi:10.1016/j.semcdb.2018.03.002

Durham BH, Diamond EL, Abdel-Wahab O. 2016. Histiocytic neoplasms in the era of personalized genomic medicine. *Curr Opin Hematol* **23:** 416–425. doi:10.1097/MOH.0000000000000256

Durham BH, Getta B, Dietrich S, Taylor J, Won H, Bogenberger JM, Scott S, Kim E, Chung YR, Chung SS, et al. 2017a. Genomic analysis of hairy cell leukemia identifies novel recurrent genetic alterations. *Blood* **130:** 1644–1648. doi:10.1182/blood-2017-01-765107

Durham BH, Roos-Weil D, Baillou C, Cohen-Aubart F, Yoshimi A, Miyara M, Papo M, Hélias-Rodzewicz Z, Terrones N, Ozkaya N, et al. 2017b. Functional evidence for derivation of systemic histiocytic neoplasms from hematopoietic stem/progenitor cells. *Blood* **130:** 176–180. doi:10.1182/blood-2016-12-757377

Durham BH, Lopez Rodrigo E, Picarsic J, Abramson D, Rotemberg V, De Munck S, Pannecoucke E, Lu SX, Pastore A, Yoshimi A, et al. 2019. Activating mutations in CSF1R and additional receptor tyrosine kinases in histiocytic neoplasms. *Nat Med* **25:** 1839–1842. doi:10.1038/s41591-019-0653-6

Else M, Dearden CE, Matutes E, Forconi F, Lauria F, Ahmad H, Kelly S, Liyanage A, Ratnayake V, Shankari J, et al. 2011. Rituximab with pentostatin or cladribine: An effective combination treatment for hairy cell leukemia after disease recurrence. *Leuk Lymphoma* **52** (Suppl. 2)**:** 75–78. doi:10.3109/10428194.2011.568650

Else M, Dearden CE, Catovsky D. 2015. Long-term follow-up after purine analogue therapy in hairy cell leukaemia. *Best Pract Res Clin Haematol* **28:** 217–229. doi:10.1016/j.beha.2015.09.004

Emile JF, Diamond EL, Hélias-Rodzewicz Z, Cohen-Aubart F, Charlotte F, Hyman DM, Kim E, Rampal R, Patel M, Ganzel C, et al. 2014. Recurrent *RAS* and *PIK3CA* mutations in Erdheim–Chester disease. *Blood* **124:** 3016–3019. doi:10.1182/blood-2014-04-570937

Emile J, Abla O, Fraitag S, Horne A, Haroche J, Donadieu J, Emile J, Abla O, Fraitag S, Horne A, et al. 2016. Revised



Cold Spring Harbor Perspectives in Medicine
www.perspectivesinmedicine.org

Downloaded from http://perspectivesinmedicine.cshlp.org/ on September 20, 2020 - Published by Cold Spring Harbor Laboratory Press



Cold Spring Harbor Perspectives in Medicine
www.perspectivesinmedicine.org



classification of histiocytoses and neoplasms of the macrophage-dendritic cell lineages. *Blood* **127:** 2672–2681. doi:10.1182/blood-2016-01-690636

Estrada-Veras JI, O'Brien KJ, Boyd LC, Dave RH, Durham B, Xi L, Malayeri AA, Chen MY, Gardner PJ, Alvarado-Enriquez JR, et al. 2017. The clinical spectrum of Erdheim–Chester disease: An observational cohort study. *Blood Adv* **1:** 357–366. doi:10.1182/bloodadvances.2016001784

Falini B, Martelli MP, Tiacci E. 2016. *BRAF* V600E mutation in hairy cell leukemia: From bench to bedside. *Blood* **128:** 1918–1927. doi:10.1182/blood-2016-07-418434

Farber S. 1941. The nature of "solitary or eosinophilic granuloma" of bone. *Am J Pathol* **17:** 84–102.

Fatobene G, Haroche J, Hélias-Rodzwicz Z, Charlotte F, Taly V, Ferreira AM, Abdo ANR, Rocha V, Emile JF. 2018. *BRAF* V600E mutation detected in a case of Rosai–Dorfman disease. *Haematologica* **103:** e377–e379. doi:10.3324/haematol.2018.190934

Favara BE, Feller AC, Pauli M, Jaffe ES, Weiss LM, Arico M, Bucsky P, Egeler RM, Elinder G, Gadner H, et al. 1997. Contemporary classification of histiocytic disorders. The WHO committee on histiocytic/reticulum cell proliferations. Reclassification working group of the histiocyte society. *Med Pediatr Oncol* **29:** 157–166.

Forconi F, Sozzi E, Cencini E, Zaja F, Intermesoli T, Stelitano C, Rigacci L, Gherlinzoni F, Cantaffa R, Baraldi A, et al. 2009. Hairy cell leukemias with unmutated *IGHV* genes define the minor subset refractory to single-agent cladribine and with more aggressive behavior. *Blood* **114:** 4696–4702. doi:10.1182/blood-2009-03-212449

Gadner H, Minkov M, Grois N, Pötschger U, Thiem E, Aricò M, Astigarraga I, Braier J, Donadieu J, Henter JI, et al. 2013. Therapy prolongation improves outcome in multisystem Langerhans cell histiocytosis. *Blood* **121:** 5006–5014. doi:10.1182/blood-2012-09-455774

Garces S, Medeiros LJ, Patel KP, Li S, Pina-Oviedo S, Li J, Garces JC, Khoury JD, Yin CC. 2017. Mutually exclusive recurrent *KRAS* and *MAP2K1* mutations in Rosai–Dorfman disease. *Mod Pathol* **30:** 1367–1377. doi:10.1038/modpathol.2017.55

Gomez Perdiguero E, Klapproth K, Schulz C, Busch K, Azzoni E, Crozet L, Garner H, Trouillet C, de Bruijn MF, Geissmann F, et al. 2015. Tissue-resident macrophages originate from yolk-sac-derived erythro-myeloid progenitors. *Nature* **518:** 547–551. doi:10.1038/nature13989

Grever MR, Abdel-Wahab O, Andritsos LA, Banerji V, Barrientos J, Blachly JS, Call TG, Catovsky D, Dearden C, Demeter J, et al. 2017. Consensus guidelines for the diagnosis and management of patients with classic hairy cell leukemia. *Blood* **129:** 553–560. doi:10.1182/blood-2016-01-689422

Grois NG, Favara BE, Mostbeck GH, Prayer D. 1998. Central nervous system disease in Langerhans cell histiocytosis. *Hematol Oncol Clin North Am* **12:** 287–305. doi:10.1016/S0889-8588(05)70511-6

Grois N, Fahrner B, Arceci RJ, Henter JI, McClain K, Lassmann H, Nanduri V, Prosch H, Prayer D, Histiocyte Society CNS LCH Study Group. 2010. Central nervous system disease in Langerhans cell histiocytosis. *J Pediatr* **156:** 873–881.e1. doi:10.1016/j.jpeds.2010.03.001

Guyot-Goubin A, Donadieu J, Barkaoui M, Bellec S, Thomas C, Clavel J. 2008. Descriptive epidemiology of childhood Langerhans cell histiocytosis in France, 2000–2004. *Pediatr Blood Cancer* **51:** 71–75. doi:10.1002/pbc.21498

Hand A. 1893. Polyuria and tuberculosis. *Arch Pediatr* **10:** 673–675.

Haroche J, Abla O. 2015. Uncommon histiocytic disorders: Rosai–Dorfman, juvenile xanthogranuloma, and Erdheim–Chester disease. *Hematology Am Soc Hematol Educ Program* **2015:** 571–578. doi:10.1182/asheducation-2015.1.571

Haroche J, Charlotte F, Arnaud L, von Deimling A, Hélias-Rodzewicz Z, Hervier B, Cohen-Aubart F, Launay D, Lesot A, Mokhtari K, et al. 2012. High prevalence of *BRAF* V600E mutations in Erdheim–Chester disease but not in other non-Langerhans cell histiocytoses. *Blood* **120:** 2700–2703. doi:10.1182/blood-2012-05-430140

Haroche J, Cohen-Aubart F, Emile JF, Arnaud L, Maksud P, Charlotte F, Cluzel P, Drier A, Hervier B, Benameur N, et al. 2013. Dramatic efficacy of vemurafenib in both multisystemic and refractory Erdheim-Chester disease and Langerhans cell histiocytosis harboring the *BRAF* V600E mutation. *Blood* **121:** 1495–1500. doi:10.1182/blood-2012-07-446286

Haroche J, Cohen-Aubart F, Emile JF, Maksud P, Drier A, Tolédano D, Barete S, Charlotte F, Cluzel P, Donadieu J, et al. 2015. Reproducible and sustained efficacy of targeted therapy with vemurafenib in patients with $BRAF^{V600E}$-mutated Erdheim–Chester disease. *J Clin Oncol* **33:** 411–418. doi:10.1200/JCO.2014.57.1950

Haroche J, Cohen-Aubart F, Rollins BJ, Donadieu J, Charlotte F, Idbaih A, Vaglio A, Abdel-Wahab O, Emile JF, Amoura Z. 2017. Histiocytoses: Emerging neoplasia behind inflammation. *Lancet Oncol* **18:** e113–e125. doi:10.1016/S1470-2045(17)30031-1

Héritier S, Saffroy R, Radosevic-Robin N, Pothin Y, Pacquement H, Peuchmaur M, Lemoine A, Haroche J, Donadieu J, Emile JF. 2015. Common cancer-associated *PIK3CA* activating mutations rarely occur in Langerhans cell histiocytosis. *Blood* **125:** 2448–2449. doi:10.1182/blood-2015-01-625491

Héritier S, Hélias-Rodzewicz Z, Chakraborty R, Sengal AG, Bellanné-Chantelot C, Thomas C, Moreau A, Fraitag S, Allen CE, Donadieu J, et al. 2017. New somatic *BRAF* splicing mutation in Langerhans cell histiocytosis. *Mol Cancer* **16:** 115. doi:10.1186/s12943-017-0690-z

Héritier S, Barkaoui MA, Miron J, Thomas C, Moshous D, Lambilliotte A, Mazingue F, Kebaili K, Jeziorski E, Plat G, et al. 2018. Incidence and risk factors for clinical neurodegenerative Langerhans cell histiocytosis: A longitudinal cohort study. *Br J Haematol* **183:** 608–617. doi:10.1111/bjh.15577

Holderfield M, Deuker MM, McCormick F, McMahon M. 2014. Targeting RAF kinases for cancer therapy: *BRAF*-mutated melanoma and beyond. *Nat Rev Cancer* **14:** 455–467. doi:10.1038/nrc3760

Hyman DM, Puzanov I, Subbiah V, Faris JE, Chau I, Blay JY, Wolf J, Raje NS, Diamond EL, Hollebecque A, et al. 2015. Vemurafenib in multiple nonmelanoma cancers with *BRAF* V600 mutations. *N Engl J Med* **373:** 726–736. doi:10.1056/NEJMoa1502309

Jallades L, Baseggio L, Sujobert P, Huet S, Chabane K, Callet-Bauchu E, Verney A, Hayette S, Desvignes JP, Salgado D, et al. 2017. Exome sequencing identifies recurrent *BCOR*

Downloaded from http://perspectivesinmedicine.cshlp.org/ on September 20, 2020 - Published by Cold Spring Harbor Laboratory Press



alterations and the absence of *KLF2*, *TNFAIP3* and *MYD88* mutations in splenic diffuse red pulp small B-cell lymphoma. *Haematologica* **102:** 1758–1766. doi:10.3324/haematol.2016.160192

Jebaraj BM, Kienle D, Bühler A, Winkler D, Dohner H, Stilgenbauer S, Zenz T. 2013. *BRAF* mutations in chronic lymphocytic leukemia. *Leuk Lymphoma* **54:** 1177–1182. doi:10.3109/10428194.2012.742525

Kansal R, Quintanilla-Martinez L, Datta V, Lopategui J, Garshfield G, Nathwani BN. 2013. Identification of the V600D mutation in Exon 15 of the *BRAF* oncogene in congenital, benign Langerhans cell histiocytosis. *Genes Chromosomes Cancer* **52:** 99–106. doi:10.1002/gcc.22010

Kreitman RJ, Wilson W, Calvo KR, Arons E, Roth L, Sapolsky J, Zhou H, Raffeld M, Stetler-Stevenson M. 2013. Cladribine with immediate rituximab for the treatment of patients with variant hairy cell leukemia. *Clin Cancer Res* **19:** 6873–6881. doi:10.1158/1078-0432.CCR-13-1752

Kreitman RJ, Dearden C, Zinzani PL, Delgado J, Karlin L, Robak T, Gladstone DE, le Coutre P, Dietrich S, Gotic M, et al. 2018. Moxetumomab pasudotox in relapsed/refractory hairy cell leukemia. *Leukemia* **32:** 1768-1777. doi:10.1038/s41375-018-0210-1

Laman JD, Leenen PJ, Annels NE, Hogendoorn PC, Egeler RM. 2003. Langerhans-cell histiocytosis 'insight into DC biology'. *Trends Immunol* **24:** 190–196. doi:10.1016/S1471-4906(03)00063-2

Lampert F. 1998. Langerhans cell histiocytosis. Historical perspectives. *Hematol Oncol Clin North Am* **12:** 213–219. doi:10.1016/S0889-8588(05)70506-2

Lee LH, Gasilina A, Roychoudhury J, Clark J, McCormack FX, Pressey J, Grimley MS, Lorsbach R, Ali S, Bailey M, et al. 2017. Real-time genomic profiling of histiocytoses identifies early-kinase domain *BRAF* alterations while improving treatment outcomes. *JCI Insight* **2:** e89473.

Leeksma AC, Taylor J, Wu B, Gardner JR, He J, Nahas M, Gonen M, Alemayehu WG, Te Raa D, Walther T, et al. 2019. Clonal diversity predicts adverse outcome in chronic lymphocytic leukemia. *Leukemia* **33:** 390–402. doi:10.1038/s41375-018-0215-9

Letterer E. 1924. Aleukämische Retikulose ein Beitrag zu den Proliferativen Erkraukungen des Retikuloendothelial Apparates. *Frankfurt Z Pathol* **50:** 377–393.

Lichtenstein L. 1953. Histiocytosis X: Integration of eosinophilic granuloma of bone," Letterer–Siwe disease," and "Schuller–Christian disease" as related manifestations of a single nosologic entity. *Arch Pathol* **56:** 84–102.

Lohr JG, Stojanov P, Carter SL, Cruz-Gordillo P, Lawrence MS, Auclair D, Sougnez C, Knoechel B, Gould J, Saksena G, et al. 2014. Widespread genetic heterogeneity in multiple myeloma: Implications for targeted therapy. *Cancer Cell* **25:** 91–101. doi:10.1016/j.ccr.2013.12.015

Maitre E, Bertrand P, Maingonnat C, Viailly PJ, Wiber M, Naguib D, Salaun V, Cornet E, Damaj G, Sola B, et al. 2018. New generation sequencing of targeted genes in the classical and the variant form of hairy cell leukemia highlights mutations in epigenetic regulation genes. *Oncotarget* **9:** 28866–28876. doi:10.18632/oncotarget.25601

Maitre E, Cornet E, Troussard X. 2019. Hairy cell leukemia: 2020 update on diagnosis, risk stratification, and treatment. *Am J Hematol* **94:** 1413–1422. doi:10.1002/ajh.25653

Mass E, Jacome-Galarza CE, Blank T, Lazarov T, Durham BH, Ozkaya N, Pastore A, Schwabenland M, Chung YR, Rosenblum MK, et al. 2017. A somatic mutation in erythro-myeloid progenitors causes neurodegenerative disease. *Nature* **549:** 389–393. doi:10.1038/nature23672

McClain KL, Natkunam Y, Swerdlow SH. 2004. Atypical cellular disorders. *Hematology* **2004:** 283–296. doi:10.1182/asheducation-2004.1.283

McDonagh J, McDonagh J. 1912. A contribution to our knowledge of the naevo-xantho-endotheliomata. *Br J Dermatol* **24:** 85–99. doi:10.1111/j.1365-2133.1912.tb16720.x

Merad M, Manz MG, Karsunky H, Wagers A, Peters W, Charo I, Weissman IL, Cyster JG, Engleman EG. 2002. Langerhans cells renew in the skin throughout life under steady-state conditions. *Nat Immunol* **3:** 1135–1141. doi:10.1038/ni852

Mesquita B, Lopes P, Rodrigues A, Pereira D, Afonso M, Leal C, Henrique R, Lind GE, Jeronimo C, Lothe RA, et al. 2013. Frequent copy number gains at 1q21 and 1q32 are associated with overexpression of the ETS transcription factors *ETV3* and *ELF3* in breast cancer irrespective of molecular subtypes. *Breast Cancer Res Treat* **138:** 37–45. doi:10.1007/s10549-013-2408-2

Milne P, Bigley V, Bacon CM, Néel A, McGovern N, Bomken S, Haniffa M, Diamond EL, Durham BH, Visser J, et al. 2017. Hematopoietic origin of Langerhans cell histiocytosis and Erdheim–Chester disease in adults. *Blood* **130:** 167–175. doi:10.1182/blood-2016-12-757823

Nelson DS, Quispel W, Badalian-Very G, van Halteren AG, van den Bos C, Bovée JV, Tian SY, Van Hummelen P, Ducar M, MacConaill LE, et al. 2014. Somatic activating ARAF mutations in Langerhans cell histiocytosis. *Blood* **123:** 3152–3155. doi:10.1182/blood-2013-06-511139

Nelson DS, van Halteren A, Quispel WT, van den Bos C, Bovée JV, Patel B, Badalian-Very G, van Hummelen P, Ducar M, Lin L, et al. 2015. *MAP2K1* and *MAP3K1* mutations in Langerhans cell histiocytosis. *Genes Chromosomes Cancer* **54:** 361–368. doi:10.1002/gcc.22247

Nezelof C, Basset F. 2001. From histiocytosis X to Langerhans cell histiocytosis: A personal account. *Int J Surg Pathol* **9:** 137–146. doi:10.1177/106689690100900208

Nezelof C, Basset F, Rousseau M. 1973. Histiocytosis X histogenetic arguments for a Langerhans cell origin. *Biomedicine* **18:** 365–371.

Nordmann TM, Juengling FD, Recher M, Berger CT, Kalbermatten D, Wicki A, Paasinen-Sohns A, Cathomas G, Tzankov A, Daikeler T. 2017. Trametinib after disease reactivation under dabrafenib in Erdheim–Chester disease with both *BRAF* and *KRAS* mutations. *Blood* **129:** 879–882. doi:10.1182/blood-2016-09-740217

O'Malley DP, Agrawal R, Grimm KE, Hummel J, Glazyrin A, Dim DC, Madhusudhana S, Weiss LM. 2015. Evidence of *BRAF* V600E in indeterminate cell tumor and interdigitating dendritic cell sarcoma. *Ann Diagn Pathol* **19:** 113–116. doi:10.1016/j.anndiagpath.2015.02.008

Ozkaya N, Rosenblum MK, Durham BH, Pichardo JD, Abdel-Wahab O, Hameed MR, Busam KJ, Travis WD, Diamond EL, Dogan A. 2018. The histopathology of Erdheim–Chester disease: A comprehensive review of a molecularly characterized cohort. *Mod Pathol* **31:** 581–597. doi:10.1038/modpathol.2017.160

Cold Spring Harbor Perspectives in Medicine
www.perspectivesinmedicine.org

Downloaded from http://perspectivesinmedicine.cshlp.org/ on September 20, 2020 - Published by Cold Spring Harbor Laboratory Press



Cold Spring Harbor Perspectives in Medicine
www.perspectivesinmedicine.org



Ozono S, Inada H, Nakagawa SI, Ueda K, Matsumura H, Kojima S, Koga H, Hashimoto T, Oshima K, Matsuishi T. 2011. Juvenile myelomonocytic leukemia characterized by cutaneous lesion containing Langerhans cell histiocytosis-like cells. *Int J Hematol* **93:** 389–393. doi:10.1007/s12185-011-0787-x

Papaemmanuil E, Gerstung M, Bullinger L, Gaidzik VI, Paschka P, Roberts ND, Potter NE, Heuser M, Thol F, Bolli N, et al. 2016. Genomic classification and prognosis in acute myeloid leukemia. *N Engl J Med* **374:** 2209–2221. doi:10.1056/NEJMoa1516192

Pettirossi V, Santi A, Imperi E, Russo G, Pucciarini A, Bigerna B, Schiavoni G, Fortini E, Spanhol-Rosseto A, Sportoletti P, et al. 2015. *BRAF* inhibitors reverse the unique molecular signature and phenotype of hairy cell leukemia and exert potent antileukemic activity. *Blood* **125:** 1207–1216. doi:10.1182/blood-2014-10-603100

Piva R, Deaglio S, Famà R, Buonincontri R, Scarfò I, Bruscaggin A, Mereu E, Serra S, Spina V, Brusa D, et al. 2015. The Krüppel-like factor 2 transcription factor gene is recurrently mutated in splenic marginal zone lymphoma. *Leukemia* **29:** 503–507. doi:10.1038/leu.2014.294

Poret N, Fu Q, Guihard S, Cheok M, Miller K, Zeng G, Quesnel B, Troussard X, Galiègue-Zouitina S, Shelley CS. 2015. CD38 in hairy cell leukemia is a marker of poor prognosis and a new target for therapy. *Cancer Res* **75:** 3902–3911. doi:10.1158/0008-5472.CAN-15-0893

Raje N, Chau I, Hyman DM, Ribrag V, Blay JY, Tabernero J, Elez E, Wolf J, Yee AJ, Kaiser M, et al. 2018. Vemurafenib in patients with relapsed refractory multiple myeloma harboring $BRAF^{V600}$ mutations: A cohort of the histology-independent VE-BASKET Study. *JCO Precis Oncol* **2:** 1–9. doi:10.1200/PO.18.00070

Rezk SA, Spagnolo DV, Brynes RK, Weiss LM. 2008. Indeterminate cell tumor: A rare dendritic neoplasm. *Am J Surg Pathol* **32:** 1868–1876. doi:10.1097/PAS.0b013e31818593d6

Rosai J, Dorfman RF. 1969. Sinus histiocytosis with massive lymphadenopathy. A newly recognized benign clinicopathological entity. *Arch Pathol* **87:** 63–70.

Rosai J, Dorfman RF. 1972. Sinus histiocytosis with massive lymphadenopathy: A pseudolymphomatous benign disorder. Analysis of 34 cases. *Cancer* **30:** 1174–1188. doi:10.1002/1097-0142(197211)30:5<1174::AID-CNCR2820300507>3.0.CO;2-S

Sadeghi N, Li HC. 2018. MRD-negative complete remission in relapsed refractory hairy cell leukemia with bendamustine and obinutuzumab. *Ann Hematol* **97:** 723–724. doi:10.1007/s00277-017-3219-z

Sarvaria A, Topp Z, Saven A. 2016. Current therapy and new directions in the treatment of hairy cell leukemia: A review. *JAMA Oncol* **2:** 123–129. doi:10.1001/jamaoncol.2015.4134

Satoh T, Smith A, Sarde A, Lu HC, Mian S, Trouillet C, Mufti G, Emile JF, Fraternali F, Donadieu J, et al. 2012. B-RAF mutant alleles associated with Langerhans cell histiocytosis, a granulomatous pediatric disease. *PLoS One* **7:** e33891. doi:10.1371/journal.pone.0033891

Schüller A. 1915. Über eigenartige schädeldefekte im jugendalter. *Fortschr Röntgenstr* **23:** 1916.

Senechal B, Elain G, Jeziorski E, Grondin V, Patey-Mariaud de Serre N, Jaubert F, Beldjord K, Lellouch A, Glorion C, Zerah M, et al. 2007. Expansion of regulatory T cells in patients with Langerhans cell histiocytosis. *PLoS Med* **4:** e253. doi:10.1371/journal.pmed.0040253

Shalem O, Sanjana NE, Hartenian E, Shi X, Scott DA, Mikkelson T, Heckl D, Ebert BL, Root DE, Doench JG, et al. 2014. Genome-scale CRISPR–Cas9 knockout screening in human cells. *Science* **343:** 84–87. doi:10.1126/science.1247005

Shanmugam V, Margolskee E, Kluk M, Giorgadze T, Orazi A. 2016. Rosai–Dorfman disease harboring an activating KRAS K117N missense mutation. *Head Neck Pathol* **10:** 394–399. doi:10.1007/s12105-016-0709-6

Siwe SA. 1933. Die reiticuloendotheliose—ein neues krankheitsbild unter den hepatosphlenomegalien. *Eur J Pediatr* **55:** 212–247.

Stålemark H, Laurencikas E, Karis J, Gavhed D, Fadeel B, Henter JI. 2008. Incidence of Langerhans cell histiocytosis in children: A population-based study. *Pediatr Blood Cancer* **51:** 76–81. doi:10.1002/pbc.21504

Strehl S, Nebral K, Konig M, Harbott J, Strobl H, Ratei R, Struski S, Bielorai B, Lessard M, Zimmermann M, et al. 2008. *ETV6-NCOA2*: A novel fusion gene in acute leukemia associated with coexpression of T-lymphoid and myeloid markers and frequent *NOTCH1* mutations. *Clin Cancer Res* **14:** 977–983. doi:10.1158/1078-0432.CCR-07-4022

Sumegi J, Streblow R, Frayer RW, Dal Cin P, Rosenberg A, Meloni-Ehrig A, Bridge JA. 2010. Recurrent t(2;2) and t(2;8) translocations in rhabdomyosarcoma without the canonical *PAX-FOXO1* fuse *PAX3* to members of the nuclear receptor transcriptional coactivator family. *Genes Chromosomes Cancer* **49:** 224–236.

Swerdlow SH, Campo E, Harris NL, Jaffe ES, Pileri SA, Stein H, Thiele J. 2017. *WHO classification of tumours of haematopoietic and lymphoid tissues, revised 4th ed.* International Agency for Research on Cancer, Lyon.

Taylor J, Pavlick D, Yoshimi A, Marcelus C, Chung SS, Hechtman JF, Benayed R, Cocco E, Durham BH, Bitner L, et al. 2018. Oncogenic TRK fusions are amenable to inhibition in hematologic malignancies. *J Clin Invest* **128:** 3819–3825. doi:10.1172/JCI120787

Techavichit P, Sosothikul D, Chaichana T, Teerapakpinyo C, Thorner PS, Shuangshoti S. 2017. *BRAF* V600E mutation in pediatric intracranial and cranial juvenile xanthogranuloma. *Hum Pathol* **69:** 118–122. doi:10.1016/j.humpath.2017.04.026

Thompson PA, Ravandi F. 2017. How I manage patients with hairy cell leukaemia. *Br J Haematol* **177:** 543–556. doi:10.1111/bjh.14524

Tiacci E, Trifonov V, Schiavoni G, Holmes A, Kern W, Martelli MP, Pucciarini A, Bigerna B, Pacini R, Wells VA, et al. 2011. *BRAF* mutations in hairy-cell leukemia. *N Engl J Med* **364:** 2305–2315. doi:10.1056/NEJMoa1014209

Tiacci E, Park JH, De Carolis L, Chung SS, Broccoli A, Scott S, Zaja F, Devlin S, Pulsoni A, Chung YR, et al. 2015. Targeting mutant *BRAF* in relapsed or refractory hairy-cell leukemia. *N Engl J Med* **373:** 1733–1747. doi:10.1056/NEJMoa1506583

Trunzer K, Pavlick AC, Schuchter L, Gonzalez R, McArthur GA, Hutson TE, Moschos SJ, Flaherty KT, Kim KB, Weber JS, et al. 2013. Pharmacodynamic effects and mechanisms of resistance to vemurafenib in patients

Downloaded from http://perspectivesinmedicine.cshlp.org/ on September 20, 2020 - Published by Cold Spring Harbor Laboratory Press



with metastatic melanoma. *J Clin Oncol* **31:** 1767–1774. doi:10.1200/JCO.2012.44.7888

Tschernitz S, Flossbach L, Bonengel M, Roth S, Rosenwald A, Geissinger E. 2014. Alternative *BRAF* mutations in *BRAF* V600E-negative hairy cell leukaemias. *Br J Haematol* **165:** 529–533. doi:10.1111/bjh.12735

Vaglio A, Diamond EL. 2017. Erdheim–Chester disease: The "targeted" revolution. *Blood* **130:** 1282–1284. doi:10.1182/blood-2017-07-795054

Veyssier-Belot C, Cacoub P, Caparros-Lefebvre D, Wechsler J, Brun B, Remy M, Wallaert B, Petit H, Grimaldi A, Wechsler B, et al. 1996. Erdheim–Chester disease. Clinical and radiologic characteristics of 59 cases. *Medicine (Baltimore)* **75:** 157–169. doi:10.1097/00005792-199605000-00005

Wander SA, Hasserjian RP, Oduro K, Glomski K, Nardi V, Cote GM, Graubert TA, Brunner AM, Chen YBA, Fathi AT. 2017. Combined targeted therapy for *BRAF*-mutant, treatment-related acute myeloid leukemia. *JCO Precis Oncol* **1:** 1–7. doi:10.1200/PO.16.00032

Wang L, Motoi T, Khanin R, Olshen A, Mertens F, Bridge J, Dal Cin P, Antonescu CR, Singer S, Hameed M, et al. 2012. Identification of a novel, recurrent *HEY1-NCOA2* fusion in mesenchymal chondrosarcoma based on a genome-wide screen of exon-level expression data. *Genes Chromosomes Cancer* **51:** 127–139. doi:10.1002/gcc.20937

Waterfall JJ, Arons E, Walker RL, Pineda M, Roth L, Killian JK, Abaan OD, Davis SR, Kreitman RJ, Meltzer PS. 2014. High prevalence of MAP2K1 mutations in variant and IGHV4-34-expressing hairy-cell leukemias. *Nat Genet* **46:** 8–10. doi:10.1038/ng.2828

Weitzman S, Jaffe R. 2005. Uncommon histiocytic disorders: The non-Langerhans cell histiocytoses. *Pediatr Blood Cancer* **45:** 256–264. doi:10.1002/pbc.20246

Wellbrock C, Karasarides M, Marais R. 2004. The RAF proteins take centre stage. *Nat Rev Mol Cell Biol* **5:** 875–885. doi:10.1038/nrm1498

Whittaker SR, Theurillat JP, Van Allen E, Wagle N, Hsiao J, Cowley GS, Schadendorf D, Root DE, Garraway LA. 2013. A genome-scale RNA interference screen implicates NF1 loss in resistance to RAF inhibition. *Cancer Discov* **3:** 350–362. doi:10.1158/2159-8290.CD-12-0470

Wood GS, Hu CH, Beckstead JH, Turner RR, Winkelmann RK. 1985. The indeterminate cell proliferative disorder: Report of a case manifesting as an unusual cutaneous histiocytosis. *J Dermatol Surg Oncol* **11:** 1111–1119. doi:10.1111/j.1524-4725.1985.tb01399.x

Xi L, Arons E, Navarro W, Calvo KR, Stetler-Stevenson M, Raffeld M, Kreitman RJ. 2012. Both variant and IGHV4-34-expressing hairy cell leukemia lack the *BRAF* V600E mutation. *Blood* **119:** 3330–3332. doi:10.1182/blood-2011-09-379339

Zarnegar S, Durham BH, Khattar P, Shukla NN, Benayed R, Lacouture ME, Lavi E, Lyden DC, Diamond EL, Dunkel IJ, et al. 2018. Novel activating *BRAF* fusion identifies a recurrent alternative mechanism for ERK activation in pediatric Langerhans cell histiocytosis. *Pediatr Blood Cancer* **65:** e26699. doi:10.1002/pbc.26699

Cold Spring Harbor Perspectives in Medicine
www.perspectivesinmedicine.org

Downloaded from http://perspectivesinmedicine.cshlp.org/ on September 20, 2020 - Published by Cold Spring Harbor Laboratory Press

Cold Spring Harbor Perspectives in Medicine

# MAP-Kinase-Driven Hematopoietic Neoplasms: A Decade of Progress in the Molecular Age

Rikhia Chakraborty, Omar Abdel-Wahab and Benjamin H. Durham

*Cold Spring Harb Perspect Med* published online June 29, 2020

**Subject Collection** Leukemia and Lymphoma: Molecular and Therapeutic Insights

**Biological and Translational Considerations regarding the Recent Therapeutic Successes and Upcoming Challenges for Multiple Myeloma**
*Constantine S. Mitsiades*

**The Biology of B-Progenitor Acute Lymphoblastic Leukemia**
*Kathryn G. Roberts and Charles G. Mullighan*

**Biology and Molecular Pathogenesis of Mature T-Cell Lymphomas**
*José R. Cortés and Teresa Palomero*

**The Role of Somatic Mutations in Acute Myeloid Leukemia Pathogenesis**
*Ashwin Kishtagari and Ross L. Levine*

**RNA Regulators in Leukemia and Lymphoma**
*Camila Prieto and Michael G. Kharas*

**Chronic Lymphocytic Leukemia**
*Nicholas Chiorazzi, Shih-Shih Chen and Kanti R. Rai*

**The Genetics and Mechanisms of T-Cell Acute Lymphoblastic Leukemia**
*Francesca Gianni, Laura Belver and Adolfo Ferrando*

**Epigenetic Mechanisms in Leukemias and Lymphomas**
*Cihangir Duy, Wendy Béguelin and Ari Melnick*

**Oncogenic Mechanisms and Therapeutic Targeting of Metabolism in Leukemia and Lymphoma**
*Maximilian Stahl, Zachary D. Epstein-Peterson and Andrew M. Intlekofer*

**MAP-Kinase-Driven Hematopoietic Neoplasms: A Decade of Progress in the Molecular Age**
*Rikhia Chakraborty, Omar Abdel-Wahab and Benjamin H. Durham*

**Epidemiology and Etiology of Leukemia and Lymphoma**
*Jordan A. Baeker Bispo, Paulo S. Pinheiro and Erin K. Kobetz*

**Mouse Models in the Study of Mature B-Cell Malignancies**
*Laura Pasqualucci and Ulf Klein*

**Clonal Hematopoiesis and Premalignant Diseases**
*Justin Kaner, Pinkal Desai, Nuria Mencia-Trinchant, et al.*

**Non-Hodgkin Lymphomas: Malignancies Arising from Mature B Cells**
*Jennifer Shingleton, Jie Wang, Carolyn Baloh, et al.*

**Mouse Models of Myeloid Malignancies**
*Faisal Basheer and George Vassiliou*

**Acute Megakaryocytic Leukemia**
*Maureen McNulty and John D. Crispino*

For additional articles in this collection, see http://perspectivesinmedicine.cshlp.org/cgi/collection/

Copyright © 2020 Cold Spring Harbor Laboratory Press; all rights reserved